NAIST-IS-DD0761021

Doctoral Dissertation

Electrophysiological and Molecular Mechanisms of Corticostriatal Synaptic Plasticity

Takashi Nakano

February 4, 2010

Department of Bioinformatics and Genomics
Graduate School of Information Science
Nara Institute of Science and Technology

A Doctoral Dissertation
submitted to Graduate School of Information Science,
Nara Institute of Science and Technology
in partial fulfillment of the requirements for the degree of
Doctor of SCIENCE

Takashi Nakano

Thesis Committee:

Professor Shin Ishii	(Supervisor)
Professor Kotaro Minato	(Co-supervisor)
Professor Kenji Doya	(Co-supervisor)
Associate Professor Yuichi Sakumura	(Co-supervisor)
Associate Professor Junichiro Yoshimoto	(Co-supervisor)

"Art is a lie that makes us realize truth."
-Pablo Picasso

Electrophysiological and Molecular Mechanisms of Corticostriatal Synaptic Plasticity*

Takashi Nakano

Abstract

The striatum is a part of the brain that is involved in learning through "trial-and-error". The striatum receives glutamatergic input from the cortex and dopaminergic input from the substantia nigra. These inputs, acting together, induce long-term change of corticostriatal synaptic strength. A number of laboratories have investigated corticostriatal synaptic plasticity: however, contradictory results and properties have been reported, and the underlying electrophysiological and molecular mechanisms have not been understood well. It is difficult to elucidate the dependence of corticostriatal synaptic plasticity on dopamine, as well as the timing of presynaptic inputs and spike output only by experimentation. To clarify the mechanisms behind the plasticity of striatal synapses, I have performed experiments and constructed realistic models at two different levels: cellular and molecular.

First, I studied synaptic plasticity in the principal neurons of the striatum, of which these are two types. To verify whether the properties of synaptic plasticity depended on cell type or not, electrophysiological experiments were performed in which cell types could be distinguished. I found that similar properties were observed in both cell types. Second, to investigate the electrophysiological mechanisms underlying spike-timing dependent synaptic plasticity (STDP) in the striatum, as well as dopamine timing effects on STDP, I constructed an electric compartment model with realistic morphology obtained from my experiments. The

*Doctoral Dissertation, Department of Bioinformatics and Genomics, Graduate School of Information Science, Nara Institute of Science and Technology, NAIST-IS-DD0761021, February 4, 2010.

model prediction was that the dependence of the calcium response on the timing of glutamate input depends on dopamine timing, which indicates dopamine timing regulates STDP. Third, to examine the dynamics of dopamine- and calcium-dependent plasticity, I constructed a signaling pathway model of synaptic spines expressing D1-type dopamine receptors, and I then analyzed the system. According to the simulation results, the direction of change in the phosphorylation level of dopamine- and cAMP-regulated phosphoprotein of molecular weight 32 kDa (DARPP-32) is dependent on calcium input strength, and a positive feedback loop including DARPP-32 shows bistability, which induces dopamine dependent long-term potentiation (LTP). Finally, by connecting the two models, I predicted synaptic efficacy induced by physiological triggers. The model reproduced calcium (membrane potential) dependent synaptic plasticity, dopamine dependent synaptic plasticity, and spike-timing dependent synaptic plasticity. The model showed that leaky integration of calcium was a good approximation of change in synaptic efficacy and that it was mediated by Ca^{2+}/calmodulin-dependent protein kinase II (CaMKII) activity. Also dopamine timing effect on synaptic efficacy was via calcium influx.

Keywords:

Striatum, Synaptic Plasticity, Calcium, Dopamine, Multi-Scale Simulation, Patch Clamp Experiment

Contents

List of Figures

List of Tables

Acknowledgements

First of all, I completed my thesis with the help of a number of people. I would like to express my appreciation to all of them.

I have studied under Professor Kenji Doya and Associate Professor Junichiro Yoshimoto. Professor Doya gave me the wonderful opportunity to study in the Okinawa Institute of Science and Technology (OIST). I received an excellent education from him, and he gave me many insightful ideas and much advice, in addition to a scientific attitude of mind. He also gave me many opportunities to meet numerous scientists from home and abroad, which gave me great experience.. Associate Professor Yoshimoto supervised me with his kind help and he gave me beneficial comments from the viewpoint of computation theory. I have had great feedback in meetings and reading groups from researchers at the Doya Neural Computation Unit. I would especially like to thank Dr. Eiji Uchibe, Dr. Makoto Ito, Dr. Katsuhiko Miyazaki, and Dr. Kayoko Miyazaki, who gave me a much advice from their great knowledge. I also thank Dr. Tetsuro Morimura and Dr. Takumi Kamioka, who have already graduated, and who gave me a mass of advice on various matters, starting with student life. I developed myself through friendly competition with Mr. Makoto Otsuka, who joined NAIST and OIST and moved to Okinawa in the same year as I.

In the year I spent in Nara which was the first year of the Ph.D. course, I received advice from various people in NAIST including Professor Shin Ishii and Associate Professor Yuichi Sakumura. Dr. Tomokazu Doi generously supervised me at the start of my simulation study. I was impressed with the dynamism of Dr. Yasunobu Igarashi and Dr. Honda Naoki. My experience in Nara became the foundation of my research life.

To start the experiments for my doctorate, Dr. Jeff Wickens accepted me into his Neurobiology Research Unit with good cheer. He gave me a great amount of advice and discussed matters of experimentation and modeling with me despite my clumsy English. Dr. Cathy Vickers cheerfully supervised me, although I was a complete beginner regarding the patch clamp. I received a great amount of advice from Dr. Tomomi Shindo and Dr. Mayumi Shindo, and I was supported during experiments by Dr. Saori Miura, Mr. Kiyoshi Baba and Ms. Yukako Suzuki. In addition, I had many things to learn from Dr. Takayuki Yamashita in

OIST and Mr. Akihiro Funamizu in the University of Tokyo. They held sincere but fun attitudes to life, both inside and outside the lab.

Although I am unable to list all names, I have gained inspiration through discussion with current and former members and visitors of OIST, including people at the Doya Unit and the Wickens Unit, as well as people in the Theoretical Life-Science Laboratory and the Systems Biology Laboratory in NAIST, the Integrated Systems Biology Laboratory in Kyoto University, the Computational Neuroscience Laboratories in ATR and all the people who I met at conferences.

Mr. Yasuhiro Inamine and Mr. Tomofumi Inoue supported me in computer management. Ms. Eri Saito from the Systems Biology Laboratory and Ms. Aya Tanimoto from the Life-Science Laboratory in NAIST, as well as Ms. Emiko Asato, Ms. Chikako Uehara and Ms. Izumi Nagano in the Neural Computation Unit in OIST, kindly helped me with secretarial work beyond their obligations. I was aided by people from companies, such as Mr. Takuya Okada from Physio-Tech, Mr. Kenji Tsubokura from Brain Vision, Dr. Yutaka Sugimoto from Olympus, Mr. Isamu Uehara from Chuoiryoki, and Mr. Takuma Taira from TOMY SEIKO. Ms. Mizuki Ihara, also a student in NAIST, helped me to submit my thesis, as well as helping me to get to know the atmosphere of NAIST. I could not complete this thesis without their unstinting support. Also, I would like to thank my friends, with whom I played, drank and talked. I especially thank my family and, above all, my parents, Mitsuo Nakano and Machiko Nakano, who gave birth to me with a healthy body, and who have raised and supported me up to today. I am also thankful for the beautiful ocean in Okinawa. Again, I would like to acknowledge Professor Shin Ishii, Professor Kotaro Minato, Professor Kenji Doya, Associate Professor Yuichi Sakumura and Associate Professor Junichiro Yoshimoto for having reviewed this thesis. Finally, I would like to thank all of those who read this thesis.

1. General Introduction

In our daily life, we make many decisions. For example, when we go out for dinner, we have choices: Which restaurant do we go to? Who do we go with? How do we get there? In such decision-making, we learn which are better choices based on our past experiences through a "trial-and-error" process. This kind of learning is called "reinforcement learning", and is hypothesized to occur in the basal ganglia of the brain [61]. According to this hypothesis, a region in the basal ganglia called the striatum computes the value (goodness) of a state and an action. This is based on a state signal from the cortex, and a reward prediction error signal that indicates whether the state and action are better or not than expected. Thus, in the computational model of the basal ganglia, the striatum is thought to estimate value. In this thesis, an investigation of the cellular and molecular mechanisms underlying this type of learning is reported.

The computation of the update of a value is the essence of this learning and is realized by the plasticity of the connection between the cortex and striatum. This is called corticostriatal synaptic plasticity. The plasticity is regulated by glutamatergic input from the cortex, dopaminergic input from the substantia nigra, and activation of striatal cell, as well as the relative timing of these signals. The deep involvement of the neuromodulator dopamine is a major characteristic in striatal synaptic plasticity. Although, many studies of corticostriatal synaptic plasticity have been performed since the first such study by Calabresi *et. al.* in 1992 [28], some reports are conflicting, and the characteristics and the mechanisms are not well understood.

Recently, computer simulation has become an important method to complement traditional theoretical and experimental approaches. Computer simulation can examine the behavior of a complicated system with many interactions. For example, although a signaling cascade is a highly complicated system and it is difficult to understand the overall dynamics by experimentation, simulation can make it possible to understand and analyze the system mathematically. Experiments, meanwhile, often have many constraints. For instance, experimental conditions are often different from those that actually occur *in vivo*. However, computer modeling can simulate such conditions. In addition, simulation can easily investigate various different conditions, saving time and money. More im-

portantly, simulations can predict mechanisms underlying phenomena, and can identify novel phenomena. "A model is a lie that helps us see the truth." Even though a model can be too simplified or even wrong, it makes the phenomenon clearer. Ideally, model prediction should be tested by experiment, and models should be improved based on experimental results. This cycle of simulation and experiment leads to improved understanding, even if the prediction is not correct.

In this thesis, to elucidate electrophysiological and molecular mechanisms of striatal synaptic plasticity that underlie the learning system in the basal ganglia and which are related to dopamine and to the timing of inputs, I performed experiments to investigate synaptic plasticity in different striatal projection neuron cell types. I also constructed a signaling cascade model and an electric compartment model with realistic morphology based on experimental data to investigate the molecular dynamics and mechanisms of synaptic plasticity. Finally, I integrated these two models and predicted changes in synaptic efficacy induced by physiological triggers.

1.1 Striatum

1.1.1 Features of the striatum in the basal ganglia circuit

The basal ganglia integrates sensory and motivational signals to achieve goal-directed actions and cognition [6,62,111]. The basal ganglia comprises four brain regions; striatum, substantia nigra (SN), globus pallidus (GP) and subthalamic nucleus (STN). The striatum consists of the caudate nucleus, putamen and nucleus accumbens. Combined the putamen and the globus pallidus are sometimes called the lenticular nucleus.

The circuit of the basal ganglia forms a loop structure (Fig. 1.1). The striatum, the input site of the basal ganglia, receives glutamatergic input from the cortex and sends signals to the substantia nigra and globus pallidus, which then send signals back to the cortex via thalamus. There are independent parallel loops such as the motor loop, oculomotor loop, prefrontal loop, and limbic loop [3,159].

This output from the striatum is divided into two pathways. One is called the direct pathway consisting of striatal projection neurons that express γ-Amino Butyric Acid (GABA), dynorphin and enkephalin and that project to the basal

ganglia output nucleus reticular part of the substantia nigra (SNr) and internal segment of the globus pallidus). The other is the indirect pathway that consists of GABA and substance P expressing striatal projection neurons that project to the external segment of the globus pallidus [110, 128]. In addition, there is a hyper direct pathway from the STN to the SNr.

The striatum has two compartments, patch and matrix, which can be distinguished by chemical markers. The patches are also called striosomes. Immunohistochemically, the calcium-binding protein calbindin D28k is localized to matrix cells, but not to the patch cells [75]. Neurons in patch compartments, which constitute approximately 15% of the striatum, receive glutamatergic projections from layer Vb and VI of the cortex. Matrix neurons receive glutamatergic input from cortical layer III and Va [125, 128]. Interestingly, the topology of the corticostriatal projection is many-to-one rather than many-to-many connections [234].

The striatum also receives dopaminergic input from the substantia nigra pars compacta and from the ventral tegmental area. Dopaminergic input to the striatum plays a critical role in motor and cognitive control, as evidenced in Parkinson's disease and drug addiction [87, 130, 165]. Moreover, the striatum is involved in learning through "trial-and-error" as described below.

1.1.2 Basal ganglia and reinforcement learning theory

The reinforcement learning model is proposed as an information processing model in the basal ganglia. Reinforcement learning is a framework of leaning that expects future rewards and that obtains better action outcomes based on experiences of reward or punishment through trial-and-error.

One of the origins of the hypothesis is an experiment by Schultz *et. al.*, which measured the activity of dopamine neurons in monkeys during tasks [202]. After learning, the dopamine neurons responded to the cue preceding the actual reward, but not to the actual reward itself. When the actual reward was omitted, the activity of the dopamine neurons decreased at the time that the reward should have been given.

The activity patterns of dopamine neurons relative to basal levels are explained by the reward prediction error in the reinforcement learning model. In addition, the cerebral cortex converts information from the outside world into a

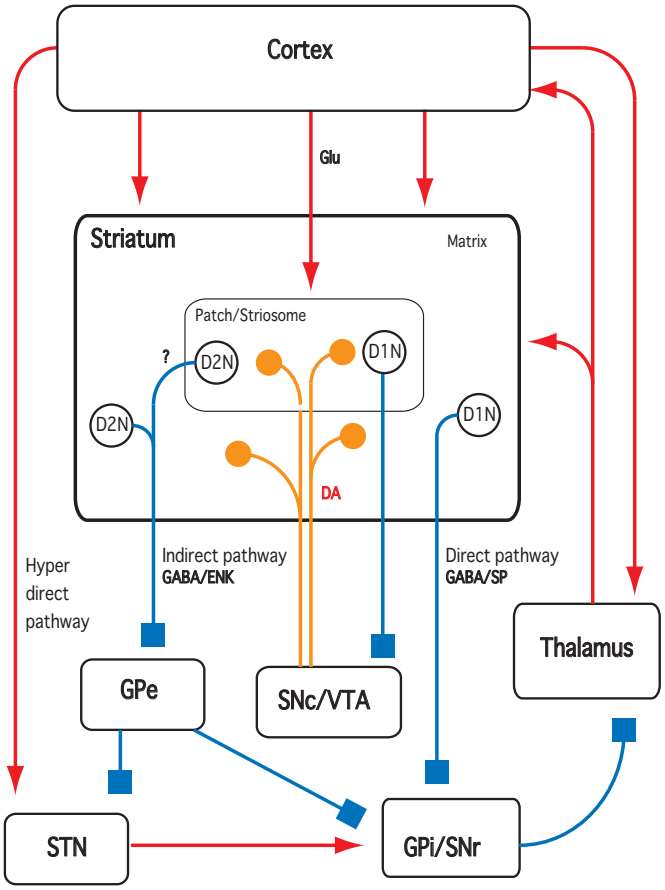

Figure 1.1. The basal ganglia circuit. The striatum receives glutamatergic input (Glu) from cortex and dopaminergic input (DA) from the substantia nigra pars compacta and ventral tegmental area. Projection neurons in the striatum are medium spiny neurons, which are divided into two groups depending on the type of dopamine receptor expressed and on the output pathways. Cells expressing the D1 type dopamine receptor (D1Ns) in the matrix express GABA and enkephalin (ENK) and project to the substantia nigra pars reticulata and the internal segment of the globus pallidus (direct pathway). D1Ns in patches project to the substantia nigra pars compacta and the ventral tegmental area. Cells expressing the D2 type dopamine receptor (D2Ns) express GABA and substance P (SP) and project to the external segment of the globus pallidus (indirect pathway). The red arrows indicate excitatory projections and the blue arrows indicate inhibitory projections.

proper representation of this state in the brain. The striatum receives cortical signals, as well as dopamine signals representing reward prediction error. To integrate these, we can presume that the basal ganglia perform reinforcement learning and that the striatum encodes the estimation of the values of the state and action. Indeed, some experiments have suggested that the striatum represents expected future reward [199].

1.1.3 Cells in the striatum

The striatum consists of five types of neurons [141]. Medium spiny neurons are the only projection neurons in the striatum and more than 90 % of striatal neurons are medium spiny neurons. The medium spiny neurons receive glutamatergic input from cortex and dopamine input from the substantia nigra. The glutamate synapses are located on spine heads and dendritic shafts. The dopamine synapses are located on spine necks, shafts and soma [76]. The glutamate synapses are about 10 times as numerous as the dopamine synapses. Although synaptic terminals of corticostriatal axons make contacts with postsynapse, dopamine receptors are not located within the nigrostriatal synapse but are located some distance away. Dopamine diffuses from the synaptic cleft into the surrounding extracellular tissue and affects multiple distant dopamine receptors [233].

In anesthetized in vivo preparations or co-cultures, the resting membrane potential of medium spiny neurons alternates between an up-state of -60 mV and a down-state of -85 mV, with a low frequency of approximately 1 Hz caused by a massive amount of cortical input.

Medium spiny neurons are divided into two subclasses: those expressing D1-type dopamine receptors (D1Rs), which are neurons of the direct pathway, and those expressing D2-type dopamine receptors (D2Rs), which are neurons of the indirect pathway. These neurons are almost the same in number and have very similar characteristics [43, 79]. The distribution of the different classes of medium spiny neuron are independent of localization to patch or matrix [77]; however, dendrites and axons do not cross compartment borders.

Other neurons in the striatum are all interneurons. They are divided to cholinergic interneuron and GABAergic interneurons [129]. Cholinergic interneurons are morphologically called large aspiny neurons and are electrophysiologically

called tonically active neurons. GABAergic neurons are divided to three types. One is a parvalbumin positive neuron that is called a fast spiking neuron. The second is a low-threshold spike cell which co-expresses somatostatin, nitric oxide synthase (NOS), and neuropeptide Y. The third is a calretininergic neuron. These interneurons are thought to regulate intercompartment transmission between patch and matrix [128, 196]. .

1.1.4 Receptors and signaling cascades in medium spiny neurons

There are five types of dopamine receptors, which can be grouped into D1Rs and D2Rs [216]. Dopamine receptors are G protein-coupled receptors (GPCRs): D1Rs couple with G_s and D2Rs couples with $G_{i/o}$. G_s promotes the production of cyclic adenosine 3',5'-monophosphate (cAMP) by activating adenylyl cyclase 5 (AC5). In contrast, $G_{i/o}$ inhibits AC5. cAMP is a second messenger and activates cAMP-dependent protein kinase (PKA). In addition, the G protein $\beta\gamma$ complex increases calcium release from inositol 1,4,5-trisphosphate (IP_3) receptors on the endoplasmic reticulum (ER) via activation of phospholipase C (PLC)β [49, 160, 166].

Glutamate receptors on the medium spiny neurons are α-amino-3-hydroxy-5-methylisoxazole- 4-proprionate (AMPA) type glutamate receptors (AMPARs), N-methyl-D-aspartate, N-methyl-D-aspartic acid (NMDA) type glutamate receptors (NMDARs) and metabotropic glutamate receptors (mGluRs).

When AMPARs bind glutamate, the channels open and permit the passage of Na^+ and K^+. AMPARs without the GluR2 subunit also permit the passage of Ca^{2+}. Similar to AMPARs, glutamate binding to NMDARs permit the passage of Na^+, K^+, and Ca^{2+}. However, NMDARs are normally blocked by Mg^{2+}. This inhibition is disinhibited when membrane potential increases. Therefore, NMDARs permit the passage of ions depending on both glutamate and membrane potential.

The striatum expresses mGluRs, especially mGluR1 and mGluR5. mGluRs are GPCRs and increase the intracellular calcium concentration via IP_3 receptors on the ER. IP_3 receptors open when IP_3 receptors bind IP_3 and Ca^{2+}. The open probability of IP_3 receptors is bell-shaped for calcium concentration, and IP_3 receptors do not open when calcium levels are too high [60, 242]. In addition,

calcium concentration can increase via entry through calcium channels.

Calcium is stored in the ER and in the extracellular medium. The concentration is a few mM outside the cell and in the tens to several hundred nM range inside the cell in the resting condition, but intracellular concentration reaches 10 μM on excitation. Calcium works as a second messenger and activates calmodulin (CaM), protein phosphatase 2B, (Calcineurin, PP2B), and Ca^{2+}/calmodulin-dependent protein kinase II (CaMKII).

In comparison with the intracellular molecules involved in the synaptic plasticity of the hippocampus and cerebellum, a major difference in the striatum is the presence of the protein: dopamine and cAMP-regulated phosphoprotein of 32 kDa (DARPP-32). DARPP-32 receives both dopamine and glutamate signals and is thought to integrate these signals and to regulate signaling cascades involved in synaptic plasticity. I describe this in detail in Chapter 4.

1.2 Neurobiology of Corticostriatal Synaptic Plasticity

Glutamatergic and dopaminergic fibers converge onto single synapses of medium spiny neurons [4], which are the striatal output neurons. Corticostriatal synapse efficacy is regulated by cortical glutamatergic input and dopaminergic input. Synaptic plasticity of the corticostriatum was investigated by Calabresi *et. al.* in 1992. They reported that high frequency stimulation of the cortex and postsynaptic activation induced long-term depression (LTD), and that tetanic stimulation in magnesium-free solution induced long-term potentiation (LTP) [28] Subsequent studies reported that coincident tetanus stimulation and dopaminergic input can cause LTP [235]. This dopamine dependence of synaptic plasticity is unique in the striatum and is different from synaptic plasticity in the hippocampus and cerebellum. This dopamine-dependent plasticity is a critical element for linking sensory and cognitive inputs from the cortex with reward-related signals from dopaminergic neurons to establish goal-directed behaviors [62].

Furthermore, some studies have reported that LTP was induced by glutamate stimulation coincident with the up-state even in the presence of magnesium. In addition, other groups reported that both LTD and LTP were induced by cortical tetanic stimulation alone, without dopamine [2, 45, 46, 213]. These varied results have meant that the study of corticostriatal synaptic plasticity has been confused.

Recently, spike-timing has been found to be an important factor in synaptic plasticity. Basically, a presynaptic spike preceding a postsynaptic spike induced LTP, and a postsynaptic spike preceding a presynaptic spike induced LTD [32, 51, 69]. The NMDA receptor was considered as a timing coincidence detector [126, 209, 229]. The NMDA receptor elevates intracellular calcium [155]. The presynaptic spike leads to glutamate release from presynaptic terminals and activates the NMDA receptor. However, ions cannot flow through the NMDA receptor because of the magnesium block. Postsynaptic depolarization causes removal of the block. The duration of the depolarization is much shorter than the duration of NMDA receptor activations by glutamate. Therefore, a postsynaptic spike following a presynaptic spike elevates calcium levels higher than if the timing is reversed. A second hypothesis of the NMDA receptor as a coincidence detector is that calcium influx from calcium channels following a postsynaptic spike inhibits NMDA receptors, therefore, decreasing calcium influx in response to glutamate [229]. Although, other types of STDP are also known, the involvement of NMDA receptors and calcium elevation have been highlighted [32]. In addition, IP_3 receptors and PLC_β were also suggested as coincidence detectors [10, 102]. PLC_β, induces presynaptic changes via endocannabinoid and is activated most strongly when mGluR signal and calcium elevation are coincident. PLC also activates IP_3 and induces calcium release from the ER via IP_3 receptors, which open when calcium and IP_3 are coincident. The calcium level is thought to determine the direction of STDP [5, 239]. However, it is also reported that the peak calcium determines the magnitude of the change in synaptic efficacy, rather than the direction of STDP [167]. The STDP depends on dendritic location [70, 145] and is considered to be caused by the back propagation of action potentials. In the striatum, some groups studied STDP of corticostriatal synapses and reported contradictory results [66, 185, 204], which are described in Section 1.2.3.

1.2.1 Dopamine dependent synaptic plasticity

In corticostriatal slices or co-culture preparations, tetanic stimulation of cortical fibers induces striatal cell firing that results in long-term depression (LTD) of corticostriatal synapses [23, 28, 47]. In contrast, simultaneous stimulation of dopaminergic neurons in the substantia nigra during cortical stimulation results in

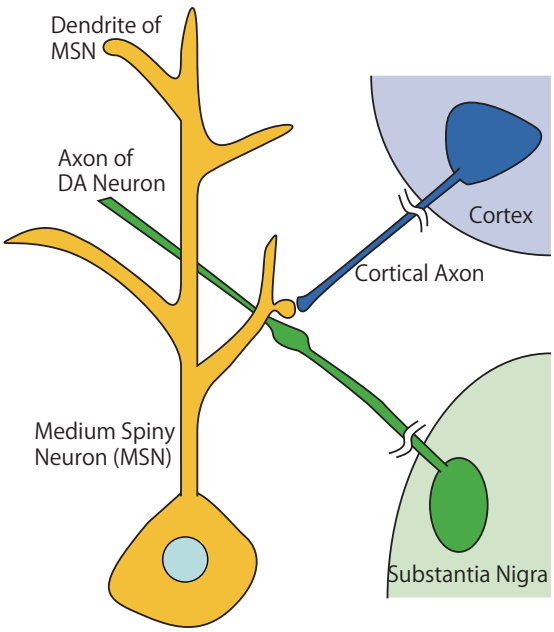

Figure 1.2. Projections to MSNs. Dopaminergic fibers originating in the SNc form synapses on the dendrites of medium spiny neurons. Cortical axons connected to spines on the dendrites of medium spiny neurons.

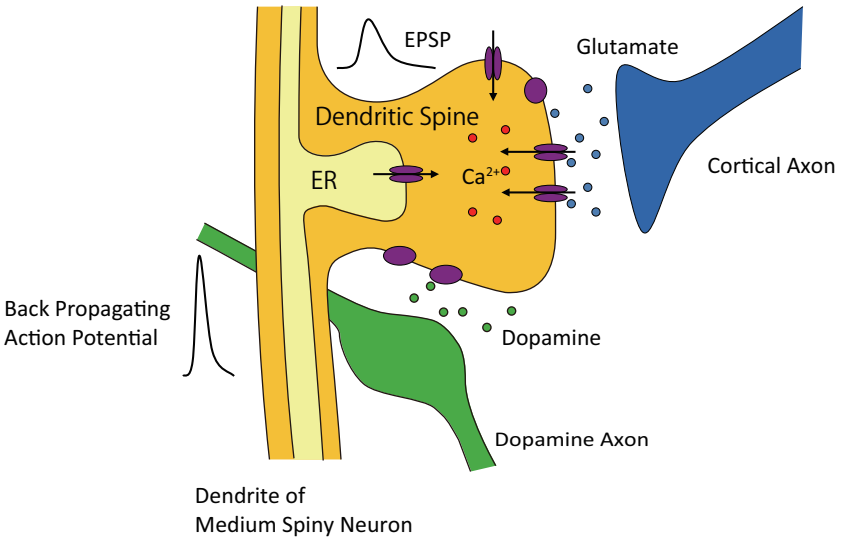

Figure 1.3. Image of striatal dendritic spine. Glutamate and dopamine are released at a spine. Glutamate activates ionotropic receptors and induces excitatory postsynaptic potentials (EPSPs). Glutamate also activates metabotropic receptors which induces calcium release from the ER. Calcium influx from outside the cell is through ionotropic glutamate receptors and calcium channels. Voltage-dependent calcium channels are activated by back-propagating action potentials (bAPs). Dopamine modulates conductance of channels and receptors.

long-term potentiation (LTP) with high frequency dopaminergic stimulation, and no change in synaptic efficacy at low frequency dopaminergic stimulation (i.e., levels corresponding to spontaneous firing) [191–193, 235]. In addition, under dopamine depletion, cortical stimulation does not alter corticostriatal synaptic efficacy [28]. Fig. 1.4A shows that cortical glutamatergic input can cause either LTD or LTP of corticostriatal synapses depending on the strength of the simultaneous dopaminergic input.

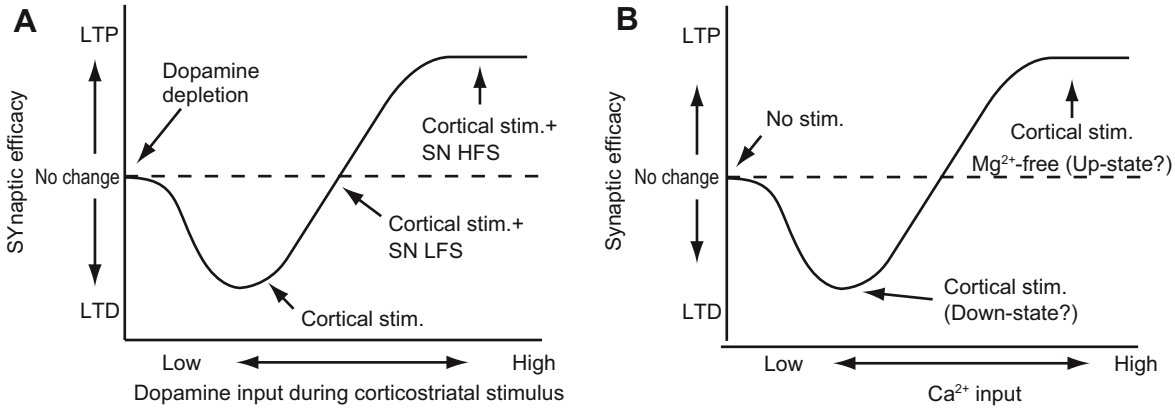

Figure 1.4. Schematic diagrams of dopamine- and calcium-dependent synaptic plasticity. (A) Dopamine-dependent synaptic plasticity (modified from [193]). (B) Calcium-dependent synaptic plasticity. The abbreviations used are as follows: SN - substantia nigra; LFS - low-frequency stimulation; and HFS - high-frequency stimulation. The altered direction of synaptic efficacy depends on input intensity of dopamine and calcium.

1.2.2 Calcium dependent synaptic plasticity

Cortical stimulation without dopamine input induces LTP of corticostriatal synapses. In slice preparations cultured in magnesium-free solutions, tetanic stimulation of cortical fibers induces LTP [24,30,42]. During the up-state, when magnesium inhibition of NMDA receptors is removed [34], tetanic stimulation of cortical fibers induces LTP in corticostriatal synapses [2, 45, 46, 213]. Therefore, even with little or no dopamine, high levels of intracellular calcium, either through calcium entry via inotropic glutamate receptors and voltage-dependent calcium channels

(VDCCs) or through endoplasmic reticulum (ER) calcium release via activation of metabotropic glutamate receptors (mGluRs), can revert LTD of corticostriatal synapses to LTP but Mg^{2+}-free LTP is blocked by DA depletion and dopamine D1 receptor antagonism [131] (Fig. 1.4B). Some studies have used caged calcium to directly examine the relationship between calcium and synaptic plasticity in the cerebellum and hippocampus [224, 239]. In the striatum, a rise in calcium by strong paired stimulation to the cortex and striatum induced LTD, whereas a small rise in calcium by weak paired stimulation to the cortex and striatum did not induce synaptic change [18].

1.2.3 Spike-timing dependent plasticity

STDP studies of corticostriatal synapses are conflicting. One reported that cortical input preceding the postsynaptic spike induced LTP whereas cortical input following the postsynaptic spike induced LTD (normal STDP) [185]. In this experiment, oblique slices were used with glycine (NMDA receptor coagonist) and picrotoxin ($GABA_A$ receptor blocker). 60-paired stimulation was applied at 0.1 Hz. To evoke a postsynaptic action potential, 2 ms current pulses were used. The change in the excitatory postsynaptic potential (EPSP) evoked by layer V stimulation was measured.

Another study reported that cortical input preceding the postsynaptic spike induced LTP whereas cortical input following the postsynaptic spike induced nothing [204]. In this experiment, parasagittal corticostriatal slices were used. Long lasting synaptic plasticity was induced using protocols of 10-15 trains of five bursts repeated at 0.1 Hz, with each burst composed of three bAPs preceded with three EPSPs at 50 Hz. To evoke a postsynaptic action potential, 5 ms current pulses were used. The change to the EPSPs evoked by focal extracellular stimulation with a small theta glass electrode was measured.

Yet another study reported the opposite coupling, in which cortical input following the postsynaptic spike induced LTD and cortical input preceding the postsynaptic spike induced LTP (reversed STDP) [66]. In this experiment, horizontal slices were used. 100-paired stimulation was applied at 1 Hz. To evoke a postsynaptic action potential, 30 ms current pulses were used. The change to the EPSCs evoked by layer V stimulation was measured. It was suggested that

spike timing dependent LTP arose from the presynaptic element.

Although the literature [185,204] suggested that the activation of D1 receptors was necessary to induce both LTD and LTP, the effect of timing of the dopamine input on STDP is still an open issue.

1.2.4 Interneurons and synaptic plasticity in striatum

Inhibition of neurotransmitter release by striatal interneurons blocks changes in synaptic efficacy of corticostriatum; therefore, interneurons are thought to be involved in the plasticity of corticostriatal synapses in medium spiny neurons.

Long term depression (LTD) of the synapse in both D1R expressing medium spiny neurons (D1Ns) and D2Rs expressing medium spiny neurons (D2Ns) requires D2R [27,30,225]. However, D1Rs and D2Rs are not expressed in the same cell [110]. The role of D2Rs on D1Ns is thought to be via cholinergic interneurons that express D2Rs [236], and M_1 muscarinic receptors on the medium spiny neurons [22, 225, 231]. This LTD also required Group 1 mGluRs [214]. LTP in magnesium-free solution required calcium influx from calcium channels and dopamine receptor activations [4,40,131]. This LTP also needs mGluRs, because LTP did not occur following mGluR inhibition [31, 92, 93]. Furthermore, inhibition of interneuronal nitric oxide synthase (NOS) blocked LTD by glutamate stimulation [26, 39, 41]. In addition, synaptic plasticity in Cholinergic neurons depends on dopamine [219] From these results, acetylcholine and nitric oxide projections from interneurons play important roles in the plasticity of corticostriatal synapses in medium spiny neurons. In this thesis, however, interneurons were ignored for the sake of simplicity.

1.3 Simulation Studies on Synaptic Plasticity

There is an approach to understand biological phenomena as systems, which is called systems biology. Computer simulation is a powerful tool for understanding the underlying mechanisms behind synaptic plasticity. Synaptic efficacy is regulated by intracellular chemical reactions, which are highly interactive and form a complicated network. This complexity makes it difficult to intuitively understand the behavior of the system based on experimental results only. It,

therefore, became popular to construct kinetic models of signaling cascades based on experimental results. Although such systems biology approaches have been attempted for the hippocampus and cerebellum [60, 142], in the striatum, there are only models of chemical pathways which are not connected to synaptic change.

Several models were proposed to explain STDP in the hippocampus. They assumed that the amplitude of calcium responses determined the direction of synaptic change and suggested that NMDA receptors functioned as timing coincidence detectors [195, 205, 206, 229, 240]

Biological systems have multiple levels, such as molecular, cellular, and network levels. These have different spatial and time scales, which makes modeling difficult. Therefore, most models incorporate degrees of simplification. For example, kinetic models can ignore whole cell dynamics, and neuronal models can assume that calcium determines synaptic change, while ignoring the chemical cascades that directly influence synaptic change.

1.4 Aims and Composition of This Thesis

As described above, mechanisms of synaptic plasticity are open to question. Synaptic plasticity is caused by intracellular molecules. For example, dopamine activates PKA through dopamine D1Rs. Glutamate receptors, as well as calcium channels, increase intracellular calcium, which activates CaMKII and protein phosphatase 1 (PP1). These kinases and phosphatases regulate synaptic efficacy. In this thesis, I aimed to predict electrophysiological mechanisms and molecular interactions that underlie synaptic plasticity and to explain various properties of corticostriatal synaptic plasticity.

Although there are two types of medium spiny neuron and each neuron has different types of dopamine receptors and different projection pathways, these two have rarely been distinguished in functional studies. This lack of distinction may cause divergence of synaptic plasticity data in the striatum. Therefore, I performed electrophysiological experiments that distinguish between the two types of cell using transgenic mice. This is presented in Chapter 2.

Next, I investigated the molecular mechanisms underlying the synaptic plasticity of D1Ns, because D1Rs are better understood than D2Rs. I constructed two models to understand the molecular and cellular mechanisms underlying synaptic

plasticity depending on dopamine and spike timing. One is a neuron model with realistic morphology at the cellular level. The morphology was obtained from experiments described in Chapter 2. This model receives physiological triggers such as glutamate, dopamine, and also postsynaptic spikes, then estimates output calcium elevation in spines. This is described in Chapter 3. The second model is a signaling cascade model at the molecular level, which is presented in Chapter 4. This model receives dopamine and calcium as inputs and determines output as synaptic efficacy. These two models are separate models. The reason why these models were separated was that calcium responses depended on whole cell activity and it was impossible to calculate it precisely in the signaling cascade model. Strictly speaking, however, these models should not be separated. Indeed, the dopamine effect on calcium is through the intracellular chemical network. However, to accommodate the difficulty of multi scale simulation, two separate models were constructed and then I integrated these models as described in Chapter 5.

Fig. 1.5 shows the relationship of modeling and experimental studies in this thesis. An electric compartment model was constructed based on experimentally derived morphology and parameters were estimated based on experimental data. The signaling cascade model predicted synaptic plasticity following dopamine and calcium inputs, and molecular mechanisms underlying synaptic plasticity. By connecting the models, I was able to predict synaptic change by physiological triggers. The model predictions should, of course, be tested by experiment and I discuss the experiments for model validation and the future possibilities of this study in Chapter 6.

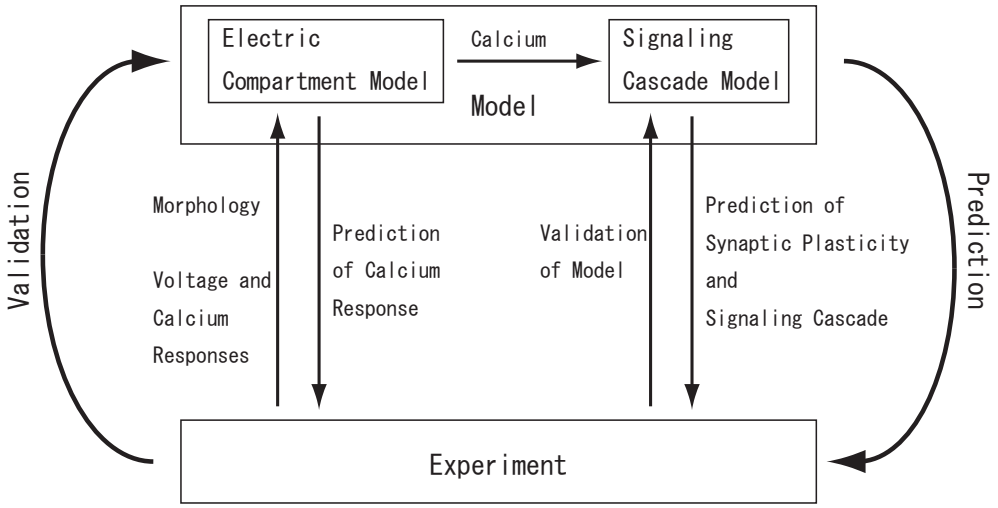

Figure 1.5. The relationships among the studies in this thesis.

2. Electrophysiological Experiment

2.1 Introduction

In corticostriatal synaptic plasticity experiments, divergent results have been reported even when similar protocols were used. For example, some groups reported LTD, but others reported LTP using high-frequency stimulation (HFS) [2, 28, 45, 46, 213]. One possible reason of these diverse results is the different medium spiny neuron cell types; D1Ns and D2Ns. To date, although these cells have different projection pathways, most synaptic plasticity studies in the striatum have been performed with no distinction being made between medium spiny neuron cell types. This is because they have a similar appearance and similar electrophysiological properties. Recently, however, transgenic mice have been engineered that enable the two cell types to be distinguished [43, 204], although no study has yet been performed to investigate the change in synaptic efficacy induced by high-frequency stimulation of the cortex and striatal postsynaptic activation in the two distinct cell types. Therefore, I first investigated synaptic plasticity having identified cell types using dopamine receptor transgenic mice, in which dopamine receptors were tagged with enhanced green fluorescent protein (eGFP).

In addition, this thesis aimed to integrate experimentation and modeling. Construction of the model is based on experimental data and the model should be tested by experimentation; the model should inform the experiment and this feedback should lead us to greater understanding. I performed experiments to collect data for improving the model in consideration of this feedback. Unfortunately, I could not test the model predictions in this thesis. In this chapter, I report synaptic plasticity experiments with cell identification, and the data collected for modeling.

2.2 Materials and Methods

2.2.1 Brain slice preparation

Acute coronal corticostriatal slices (300 μm) were prepared from p21-25 Drd1a-eGFP or Drd2-eGFP Swiss Webster mice [84]. Mice were obtained from the Gensat project, USA.

The mice were anesthetized with isoflurane (Abbott) and decapitated. Brains were rapidly removed and sectioned in oxygenated, ice-cold, artificial cerebrospinal fluid (aCSF) without calcium using a Leica VT1000S vibratome (Leica Microsystems). The aCSF contained the following (in mM): 126 NaCl, 2.5 KCl, 1.3 $MgCl_2$, 26 $NaHCO_3$. Unless otherwise noted, all chemicals and reagents were obtained from Nacalai Tesque.

The slices were transferred to a holding chamber where they were incubated in aCSF contained the following (in mM): 126 NaCl, 2.5 KCl, 2.5 $CaCl_2$, 1.3 $MgCl_2$, 26 $NaHCO_3$ for 1 h, after which they were stored at room temperature until whole-cell recording experiments (1-5 h). The external aCSF solutions were gassed with 95% O2/5% CO2 at all times. Solutions were made with Millipore Milli-Q water.

The Okinawa Institute of Science and Technology Animal Research Committee approved the study,

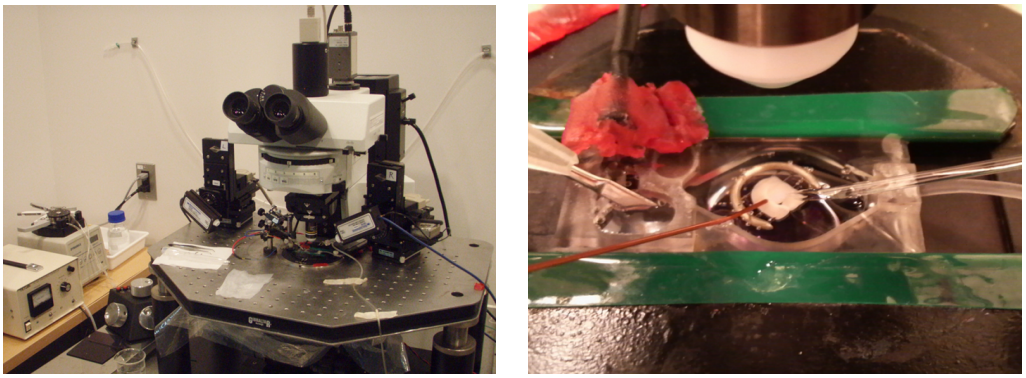

Figure 2.1. Devices. (Left) Microscope and other devices. (Right) slice set in microscope. The right electrode is the recording electrode and the left electrode is the stimulation electrode.

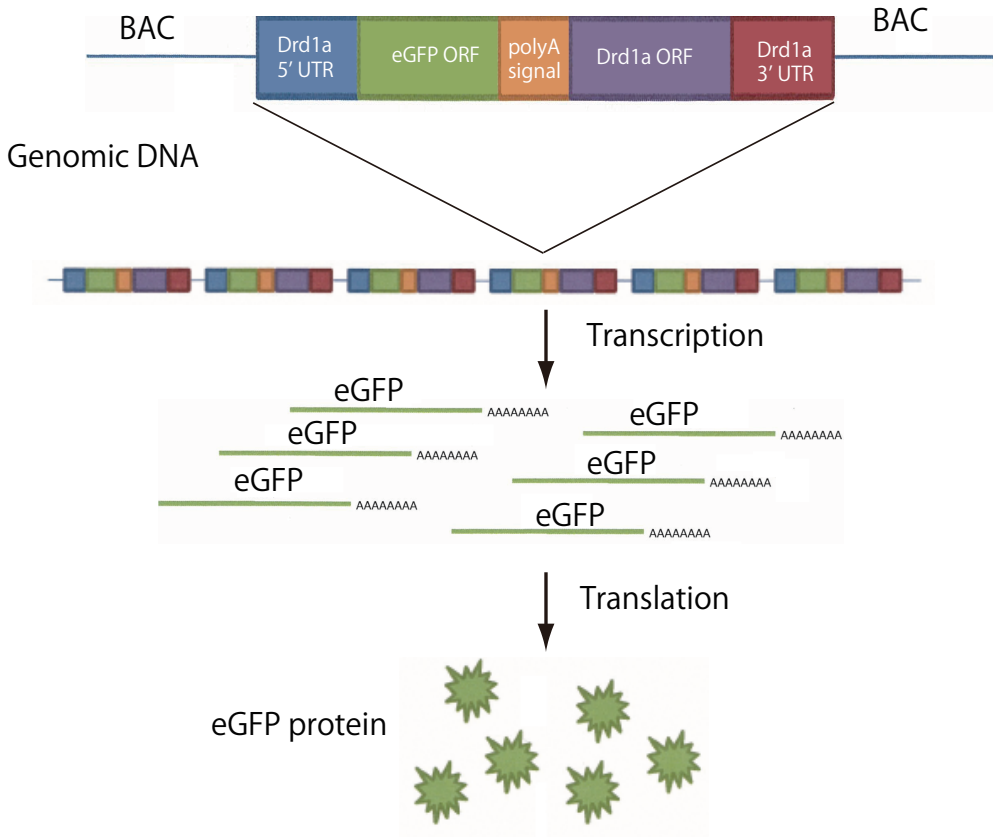

Figure 2.2. DR transgenic mice. The eGFP gene was inserted into the mouse dopamine receptor gene using Bacterial Artificial Chromosomes (BAC). For Drd1a, the eGFP mRNA was inserted in the Drd1a promoter and terminated at the polyA signal. The coding region of Drd1a is not transcribed. Drd1a mice have approximately six copies of the transgene per allele. The expression of eGFP is controlled by the dopamine receptor promoter (Drd1a or Drd2).
[83, 84]

2.2.2 Electrophysiological recordings

D1 (Drd1a-eGFP) or D2 (Drd2-eGFP) receptor-expressing MSNs in 300 μm-thick corticostriatal slices were identified by somatic eGFP excited fluorescence using an Olympus BX51WI microscope. A infra-red differential interference contrast (IR-DIC) was used to provide a bright-field transmission image. The green GFP signals (490-560 nm) were acquired using mercury lamp (USH-103OL, Olym-

pus) and a camera (JK-TU53H, TOSHIBA or MiCAM02, Brain Vision). During recordings, external aCSF was pumped using a Rainin peristaltic pump (model RP-10) and a PC-20A (K.T. labs), and maintained at 37 $^{\circ}C$ (TC-344B, Warner Instruments). MSNs were patched using video microscopy with an IR filtered halogen lamp (12V100WHAL-L, Olympus), a DIC camera (C2741, Hamamatsu) and an Olympus LUMPlanFL 40x/0.8 NA water-immersion objective. Patch electrodes were made by pulling GC150F-7.5 glass (HARVARD Apparatus) on a P-97 Flaming/Brown micropipette puller (Sutter Instrument). The pipette solution contained the following (in mM): 132 K glucose (Sigma/RBI), 6 KCl, 8 NaCl, 10 HEPES(Sigma/RBI), 2 MgATP(Sigma/RBI), 0.4 NaGTA(Sigma/RBI) and 0.5 EGTA(Sigma/RBI), pH % 7.2-7.3 with KOH(Sigma/RBI), 300 mOsm/L. In calcium imaging experiments, Alexa 594 or Oregon Green BAPTA 1, 2 or 6F were added to the pipette solution (These reagents were obtained from Invitrogen). Biocytin (Invitrogen) was added to the pipette solution to trace cell morphology.

All experiments were performed on a Burleigh Gibraltar stage. Patch electrodes were controlled using an MP-285 micromanipulator (SUTTER Instrument). As measured in the recording bath, the pipette resistance was $4 - 8$ MΩ. High-resistance (> 1 GΩ) seals were formed in the voltage-clamp mode on somata. After patch rupture, the series resistance decreased to $10 - 15$ MΩ.

To evoke EPSPs, cortical stimulation was evoked using a stimulating electrode, 0.195 mm diameter tungsten concentric electrodes (WE3CEA5, Microprobe), placed on the corpus callosum using a micromanipulator (M-44 Narishige). Stimulating intensity and duration were controlled using a Digitimer current stimulator (model DS3)

Signals (voltage and current) were amplified with a Multiclamp 700B (Molecular Devices) with CV-7B headstages (Molecular Devices) and sampled online with the use of a Digidata 1440A interface (Molecular Devices) connected to a personal computer. Acquisition and subsequent analysis of the acquired data were performed with the Clampex suite software 10 (Molecular Devices). Data were analyzed offline and is displayed here using MATLAB software. The resting membrane potentials were the potentials recorded in current clamp without any holding current after whole-cell recordings were established

After a stable baseline was established for at least 10 minutes, 6×100 Hz cortical stimulation was paired with supra-spike threshold depolarization of the postsynaptic cell. Postsynaptic high frequency stimulation responses were then monitored for at least 20 minutes.

In Mg-free experiments, I used magnesium-free aCSF containing the following (in mM): 126 NaCl, 2.5 KCl, 2.8 $CaCl_2$, 26 $NaHCO_3$.

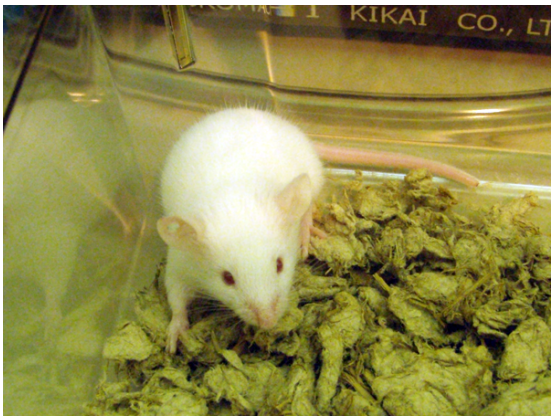

Figure 2.3. DR transgenic mouse. Original strain was Swiss Webster. I used only p21-25 male mice.

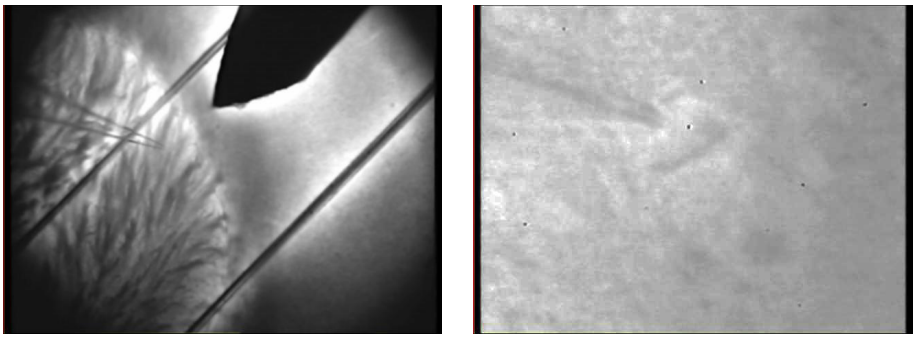

Figure 2.4. Appearance of striatum. Left figure is an image through a 10× objective and a magnification changer. The stimulation electrode was placed using this objective. Right figure is an image through a 40× objective and a magnification changer. Patch clamp was done using this objective.

2.2.3 Cell morphology tracing

I used an immunohistochemical method to obtain morphological images. A neuron was filled with biocytin (Invitrogen) through the patch pipette. The slice was fixed using 4 % w/v formaldehyde (Sigma/RBI) The biocytin has high binding affinity for streptavidin and was visualized using streptavidin conjugated Alexa 488 (Invitrogen).

Slices were not re-sectioned. For three-dimensional morphological reconstructions, the Neurolucida system (MicroBrightField) was used in conjunction with an Olympus disk scanning unit (DSU) confocal system which includes an Olympus BX51 microscope, a UPlanSApo 60x(1.35 numerical aperture (NA), oil) objectives and a DSU device (BX-DSU, Olympus). Alexa 488 was excited by mercury light (USH-103OL, Olympus) and a stack of 141 digital images were taken at 1 μm intervals using a cooled CCD camera (C9100, Hamamatsu) attached to a dedicated PC. Morphological measurements of dendrites including thickness and length with spines were made manually offline.

2.3 Identification of Medium Spiny Neurons

D1R and D2R transgenic mice were used to identify MSN cell-types. In Drd1a transgenic mice, eGFP is expressed only in D1R expressing cells. In contrast, in Drd2 transgenic mice eGFP is expressed only in D2Rs expressing cells. The eGFP was excited by blue light from a mercury lamp. The appearance of eGFP is shown in Fig. 2.5. I could see several bright green areas, which indicate the soma of D1R or D2R positive cells. eGFP fluorescence in D1R transgenic mice was darker than that in D2R transgenic mice. By comparing these fluorescence images with IR images, I identified D1Ns or D2Ns. eGFP negative cells could not be identified because half of the neurons, which should have had fluorescence, lacked fluorescence in transgenic mice [207]. In all whole cell recordings, the identity of cell types was confirmed.

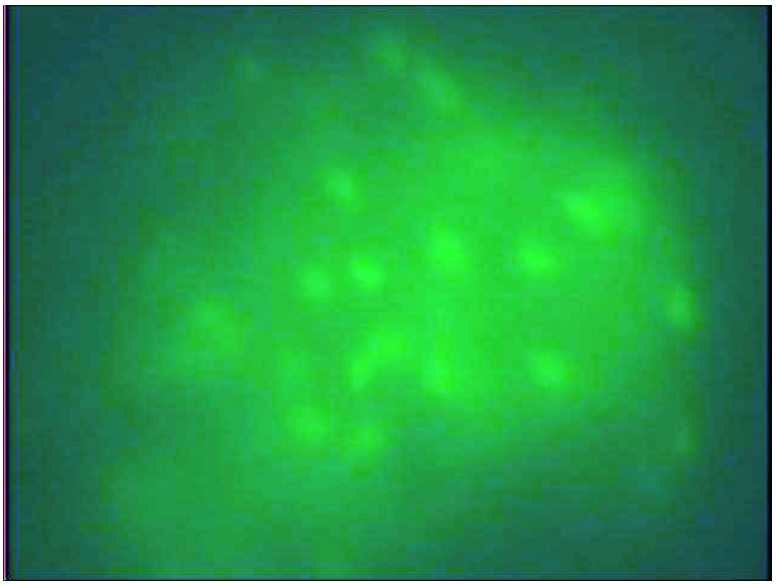

Figure 2.5. GFP imaging. Green bright areas are eGFP fluorescence from Drd2 transgenic mice. Thus, the green areas indicate somas of D2R positive cells. eGFP is excited by blue light and the emission light is green.

2.4 Synaptic Plasticity in D1Ns and D2Ns

Next, I investigated the dependence of synaptic plasticity on cell type. Most recordings were done in the dorsal striatum. After a stable baseline was established for at least 10 minutes, 6 trains of 1 second 100 Hz cortical stimulation was paired with 1 second supra-spike threshold depolarization of the postsynaptic cell. Post high frequency stimulation responses were then monitored for at least 20 minutes. EPSPs were measured three times a minute at 20 second intervals. During recordings, input resistance and resting potential were also checked. Current-voltage (IV) characteristics (voltage responses to current steps from -0.3 nA to 0.24 nA at intervals of 0.04 nA) were measured before and after conditioning. Neurons, in which input resistance or resting potential or IV characteristics changed during recording were removed from analysis. Input resistance was a ratio of voltage response to 50 pA hyperpolarizing current.

2.4.1 Synaptic plasticity experiment

Synaptic plasticity was investigated in eGFP positive and negative cells in both D1R and D2R transgenic mice. The results showed that the properties of synaptic plasticity were the same in all four cell types;(Fig. 2.8 and 2.9) some cells showed LTD, some cells showed LTP, but most cells did not show long-lasting changes (Table 2.1). On an average, D1Ns and D2Ns showed short-term potentiation, which did not last long and soon returned to baseline.

	D1p	D2p	D1n	D2n
LTP	3	2	2	1
No change	6	3	3	0
LTD	3	3	0	1

Table 2.1. The number of individual neurons showing long-term changes. D1p and D2p indicate eGFP positive neurons in Drd1a and Drd2 dopamine receptor transgenic mice, respectively. D1n and D2n indicate eGFP negative neurons in Drd1a and Drd2 dopamine receptor transgenic mice, respectively. The dopamine receptor subtype in eGFP positive neurons is known according to the transgenic line, but which dopamine receptor is expressed by eGFP negative neurons is not known. "No change" included short-term potentiation.

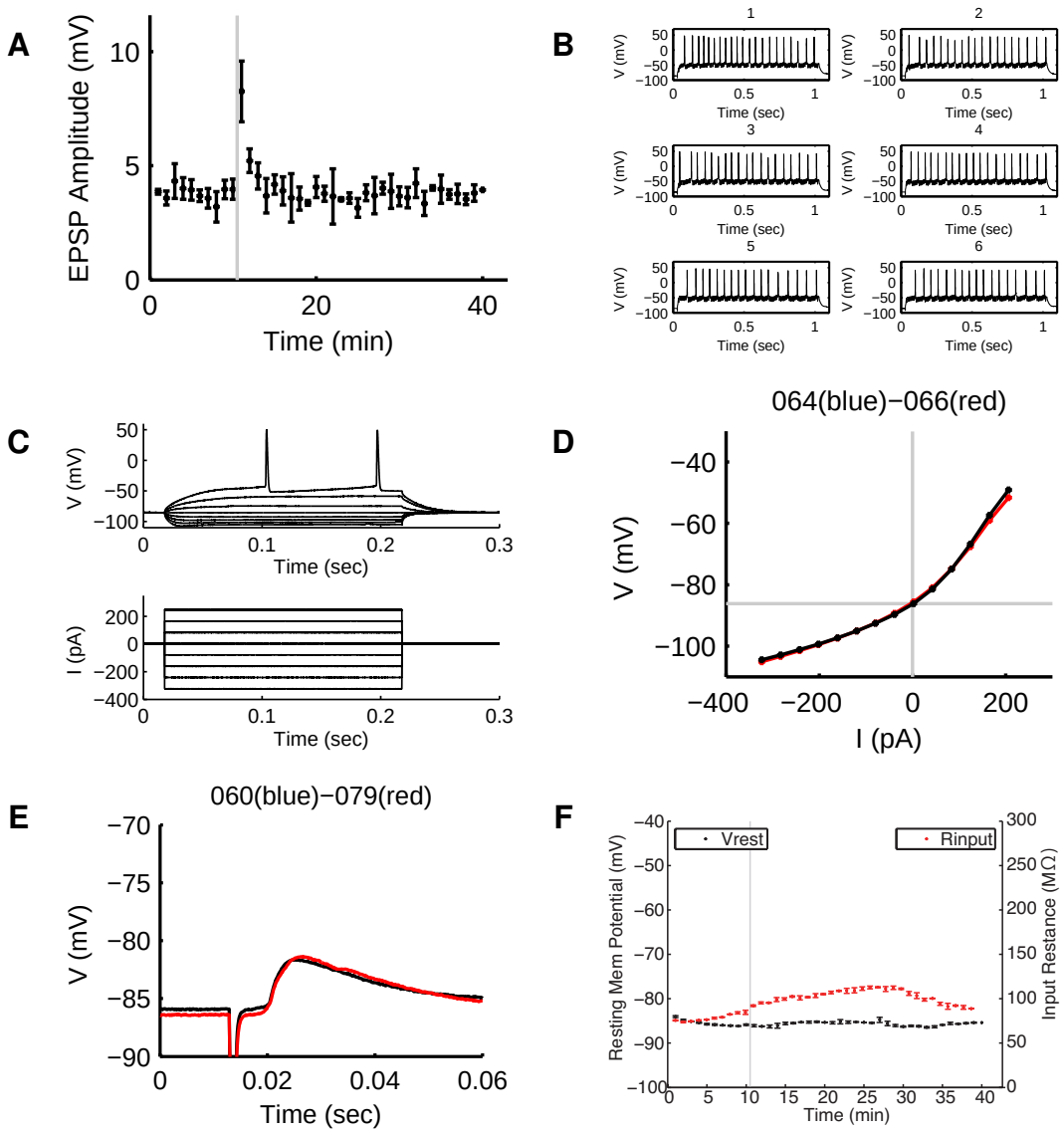

Figure 2.6. An example of synaptic plasticity in a D1N. (A) This neuron showed short-term potentiation. (B) Voltage responses to conditioning protocol. Paired simulation of cortical stimulation and postsynaptic activation were repeated 6 times. (C) Voltage responses (upper) to current steps (lower). The cell showed the property of medium spiny neurons: small responses to hyperpolarizing current, small after-hyperpolarization, and deep resting potential. (D) IV curve from voltage responses to current steps in panel (C). IV curves before (black) and after (red) conditioning were overlapped. (E) Samples of EPSPs before (black) and after (red) conditioning. (F) Input resistances (red) and resting potentials (black) were measured at 0.05 Hz.

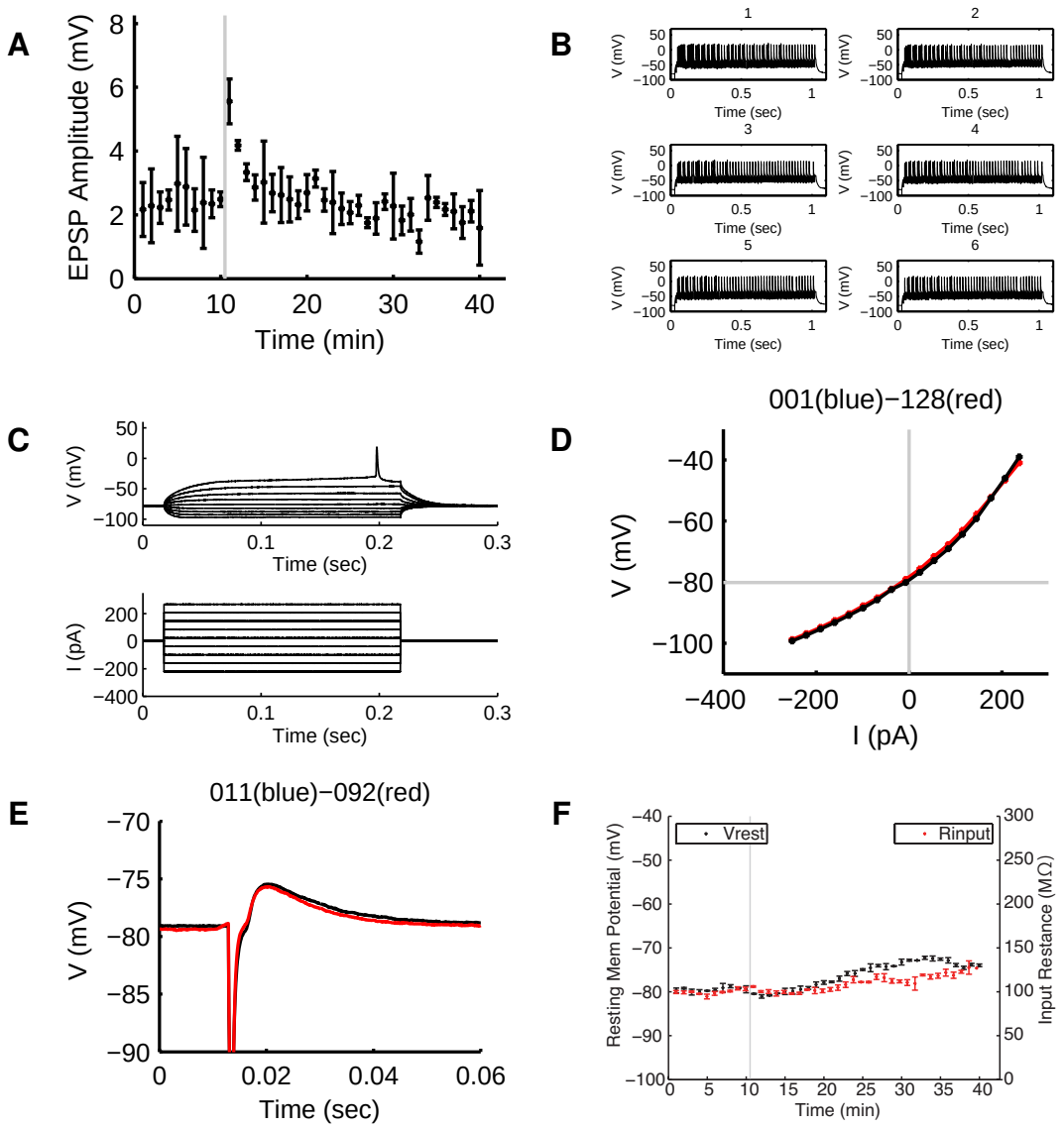

Figure 2.7. An example of synaptic plasticity in a D2N. (A) Change in EPSPs before and after conditioning. (B) Voltage responses to conditioning protocol. Paired simulation of cortical stimulation and postsynaptic activation were repeated 6 times. (C) Voltage responses (upper) to current steps (lower). The cell showed the property of medium spiny neurons: small responses to hyperpolarizing current, small after-hyperpolarization, and deep resting potential. (D) IV curve from voltage responses to current steps in panel (C). IV curves before (black) and after (red) conditioning were overlapped. (E) Samples of EPSPs before (black) and after (red) conditioning. (F) Input resistances (red) and resting potentials (black) were measured at 0.05 Hz.

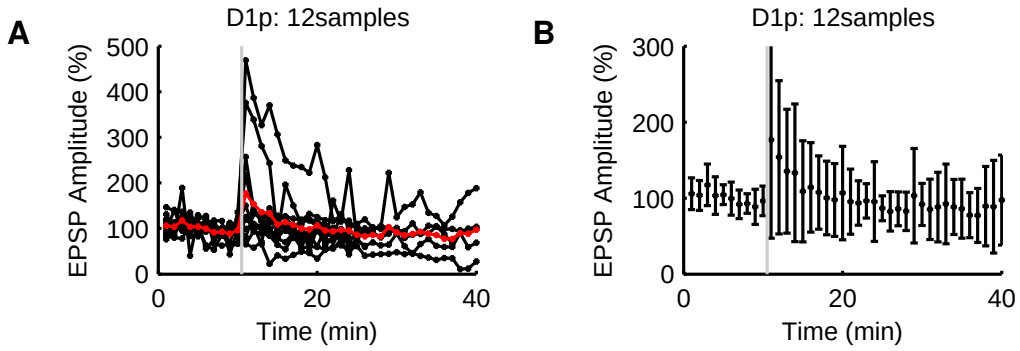

Figure 2.8. Synaptic plasticity in Drd1a eGFP positive neurons. (A) Sample paths of changes in EPSPs. (B) Average and standard deviation of EPSPs.

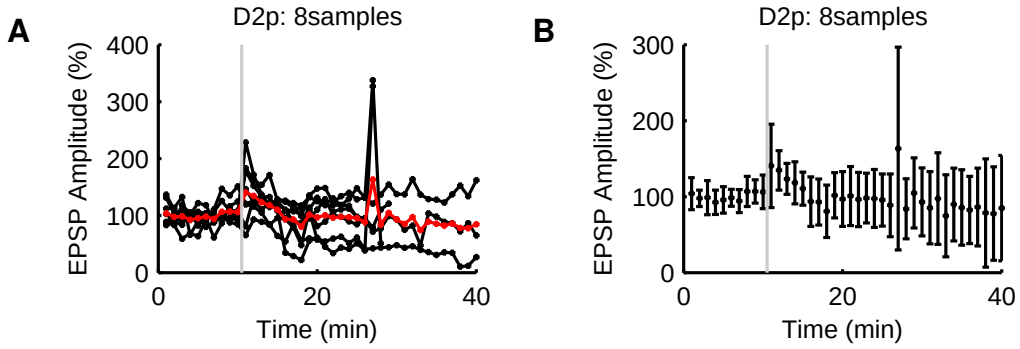

Figure 2.9. Synaptic plasticity in Drd2 eGFP positive neurons. (A) Sample paths of changes in EPSPs. (B) Average and standard deviation of EPSPs.

	D1p	D2p
LTP	3	3
No change	2	2
LTD	0	0

Table 2.2. The number of individual neurons showing long-term changes in magnesium free solution. D1p and D2p indicate eGFP positive neurons in Drd1a and Drd2 dopamine receptor transgenic mice respectively. eGFP positive neurons express the dopamine receptor according to the transgenic line. "No change" included short-term potentiation.

2.4.2 Synaptic plasticity in magnesium-free solution

The same experiments as above were performed, except using magnesium-free aCSF. First, I tested the effect of magnesium-free conditions on EPSPs. The amplitude of EPSPs became bigger and EPSPs also became longer, because the response of NMDA receptors is longer than that of AMPA receptors. This indicated that the NMDA receptor was dominant in magnesium free conditions.

Next, changes in EPSPs by conditioning were performed in D1Ns and D2Ns in magnesium-free solution. For these recordings, slices were bathed from the beginning of the experiment. Both D1N and D2N showed LTP in magnesium-free solution (Figs. 2.13 and 2.14).

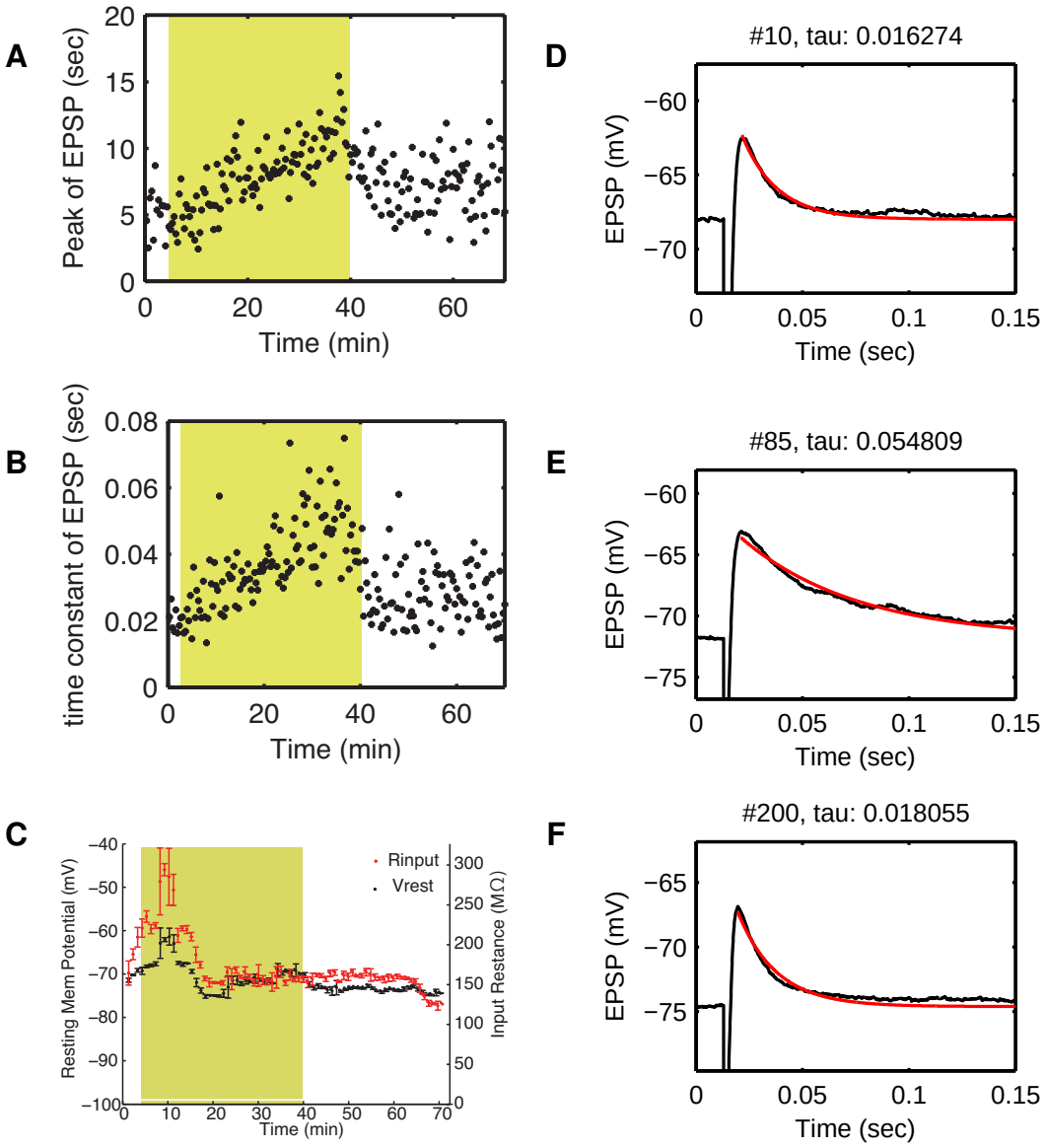

Figure 2.10. EPSPs in magnesium-free solution. Slice was bathed in magnesium-free aCSF from 5 minutes and washed by normal aCSF from 40 minutes (yellow area in (A-C)). (A) Changes in EPSP amplitude. (B) Decay constant of EPSPs. (C) Input resistances (red) and resting potentials (black). (D-F) Examples of EPSP (D) before, (E) during, and (F) after bath application of magnesium-free solution.

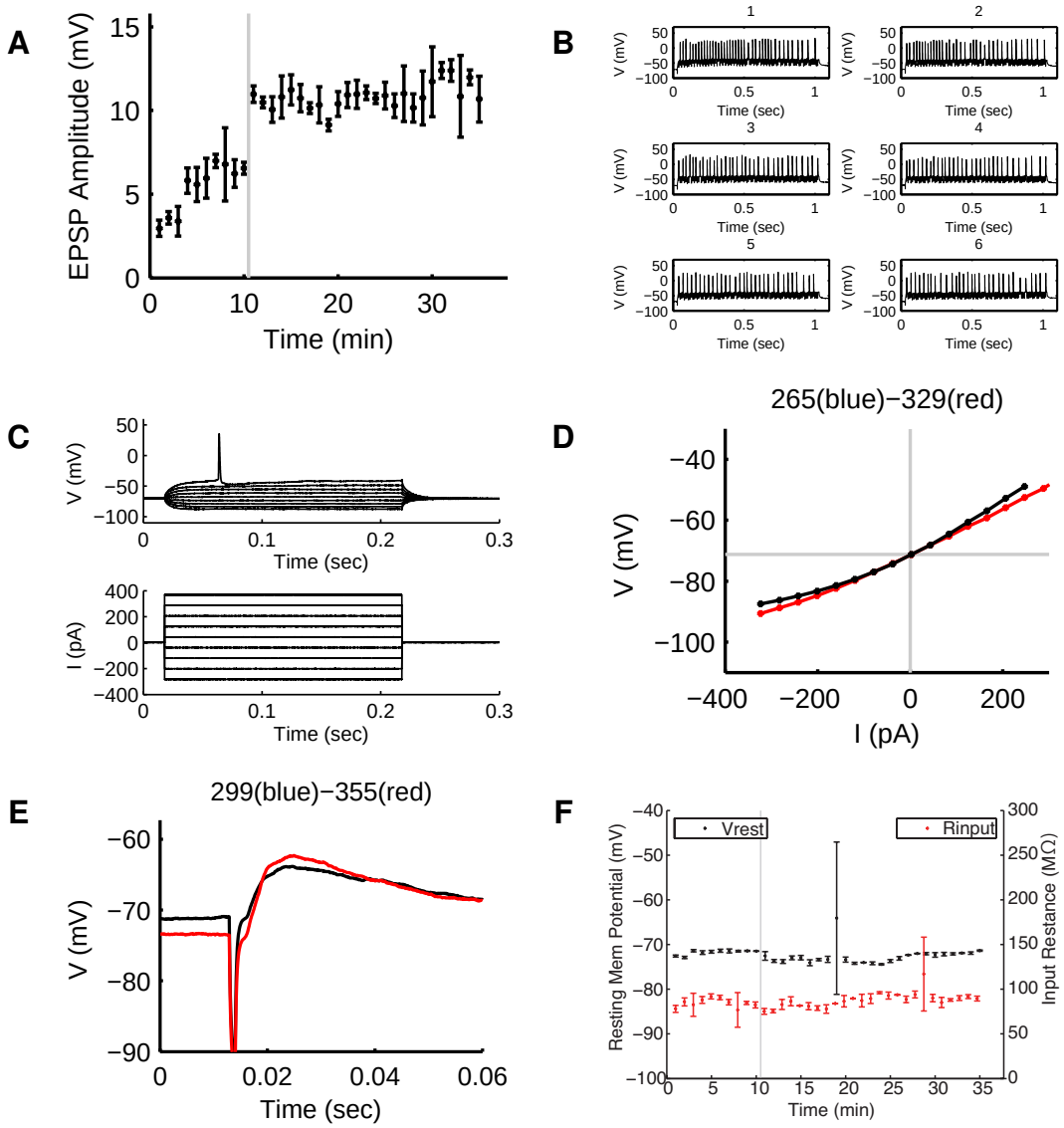

Figure 2.11. An example of synaptic plasticity in a D1N in magnesium-free solution. (A) Change in EPSPs before and after conditioning. (B) Voltage responses to conditioning protocol. Paired simulation of cortical stimulation and postsynaptic activation were repeated 6 times. (C) Voltage responses (upper) to current steps (lower). The cell showed the property of medium spiny neurons: small responses to hyperpolarizing current, small after-hyperpolarization, and deep resting potential. (D) IV curve from voltage responses to current steps in panel (C). IV curves before (black) and after (red) conditioning were overlapped. (E) Samples of EPSPs before (black) and after (red) conditioning. (F) Input resistances (red) and resting potentials (black).

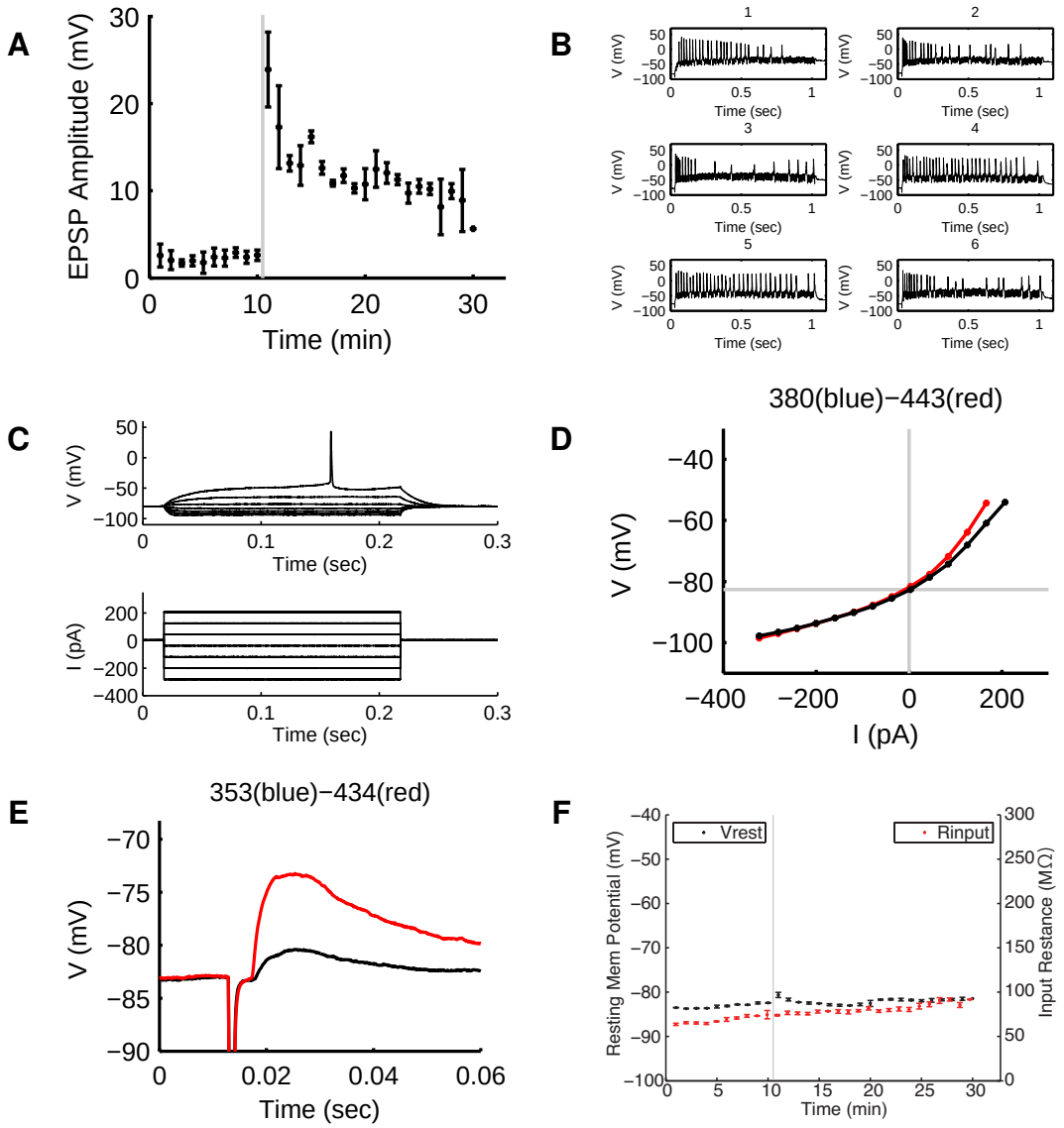

Figure 2.12. An example of synaptic plasticity in a D2N in magnesium-free solution. (A) Change in EPSPs before and after conditioning. (B) Voltage responses to conditioning protocol. Paired simulation of cortical stimulation and postsynaptic activation were repeated 6 times. (C) Voltage responses (upper) to current steps (lower). The cell showed the property of medium spiny neurons: small responses to hyperpolarizing current, small after-hyperpolarization, and deep resting potential. (D) IV curve from voltage responses to current steps in panel (C). IV curves before (black) and after (red) conditioning were overlapped. (E) Samples of EPSPs before (black) and after (red) conditioning. (F) Input resistances (red) and resting potentials (black).

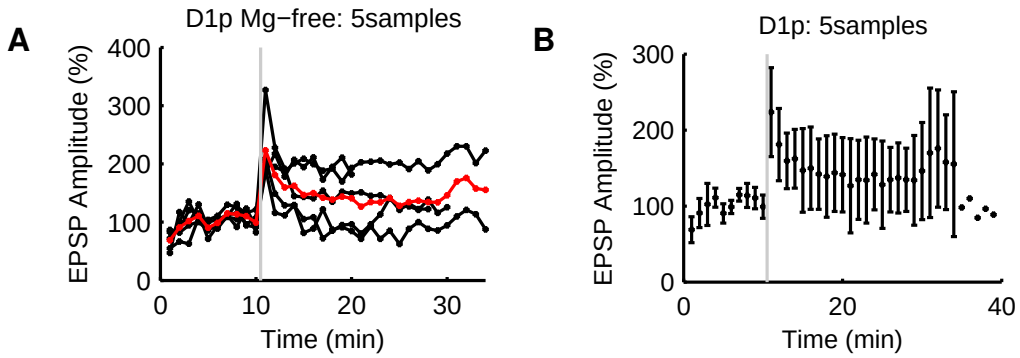

Figure 2.13. Synaptic plasticity in Drd1a eGFP positive neurons in magnesium-free solution. (A) Sample paths of changes in EPSPs. (B) Average and standard deviation of EPSPs.

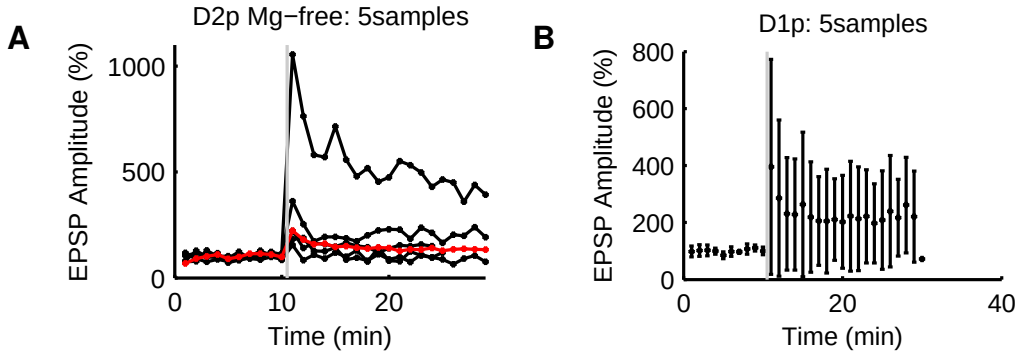

Figure 2.14. Synaptic plasticity in Drd2 eGFP positive neurons in magnesium-free solution. (A) Sample paths of changes in EPSPs. (B) Average and standard deviation of EPSPs.

2.4.3 Conclusion

No differences were observed between D1Ns and D2Ns. Both cells showed mixed changes by tetanic stimulation: LTP, LTD and no change. However, both cells showed LTP in magnesium-free solution.

2.5 Morphological Tracing

To construct a realistic dendrite model, I obtained actual cell morphology, using the same neurons that were used for the synaptic plasticity experiment. Fig. 2.15 shows samples of dendritic morphology of D1Ns. Medium spiny neurons had widespread dendrites.

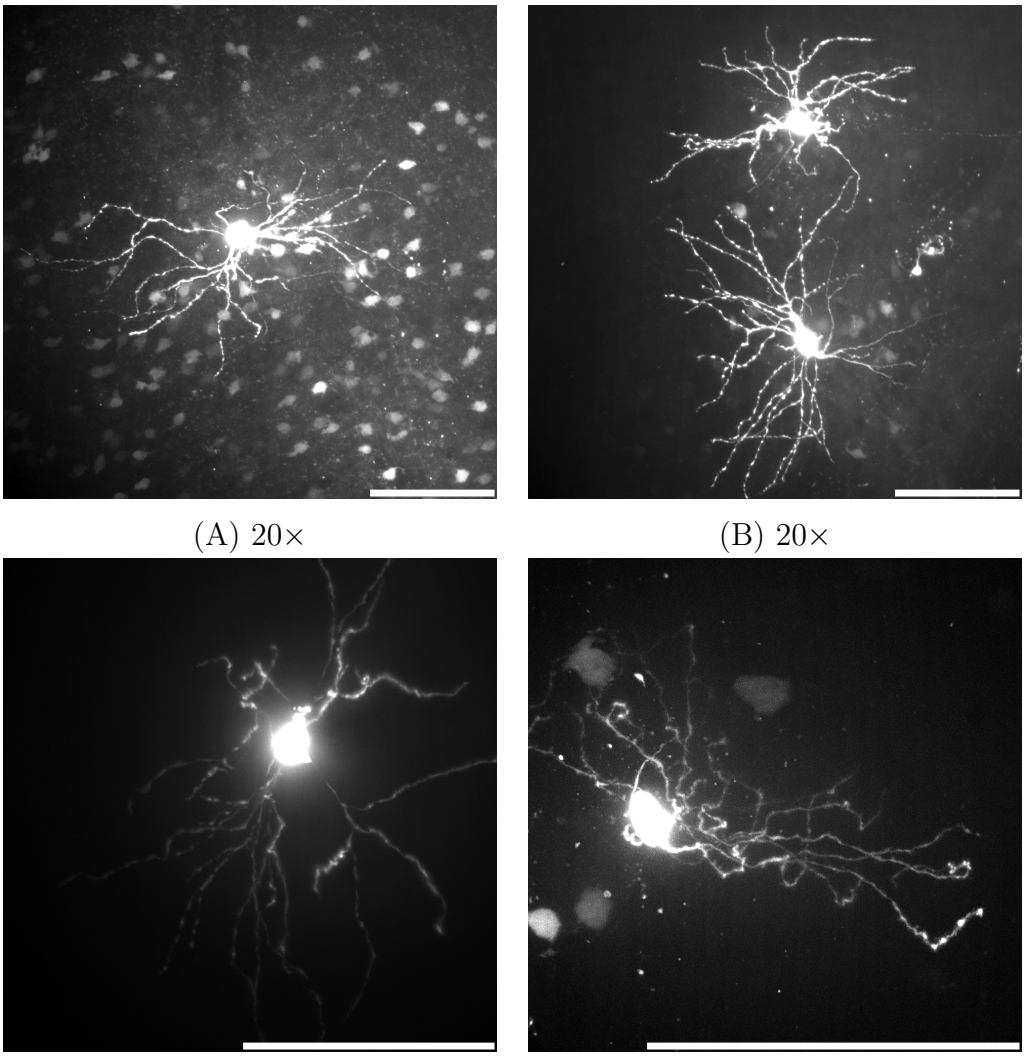

(A) 20× (B) 20×

(C) 40× (D) 60×

Figure 2.15. Morphology of medium spiny neuron. All cells were Drd1a eGFP positive cells. White bars indicate 100 μm. (A, B) 20×, (C) 40×, and (D) 60× objectives were used.

2.6 Discussion

2.6.1 Synaptic plasticity in D1Ns and D2Ns

Although differences between D1Ns and D2Ns have been reported using an STDP protocol [204], in this study, no difference in synaptic plasticity induced by HFS between D1N and D2N could be observed. Both LTD and LTP were observed in normal aCSF, but only LTP and no change was observed in magnesium-free solution. This could be explained by the calcium level being around the threshold of LTD and LTP in normal aCSF, while the calcium level is supra-threshold in magnesium-free solution. This is consistent with the hypothesis of calcium dependent synaptic plasticity.

2.6.2 Difference between *in vivo* and *in vitro* experiments

In vivo, the membrane potential of medium spiny neurons fluctuates. This fluctuation is caused by cortical inputs. However, this was not observed in the slice preparation. The aCSF solution surrounding the slices replaced the *in vivo* extracellular fluid. A consequence of this is that the dopamine concentration was different. This is because dopamine neurons show tonic activity and the basal dopamine level would be maintained at some level. Thus, the dopamine basal level *in vitro* would be lower than that *in vivo*.

2.6.3 Morphological tracing

Here I mention the issues of neuronal tracing. In my experiment, I used fluorescent dye to visualize a dendrite. The fluorescence images were blurred, so the apparent diameter of a dendrite may be larger than it really is. This problem could possibly be resolved using 3,3'-Diaminobenzidine (DAB) staining which can be observed in bright field. There is a possibility that the fixation process caused shrinkage of the slice. Also, there is a possibility that I did not measure all dendrites and spines, because the dye may not diffuse to the dendrites widely.

3. Electric Compartment Model

3.1 Introduction

STDP in the striatum is controversial, as I have discussed in Section 1.2.3. Glutamate release preceding a postsynaptic spike induced LTP, and glutamate release following a postsynaptic spike induced LTD [185, 204], which is similar to STDP in other brain areas (normal STDP). However, the converse has also been reported; glutamate release preceding a postsynaptic spike induced LTD, and glutamate release following a postsynaptic spike induced LTD [66], which is a reversed timing window compared with other areas (reversed STDP). Although the literature [185, 204] suggested that the activation of D1 receptors was necessary to induce both LTD and LTP, the timing effect of dopamine input on STDP was still unresolved. In addition, these STDP studies used different post-synaptic pulse durations: 30 ms [66], 2 ms [185] and 5 ms [204]. This may be a possible cause of the conflict between the reports of [185, 204] and [66].

The dynamics of the calcium influx is likely to be an important factor in the mechanisms behind STDP in corticostriatal synapses. It has been shown in cortical and hippocampal neurons that there is a threshold level of calcium ion influx into the postsynaptic spines, which determines whether a synapse is potentiated or depressed [5, 99, 150, 245]. Synaptic efficacy is unaffected with no calcium influx, depressed by an intermediate level of calcium elevation, and potentiated with a large increase in calcium levels. However, the detailed relationship between calcium and synaptic efficacy was unclear. Although it was thought that the peak value of calcium transient controlled the magnitude of synaptic plasticity, an uncaging study in the cerebellum have reported leaky integration of calcium was a better approximation of the magnitude of synaptic plasticity than the calcium peak. However the leaky integration of calcium was performed by a positive feedback loop in the cerebellum and there was no signaling cascade corresponding to the loop.

Moreover, the membrane potential on medium spiny neurons exhibited spontaneous oscillations between the up-state and down-state, which is related to synaptic plasticity [45]. However, *in vitro* experiments cannot reproduce these oscillations. In addition, it is difficult to experimentally test these various condi-

tions. In particular, to investigate three timing variables: glutamate, dopamine, and postsynaptic action potential. This would require a lot of time, funding, and hard work.

STDP depends on the synapse location on the dendrite [127]. To consider this dendritic effect precisely, we have to consider with actual dendritic morphology.

In this study, I constructed a multi-compartmental model using a morphologically realistic striatal neuron. To give predictions of the electrophysiological mechanisms of dopamine related STDP in the striatum and how the timing of cortical input, dopamine input, and postsynaptic spiking affect calcium influx, I ran the simulation using timed inputs of dopamine, glutamate, and postsynaptic spike, while mimicking the states of the oscillation.

3.2 Methods

3.2.1 Morphological modeling

The electric compartment model was constructed with realistic morphology based on my measurements from actual medium spiny neurons. This allowed us to precisely evaluate the effect of back-propagating action potentials.

To obtain morphological images, acute corticostriatal slices (300 μm thickness) were prepared from p21-25 Drd1a eGFP Swiss Webster mice [84]. A neuron was filled with biocytin through the patch pipette and was tagged with Alexa 488 after the whole cell recording. A 3D morphological image (Fig. 3.1) was obtained using the Neurolucida neuronal tracing system with a DSU confocal microscope. Cell morphology was manually traced using Neurolucida. The traced data included information about the lengths and diameters of the dendrites [112] (see detail in Section 2.2.3). The traced data were converted to NEURON hoc files using NLMorphologyViewer/NLMorphologyConverter software (neuronland.org). In this process, all spines were ignored.

I added two spines of diameter 1 μm and length 1.273 μm, giving a volume of 10^{-18} m^3, to proximal and distal dendrites 25 μm and 100 μm away from the soma, respectively, to measure the calcium transient in the different spines (see arrows in Fig. 3.1). Although most dendritic spines were ignored, the effect of the presence of spines can be mimicked by decreasing membrane potential R_m

(which is the reciprocal of the passive capacitance $G_{pas} = 1.7 \times 10^{-5}$ Scm^{-2}) and increasing membrane capacitance $C_m = 1$ μFcm^2, according to the membrane area increase caused by the spines [115, 137]. The channel density on the spines was set at the same density as that on the dendrite where the spine was located.

$$F = \frac{A_{dend}+A_{spine}}{A_{dend}}, \tag{3.1}$$

$$R'_m = R_m/F, \qquad C'_m = C_m F, \tag{3.2}$$

where A_{dend} and A_{spine} are the area of dendrites and spines, respectively.

The F value used in the model is shown in Table 3.1. The value was different depending on the area of the dendrite.

	Soma and proximal	Mid	Distal
F	1	1.3	3

Table 3.1. F value.

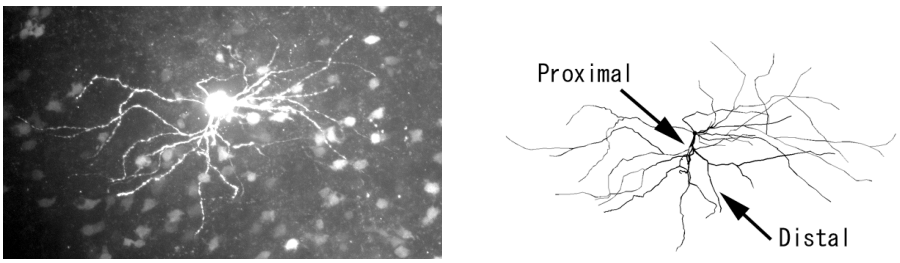

Figure 3.1. Morphology of a D1-type dopamine receptor-expressing medium spiny neuron. Left: a medium spiny neuron was filled with the fluorescent dye Alexa 488 and observed using a DSU confocal microscope. Right: morphological data imported into the NEURON simulator. The arrows heads indicate the proximal and distal dendrites described in the results section.

3.2.2 Multi-compartment model

Real dendrites have a continuous variable along with dendrite. To model the neuron, it was split into separate small compartments that could be treated as

isolated elements to approximate the continuous variable. The membrane potential of the jth compartment was represented as,

$$\begin{aligned} C_m \frac{dV_{m,j}}{dt} &= -I_{leak,j} - I_{syn,j} - I_{chan_j} - I_{stim_j} \\ &\quad + g_{j-1,j}(V_{j-1} - V_j) - g_{j,j+1}(V_j - V_{j+1}). \end{aligned} \tag{3.3}$$

$I_{leak,j}$ is a leak current through passive channels of the jth compartment and is represented by $I_{leak,j} = g_{leak,j}(V_{m,j} - E_{leak,j})$, where $g_{leak,j}$ is transmembrane conductance, $V_{m,j}$ is membrane potential, and $E_{leak,j}$ is fixed reversal potential of the passive channel. $I_{chan,j}$ and $I_{syn,j}$ are ionic currents through active channels and synaptic channels in the jth compartment, respectively, which are described in detail in Section 3.2.3. There are also membrane currents from neighbor compartments with axial conductance (Fig. reffig:compartmentmodel).

Spatial discretization of model neurons was done automatically according to the d_lambda rule [112].

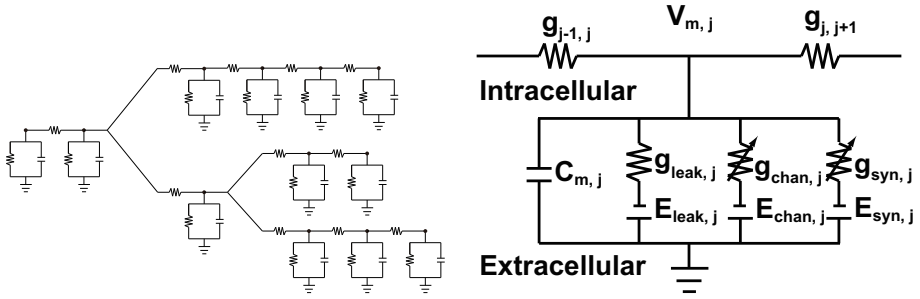

Figure 3.2. Equivalent circuit for a compartment model. Each compartment had several membrane elements. $C_{m,j}$ is the membrane capacitance of the compartment. $V_{m,j}$ is the membrane potential. $g_{j,j+1}$ is the axial conductance between the (j-1)th and the j th compartment. $g_{leak,j}$ is a constant conductance, in series with a constant battery E_{leak} through which the passive ionic current flow. $g_{chan,j}$ and $g_{syn,j}$ are conductances which are in series with a battery E whose value is the equilibrium potential of each component. $E_{chan,j}$ is the abstraction battery of reversal potential for channels, which is defined for all types of channel. $E_{syn,j}$ is synaptic reversal potential.

3.2.3 Ionic currents

My model had two types of sodium channels: fast (NaF) and persistent (NaP), and six different potassium channels: inwardly rectifying (KIR), slow A-type (KAs), fast A-type (KAf), 4-AP resistant persistent (KRP), small conductance calcium dependent (SK), and large-conductance calcium dependent (BK), and six calcium currents: N- (CaN), Q- (CaQ), R- (CaR), T- (CaT), Cav1.2 [high-voltage activated (HVA)] L- (CaL) and Cav1.3 [low-voltage activated (LVA)] (CaL13) types [38]. These channels were based on Wolf's model [238].

$$\begin{aligned} I_{NaChan} &= I_{\mathrm{NaF}} + I_{\mathrm{NaP}} \\ I_{KChan} &= I_{\mathrm{Kir}} + I_{\mathrm{KAs}} + I_{\mathrm{KAf}} + I_{\mathrm{KRP}} + I_{\mathrm{SK}} + I_{\mathrm{BK}} \\ I_{CaChan} &= I_{\mathrm{CaN}} + I_{\mathrm{CaQ}} + I_{\mathrm{CaR}} + I_{\mathrm{CaT}} + I_{\mathrm{CaL1.2}} + I_{\mathrm{CaL1.3}} \end{aligned} \tag{3.4}$$

In general, sodium and potassium channel currents are determined by

$$I(t,V) = g(t,V)(V - E_{rev}). \tag{3.5}$$

Here, E_{rev} is the reversal potential and $g(t,V)$ is

$$g(t,V) = g_{\max} m^M h^H, \tag{3.6}$$

where, the parameters m and h are the activation and inactivation state of the channel, which is given by,

$$\frac{dm}{dt} = \frac{m_\infty - m}{\tau_m}, \tag{3.7}$$

$$\frac{dh}{dt} = \frac{h_\infty - h}{\tau_h}, \tag{3.8}$$

$$\tag{3.9}$$

where,

$$m_\infty = \frac{1}{1 + \exp((V_m - V_{half,m})/V_{slope,m})}, \tag{3.10}$$

$$h_\infty = \frac{1}{1 + \exp((V_m - V_{half,h})/V_{slope,h})}. \tag{3.11}$$

Some currents (K_{AP}, K_{RP}, CaN and CaL1.2) are described as partially inactivating by

$$g(t, V) = g_{\max} m^M (ah + (1 - a)). \tag{3.12}$$

Calcium currents were modeled using the Goldman-Hodgkin-Katz (GHK) equation.

$$I = P_A z^2 \frac{V_m F^2}{RT} \frac{[A^{z+}]_i - [A^{z+}]_o \exp(-zFV_m/RT)}{1 - \exp(-zFV_m/RT)} \tag{3.13}$$

where A=Ca, z=2, $T = 30\,^{\circ}$C, F=96.489 C/mol, R=8.31 J/mol-K. $P_A = P_{\max,Ca} m^M h^H$ is channel permeability to ions. m and h are given by equation 3.11.

Time constants of channels are described as:

- NaP

$$\tau_m = 0.025 + 0.14 \exp\left(\frac{v + 40}{10}\right), \qquad V_m < -40 \text{ mV} \tag{3.14}$$

$$\tau_m = 0.02 + 0.145 \exp\left(-\frac{v + 40}{10}\right), \qquad V_m \geq -40 \text{ mV} \tag{3.15}$$

- Kas

$$\tau_m = 0.378 + 9.91 \exp\left(-\left(\tfrac{v+34.3}{30.1}\right)^2\right) \tag{3.16}$$

$$\tau_h = 1097.4 \Big/ \left(\exp\left(-\tfrac{v+0.96+90}{29.01}\right) + \exp\left(\tfrac{v+0.96+90}{100}\right)\right) \tag{3.17}$$

- CaL and CaL13

$$\tau_m = 1 \Big/ \left(\frac{0.1194(v + 8.124)}{\exp\left(\frac{v+8.124}{9.005} - 1\right)} + 2.97 \exp\left(\frac{v}{31.4}\right)\right) \tag{3.18}$$

- CaN

$$\tau_m = 1 \Big/ \left(\frac{0.1157(v + 17.19)}{\exp\left(\frac{v+17.19}{15.22} - 1\right)} + 1.15 \exp\left(\frac{v}{23.82}\right)\right) \tag{3.19}$$

The model also had ionic currents through AMPA- and NMDA-type glutamate receptors and GABA receptors.

$$I_{syn} = I_{\text{AMPA}} + I_{\text{NMDA}} + I_{\text{GABA}} \tag{3.20}$$

These currents are described as,

$$I_z(t, V) = g_{\max}(h - m)(V - E_{rev}), \tag{3.21}$$

where,

$$m' = \frac{-m}{\tau_{rise}}, \tag{3.22}$$

$$h' = \frac{-h}{\tau_{decay}}. \tag{3.23}$$

The NMDAR current was modified to account for voltage dependent magnesium blockade by multiplying equation 3.21 by a factor B (Fig. 3.3), where

$$B(V_m) = 1 \Big/ \left(1 + \frac{[Mg^{2+}]_o}{3.57 \text{ mM}} \exp(-V_m \cdot 0.062 \text{ mV}^{-1})\right). \tag{3.24}$$

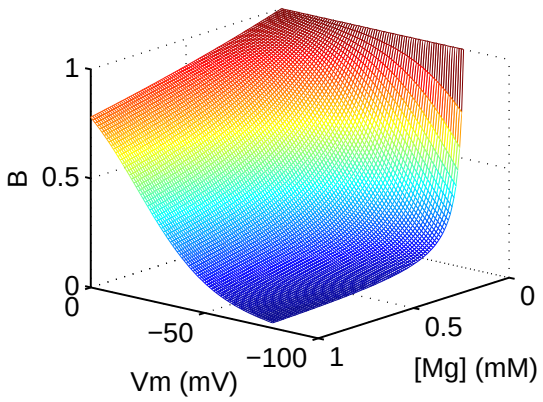

Figure 3.3. Magnesium block.

I adjusted the conductance parameters to fit my experimental data using Neurofitter [74]. The parameters used in the model are listed in Tables 3.2, 3.3, and 3.4. I tested two different parameter settings. The difference between the two settings was the conductance of calcium channels, AMPAR and NMDAR. In this thesis, the parameter settings of CaT, AMPAR and NMDAR were the same as in [238] and was called the "original parameter setting". Parameter settings of high AMPAR and low NMDAR conductance were called the "high AMPAR/NMDAR conductance condition". Unless otherwise noted, the original parameter setting was used in this thesis.

	$g_{\max}$(S/cm2)	HH form		V_{half} (mV)	V_{Slope} (mV)
NaF	soma, 1.96	$m^3 \times h$	m	-23.9	-11.8
	dendrites, 0.0185		h	-62.9	10.7
NaP	soma, 7.36e-5	$m \times h$	m	-52.6	-4.6
	dendrite, 2.86e-7		h	-48.8	10
KAf	soma & proximal, 0.247	$m^2 \times h$	m	-10	-17.7
	middle & distal, 0.0429		h	-75.6	10
KAS	soma & proximal, 0.0129	$m^2 \times (a \times h + (1 - a))$	m	-27.0	-16
	middle & distal, 9.44e-4	a=0.996	h	-33.5	21.5
KIR	4.18e-4	m	m	-82	13
KRP	0.00730	$m \times (a \times h + (1 - a))$	m	-13.5	-11.8
		a=0.7	h	-54.7	18.6
BK KCa	0.00158				
SK KCa	0.0910				

Table 3.2. Channel parameters except calcium channels. These values were based on [238].

	$P_{\max}$(cm/s)	HH form		V_{half} (mV)	V_{Slope} (mV)
CaL1.2	1.34e-5	$m^2 \times (a \times h + (1 - a))$	m	-8.9	-6.7
	(† 6.7e-6)	a=0.17	h	-13.4	11.9
CaL1.3	1.7e-6	$m^2 \times h$	m	-33.0	-6.7
	(† 4.25e-7)		h	-13.4	11.9
CaN	2.0e-5	$m^2 \times (a \times h + (1 - a))$	m	-8.7	-7.4
	(† 1e-5)	a=0.21	h	-74.8	6.5
CaQ	1.2e-5 († 1e-5)	m^2	m	-9.0	-6.6
CaR	5.2e-5	$m^3 \times h$	m	-10.3	-6.6
	(† 2.6e-5)		h	-33.3	17
CaT	8e-7	$m^3 \times h$	m	-51.73	-6.53
	(† 1.8e-7)		h	-80	6.7

Table 3.3. Parameters of calcium channels. These values were based on [238]. I used parameters indicated by † in high AMPAR/NMDAR conductance conditions.

	$g_{\max,z}$(pS)	E_z (mV)	τ_{on} (ms)	τ_{off} (ms)
AMPAR	447 († 593)	0	1.1	5.75
NMDAR	226 († 24.6)	0	2.82	160
GABAR	435	-60	0.25	3.75

Table 3.4. Parameters of synaptic receptors. These values were based on [238]. I used $g_{\max}$ of 593 pS for AMPAR and 24.6 pS for NMDAR in high AMPAR/NMDAR conductance conditions (†).

3.2.4 Calcium dynamics

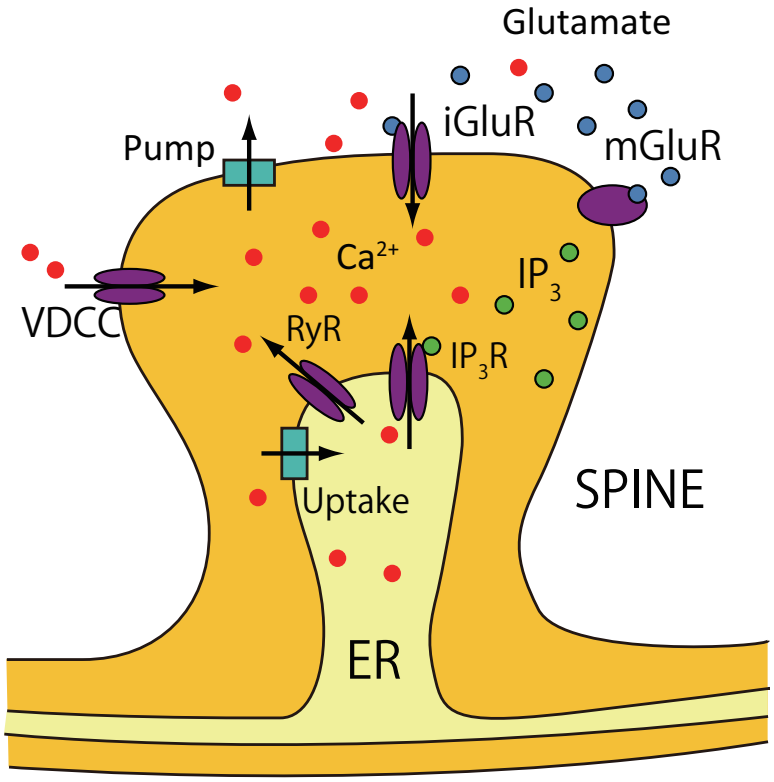

Figure 3.4. Calcium dynamics. Calcium sources are divided into two groups. One group consists of extracellular sources, and includes calcium influx from voltage-dependent calcium channels (VDCCs), from calcium permeable ionotropic glutamate receptors (iGluRs). There are two types of iGluR in my model: AMPAR and NMDAR. Calcium is also and pumped out of the cell into the extracellular matrix by calcium pumps.
The other group consists of intracellular calcium stores, in the endoplasmic reticulum (ER), which are accessed by IP_3 receptors (IP_3R), ryanodine receptors (RyR). IP_3 is produced by metabotropic glutamate receptors. Calcium uptake, mediated by Sarco/Endoplasmic Reticulum Ca^{2+}-ATPase (SERCA), and leak also occurs from the ER.

My model included several processes contributing to calcium dynamics, namely calcium influx from AMPA and NMDA-type synaptic receptors, voltage-gated

calcium channels, calcium buffer, calcium pumps, and calcium release from the intracellular calcium store (endoplasmic reticulum, ER), through ryanodine and inositol-1,4,5-triphosphate (IP_3) channels [138, 238].

The transient change in the intracellular calcium $[Ca^{2+}]_i$ was modeled as

$$\begin{aligned}\frac{d[Ca^{2+}]_i}{dt} &= k(J_{\text{CICR}} + J_{IP_3} - J_{\text{Uptake}} + J_{\text{Leak}} + J_{\text{Chan}} + J_{\text{Syn}} - J_{\text{Pump}}) \\ &\quad +([Ca^{2+}]_{inf} - [Ca^{2+}]_i)/\tau_r. \end{aligned} \tag{3.25}$$

Here, J_{CICR} is the flux caused by calcium-induced calcium release from intracellular stores. This process is mediated by a ryanodine receptor; thus, I modeled it as

$$J_{\text{CICR}} = V_{CICR}\frac{[Ca^{2+}]_i}{[Ca^{2+}]_i + K_{CICR}}([Ca^{2+}]_{ER} - [Ca^{2+}]_i]), \tag{3.26}$$

where $V_{CICR} = 3 \times 10^{-12}$ s^{-1} is the maximum rate of CICR and $K_{CICR} = 0.2$ μM.

J_{IP_3} is the flux caused by IP_3-induced calcium release from intracellular stores. $[Ca^{2+}]_{ER} = 0.20$ mM is the calcium concentration in the ER. It is known that the process has a bell-shaped steady state curve dependent on $[Ca^{2+}]_i$ with a sharp peak around 0.2 uM; thus, I modeled it as

$$J_{IP_3} = V_{IP_3} m^3 h^3 ([Ca^{2+}]_{ER} - [Ca^{2+}]_i), \tag{3.27}$$

where $V_{IP_3} = 1 \times 10^{-9}$ cm^{-2}ms^{-1} is the maximum rate of IP_3 induced release, an activation gate m and an inactivation gate h,

$$m = \frac{[IP_3]_i}{[IP_3]_i + d_{IP_3}} \frac{[Ca^{2+}]_i}{[Ca^{2+}]_i + d_{act}}, \tag{3.28}$$

$$h = \frac{d_{inh}([IP_3]_i + d_{IP_3]})}{d_{inh}([IP_3]_i + d_{IP_3}) + [Ca^{2+}]_i([IP_3]_i + d_{dis})}, \tag{3.29}$$

where $d_{IP_3} = 0.13$ μM is the dissociation constant for IP_3 binding to the uninhibited receptor, $d_{dis} = 0.94$ μM is the dissociation constant for the Ca^{2+}-inhibited receptor, $d_{act} = 8.2 \times 10^{-2}$ μM is the dissociation constant for Ca^{2+}-activation of the receptor, and $d_{inh} = 1.05$ μM is the dissociation constant for Ca^{2+}-inhibition of the receptor [138].

IP_3 was generated via G-proteins when glutamate binds to mGluRs. The transient change in the level of intracellular IP_3, $[IP_3]$ was modeled by

$$\frac{d[IP_3]_i}{dt} = \gamma t \exp(-t/\tau) - \beta([IP_3]_i - [IP_3]_{min}), \tag{3.30}$$

where $\tau = 220$ ms is the time to peak and $\gamma = 5 \times 10^{-6}$ mM/ms^2 determines the maximum amount of IP_3 production and $\beta = 0.2$ ms^{-1} is the removal rate [138].

J_{Uptake} is the calcium uptake to the endoplasmic reticulum (ER), which was modeled as

$$J_{\text{Uptake}} = V_{\text{Uptake}} \frac{[Ca^{2+}]_i^2}{K_{\text{Uptake}}^2 + [Ca^{2+}]_i^2}, \tag{3.31}$$

where $V_{\text{Uptake}} = 0.75 \times 10^{-9}$ μM/s is the maximum rate of uptake and $K_{\text{Uptake}} = 0.2$ μM is a parameter.

J_{leak} is the calcium leak from the ER, which was modeled as

$$J_{\text{Leak}} = V_{\text{Leak}}([Ca^{2+}]_{ER} - [Ca^{2+}]_i), \tag{3.32}$$

where $V_{\text{Leak}} = 6.15 \times 10^{-14}$ s^{-1} is the maximum rate of leak.

J_{Channel} and J_{Synaptic} are calcium influx through calcium channels and calcium permeable glutamate receptors respectively, which were calculated from channel or synaptic current I,

$$J_{\text{Channel}} \text{ or } J_{\text{Synaptic}} = -\frac{k * I}{z * F * d}, \tag{3.33}$$

where $F = 96489$ C is Faraday's constant, $d = 0.1$ μm is shell depth.

J_{Pump} is pumping activity to the outside of the cell,

$$J_{\text{Pump}} = -k \cdot kt \cdot [Ca^{2+}]_i / ([Ca^{2+}]_i + kd), \tag{3.34}$$

where $kt = 0.1$ μM/ms is the time constant of the pump and $kd = 0.1$ μM is the equilibrium calcium value, and parameter $k = 0.02$.

The last term in equation 3.25 is a simple diffusive or buffering process, where the diffusive term uses $\tau_r = 43$ ms and $[Ca^{2+}]_{inf} = 105$ mM [238].

3.2.5 Dopamine modulation

There are various dopamine effects on channel conductance as listed in Table 3.5. To reflect a finding of dopamine modulation, I introduced a dopamine modulation factor μ, which scaled channel currents for each current as listed in Table 3.6.

$$
\begin{aligned}
I_{NaChan} &= \mu_{\mathrm{NaF}} I_{\mathrm{NaF}} + I_{\mathrm{NaP}} \\
I_{KChan} &= \mu_{\mathrm{Kir}} I_{\mathrm{Kir}} + I_{\mathrm{KAs}} + I_{\mathrm{KAf}} + I_{\mathrm{KRP}} + I_{\mathrm{SK}} + I_{\mathrm{BK}} \qquad (3.35) \\
I_{CaChan} &= \mu_{\mathrm{CaN}} I_{\mathrm{CaN}} + \mu_{\mathrm{CaQ}} I_{\mathrm{CaQ}} + I_{\mathrm{CaR}} + I_{\mathrm{CaT}} + \mu_{\mathrm{CaL1.2}} I_{\mathrm{CaL1.2}} + I_{\mathrm{CaL1.3}} \\
I_{syn} &= I_{\mathrm{AMPA}} + \mu_{\mathrm{NMDA}} I_{\mathrm{NMDA}} + I_{\mathrm{GABA}} \qquad (3.36)
\end{aligned}
$$

μ gradually increased (or decreased) from $\mu = 1$ (corresponding to the basal dopamine level) and reached a peak ($\mu \simeq 2$), 50 milliseconds after the dopamine signal arrived (Fig. 3.5) [91].

In the case of NMDAR, the direction of dopamine modulation was positive and negative as shown in Table 3.5. Therefore, I tested two types of modulation.

	Dorsal		Ventral	
Channel	Effect	Ref.	Effect	Ref.
NaF	62.2-78%	[29, 200, 201, 217]	75%	[244]
	hV1/2 -5.6 mV			
CaQ	17-84%	[197, 215]	52%	[243]
CaN	76.5-96%	[197, 215]	20%	[243]
CaL1.2	200%	[168, 212, 215]		
	m (h?) V1/2	[215]		
KAs	80-95%	[218]	no change	[117]
	no change	[117, 169]		
Kir	125%	[182]	107%	[226, 227]
NMDAR	103-141%	[44, 67, 96, 146]	171%	[101]
	70-81%	[37, 148]		
AMPAR	121-129%	[188, 228]	44-64%	[100]
	no change	[146]		

Table 3.5. Effects of dopamine modulation. This table was adopted from [162]. % means the change of the conductance. 100 % means no change.

	mod 1	mod 2
Scaling factor: μ	max or min of μ	
μ_{NaF}	0.95	0.95
μ_{CaQ}	0.5	0.5
μ_{CaN}	0.2	0.2
$\mu_{\text{CaL1.2}}$	2	2
μ_{Kir}	1.25	1.25
μ_{NMDA}	1.3	0.7

Table 3.6. Scaling factor μ. μ values of two types of dopamine modulation: mod 1 and mod 2. These values were based on [162].

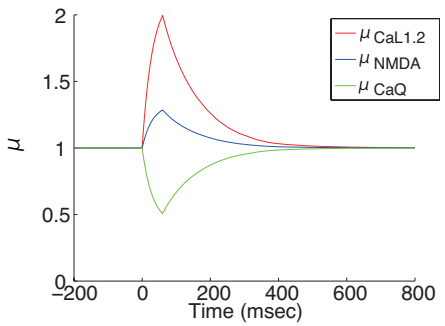

Figure 3.5. Examples of μ. Red line indicates $\mu_{CaL1.2}$. Blue line indicates μ_{NMDA}. Green line indicates μ_{CaQ} All μ show a maximum change 50 ms after dopamine input.

3.3 Results

I calibrated the model parameters to fit the electrophysiological properties of medium spiny neurons expressing D1-type dopamine receptors, which were examined by whole cell patch clamp experiments in vitro. Fig. 3.6 compares the current pulse responses of the model to those of a real neuron. The model replicated the characteristic properties of the medium spiny neurons: resting membrane potential around -85 mV, small voltage responses to hyperpolarizing current, and shallow after-hyperpolarization (AHP) after spike firing.

Using this model, I investigated the following: 1) the voltage and calcium responses of the dendrites to glutamate input and back-propagation action potentials; 2) the timing dependence of calcium response to glutamate input and postsynaptic spike; 3) the triplet interactions of glutamate input, dopamine input, and postsynaptic spike. I compared these properties at proximal and distal dendrites under different membrane potential levels, known as up-state and down-state [237]. I also tested two parameter settings, two types of dopamine modulation and two durations of current pulse injection into the soma.

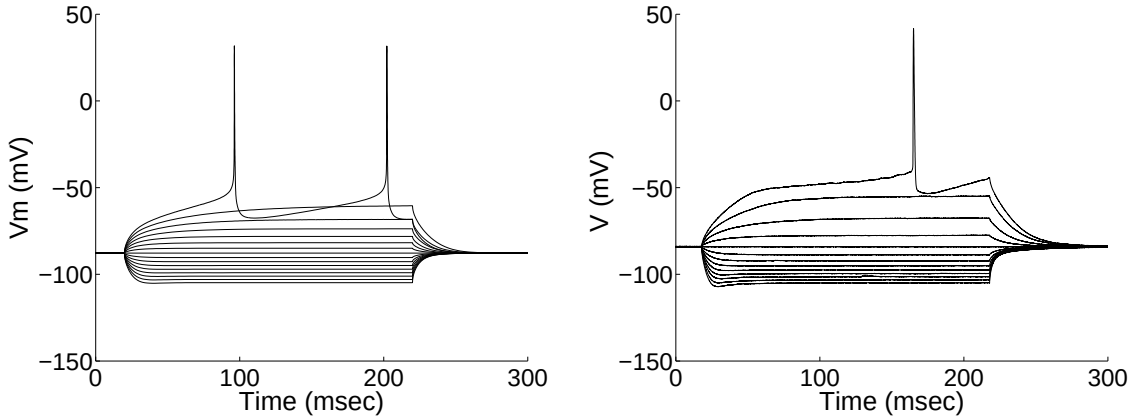

(A) Model (B) Experiment

Figure 3.6. I-V characteristics. Model and experimental responses of medium spiny neurons to current steps from -0.3 nA to 0.28 nA at intervals of 0.04 nA.

3.3.1 Voltage and calcium responses

I investigated voltage and calcium responses in dendritic spines on proximal and distal dendrites. The membrane potential of medium spiny neurons with intact cortical input fluctuates between the "down-state" at about -85 mV and the "up-state" at about -65 mV [237]. I simulated the up-state by a steady current input of 0.2 nA to the soma and the down-state by no current input.

Fig. 3.7 (A, D, G, J) shows the voltage responses (EPSPs) and calcium responses in dendritic spines to glutamatergic synaptic inputs in the original parameter setting. Unless otherwise noted, the following results were from the original parameter setting. EPSPs and calcium responses to glutamate input were the same for proximal and distal spines. The EPSPs and calcium responses were facilitated in the up-state (Figs. 3.7(A) and (D)). Fig. 3.7 (G) and (J) show the sources of calcium influx to the proximal spine during the down-state (G) and up-state (J). The increased calcium influx in the up-state was mediated by voltage-gated calcium channels and NMDA receptors as well as by calcium-dependent calcium release from the ER (compare Figs. 3.7 (G) and (J)).

Fig. 3.7 (B, E, H, K) shows the voltage and calcium responses of the proximal spine to a postsynaptic spike caused by a transient current pulse (2.5 nA, 2

msec). Again, the EPSPs and calcium responses were enhanced in the up-state (Figs. 3.7(B) and (E)), but the calcium influx, caused by the back propagating action potential (bAP), was mainly from L-type calcium channels both in the down-state and up-state (Figs. 3.7(H) and (K)). These properties held for the responses of the distal spine except that the magnitude of the bAP and the calcium flux were reduced compared with the case of the proximal spine (data not shown).

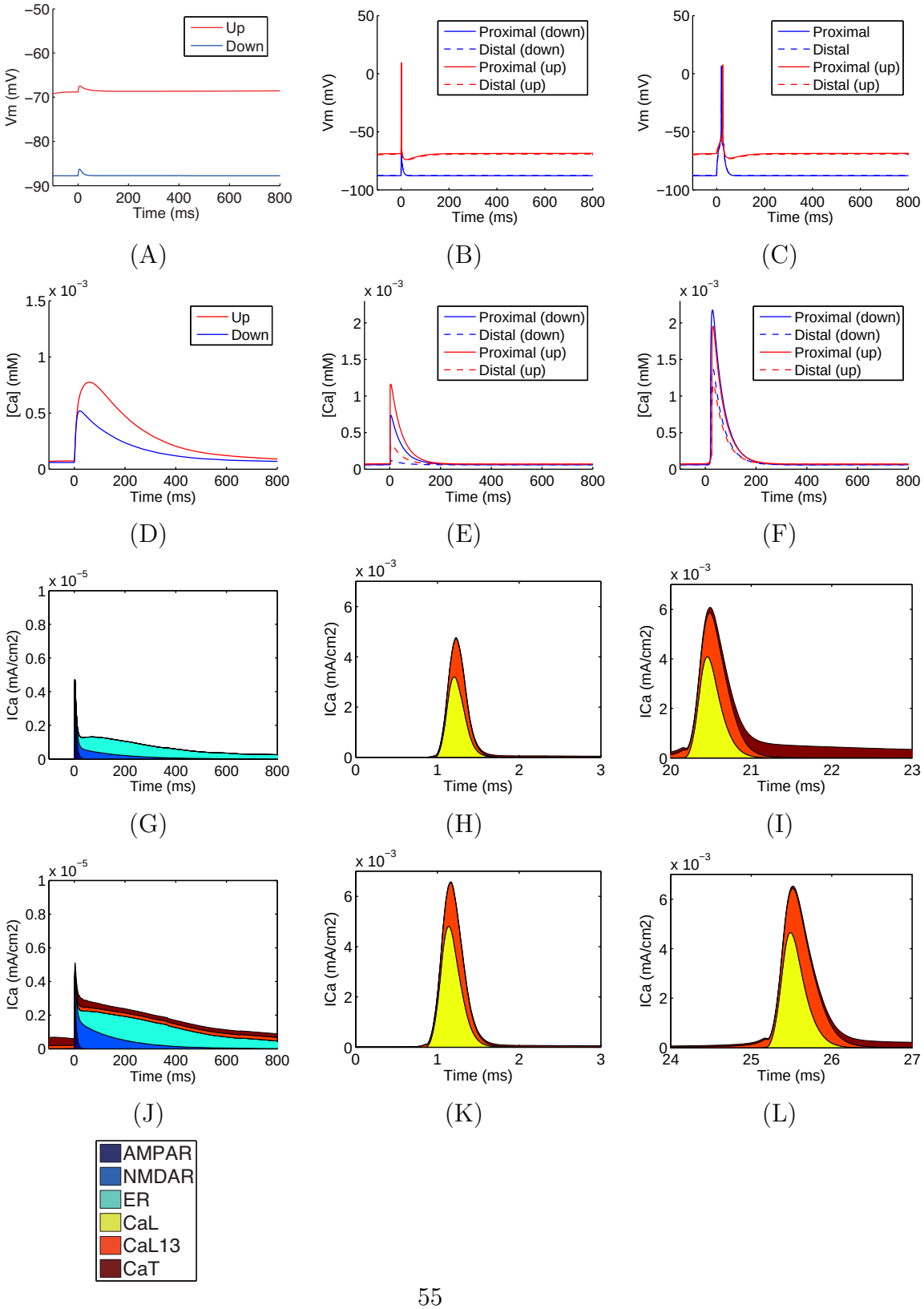
Vm (mV)
Time (ms)
Up
Down
(A)
Proximal (down)
Distal (down)
Proximal (up)
Distal (up)
(B)
Proximal
Distal
Proximal (up)
Distal (up)
(C)
[Ca] (mM)
x 10^-3
(D)
(E)
(F)
ICa (mA/cm2)
x 10^-5
x 10^-3
(G)
(H)
(I)
(J)
(K)
(L)
AMPAR
NMDAR
ER
CaL
CaL13
CaT

Figure 3.7. Voltage and calcium responses. Voltage and calcium responses of the proximal and distal dendritic spines, to glutamate input (left panels) and to 2 ms (middle panels) and 30 ms (right panels) supra threshold current pulses into the soma. Panels (A-C) show time courses of voltage and panels (D-F) show intracellular calcium concentration. The blue lines indicate down-state and the red lines indicate up-state simulated by a steady current input. The lower two rows show the distribution of sources of calcium influx to the spine in the down-state (G-I) and in the up-state (J-L). In the legends, AMPAR, NMDAR, ER, CCs, CaL, CaL13 and CaT denote calcium influx from AMPA receptors, NMDP receptors, ER, all calcium channels, L-type calcium channels (v1.2), L-type calcium channels (v1.3) and T-type calcium channels, respectively. Glutamatergic synaptic inputs were applied to the same spines in which calcium was observed.

The properties of calcium responses were compared with experimental results reported by Carter *et. al.* [34]. When I applied a wide current pulse (30 ms duration) to evoke one action potential, the calcium response in the up-state was smaller than that in the down-state (Figs. 3.7(F)), which was the opposite result evoked by a short current pulse. This result corresponds with experimental results [34]. When I blocked T-type calcium channels, the calcium transient in the up-state was larger than that in the down-state (Fig. 3.8). The calcium current through T-type calcium channels was dominant. However, T-type calcium channels were inactivated by additional current in the up-state, which caused this inversion phenomenon. Carter *et. al.* also reported that the AMPAR mediated calcium response in the down-state was larger than that in the up-state with the application of CPP (NMDAR antagonist), TTX (sodium channel blocker) and VDCC blockers. The NMDAR mediated calcium response was larger in the up-state than in the down-state, and it was smaller in the up-state than in the down-state in magnesium-free conditions in presence of NBQX (AMPAR antagonist),TTX and VDCC blockers. To test these experimental results, simulated experiments were performed under various conditions (Fig. 3.8). As a result, the properties shown in the paper by Carter *et. al.* could be accurately reproduced.

In addition, calcium spikes were observed by a step current input with the

application of 4-AP (potassium channel blocker) and TTX [177]. The model also showed calcium spike by mimicking the experimental condition (Fig. 3.9).

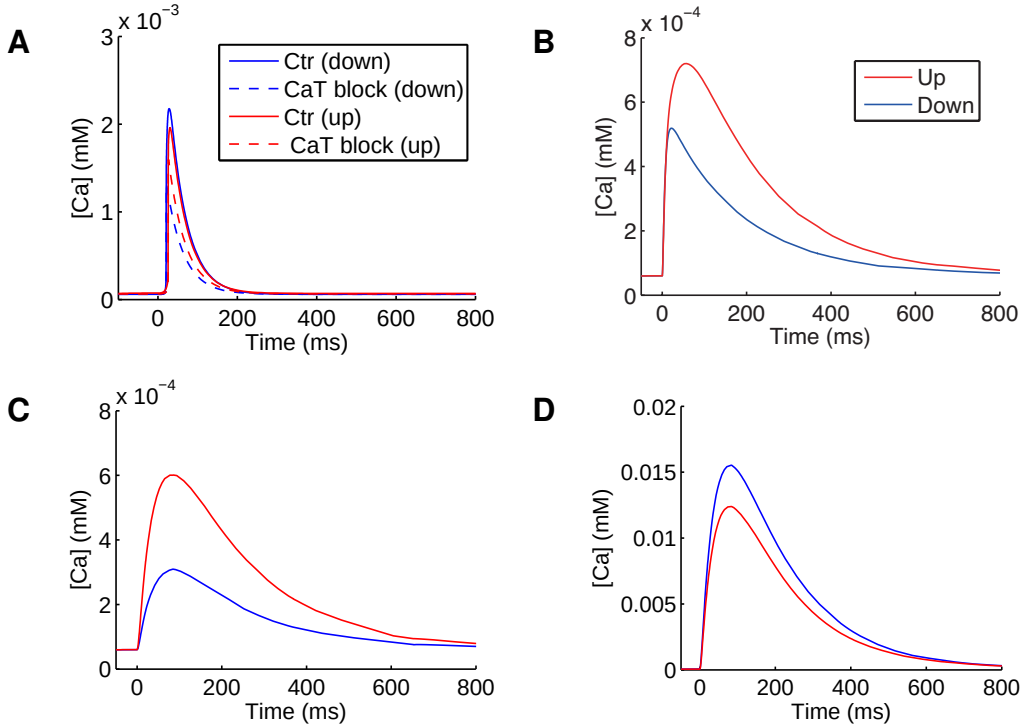

Figure 3.8. Comparison of calcium responses. Calcium responses to synaptic input in up-state (red) and down-state (blue). (A) Calcium responses to a 30 ms current pulse to the soma with blockade of T-type calcium channels. (B) AMPAR mediated calcium signals under the conditions of sodium, calcium and NMDAR currents being set at zero. (C, D) NMDAR mediated calcium responses under the conditions of sodium, calcium and AMPAR currents being set at zero. (C) 1 mM and (D) 0 mM magnesium.

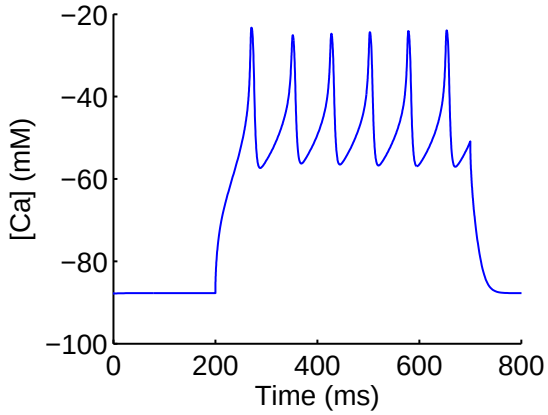

Figure 3.9. Calcium spike. Calcium spikes following a 0.3 mA current pulse were observed. Some channel conductances were multiplied: KAf conductance by 0.6, KAs by 0.4, KRP by 0.5, and NaF by 0.25 [162] to mimic experimental conditions [177].

3.3.2 Timing of glutamate input and postsynaptic spike

Next, I studied how the neuronal responses depended on the relative timing of paired inputs: glutamate input and postsynaptic spike. Fig. 3.10 (A, B) shows the calcium responses to glutamate input (Glu) preceding or following a postsynaptic action potential (Post) by 20 ms in the down-state. The postsynaptic spike was evoked by a 2 ms or 30 ms supra threshold current pulse injection into the soma. In this section, glutamate timing Δt_{Glu} was defined relative to the postsynaptic action potential. Glu-Post timing indicates that glutamate preceded the postsynaptic action potential ($\Delta t_{\mathrm{Glu}} > 0$), and Post-Glu indicates the reverse timing ($\Delta t_{\mathrm{Glu}} < 0$). Fig. 3.10 (B, C, E, F) shows the timing dependent peak calcium responses to Glu and Post inputs in down- and up-states. For both 2 and 30 ms pulses, Glu-Post timing caused higher calcium responses than Post-Glu timing.

When I studied the effect of dopamine timing relative to postsynaptic spike I saw that when dopamine preceded the postsynaptic spike the increased calcium response was higher than when dopamine followed the postsynaptic spike (Fig. 3.11).

When we saw the effect of dopamine timing relative to postsynaptic spike,

preceding dopamine increased calcium response higher than following dopamine (Fig. 3.11).

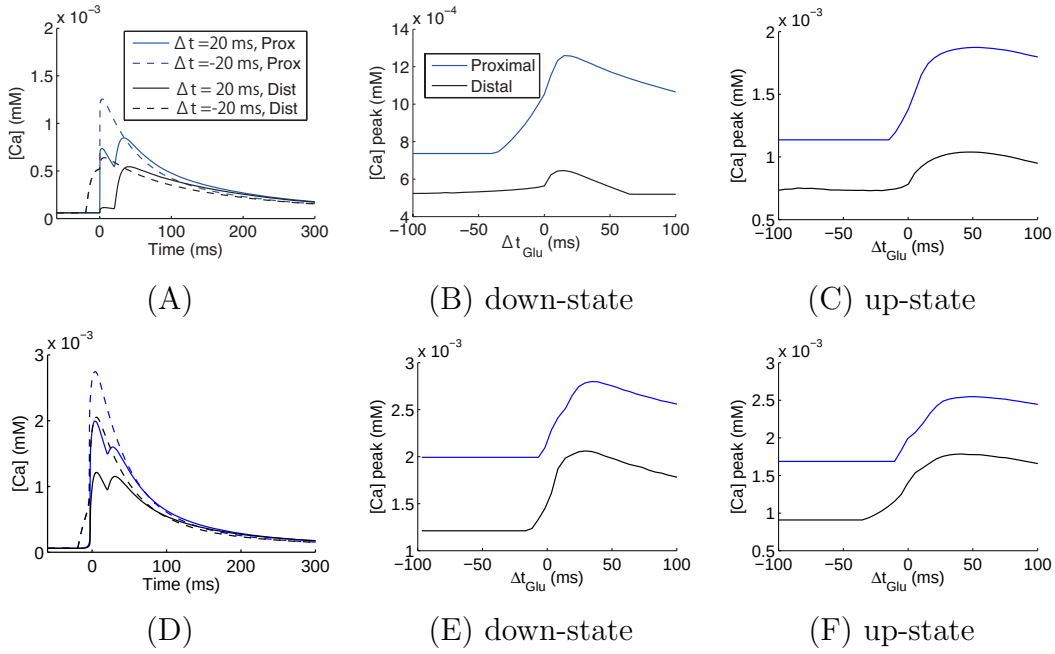

Figure 3.10. Glutamate timing dependent calcium responses. The dependence of the calcium response on the timing of glutamate synaptic input relative to postsynaptic action potential, which was evoked by a 2 ms postsynaptic current pulse (A-C), and by a 30 ms current pulse (D-F). (A, D) Typical calcium response to timed input of Glu and Post. The gray lines indicate presynaptic input leading the postsynaptic spike by 20 ms, and the black lines indicate the presynaptic input following the postsynaptic spike by 20 ms. (B, C, E, F) Peak of the calcium transient for each timed input in the down-state (B, E) and up-state (C, F). Δt_{Glu} means the time difference between presynaptic glutamate input and postsynaptic action potential. A positive time means the presynaptic input precedes the postsynaptic action potential.

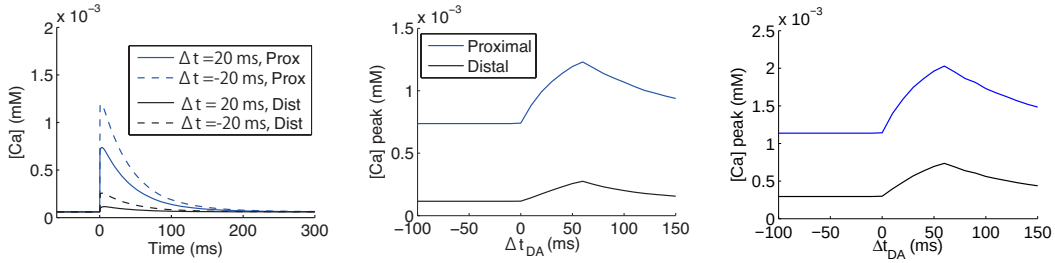

(A) (B) down-state (C) up-state

Figure 3.11. Dopamine timing dependent calcium responses. The dependence of the calcium response on the timing of dopamine synaptic input relative to postsynaptic action potential, which was evoked by a 2 ms postsynaptic current pulse. (A) Typical calcium response to timed input of DA and Post. The gray lines indicate presynaptic input leading the postsynaptic spike by 20 ms, and the black lines indicate the presynaptic input following the postsynaptic spike by 20 ms. (B) Peak of the calcium transient for each timed input at the proximal spine (blue) and the distal spine (black) in (B) down-state and (C) up-state. Δt_{Glu} means the time difference from presynaptic dopamine input to postsynaptic action potential. A positive value means the presynaptic input precedes the postsynaptic action potential.

Fig. 3.12 shows the sources of calcium influx. For the glutamate input (upper panels), the increased calcium response to Glu and Post timing input was due to enhanced calcium influx through NMDA receptors following bAP. This is consistent with previous findings [34, 132, 133] For dopamine input (lower panels), the increased calcium response to DA and Post timing input was due to enhanced calcium influx through L-type calcium channels.

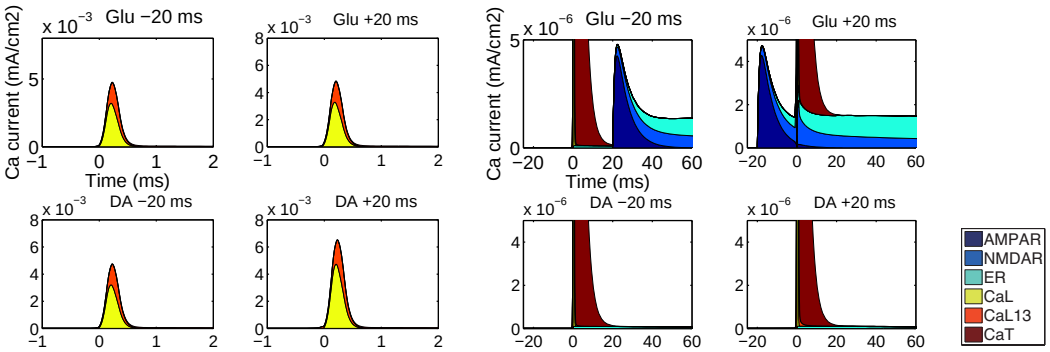

Figure 3.12. Timing dependent calcium responses. Distribution of calcium response sources to timed presynaptic input (glutamate or dopamine) relative to postsynaptic action potential at proximal spines in the down-state. The right four figures are magnifications of the left four figures. The conditions are $\Delta t_{\mathrm{Glu}} = -20$ (upper-left), $\Delta t_{\mathrm{Glu}} = +20$ (upper-right), $\Delta t_{\mathrm{DA}} = -20$ (lower-left), $\Delta t_{\mathrm{DA}} = +20$ (lower-right). The abbreviations in the legend are the same as those in Fig. 3.7.

3.3.3 Triplet interaction

I then investigated the dependence of calcium responses on the timing of both glutamate (Glu) and dopamine (DA) inputs relative to the postsynaptic spike. Dopamine timing Δt_{DA} and glutamate timing Δt_{Glu} were defined relative to postsynaptic action potential as in the previous section. Positive values meant dopamine or glutamate preceded the postsynaptic spike. The temporal order of input timings is shown in Fig. 3.13. This presentation is also used in later figures.

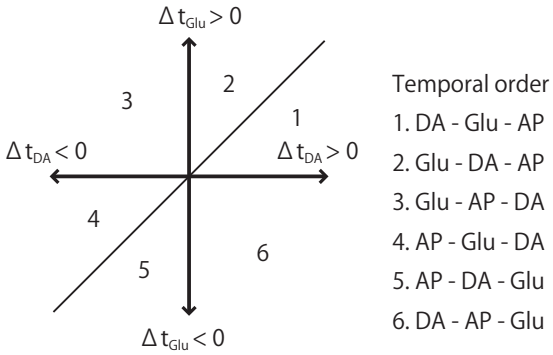

Figure 3.13. Temporal order of triplet inputs. Δt means the time difference between presynaptic glutamate input and postsynaptic action potential. Positive values mean the presynaptic input precedes the postsynaptic action potential. For example, in timing area 1, the temporal order of inputs was dopamine first, glutamate second, and finally the postsynaptic spike.

Fig. 3.14 shows the peak calcium concentration in the proximal and distal spines. In the down-state the effect of dopamine input was most pronounced when the dopamine input preceded the postsynaptic spike by about 50 ms. This tendency was also observed in the up-state (Fig. 3.15). In the distal spine, the calcium peak was lower than that in the proximal spine because the bAP was attenuated at the distal dendrite and such a small bAP was not enough to activate L-type calcium channels. Although this occurred for a 2 ms current pulse, it did not occur for a 30 ms current pulse. Timing dependence of the glutamate and postsynaptic spike was weakened by blocking NMDA receptors. Timing dependence of the dopamine and postsynaptic spike disappeared when NMDAR and L-type calcium channels were blocked (Fig. 3.16). It is noteworthy that the modulation by dopamine input was not just a linear summation. Calcium levels were elevated drastically only when the glutamate and dopamine input timing adequately preceded postsynaptic input. In the up-state, the calcium responses were enhanced, and their peaks were shifted to $\Delta t_{\mathrm{Glu}} = +50$ ms from $\Delta t_{\mathrm{Glu}} = +20$ ms in the down-state.

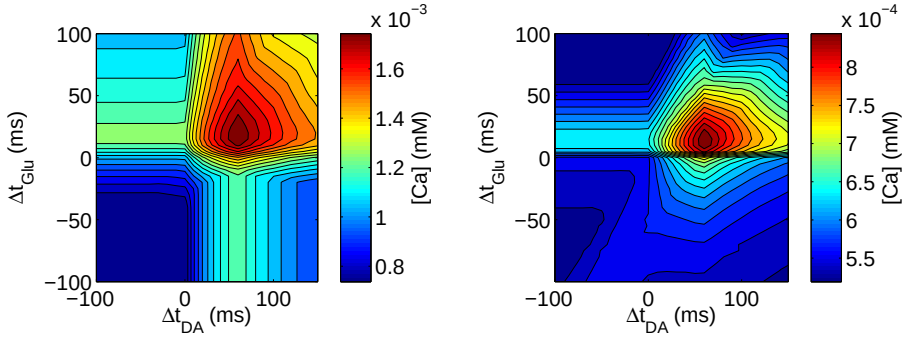

(A) Proximal, 2 ms pulse

(B)Distal, 2 ms pulse

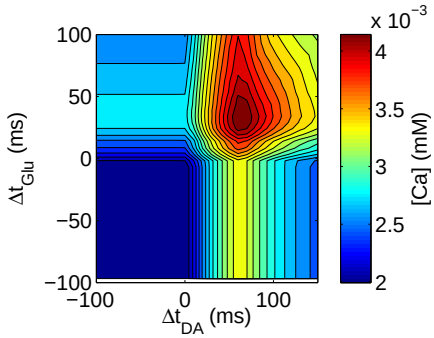

(C) Proximal, 30 ms pulse

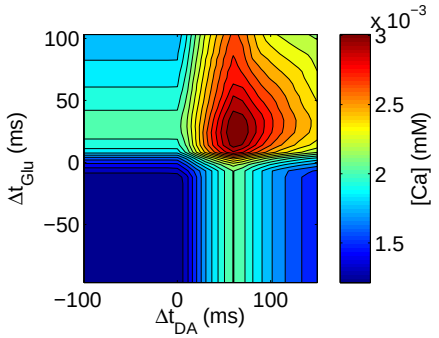

(D)Distal, 30 ms pulse

Figure 3.14. Calcium responses to triplet timed inputs in the down-state. Peak calcium in the proximal spine (A, C) and distal spine (B, D) was plotted in response to different timings of glutamate and dopamine inputs relative to a postsynaptic spike. Postsynaptic spikes were evoked by (A, B) 2 ms and (C, D) 30 ms current pulses, respectively.

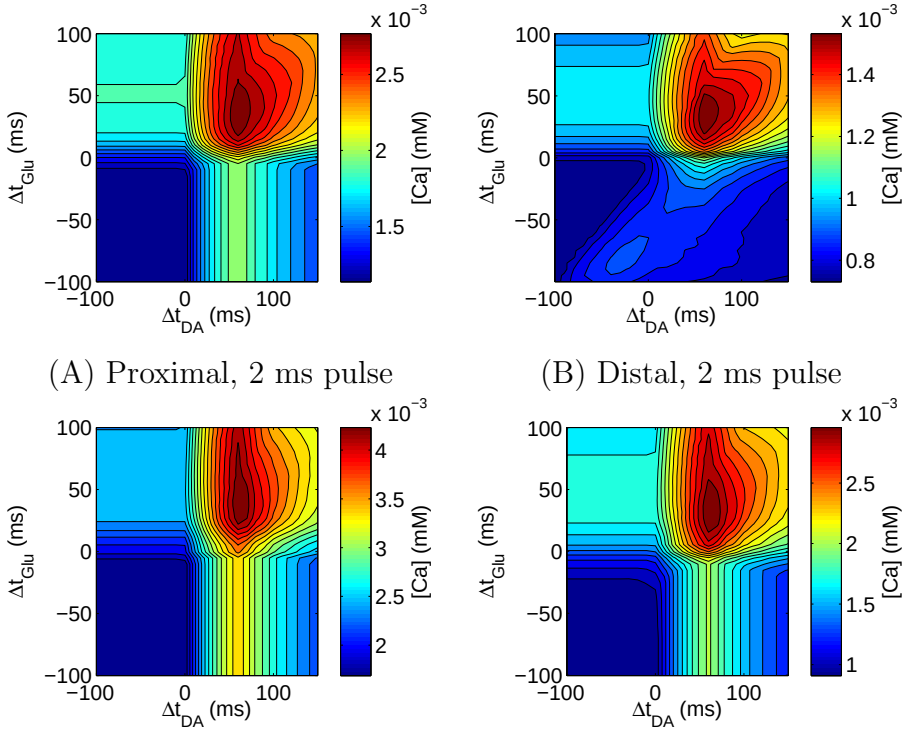

(A) Proximal, 2 ms pulse

(B) Distal, 2 ms pulse

(C) Proximal, 30 ms pulse

(D) Distal, 30 ms pulse

Figure 3.15. Calcium responses to triplet timed inputs in the up-state. Peak calcium in the proximal spine (A, C) and distal spine (B, D) was plotted in response to different timings of glutamate and dopamine inputs relative to a postsynaptic spike. Postsynaptic spikes were evoked by (A, B) 2 ms and (C, D) 30 ms current pulses, respectively.

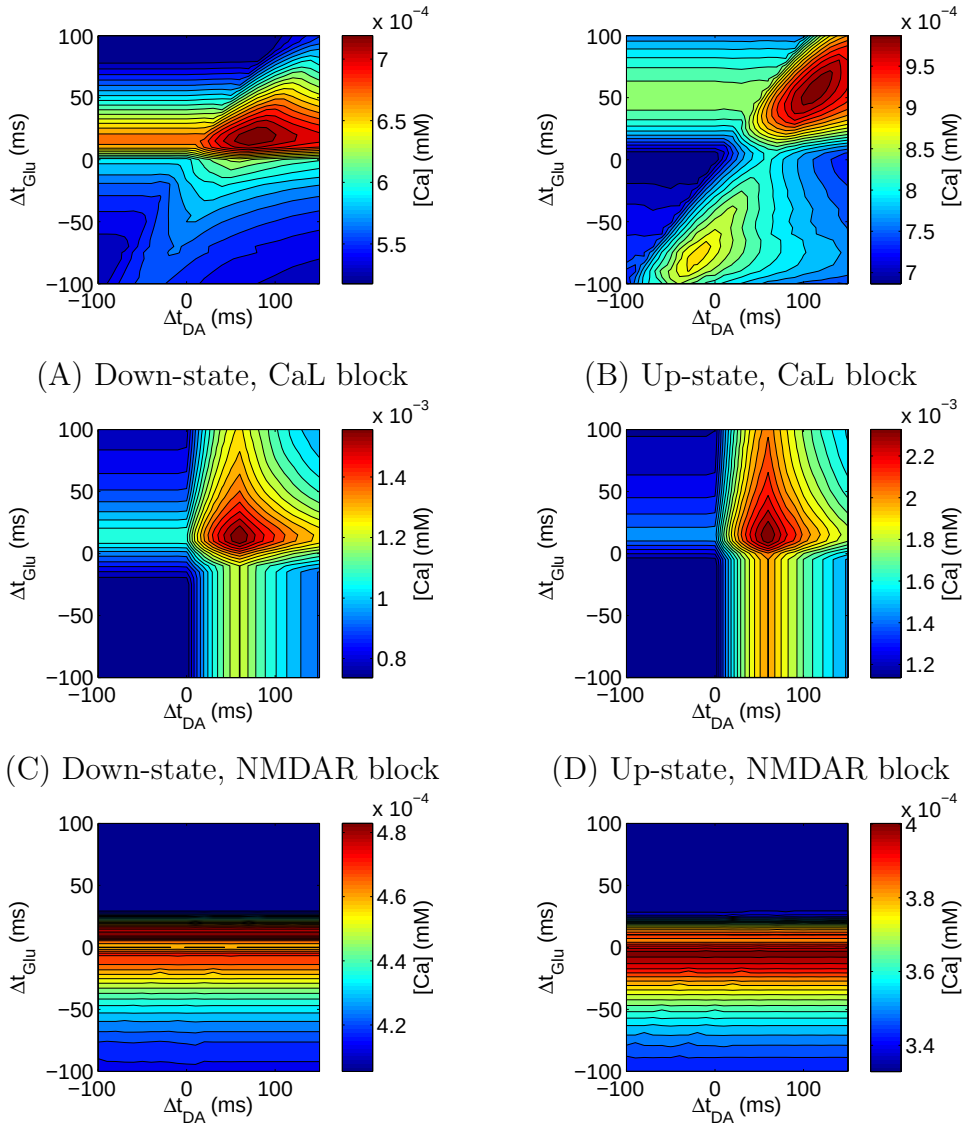

(A) Down-state, CaL block

(B) Up-state, CaL block

(C) Down-state, NMDAR block

(D) Up-state, NMDAR block

(E) Down-state, CaL+NMDAR block

(F) Up-state, CaL+NMDAR block

Figure 3.16. Calcium responses to triplet timed inputs under inhibition conditions. (A, B) L-type calcium channel (CaL) (C, D) NMDAR and (E, F) both NMDAR and CaL conductances were set to zero in the down-state (A, C, E) and up-state (B, D, F).

3.3.4 Leaky integration of calcium

An uncaging calcium study in the cerebellum reported that the amplitude of LTD was considered as a leaky integrator of calcium [224]. The leaky integrator was described by

$$\tau \frac{dx}{dt} = -x + a[Ca^{2+}](t), \text{or} \tag{3.37}$$

$$x(t) = \frac{a}{\tau} e^{-\frac{t}{\tau}} \int [Ca^{2+}](t) e^{\frac{t}{\tau}} dt, \tag{3.38}$$

where τ is the time constant of integration, x is the amount of a signal that transduces calcium into the change in synaptic efficacy, and a is a scaling factor representing the efficiency of the integrator in converting calcium into x. These two equations are mathematically the same, but are represented differently. The leaky integration of calcium was calculated with τ of 600 ms and a of 20.

Interestingly, the dependence of timed inputs on the leaky integration of calcium was different from that of the calcium peak (Fig. 3.17 and 3.18). For a 2 ms current pulse, when dopamine preceded postsynaptic spike, Glu-Post induced higher x. However, when dopamine followed the postsynaptic spike, Glu-Post induced lower x. For a 30 ms current pulse, Glu-Post induced higher x in spite of dopamine timing.

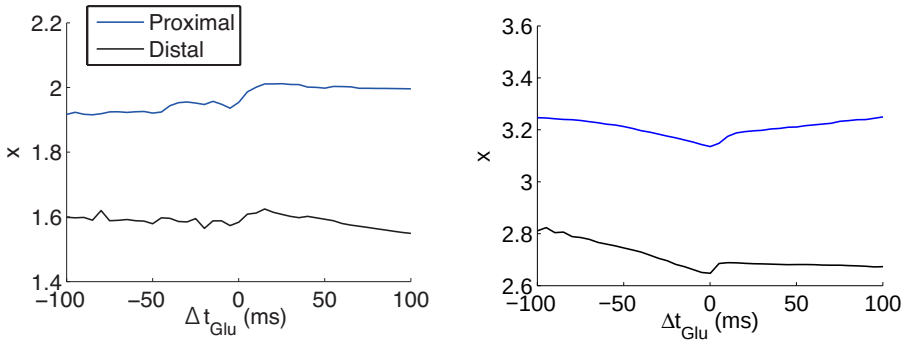

(A) Down-state, 2 ms pulse

(B) Up-state, 2 ms pulse

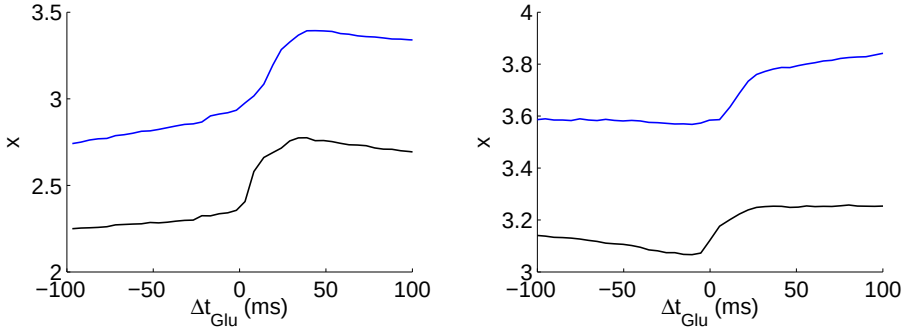

(C) Down-state, 30 ms pulse

(D) Up-state, 30 ms pulse

Figure 3.17. Leaky integration of calcium responses to timed inputs. Leaky integration of calcium responses to timed glutamate inputs relative to a postsynaptic spike in the down-state (A, C) and up-state (B, D). Postsynaptic spikes were evoked by (A, B) 2 ms and (C, D) 30 ms current pulses, respectively.

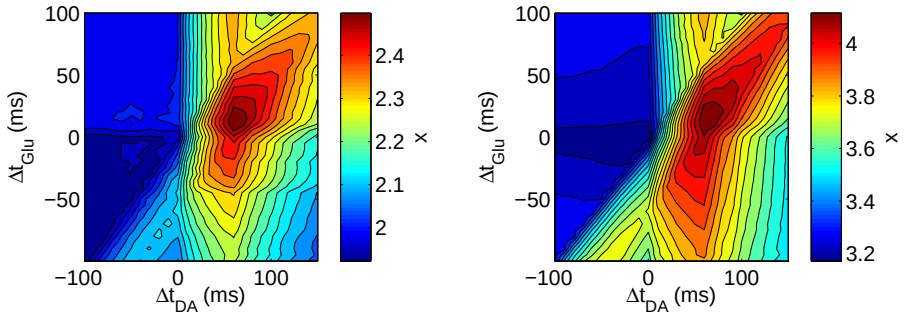

(A) Down-state, 2 ms pulse (B) Up-state, 2 ms pulse

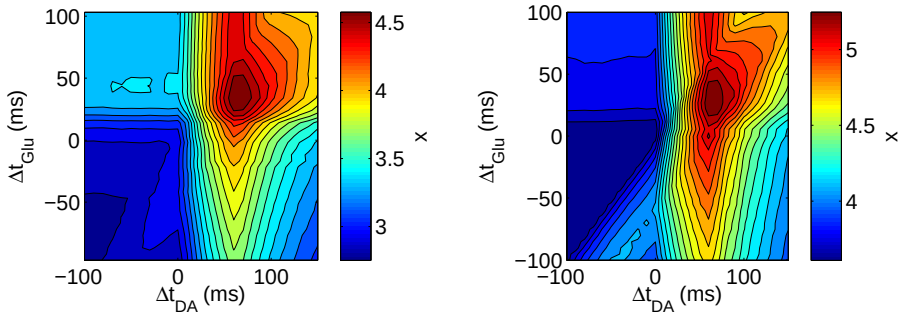

(C) Down-state, 30 ms pulse (D) Up-state, 30 ms pulse

Figure 3.18. Leaky integration of calcium responses to triplet timed inputs in proximal spines. Leaky integration of calcium in the down-state (A, C) and up-state (B, D) in response to different timings of glutamate and dopamine inputs relative to a postsynaptic spike. Postsynaptic spikes were evoked by (A, B) 2 ms and (C, D) 30 ms current pulses, respectively.

To test the mechanisms of the phenomenon by which the relationship between x and the timing of glutamate and the postsynaptic spike was dependent on dopamine timing, additional simulation was performed without the dopamine effect on the NMDAR. Accordingly, I observed that the dopamine timing effect on glutamate timing dependence disappeared (Fig. 3.19). In addition, calcium responses to Glu preceding input was more enhanced than when Glu followed input at $\Delta t_{\mathrm{DA}} = +100$ ms. Dopamine did not enhance calcium response to Glu preceding input at $\Delta t_{\mathrm{DA}} = -10$ ms.

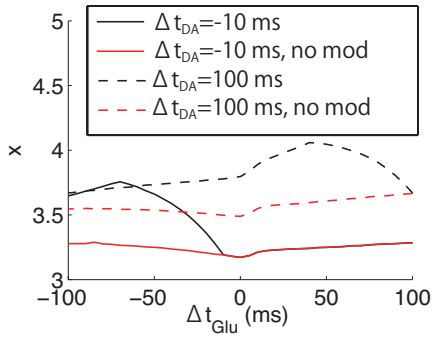

(A)

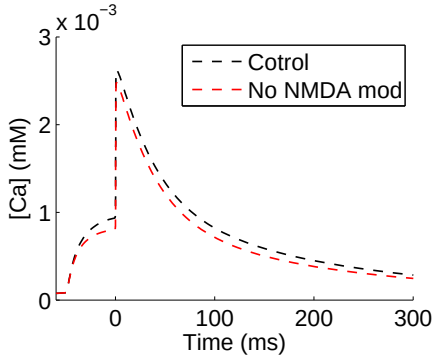

(B) $\Delta t_{\mathrm{DA}} = 100$ ms, $\Delta t_{\mathrm{Glu}} = 50$ ms

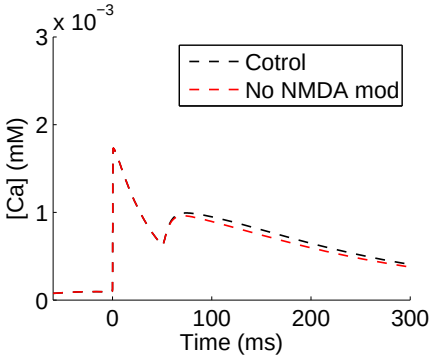

(C) $\Delta t_{\mathrm{DA}} = 100$ ms, $\Delta t_{\mathrm{Glu}} = -50$ ms

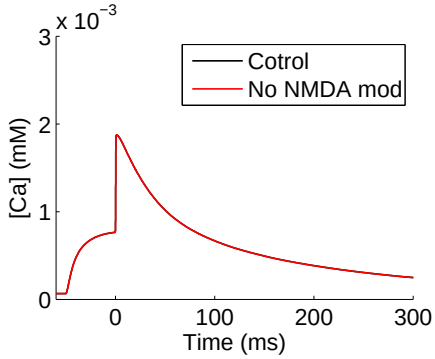

(D) $\Delta t_{\mathrm{DA}} = -10$ ms, $\Delta t_{\mathrm{Glu}} = 50$ ms

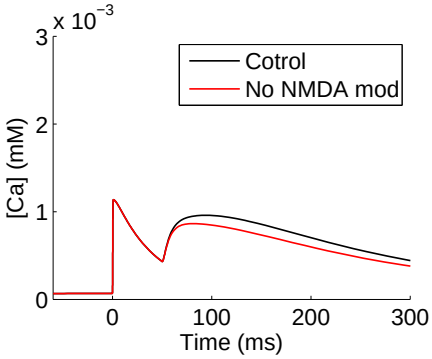

(E) $\Delta t_{\mathrm{DA}} = -10$ ms, $\Delta t_{\mathrm{Glu}} = -50$ ms

Figure 3.19. Leaky integration of calcium responses to timed inputs without a dopamine effect on the NMDAR. Spikes were evoked by 2 ms current injections to the soma in the up-state and responses were measured at proximal spines. Black lines indicate control conditions and red lines are in the absence of the effect of dopamine on the NMDAR. In panel (D), black and red lines are overlapped.

3.3.5 Different parameter conditions

To explore the possibility of reversed STDP, I tested different parameter settings (high AMPAR/NMDAR conductance conditions), which were higher AMPAR conductance and lower conductance of NMDAR and calcium channels than the original parameter settings (Table 3.3 and Table 3.4).

The voltage responses to glutamate were a little bit larger than those produced by the original parameter settings. The calcium responses to glutamate were sharp, because AMPAR was dominant. Also, reversed timing relationships, whereby Glu-Post induced lower calcium response than Post-Glu (Fig. 3.20) were produced. However, the difference of peak calcium between the two types of timed input was small.

When AMPARs were blocked, such a reversed timing relationship disappeared (Fig. 3.21), because the reverse potential of AMPAR is 0 mV and long depolarization caused a small calcium current from AMPARs.

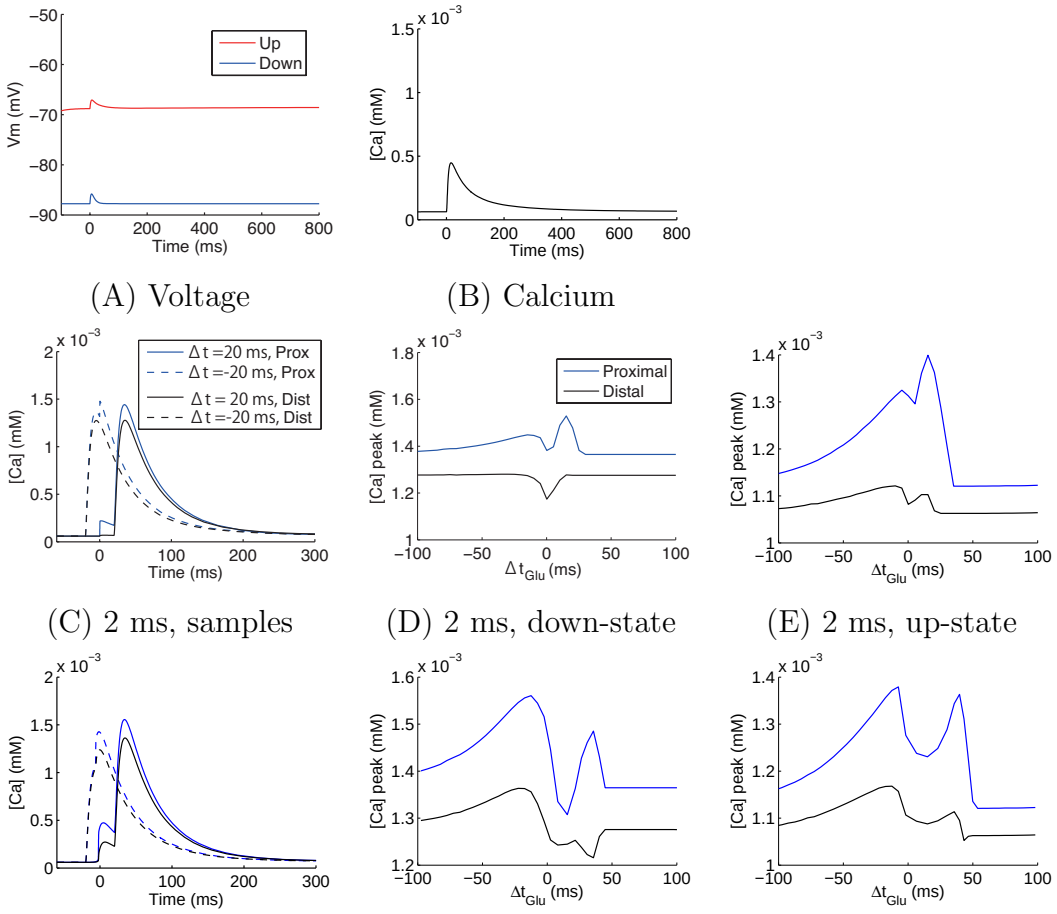

(A) Voltage (B) Calcium

(C) 2 ms, samples (D) 2 ms, down-state (E) 2 ms, up-state

(F) 30 ms, samples (G) 30 ms, down-state (H) 30 ms, up-state

Figure 3.20. Timing dependent calcium responses in high AMPAR/NMDAR conductance conditions. (A) Voltage and (B) calcium response to glutamate. (C-H) The dependence of the calcium response on the timing of glutamate synaptic input relative to postsynaptic action potential, which was evoked by a 2 ms postsynaptic current pulse (C-E), and a 30 ms current pulse (F-H). (C, F) Typical calcium responses to timed input of Glu and Post. The gray lines indicate presynaptic input leading the postsynaptic spike by 20 ms, and the black lines indicate the presynaptic input following the postsynaptic spike by 20 ms. (D, E, G, H) Peak of the calcium transient for each timed input in the down-state (D, G) and up-state (E, H).

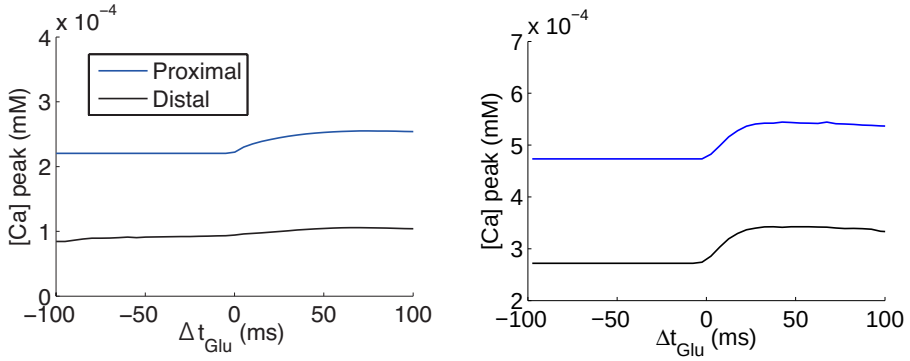

(A) 2 ms pulse (B) 30 ms pulse

Figure 3.21. Timing dependent calcium responses in high AMPAR/NMDAR conductance conditions with AMPAR block. Two types of current pulses were injected to evoke action potentials in the down-state.

When there is calcium dependence on the triplet timing input, the tendency of timing dependence of the glutamate and postsynaptic spike did not change for the 2 ms current pulse for any dopamine timing; however, the tendency did change for the 30 ms current pulse (Fig.3.22). When dopamine followed the post-synaptic spike, Glu-Post increased calcium more than Post-Glu, which was the same tendency as seen with the timed input of glutamate and postsynaptic spike in the absence of dopamine. However, when dopamine preceded the postsynaptic spike, Post-Glu increased calcium more than Glu-Post, which was the opposite tendency to that seen with the timed input of glutamate and postsynaptic spike in the absence of dopamine.

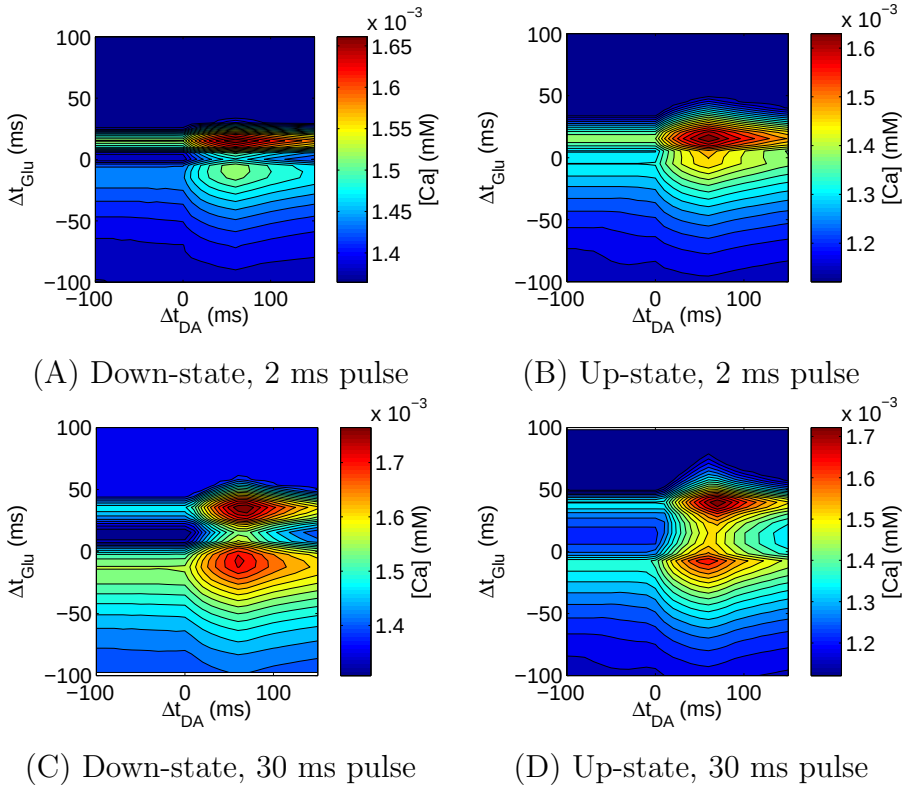

(A) Down-state, 2 ms pulse

(B) Up-state, 2 ms pulse

(C) Down-state, 30 ms pulse

(D) Up-state, 30 ms pulse

Figure 3.22. Calcium responses to triplet timed inputs in proximal dendritic spines in high AMPAR/NMDAR conductance conditions. Peak calcium in the down-state (A, C) and up-state (B, D) were plotted in response to different timings of glutamate and dopamine inputs relative to a postsynaptic spike. Postsynaptic spikes were evoked by (A, B) 2 ms and (C, D) 30 ms current pulses, respectively.

The dependence of triplet timing on leaky integration of calcium in the high AMPAR/NMDAR conductance condition was very different from that seen in the original parameter settings (Fig. 3.23). There was a dip around $\Delta t_{\text{Glu}} = 0$ ms. Leaky integration of calcium was higher when glutamate followed the postsynaptic spike for any dopamine timing for the 2 ms current pulse.

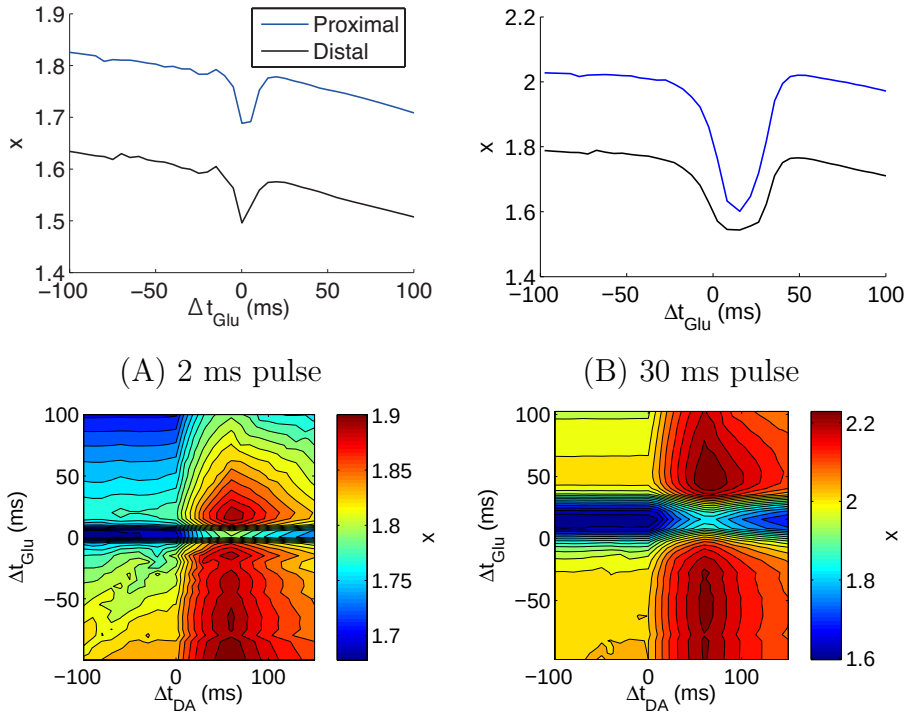

(A) 2 ms pulse (B) 30 ms pulse

(C) 2 ms pulse (D) 30 ms pulse

Figure 3.23. Leaky integration of calcium responses to timed inputs in the down-state in high AMPAR/NMDAR conductance conditions. Leaky integration of calcium in response to different timings of (A, B) glutamate and (C, D) both glutamate and dopamine relative to a postsynaptic spike. Postsynaptic spikes were evoked by (A, C) 2 ms and (B, D) 30 ms current pulses, respectively.

3.3.6 Different dopamine modulations

So far, the effect of dopamine modulation on NMDAR was enhancement. However, there were possibilities of various types of dopamine modulation. As described in Table 3.5, there were some reports that dopamine reduced NDMAR conductance. Therefore, I first tested the dependence of triplet timing on the leaky integration of calcium for dopamine reducing NMDAR conductance modulation as Table 3.6. As a result, the calcium peak response was higher when glutamate preceded the postsynaptic spike for any dopamine timing (Fig. 3.24). Leaky integration of calcium was higher when glutamate preceded the postsynap-

tic spike for late dopamine timings, but the tendency was lost for early dopamine timings.

Next, I investigated the effects of dopamine on the back-propagation of action potentials. The propagation was rapidly attenuated (Fig. 3.25) and this corresponded with [52]. When dopamine was applied to all dendrites and spines constantly, the attenuation occurred more sharply. I investigated the timing dependent calcium response with respect to the dopamine effect on back-propagation. The results showed that the tendency of the calcium response to timing was the same as in the absence of dopamine modulation in both modulation cases (Fig. 3.26).

Finally, dopamine was applied to all dendrites and spines at timing Δt_{DA}, but not constantly. The results, shown in Fig. 3.27, were similar to those from a normal dopamine effect (Fig. 3.18 and Fig. 3.14).

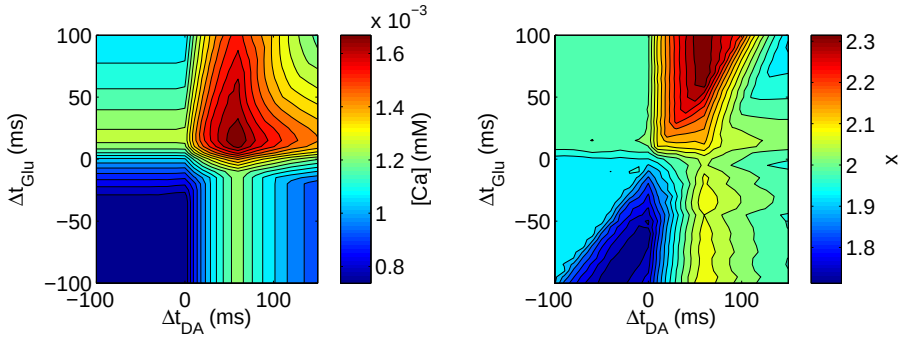

(A) Peak (B) Leaky integration

Figure 3.24. Calcium responses to triplet timed inputs in the down-state in the case of different DA modulation. Dopamine reduced the NMDAR current. (A) Peak and (B) leaky integration of calcium responses in the proximal spine in response to different timings of glutamate and dopamine inputs relative to a postsynaptic spike evoked by a 2 ms current pulse.

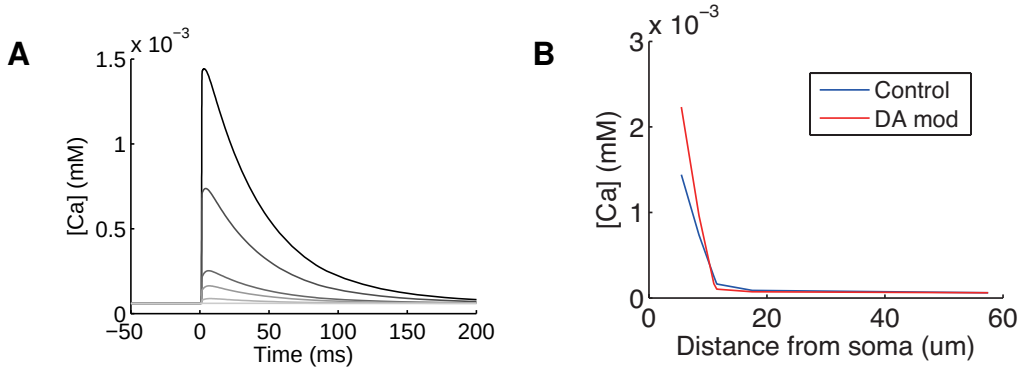

Figure 3.25. Attenuation of calcium. (A) Typical calcium responses to back-propagating action potentials. Darker lines indicate responses from the location on the dendrite nearest the soma. (B) peak of back-propagating action potential in control dendrites (blue) and under dopamine modulation for all dendrites (red). Distance is an approximation from the soma.

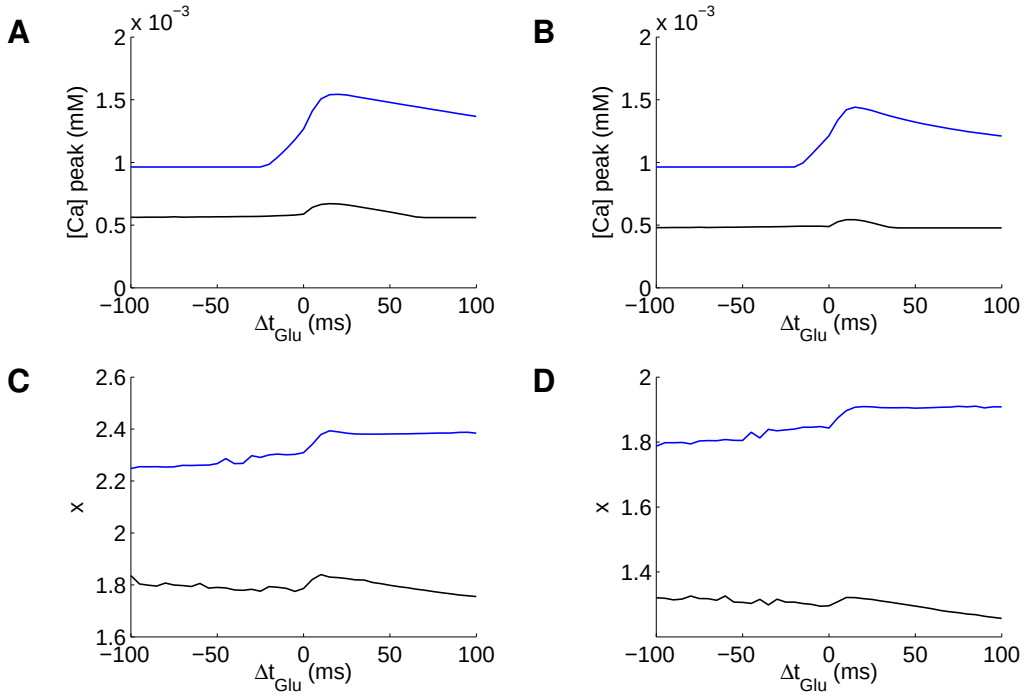

Figure 3.26. Timing dependent calcium responses under tonic DA conditions. (A, B) Peaks and (C, D) leaky integration of calcium responses under (A, C) dopamine enhanced NMDA receptor conductance, (B, D) dopamine reduced NMDA receptor conductance.

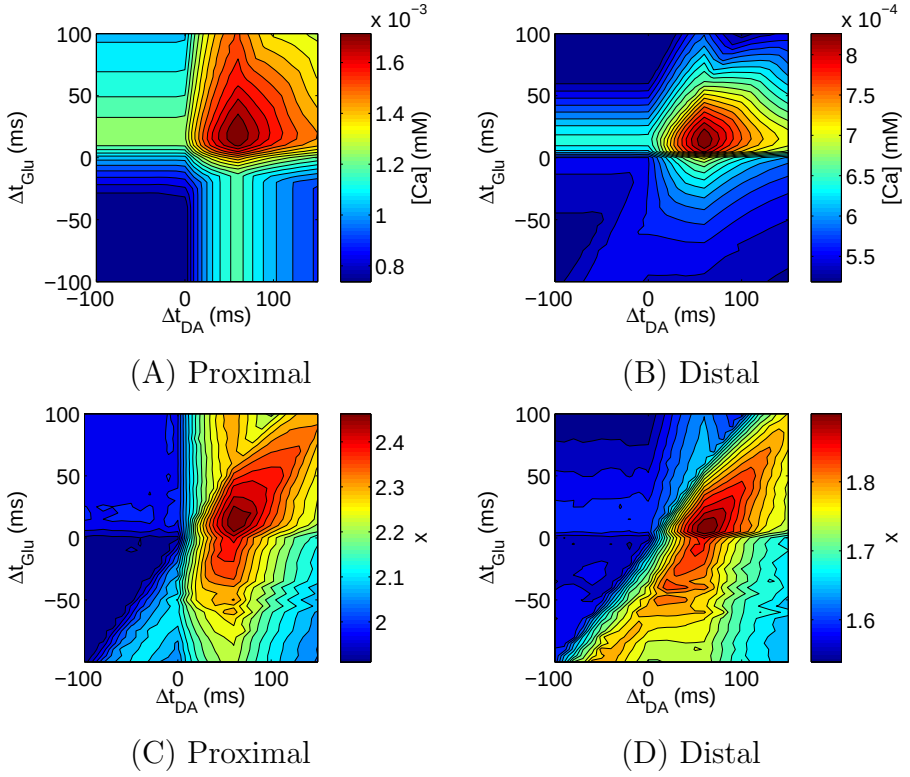

Figure 3.27. Timing dependent calcium responses for DA effect on the entire cell. Dopamine affected all dendrites and spines. (A, B) peaks and (C, D) leaky integration of calcium were measured at (A, C) proximal and (B. D) distal spines.

3.4 Conclusion and Discussion

I constructed a multi-compartment model of a medium spiny neuron of the striatum based on real morphological data. The model could reproduce several experimental results and predicted calcium responses to timed glutamate, dopamine and postsynaptic spike under several conditions: up-/down-state and two types of postsynaptic current duration to evoke postsynaptic spike, two types of parameter settings and several types of dopamine modulation. I measured from proximal and distal spines and evaluated peak and leaky integration of calcium.

The results suggested that:

1. Glutamate input preceding postsynaptic spike induced a higher calcium response, mostly caused by NMDA receptors and L-type calcium channels.

2. Dopamine input preceding postsynaptic spike induced a higher calcium response, mostly caused by L-type calcium channels.

3. Although a 2 ms current pulse in the up-state induced a higher calcium response than in the down-state, a 30 ms current pulse in the down-state induced a higher calcium response than in the up-state, which was caused by T-type calcium channels.

4. These tendencies were the same for triplet timing inputs, but dopamine modulation was not linear.

5. At distal spines, the back-propagating action potential was attenuated, and the dopamine timing effect was small.

6. Timing dependence on leaky integration of calcium was different from the timing dependence on the calcium peak. Glutamate following a postsynaptic spike induced higher a calcium response when dopamine also followed the postsynaptic spike, which was caused by dopamine modulation of NMDARs.

7. In the high AMPAR/NMDAR conductance condition, although the calcium response to Post-Glu was lower than to Glu-Post when a 2 ms current pulse was used to evoke the postsynaptic action potential, the calcium response to Post-Glu was higher than to Glu-Post when a 30 ms current pulse was used. This was caused by AMPARs.

8. Different dopamine modulations (DA inhibition of NMDARs, constant DA application, and broad effect of DA) were tested and there were no remarkable differences among the characteristics.

3.4.1 Conflicting Glu-Post timing order effects

I discuss the predictions of the simulation conditions in which the calcium response depended on the timing of glutamate and postsynaptic spike.

I consider possible conditions that caused the calcium response to Post-Glu to be higher than that to Glu-Post. If peak calcium is considered, the following conditions could be candidates: 1) A 30 ms current pulse with high AMPAR and low NMDAR conductances. 2) Dopamine followed the postsynaptic spike, for a 2 ms current pulse, in the distal spine, in the up-state, if L-type calcium channel conductance was small. 3) Dopamine followed the postsynaptic spike, for a 30 ms current pulse, in the high AMPAR/NMDAR conductance condition. If leaky integration of calcium was considered, the following conditions could be candidates: 1) 2 ms pulses were used in the up-state. 2) Dopamine timing was later than the postsynaptic spike for both 2 ms and 30 ms pulses. 3) A 2 ms current pulse was used with any dopamine timing in the high AMPAR/NMDAR conductance conditions.

As above, some conditions reproduced reversed timing relationships. If the presence of dopamine was assumed, more conditions were possible to reproduce a reversed timing relationship. My model suggested that reversed STDP occurred when dopamine input was early 3.18. However, studies by [66, 185, 204] did not use dopamine input. The problem was whether dopamine was released by cortical input or striatal activation. There has been a study suggesting that dopamine was projected by cortical high-frequency stimulation (not published). Therefore, reversed STDP could possibly be induced by dopamine.

However, dopamine input potentiated synaptic efficacy via a signaling cascade. Therefore, we should ignore the dopamine present conditions. In the dopamine absent conditions, when a 30 ms current pulse was used to evoke postsynaptic action potentials, the calcium response to Post-Glu was higher than to Glu-Post, in the high AMPAR/NMDAR conductance conditions. However, the relationship was different for the leaky integration of calcium. In addition, in a previous study by [238], NMDA/AMPA receptor conductance ratios were set 0.5, which show intrinsic bistability of membrane oscillation. The high AMPAR/NMDAR conductance conditions did not correspond with these conditions. Therefore these conditions may not be feasible and should be tested by experiment.

In addition, timing dependent elevation of calcium level was a gentle slope, which may cause ambiguous threshold of LTD and LTP. However, if we take into account the randomness of NMDAR conductance, we would get a more clear

STDP shape [206]. A stochastic simulation would be a worthwhile future study.

3.4.2 Dopamine timing and reinforcement learning

For reinforcement learning, dopamine input should come after glutamate input, because dopamine neurons calculate reward prediction error based on the expected reward signal from the striatum. However, dopamine input preceding HFS of paired cortical stimulation and postsynaptic spike induced LTP. Here, I discuss possibilities that a preceding dopamine input is an intrinsic mechanism in basal ganglia function.

One possibility is that reversed STDP is an essential form of STDP in the striatum. An action potential is evoked by the integration of cortical input, and this integration would be a gentle slope. Therefore, a 30 ms current pulse maybe more natural than sudden activation by a 2 ms short current pulse. My model reproduced reversed STDP in high AMPAR/NMDAR conductance parameter settings. In this case, late dopamine timing switched reversed STDP to normal STDP. There is a possibility that physiological striatal STDP is reversed STDP, and normal STDP at late dopamine timing is irregular.

Another possibility is that dopamine reduces NMDAR conductance. In Fig. 3.24B, Glu-Post elevated leaky integration of calcium more than Post-Glu for early dopamine input. Post-Glu elevated leaky integration of calcium more than Glu-Post for late dopamine input. Prediction by reinforcement learning maybe wrong and dopamine may come after cortical input. These predictions from my model are worth consideration. Validation by experimentation is required.

3.4.3 Thalamostriatal synaptic plasticity

Striatal neurons receive glutamate inputs from the thalamus and cerebral cortex. These are projected to different parts of the dendrite; cerebral inputs are projected to dendritic spines, whereas thalamic inputs are projected to dendritic shafts in the matrix region of the striatum [71, 72]. Thalamostriatal synaptic plasticity was different from corticostriatal synaptic plasticity in a parkinsonian monkey model [189]. In addition, corticostriatal and thalamostriatal synapses are suggested to have distinctive properties [58]. This study reported that the NMDAR/AMPAR ratio was significantly greater at corticostriatal synapses than

at thalamostriatal synapses. My results suggested that a low NMDAR/AMPAR conductance ratio reproduced both types of STDP, but a high NMDAR/AMPAR conductance ratio did not. This suggested that thalamostriatal synaptic plasticity could only be normal STDP.

4. Signaling Cascade Model

4.1 Introduction

In this chapter, a dynamic model of the intracellular signaling cascade, which links glutamatergic and dopaminergic inputs to regulation of glutamatergic receptors, was constructed to elucidate the dynamic molecular mechanisms behind the two types of corticostriatal synaptic plasticity. This model will provide a basis for understanding and predicting the effects of pharmacological manipulations and genetic variations on reward-dependent functions involving the basal ganglia, such as motor learning, cognitive control, and drug addiction.

The intracellular signaling cascade involved in synaptic regulation of corticostriatal synapses has been extensively studied [90, 97, 170–172, 174, 220, 221]. Glutamatergic input increases intracellular calcium ion concentration, and dopaminergic input increases intracellular cyclic adenosine 3',5'-monophosphate (cAMP) by activating adenylyl cyclase 5 (AC5). DARPP-32, the dopamine- and cyclic AMP-regulated phosphoprotein, with a molecular weight of 32 kDa, has multiple phosphorylation sites that are affected by calcium and cAMP. DARPP-32, in turn, regulates enzymes that influence phosphorylation of AMPA-type glutamate receptors. Insertion of phosphorylated AMPA receptors into the post-synaptic membrane is the main mechanism of glutamatergic synaptic plasticity [156]. Despite extensive knowledge of this system, multiple feedforward and feedback pathways, with excitatory and inhibitory interactions in the molecular network, results in complicated mechanisms that are difficult to comprehend with schematic diagrams or purely analytical methods. Therefore, quantitative computer simulations of the signaling cascade under various manipulations are required, such as blockades and knockouts, to understand the basic mechanism of the entire pathway and the roles of specific elements.

Existing simulation models have considered subnetworks of the signaling pathways surrounding DARPP-32. The model by Fernandez *et. al.* [65] considered intracellular calcium ion and cyclic AMP concentrations to be the inputs and simulated activation of three DARPP-32 phosphorylation sites. Lindskog *et. al.* [149] utilized intracellular calcium and D1-type dopamine receptor (D1R) binding as inputs and simulated activation of enzyme phosphorylation and de-

phosphorylation. In addition, Barbano *et. al.* [9] analyzed a model making use of glutamate and dopamine for input, demonstrating the stability of the net state of DARPP-32 phosphorylation in the presence of noise. However, none of these models included the resulting phosphorylation of AMPA receptors, which is directly related to LTP and LTD. In addition, the models only focused on dopamine-dependent plasticity and did not consider the mechanisms of calcium-dependent plasticity.

In the present study, a complete model of the signal transduction pathway was constructed, with intracellular calcium ion and extracellular dopamine concentrations serving as inputs and post-synaptic membrane insertion of AMPA-type glutamate receptors for the output. The following was demonstrated *in silico*: 1) The model reproduced both calcium- and dopamine-dependent plasticity and determined the sub-pathways responsible for different types of plasticity. 2) The model predicted that the pathway through cyclin-dependent kinase 5 (Cdk5) is crucial for inducing synaptic depression with weak calcium input. 3) The model determined that a positive (double-negative) feedback loop, which included DARPP-32, plays an important role in LTP induction, with either strong calcium input or simultaneous calcium and dopamine inputs.

In the following sections of this manuscript, the neurobiological literature for building the transduction pathway model will be reviewed, followed by an explanation of the structure, computing method, and simulation input and output. Experimental results *in silico* demonstrated the following: the pathway response to different calcium and dopamine input levels, the effect of DARPP-32 knockout, and analysis of the positive feedback loop. The study concludes with the new knowledge gained by this simulation and directions for further studies based on this model.

4.1.1 Intracellular signal transduction

The intracellular signaling cascades that regulate synaptic efficacy of the corticostriatal synapse have been extensively studied [86, 88, 89, 95, 190].

The present study modeled D1R-expressing neurons based on previous literature and databases [208]. Fig. 4.1 shows the summary block diagram of the signaling cascade model. The model details are provided in Materials and Meth-

ods.

4.2 Materials and Methods

4.2.1 Mathematical formulation

All signaling pathway reactions shown in Fig. 4.1 are represented by binding and enzymatic reactions.

Binding reaction of molecule A and molecule B to form molecule AB

$$\mathrm{A} + \mathrm{B} \underset{k_b}{\overset{k_f}{\rightleftharpoons}} \mathrm{AB}, \tag{4.1}$$

where k_f and k_b are rate constants for forward and backward reactions, is simulated by the ordinary differential equation:

$$\frac{d[\mathrm{AB}]}{dt} = -\frac{d[\mathrm{A}]}{dt} = -\frac{d[\mathrm{B}]}{dt} = k_f[\mathrm{A}][\mathrm{B}] - k_b[\mathrm{AB}]. \tag{4.2}$$

The rate constants k_f and k_b were related to the dissociation constant $K_d = k_b/k_f$ and the time constant $\tau = 1/(k_f + k_b)$, i.e., $k_f = \frac{1}{\tau(1+K_d)}$ and $k_b = \frac{K_d}{\tau(1+K_d)}$.

An enzymatic reaction of substrate S with enzyme E to produce product P was simulated by a collection of two elementary processes: 1) enzyme E bound to substrate S to form the enzyme-substrate complex ES; and 2) the complex ES dissociated into enzyme E and product P. The chemical equation can be written as

$$\mathrm{S} + \mathrm{E} \underset{k_b}{\overset{k_f}{\rightleftharpoons}} \mathrm{ES} \xrightarrow{k_{\mathrm{cat}}} \mathrm{E} + \mathrm{P}. \tag{4.3}$$

The Michaelis-Menten formulation was avoided due to problems with the steady-state assumption [65, 157]. However, many papers and databases have provided only k_{cat} and the Michaelis constant $K_M = (k_b + k_{\mathrm{cat}})/k_f$ rather than k_f and k_b. In such cases, it was assumed that k_b was four times larger than k_{cat} (i.e. $k_f = 5k_{\mathrm{cat}}/K_M$ and $k_b = 4k_{\mathrm{cat}}$), based on the default setting in GENESIS/Kinetikit simulator. (see Appendix B).

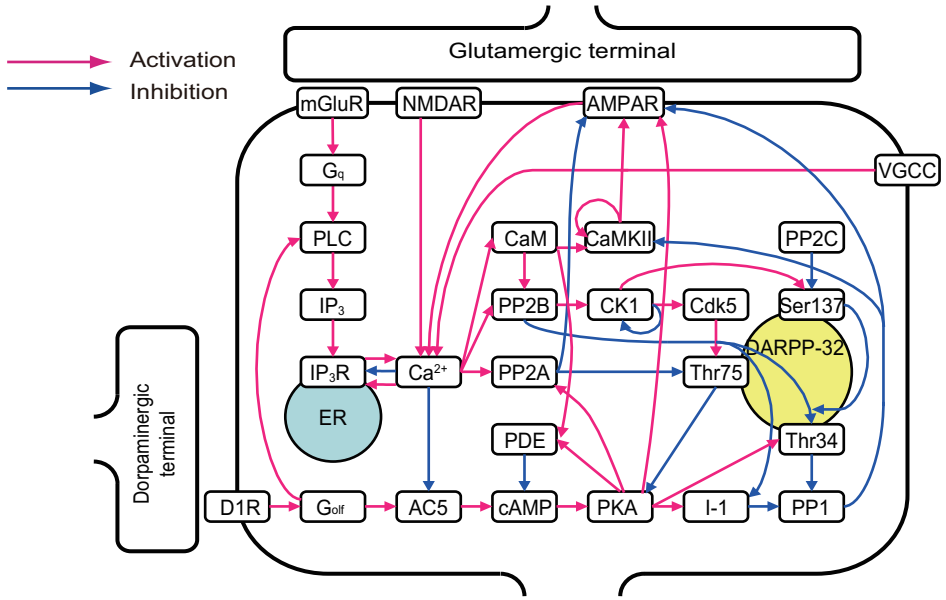

Figure 4.1. Block diagram of the signal transduction model in medium spiny neurons. The red and blue arrows indicate activation and inhibition, respectively. Detailed information on the regulatory pathways is provided in the Materials and Methods section, and the rough sketch of the signal flow is as follows. Glutamate binds to its corresponding receptors and increases intracellular calcium. D1R binding to dopamine increases cAMP. Calcium and cAMP alter the number of AMPA membrane receptors via downstream cascades and, thereby, regulate the synaptic efficacy of the neuron. The bi-directional effect of calcium on IP_3 receptor should be mentioned. The activation level (open probability) of IP_3 receptor displays a bell-shaped response curve to intracellular calcium concentrations. The IP_3 receptor activation level is maximal when intracellular calcium concentration is approximately 0.2 μM [12]. However, more (and less) calcium reduces IP_3 receptor activation. To represent this regulation, two complementary arrows represent activation and inhibition from calcium to IP_3 receptor in this diagram. In addition, one arrow originates from Ser137 and terminates at an arrow from PP2B to Thr34. Phosphorylation of Ser137 decreases the rate of Thr34 dephosphorylation by PP2B. Therefore, Ser137 contributes to disinhibition of the PP2B-Thr34 pathway [56]. The arrow from Ser137 represents this effect.

4.2.2 Intracellular signal transduction

Postsynaptic spines receive two presynaptic inputs: glutamatergic terminals from the cerebral cortex and dopaminergic terminals from the substantia nigra pars compacta. Plasticity of corticostriatal synaptic input results from phosphorylation of AMPA-type glutamatergic receptors, which promotes insertion into the postsynaptic membrane [63, 64, 156]. Below, the pathways linking glutamatergic and dopaminergic input to phosphorylation of AMPA receptors are delineated (see Fig. 4.2, Fig. 4.10, and Appendix C for illustrations of following signaling cascade).

1) Glutamate release from the cortical presynaptic terminal increases calcium concentration in the postsynaptic spine via three mechanisms: i) calcium influx from NMDA- and AMPA-type glutamatergic receptor channels, ii) calcium efflux from the ER via IP_3 receptor channels following mGluR activation, iii) calcium influx from VGCC due to EPSPs of NMDA- and AMPA-type glutamate receptors, and back-propagation of action potentials when neural firing is evoked.

2) D1Rs binding to dopamine activates the olfactory-type guanine nucleotide-binding protein (G_{olf}), which then activates adenylyl cyclase 5 (AC5) by binding G_α subunit of G_{olf}. AC5 degrades ATP into cyclic adenosine 3',5'-monophosphate (cAMP) [107] which then binds cAMP-dependent protein kinase (PKA), thereby disassociating the catalytic and regulation subunit. The catalytic subunit functions as an active PKA, which activates phosphodiesterase (PDE) and degrades cAMP, forming a negative feedback loop composed of cAMP, PKA, and PDE.

3) Calcium increases by glutamate and PKA activation by dopamine exhibit bidirectional interactions. G_{olf} activation by D1R activates phospholipase C (PLC) in the mGluR pathway to induce calcium release from the ER. Calcium inhibits AC5 [48, 94, 161] and enhances degradation of cAMP by PDE via calmodulin (CaM).

4) CaM binding to calcium activates calcium-calmodulin-dependent protein kinase II (CaMKII), which is also activated by self-phosphorylation of Thr286 and de-phosphorylated by protein phosphatase 1 (PP1) [21, 122, 123]. CaMKII phosphorylates AMPA receptors, which promotes receptor insertion into the postsynaptic membrane.

5) In contrast, calcium activates protein phosphatase 2A (PP2A) [124], which is

also activated by PKA phosphorylation. This mechanism involves several types of PP2A subunits, including catalytic C subunit, regulatory A subunit, and regulatory B subunit. Several subtypes of B subunit exist; one subunit binds calcium and another is phosphorylated by PKA [124, 230]. When these subunits bind the AC complex, PP2A functions as an enzyme and dephosphorylates AMPA receptors.

6) PKA also indirectly promotes phosphorylation of AMPA receptors by inhibiting PP1 via binding inhibitor 1 (I-1) and threonine 34 (Thr34) of DARPP-32 [56, 104–106] phosphorylated by PKA. PP1 activation can be regarded as the disinhibition resulting from release of these inhibitors. PP1 dephosphorylates AMPA receptors and CaMKII.

7) Calcium also activates protein phosphatase 2B (PP2B, or calcineurin) by binding calcium and CaM, and PP2B inhibits or activates AMPA receptors indirectly. PP2B dephosphorylates I-1 and DARPP-32 at Thr34, both of which cause disinhibition of PP1, thereby inhibiting (triple-negative) AMPA receptors. PP2B also dephosphorylates and activates casein kinase 1 (CK1), which self-inhibits via autophosphorylation [153]. Subsequently, CK1 phosphorylates DARPP-32 at serine 137 (Ser137), which then suppresses the speed of PP2B-induced DARPP-32 dephosphorylation at Thr34 [55–57, 134, 136], thereby facilitating (quadruple-negative) AMPA activity. Ser137 is dephosphorylated by PP2C [57], and DARPP-32 phosphorylation at Ser137 decreases the rate of dephosphorylation of phospho-Thr34 by PP2B [56]. CK1 also activates cyclin-dependent kinase 5 (Cdk5), a pathway that remains poorly understood. Therefore, the present study assumes the pathway to be one enzymatic reaction for simplicity. Cdk5 phosphorylates DARPP-32 at threonine 75 (Thr75) [14, 152].

8) Finally, there exists a positive (double-negative) feedback loop, composed of PKA, PP2A, and DARPP-32 at Thr75: i) PKA activates PP2A [230], ii) PP2A dephosphorylates DARPP-32 at Thr75, and iii) DARPP-32 phosphorylated at Thr75 binds and inhibits PKA [15, 173]. PKA, PP2A, and DARPP-32 form a positive feedback loop, where PP2A activation disinhibits PKA [171]. Activation of this positive feedback loop can cause direct and indirect phosphorylation of AMPA receptors by PKA, as well as dephosphorylation by PP2A.

4.2.3 Modeling strategy

The above-described signaling cascade, which links glutamatergic and dopaminergic inputs to AMPA receptor regulation, includes multiple excitatory and inhibitory pathways and feedback loops. This makes logical or intuitive inference of network behaviors virtually impossible; the outcomes depend on the strength and delay associated with each arrow in the diagram.However, logical or intuitive inference of network behaviors becomes virtually impossible, because the outcomes depend on strength and delay associated with each arrow in the diagram. This necessitates numerical simulation of a quantitative model of a signaling cascade to understand and prediction the dynamic behavior.
Therefore, the present study designed a kinetic model of the cascade with the concentrations of intracellular calcium and extracellular dopamine as the inputs and AMPA receptor concentration in the postsynaptic membrane as the output. However the cascade, which links glutamate stimulation to calcium response was not included in this model but will be addressed in a future study.
Similar to most large-scale cascade models, many reactions were adopted from previously published model [15, 56, 65, 139, 149, 210] or deposited the DOQCS database [208]. When available, models of striatal spiny neurons were utilized (e.g., DARPP-32, D1R, and AC5). Otherwise, Otherwise, hippocampal neuron models were adopted (e.g., CaM, CaMKII,PP2B, I-1, and AMPA receptor) by assuming that molecular processes are common between different brain areas. If no previous model was available (e.g., PP2A, PP1, CK1, and Cdk5), a reaction model was designed based on previous literature.

Because many of the reactions remain poorly understood, a number of assumptions and simplifications were necessary to design the cascade models. For instance, although DARPP-32 contains at least four phosphorylation sites that affect its enzymatic properties, phosphorylation of Ser102 by CK2, which facilitates phosphorylation of Thr34 by PKA, was not modeled [81]. This was because the upstream regulation mechanisms for CK2 are now well known. Therefore, an 8-state model was designed for DARPP-32 , with three phosphorylation sites: Thr34, Thr75, and Ser137.

CK1 activation is required for Cdk5 activation [152]. Although the cascade linking these two molecules has not yet been identified, a direct pathway from

CK1 to Cdk5 has been hyphothesized [9]. Although reports have described PP1 phosphorylation by Cdk5 [147], a simple model was adopted from the DOQCS database, where only inhibition and disinhibition by I-1 and Thr34 were taken into account [13].

AMPA receptor trafficking in the postsynaptic membrane was modeled using the state transition diagram shown in Fig. 4.2. AMPA receptors contain two phosphorylation sites - Ser845 phosphorylated by PKA and Ser831 phosphorylated by CaMKII. Therefore, a serial phosphorylation model was proposed for hippocampal neurons [35] where Ser831 was phosphorylated after Ser 845 phosphorylation.

Initially, the model was tested to determine whether it reproduced known features of calcium- and dopamine-dependent plasticity in medium spiny neurons. Subsequently, the dynamic characteristics of the model were analyzed to predict effects of experimental manipulation.

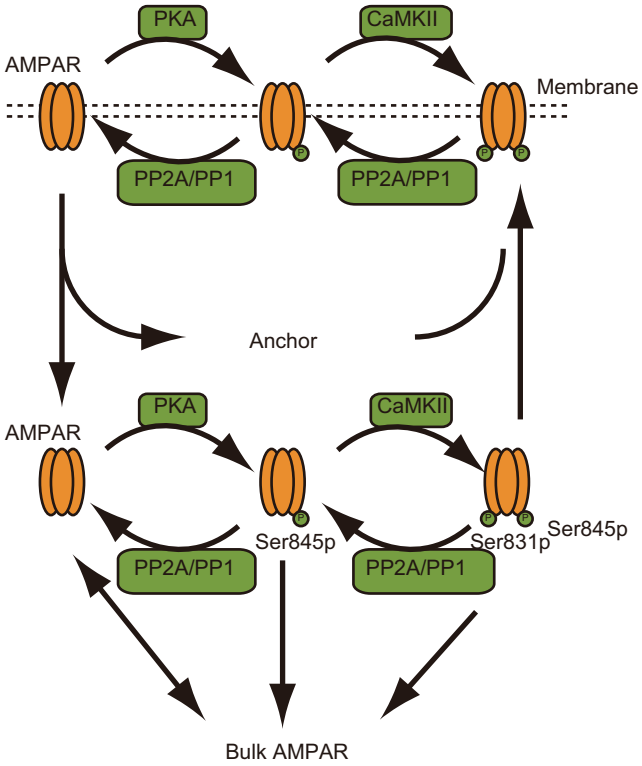

Figure 4.2. Schematic diagram of the AMPA receptor trafficking model. AMPA receptors are phosphorylated at Ser845 and Ser831 by PKA and CaMKII, respectively, and are also dephosphorylated by PP1 and PP2A. The phosphorylated AMPA receptors bind to anchor protein (Anchor) and are inserted into the cell membrane. In contrast, dephosphorylated AMPA receptors are removed from the membrane. AMPA receptors released from anchor protein are degraded and stored in cytosol (Bulk AMPAR)

4.2.4 Parameter setting and simulation

The entire model consisted of 72 reactions, with 132 reaction parameters. Among these, 83 parameters were retrieved from literature and model database. The remaining 49 parameters were hand-tuned to qualitatively reproduce the following properties:

1. The D1R agonist increases Thr34 phosphorylation levels [172], which was used to fit Thr34 responses to dopamine input.

2. Dopamine decreases Thr75 [171], which was used to fit the Thr75 response to dopamine input.
3. Group 1 mGluR agonist increases Thr75, Ser137, and Cdk5 activity [152], which was utilzed to fit Cdk5, Ser137, and Thr75 responses to 1 μM calcium input.
4. Glutamate decreases Thr75 [174], which was used to fit the Thr75 response to 10 μM calcium input.
5. AMPA and NMDA decrease Thr34 and Thr75 [170, 211], which was employed to fit Thr75 and Thr34 responses to 10 μM calcium input.
6. LTD induced by cortical high frequency stimulation leading to small increases in intracellular calcium is blocked by knocking out DARPP-32 [25]. This was used to fit synaptic efficacy by 1 μM calcium input under normal and absence of DARPP-32 conditions.
7. LTP induced by cortical high frequency stimulation in Mg-free solution leading to large increases in intracellular calcium is blocked by knocking out DARPP-32 [25]. This was used to fit synaptic efficacy by 10 μM calcium input under normal and absence of DARPP-32 conditions.

Forms and parameters of all reactions are listed in Appendix B. Because many of the parameters affected multiple features of the model behavior, it was difficult to specify which parameter was responsible for the replication of each property.

Numerical simulations were implemented by GENESIS/kinetikit (http://www.genesis-sim.org/GENESIS/). It was assumed that the postsynaptic spine was a homogeneous volume of 10^{-18} m^3 (1 femtoliter), so that each molecular species concentration represented the state variables.

4.2.5 Input time course

The two inputs to the cascade model comprised the concentrations of intracellular calcium, which were evoked by cortical glutamatergic input, and extracellular dopamine, which were evoked by nigral dopaminergic input. The time courses of the concentrations were approximated by the alpha function

$$\alpha_\tau(t) = \begin{cases} \frac{t}{\tau} \times \exp\left(1 - \frac{t}{\tau}\right) & (t \geq 0) \\ 0 & (t < 0), \end{cases} \tag{4.4}$$

which takes a maximum value of 1 when $t = \tau$.

The intracellular calcium concentration induced by a train of n cortical spikes, which begin at time t_0 with Δt inter-spike interval (ISI), was simulated by

$$\begin{aligned}[Ca^{2+}](t) &= [Ca^{2+}]_{\text{basal}} + [Ca^{2+}]_{\text{stim}} \\ &\quad \times \max\left\{\alpha_{\tau_C}(t - t_0), \alpha_{\tau_C}(t - (t_0 + \Delta t)), \ldots, \alpha_{\tau_C}(t - (t_0 + n\Delta t))\right\},\end{aligned} \tag{4.5}$$

where $[Ca^{2+}]_{\text{basal}}$ and $[Ca^{2+}]_{\text{stim}}$ were the basal level and stimulus amplitude of calcium concentration, respectively (Fig. 4.3A). The maximum function, rather than temporal summation, of calcium transients was used to replicate calcium response data from D1R-expressing striatal neurons [52]. The time constant of the alpha function was $\tau_C = 100$ ms [18, 140]. $n = 20$ spikes at $\Delta t = 10$ ms ISI (100 Hz) were simulated and repeated six times with 10-sec intervals (Fig. 4.3B). The concentrations used in the simulation were as follows: $[Ca^{2+}]_{\text{basal}} = 60$ nM and $[Ca^{2+}]_{\text{stim}} = 0$ to 10 μM.

The extracellular dopamine concentration, which was induced by a single presynaptic spike at time t_0, was simulated by:

$$[DA](t) = [DA]_{\text{basal}} + [DA]_{\text{stim}} \times \alpha_{\tau_D}(t - t_0), \tag{4.6}$$

where $[DA]_{\text{basal}}$ and $[DA]_{\text{stim}}$ were the basal level and stimulus amplitude of dopamine concentration, respectively (Fig. 4.3C). The time constant of the alpha function was $\tau_D = 100$ ms [85, 140]. Dopamine input simulation was repeated six times with 10-sec intervals (Fig. 4.3D). The concentrations used in the simulation were as follows: $[DA]_{\text{basal}} = 10$ nM and $[DA]_{\text{stim}} = 0$ to 2 μM.

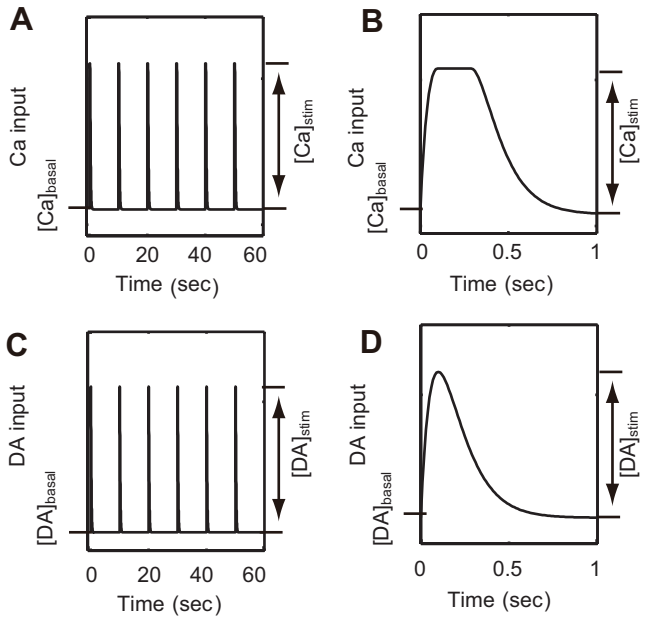

Figure 4.3. Transient time courses from two input sources. (A) Calcium input and (B) magnification from 0 to 1 second. (C) Dopamine input and (D) magnification from 0 to 1 second.

4.3 Results

First, the responses to intracellular molecules and AMPA receptor activation under four different levels of calcium and dopamine inputs were simulated. Then, changes in the post-synaptic AMPA receptors were predicted at different levels of calcium and dopamine inputs. Finally, *in silico* experiments with blockades of different pathways were developed to elucidate the dynamic mechanisms of calcium- and dopamine-dependent plasticity.

4.3.1 Cascade responses to calcium and dopamine inputs

The activities of intracellular molecules were simulated in response to four input conditions: i) weak calcium input alone ($[Ca^{2+}]_{\text{stim}} = 1$ μM and $[DA]_{\text{stim}} = 0$ μM); ii) strong calcium input alone ($[Ca^{2+}]_{\text{stim}} = 10$ μM and $[DA]_{\text{stim}} = 0$ μM); iii) dopamine input alone ($[Ca^{2+}]_{\text{stim}} = 0$ μM and $[DA]_{\text{stim}} = 2$ μM). iv) weak

calcium input coincident with dopamine input ($[Ca^{2+}]_{\text{stim}} = 1$ μM and $[DA]_{\text{stim}} = 2$ μM); The detailed input forms are explained by Eqs. (4)-(6) in Materials and Methods, and the transient time courses are shown in Fig. 4.3. Results are shown in Fig. 4.4.

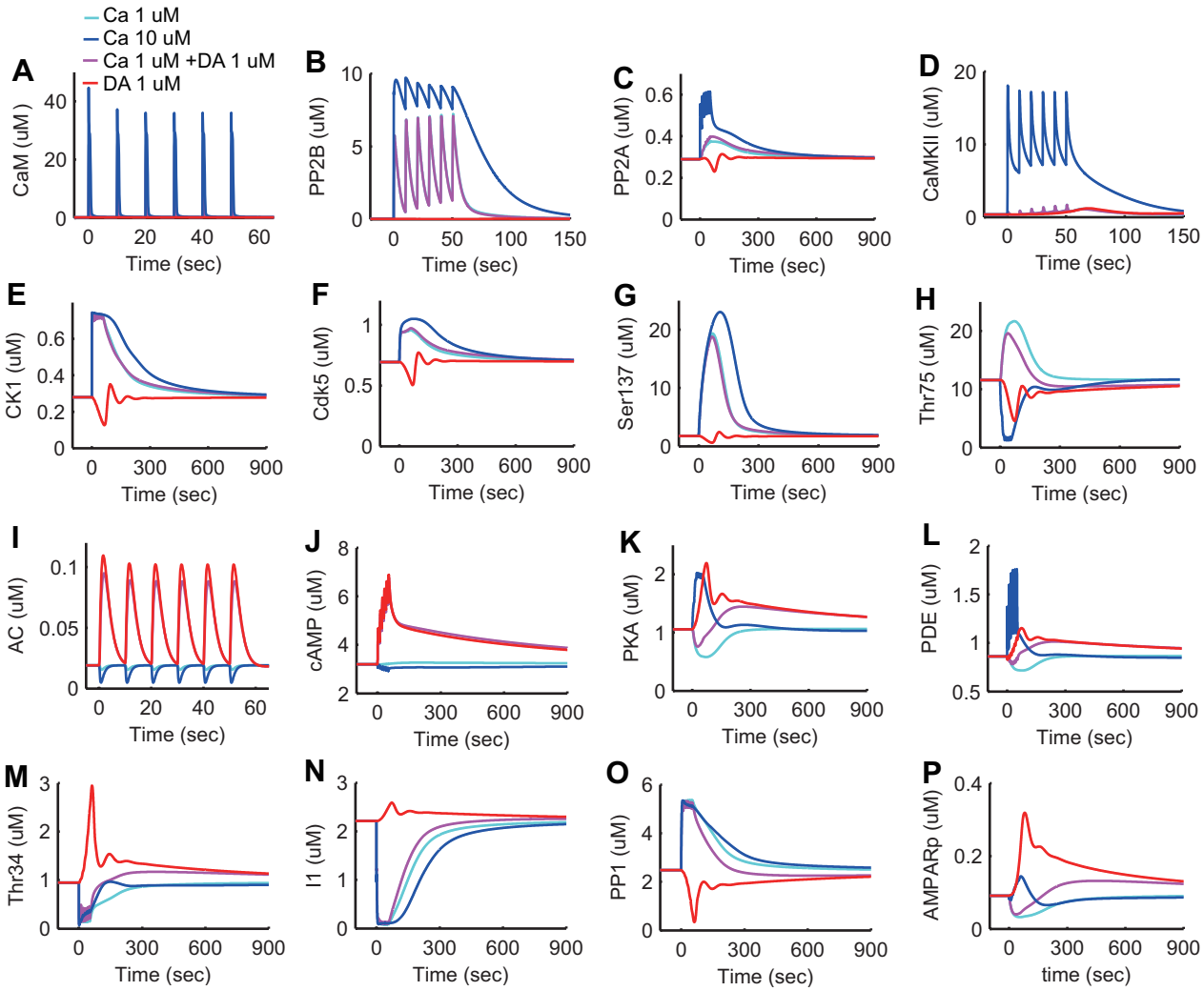

Figure 4.4. Transient activation responses of intracellular molecules from the original model. Line colors denote four different conditions: 1 μM calcium influx without dopamine input (cyan); 10 μM calcium influx without dopamine input (blue); 1 μM calcium influx coincident with 1 μM dopamine input (magenta); and 1 μM dopamine input in the absence of calcium influx (red). (A-O) Each plot indicates the activation state of each protein. (P) AMPARp indicates total concentration of phosphorylated AMPA receptor from at least one phosphorylation site.

Direct downstream of calcium, CaM (Fig. 4.4A), PP2B (Fig. 4.4B), and PP2A

(Fig. 4.4C) were moderately activated by weak calcium input (cyan), but more highly activated by strong calcium input (blue). In contrast, CaMKII (Fig. 4.4D), which self-phosphorylates, did not respond to weak calcium input (cyan), but responded drastically to strong calcium input (blue). The differential activation profiles of PP2A, which dephosphorylates AMPA receptors, and CaMKII, which phosphorylates AMPA receptors, can be a source of bi-directional plasticity due to calcium input.

CK1 (Fig. 4.4E) was activated by PP2B, but the response to strong calcium input was saturated due to a self-inhibitory mechanism. CK1 subsequently activated Cdk5 (Fig. 4.4F) and the Ser137 phosphorylation site of DARPP-32 (Fig. 4.4G).

Phosphorylation of Thr75 in DARPP-32 (Fig. 4.4H) increased with weak calcium input (cyan) via Cdk5 activation (Fig. 4.4F), but decreased with strong calcium input (blue) via PP2A activation (Fig. 4.4C). This bi-directional calcium effect on Thr75 was consistent with experiments showing phosphorylation of Thr75 with a glutamate receptor agonist [170, 174].

Downstream of the D1Rs, AC5 (Fig. 4.4I) increased with dopamine input, but decreased with strong calcium input due to calcium inhibition. cAMP concentration (Fig. 4.4J) increased or decreased depending on AC5 activation level, and subsequently slowly decayed. Phosphorylated PKA (Fig. 4.4K) decreased with weak calcium input (cyan) and increased with strong calcium input (blue), mirroring the bi-directional changes of Thr75 (Fig. 4.4H). PKA increased at a slower rate with dopamine input (red), subsequent to increased cAMP. Simultaneous stimulation of weak calcium and dopamine resulted in a bi-phasic response, including an initial dip followed by a sustained elevation. PDE activation (Fig. 4.4L) was similar to the activation profile of PKA.

Dopamine input (red) resulted in increased Thr34 phosphorylation of DARPP-32 (Fig. 4.4M) via PKA activation. Calcium input (cyan and blue) reduced Thr34 phosphorylation due to stronger inhibition by PP2B. The decreased Thr34 phosphorylation due to calcium input was consistent with experimental results utilizing AMPA and NMDA [170]. Coincident calcium input (magenta) reduced the response of Thr34 to dopamine input (red). These results were consistent with experimental responses to different levels of dopamine and NMDA inputs [211].

Dopamine input alone increased phosphorylation of Inhibitor-1 (I-1) (Fig. 4.4N) via PKA activation. However, I-1 phosphorylation decreased due to either weak or strong calcium input, or simultaneous calcium and dopamine inputs, via PP2B inhibition. Phosphorylation of PP1 (Fig. 4.4O) was opposite to that of I-1 by dopamine input (red), but similarly phosphorylated by both strong (blue) and weak (cyan) calcium inputs, even under simultaneous dopamine input (magenta).

Finally, via phosphorylation by CaMKII (Fig. 4.4D) and PKA (Fig. 4.4K), and dephosphorylation by PP2A (Fig. 4.4C) and PP1 (Fig. 4.4O), AMPA receptor phosphorylation at Ser845 decreased due to weak calcium input, but increased due to strong calcium input and simultaneous calcium and dopamine inputs (Fig. 4.4P).

4.3.2 Dopamine- and calcium-dependent synaptic plasticity

Fig. 4.5A shows the time course of synaptic efficacy (AMPA receptor concentration in the post-synaptic membrane) induced by different levels of dopamine input coincident with a weak calcium input. While the absence of dopamine input caused depression of the synapse (solid), increased dopamine levels resulted in potentiation.

Fig. 4.5B shows the time course of synaptic efficacy in three different levels of calcium input without dopamine input. While weak calcium input causes depression, increased calcium input resulted in potentiation.

Synaptic efficacy was evaluated 10 min after conditioning as an index of long-term synaptic plasticity. Synaptic efficacy increased with increasing dopamine input coincident with calcium input (Fig. 4.5C). In conditions of dopamine depletion, where both $[DA]_{\text{basal}}$ and $[DA]_{\text{stim}}$ were set at 0 μM, the calcium input did not alter synaptic efficacy. These results were in accordance with dopamine-dependent synaptic plasticity [193], as characterized in Fig. 1.4A.

Fig. 4.5D shows synaptic plasticity dependence on calcium input levels in the absence of dopamine input. Weaker calcium input resulted in LTD, but stronger calcium input caused LTP. These results were consistent with previous experimental observations [24, 30, 42], as schematized in Fig. 1.4B.

To further clarify the interactions between calcium and dopamine inputs and the roles of molecules in the signaling cascade, 2D maps of synaptic plasticity

were plotted with different levels of calcium and dopamine inputs using standard and modified models.

Fig. 4.6A shows synaptic plasticity after 10 minutes stimulation in the standard model. LTD was induced by weak calcium input in the absence of dopamine (blue area), and LTP was induced by either strong calcium or strong dopamine input (red area).

When CaMKII activation was fixed at a steady-state level (Fig. 4.6B), increased calcium input did not induce LTP. Rather, LTD occurred only at low levels of dopamine input. When PKA was fixed at the steady-state level (Fig. 4.6C), dopamine-dependent plasticity disappeared. Fixing PP1 produced LTP, regardless of the strength of calcium and dopamine inputs (Fig. 4.6D). The potentiation induced by strong dopamine alone disappeared, because the disinhibition due to decreased PP1 (corresponding to the red line in Fig. 4.4O) was removed.

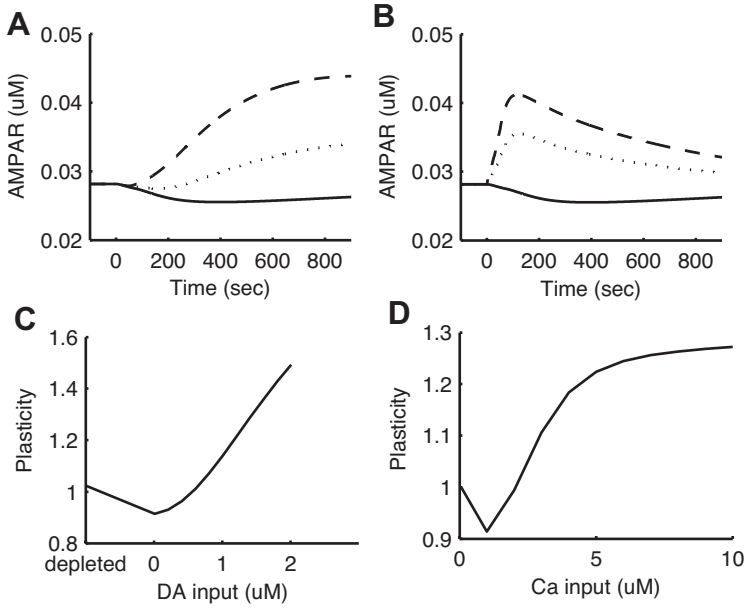

Figure 4.5. Dopamine- and calcium-dependent synaptic plasticity reproduced by the model. (A) Transient time courses of synaptic efficacy induced by 0 μM (solid line), 1 μM (dotted line), and 2 μM (dashed line) dopamine input coincident with 1 μM calcium input. (B) Transient time courses of synaptic efficacy induced by 1 μM (solid line), 3 μM (dotted line), and 5 μM (dashed line) calcium input without dopamine input. In all cases from (A) and (B), input was initiated at 0 seconds and synaptic efficacy was evaluated by the number of AMPA receptors in the post-synaptic membrane. (C) Synaptic plasticity as a function of dopamine input with 1 μM calcium input. The dopamine concentration was fixed at 0 μM in the depleted condition, but set to 0.01 μM steady state in the remaining conditions. (D) Synaptic plasticity as a function of calcium input. For (C) and (D), plasticity was evaluated by the ratio of the number of AMPA receptors in the post-synaptic membrane prior to and 10 minutes after stimulation onset.

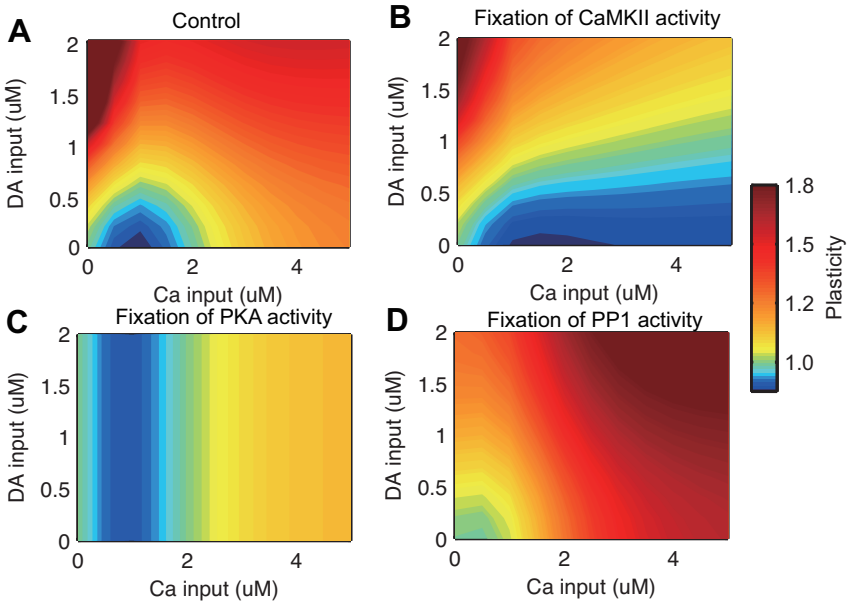

Figure 4.6. Contour plot of synaptic plasticity during dopamine and calcium input. Panels (A-D) show results from four different conditions: (A) control with the original model; (B) fixation of CaMKII activity; (C) fixation of PKA activity; and (D) fixation of PP1 activity. The quantitative evaluation of synaptic plasticity was identical to Fig. 4.5. Green (corresponding to 1.0 in the right color-bar) indicates areas where synaptic efficacy was not altered. Hotter and colder colors indicate areas where LTP and LTD are induced, respectively.

4.3.3 Dynamic mechanisms behind calcium and dopamine-dependent plasticity

4.3.3.1 The role of the CK1-Cdk5 pathway in calcium-dependent plasticity

To determine the mechanisms of bidirectional change in Thr75 phosphorylation due to weak and strong calcium inputs (Fig. 4.4H), Cdk5 and PP2A responses to different levels of calcium inputs were analyzed (Fig. 4.7). Although Cdk5 was steeply activated at a low level of calcium input (Fig. 4.7A), PP2A was gradually activated with increased calcium input levels (Fig. 4.7B). The Cdk5

effect was dominant with a weak calcium input, leading to Thr75 phosphorylation (cyan line in Fig. 4.4H). When Cdk5 was saturated due to stronger calcium input, the stronger effect of PP2A resulted in Thr75 dephosphorylation (blue line in Fig. 4.4H). To verify the role of the CK1-Cdk5 pathway, a simulation was performed with the removal of this pathway. Results demonstrated that inhibition of the CK1-Cdk5 pathway drastically decreased Thr75 phosphorylation under conditions of weak calcium input (red lines in Fig. 4.7C).

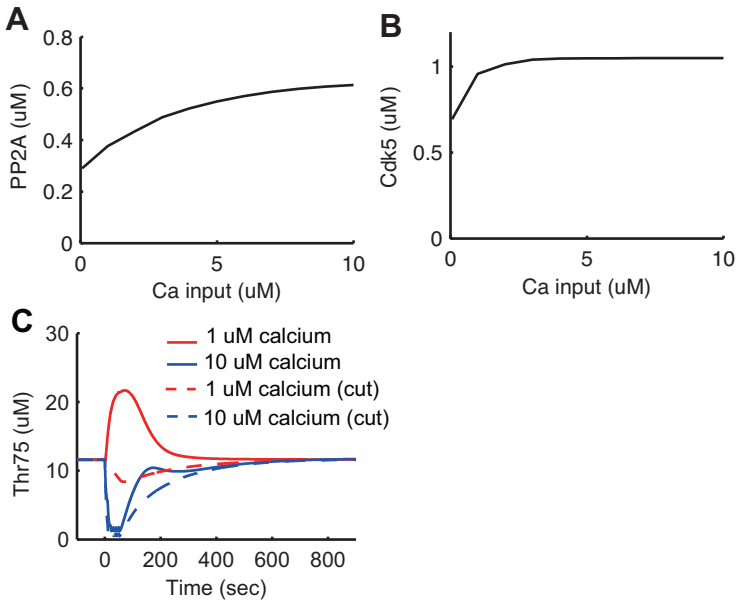

Figure 4.7. The role of the CK1-Cdk5 pathway. The maximum response of (A) Cdk5 and (B) PP2A activities to different levels of calcium input. (C) Altered transient responses of phosphorylated Thr75 by removing the Ck1-Cdk5 pathway. The solid lines are responses from the original model. Dotted lines are the responses from the modified model, where the CK1-Cdk5 pathway was removed from the original model. Different levels of calcium input are denoted by different colors: red for 1 μM calcium input; and blue for 10 μM calcium input.

4.3.3.2 The role of DARPP-32

Although DARPP-32 affects striatal synaptic plasticity, the signaling cascade diagram (Fig. 4.1) includes pathways to PKA and PP1 from either dopamine

input or calcium input without going through DARPP-32.

To examine the role of DARPP-32 in synaptic plasticity, a DARPP-32 knockout was simulated by maintaining a DARPP-32 concentration of 0 μM (Fig. 4.8). Under this condition, dopamine-induced PKA activation became much weaker (Fig. 4.8A) and stayed almost constant with increased calcium input (Fig. 4.8B). Dopamine-induced PP1 inhibition was abolished (Fig. 4.8C), while its activation by calcium input was maintained (Fig. 4.8D).

Fig. 4.9 shows dopamine- and calcium-dependent plasticity in the absence of DARPP-32. Dopamine-dependent plasticity almost disappeared, and calcium-dependent plasticity lost the LTP component and retained only a weak LTD component. These results were consistent with experimental results from DARPP-32 knockout mice [25].

These results suggested: 1) PKA was critical for both dopamine- and calcium-dependent LTP; 2) PP1 played an important role in calcium-dependent LTD; and 3) DARPP-32 played a critical role in the bi-directional regulation of dopamine- and calcium-dependent synaptic plasticity.

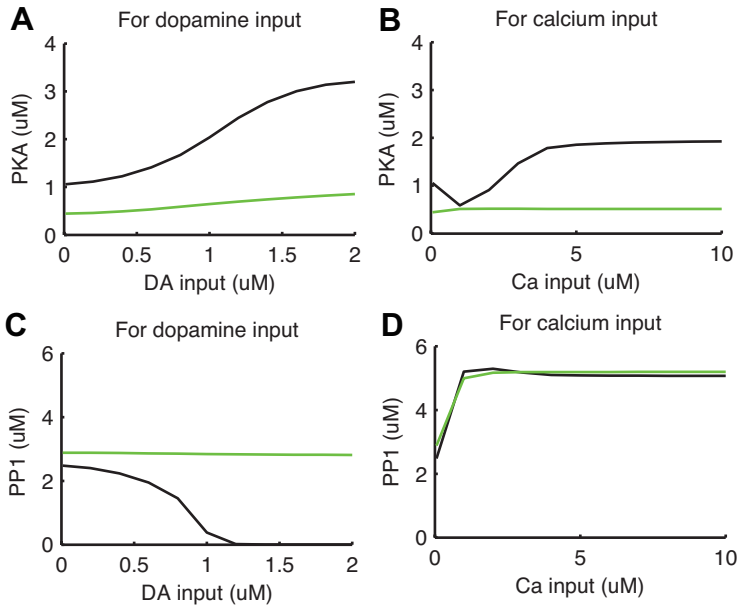

Figure 4.8. Responses of PKA and PP1 in the absence of DARPP-32. (A-B) Maximal responses of active PKA to various levels of dopamine and calcium input, respectively. (C-D) Maximal responses of active PP1 to various levels of dopamine and calcium input, respectively. For all panels, black lines indicate results from the original model (control), and green lines indicate results from the modified model, where DARPP-32 is fixed at 0 μM (DARPP-32 knockout condition).

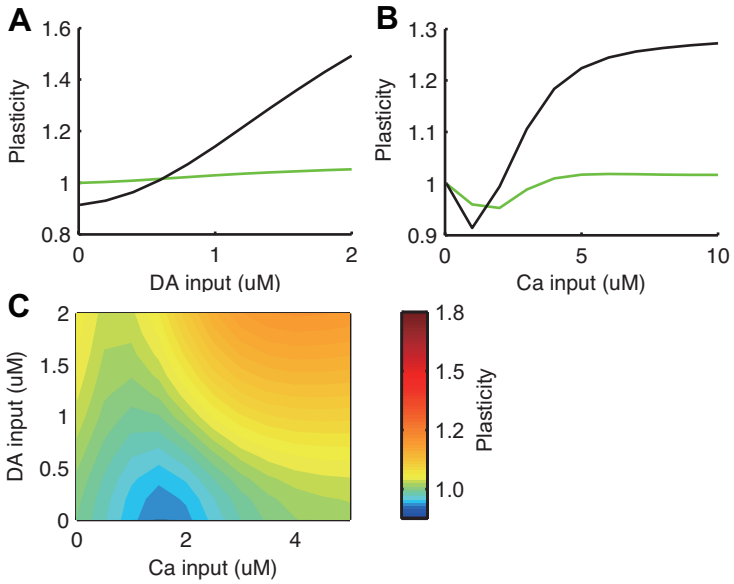

Figure 4.9. Synaptic plasticity in the absence of DARPP-32. (A) Synaptic plasticity due to varying strengths of dopamine input combined with 1 μM calcium input. (B) Synaptic plasticity due to varying strengths of calcium input without dopamine input. Black lines indicate results from the original model (control), and green lines indicate results from the modified model, where DARPP-32 is fixed at 0 μM (DARPP-32 knockout condition). (C) Contour plot of synaptic plasticity in the DARPP-32 knockout condition as a function of calcium and dopamine input.

4.3.3.3 PKA-PP2A-DARPP-32 positive feedback loop

Results from DARPP-32 knockout simulation suggested that direct activation of PKA through the D1R-AC5-cAMP pathway was not sufficient. In addition, amplification via the PKA-PP2A-Thr75-PKA-positive (double-inhibitory) feedback loop played an essential role in LTP induction.

To determine the effects of this positive feedback loop, the sub-network dynamics were analyzed, which consisted of a PKA-PP2A-Thr75 loop containing calcium, Cdk5, and cAMP as parametric inputs (Fig. 4.10A). Calcium and Cdk5 were set to baseline levels, and cAMP concentration was gradually increased starting with 3.2 μM (Fig. 4.10B). The steady-state level of active PKA gradually increased to approximately 1.2 μM, but drastically increased to approx-

imately 1.5 μM when the cAMP concentration exceeded 3.4 μM. In contrast, when the cAMP concentration was gradually decreased from 3.5 μM, steady-state PKA activation gradually decreased to approximately 1.4 μM and then was abruptly reduced to around 1.2 μM as cAMP concentrations fell below 3.33 μM (see Fig. 4.10 caption for an exact description). This hysteresis suggested bistability of the positive feedback loop at intermediate levels of cAMP input.

To more rigorously examine subnetwork bistability (Fig. 4.10A), a steady state analysis was performed with COPASI [116]. For each cAMP and Cdk5 level, steady states were identified from multiple initial states using the Newton method, and stabilities were determined by calculating eigenvalues of the Jacobians. Fig. 4.11A shows the resulting bifurcation diagrams using cAMP level as the parameter. The subsystem exhibited one stable state when cAMP was less than 3.29 μM or greater than 3.41 μM. In the cAMP middle range, the subsystem exhibited three steady states: two asymptotically stable steady states and one unstable steady state in the middle. Bistability was also observed in an analysis using Cdk5 level as the parameter (Fig. 4.11B).

Fig. 4.11C shows the bifurcation diagram of the two-dimensional parameter space by cAMP and Cdk5 levels. Two planes of stable steady states (blue and red) existed, which were connected by a band of unstable stable states (not shown for clarity). The higher Cdk5 level shifted the threshold of cAMP input for PKA activation (the end of blue plane) higher. As Cdk5 is activated by the calcium input and cAMP is activated by the dopamine input, this interdependency of Cdk5 and cAMP for PKA activation could be a cause of calcium and dopamine interaction in producing LTP and LTD. In fact, this bifurcation diagram is consistent with my analysis of the plasticity in the 2D parameter space of calcium and dopamine inputs shown in (Fig. 4.6B), where the activation of AMPA receptors by CaMKII was held constant. In addition, PKA trajectories from several initial conditions were confirmed and plotted in Fig. 4.11D. The trajectories converged toward one of the two stable steady states.

To test the robustness of the threshold dynamic of the positive feedback loop, the dissociation constants in the loop were varied up to ten-fold. The stationary concentration of active PKA, which started at a low initial level (1.2 μM), was observed with different level of Cdk5. As shown in Fig. 4.12, active steady

state PKA abruptly decreased (failed to increase to the upper branch) when initial Cdk5 concentrations exceeded a threshold. Although the threshold value of Cdk5 varied according to altered dissociation constants, the threshold behavior was robust under wide ranges of model parameters. These results suggested that bistable dynamics of the positive feedback loop by PKA, PP2A, and Thr75 of DARPP-32 contributed to a robust nonlinear threshold response of PKA.

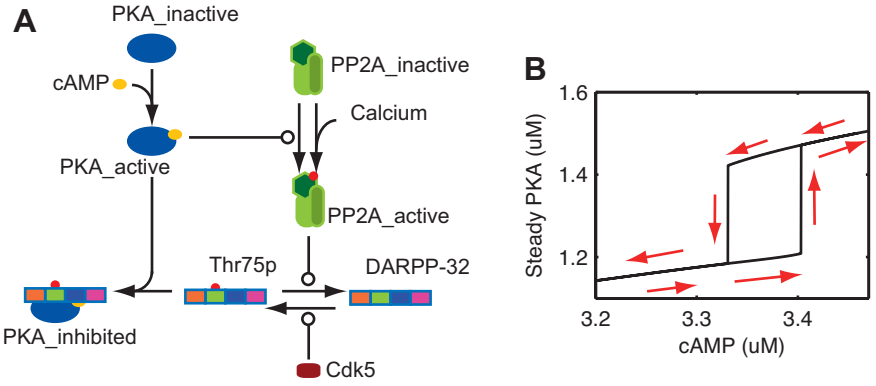

Figure 4.10. Hysteresis of PKA-PP2A-DARPP-32 positive feedback loop. (A) Schematic diagram of the sub-network forming the PKA-PP2A-DARPP-32 positive feedback loop. Blocks indicate different molecular states. Specifically, DARPP-32 has four phosphorylation cites (Thr34, Thr75, Ser102, and Ser137), which are indicated by different colors in this diagram. Round arrowheads are enzymatic actions and red dots indicate phosphorylated states. (B) Active PKA changes at steady states, with gradual changes in cAMP concentration at fixed concentrations of calcium at 0.06 μM and Cdk5 at 0.67 μM. First, cAMP concentration was set to 3.2 μM, and active PKA steady state was calculated by COPASI. Subsequently, cAMP concentration was increased by a step of 0.003 μM to 3.5 μM, and steady state level of active PKA was calculated at each setting. Next, cAMP concentration was reduced by a step of 0.003 μM to 3.2 μM, and steady state of active PKA was analyzed again. The arrows along the lines show the direction of the trajectory in the two-dimensional space of cAMP conditions and steady states of active PKA.

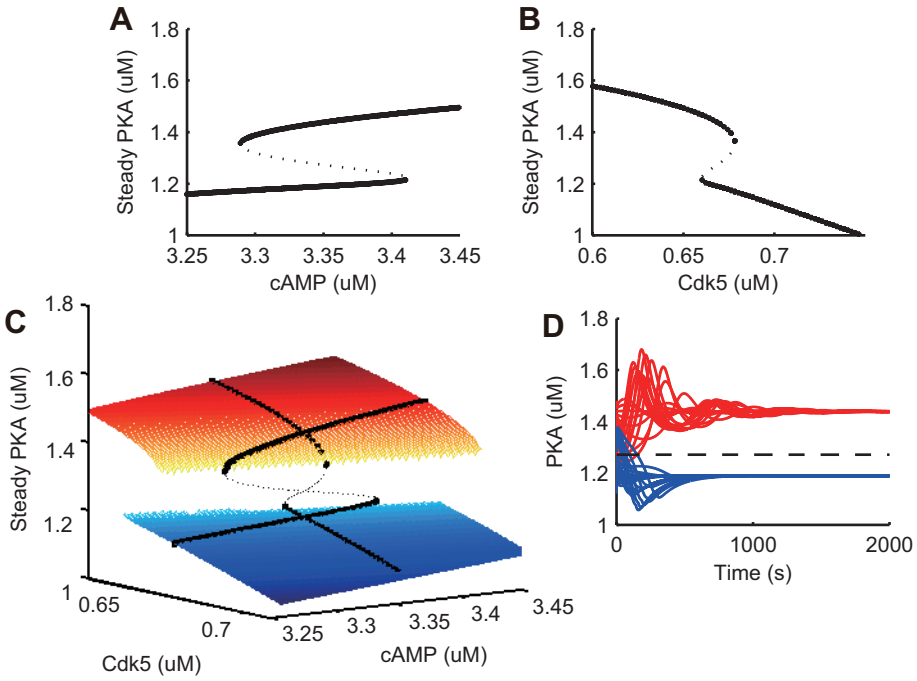

Figure 4.11. Bi-stability of PKA-PP2A-Thr75 positive feedback. (A, B) Bifurcation diagrams created by identification of steady states using the Newton method and determination of stabilities using the eigenvalues of the Jacobian. Large points indicate stable steady states and small points indicate unstable steady states. (A) Bifurcation diagram for the altered cAMP, with fixed parameters of 0.06 μM calcium and 0.67 μM Cdk5. The subsystem has one stable state when cAMP is less than 3.29 μM or greater than 3.41 μM. At middle range of cAMP, three steady states exist: two stable states and one unstable state. (B) Bifurcation diagram for the altered Cdk5, with fixed parameters of 0.06 μM calcium and 3.352 μM cAMP. The subsystem has one stable state when Cdk5 is less than 0.66 μM or greater than 0.68 μM. At middle range of Cdk5, three steady states exist: two stable states and one unstable state. (C) Steady state level of PKA in the 2D parameter space of cAMP and Cdk5. The calcium concentration was fixed at 0.06 μM. The blue and red planes are steady states of PKA at low and high levels, respectively. The black dots indicate steady states with Cdk5 fixed at 0.67 μM or cAMP fixed at 3.352 μM, as plotted in panels A and B. (D) PKA trajectories from several initial conditions at a cAMP level of 3.352 μM and Cdk5 level of 0.67 μM. The trajectories funnel toward a stable steady state. The dotted line indicates PKA levels at an unstable steady state.

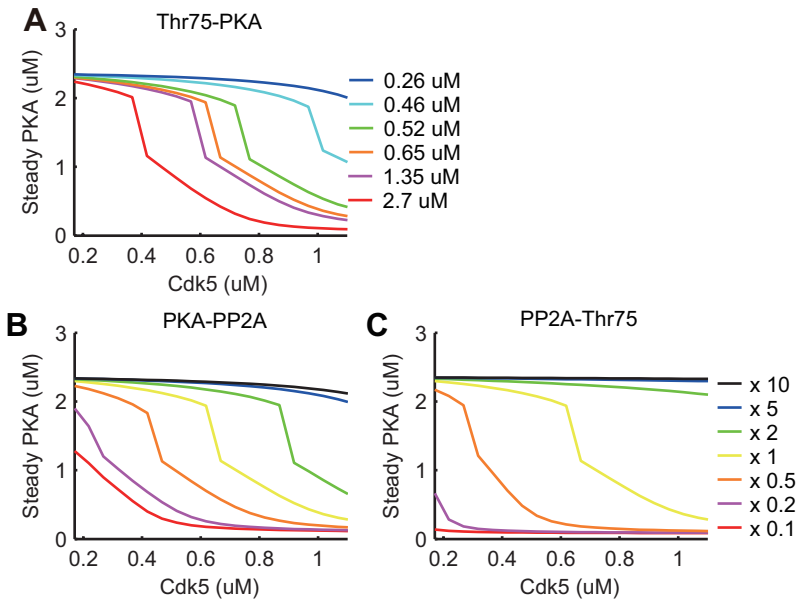

Figure 4.12. Robustness of the PKA-PP2A-DARPP-32 positive feedback loop. (A-C) Robustness of the threshold-like PKA activation as a function of total concentration of Cdk5 in the sub-system shown in Fig. 4.10, when three parameters were independently altered: (A) A dissociation constant Kd in a reaction where Thr75 is dissociated from inhibited PKA, was given by 0.26 μM (blue), 0.46 μM (cyan), 0.52 μM (green), 0.65 μM (orange), 1.35 μM (magenta) or 2.7 μM (red); (B) A catalytic constant k_{cat} in a reaction where active PKA phosphorylates PP2A, is given by 10 times (black), 5 times (blue), 2 times (green), control (yellow), 0.5 times (orange), 0.2 times (magenta), 0.1 times (red), larger than the control value in the original model (yellow); and (C) A catalytic constant k_{cat} in a reaction where active PP2A dephosphorylates Thr75, is given by 10 times (black), 5 times (blue), 2 times (green), control (yellow), 0.5 times (orange), 0.2 times (magenta), 0.1 times (red), larger than the control value in the original model (yellow). Please note that the dissociation constant Kd in panel (A) was set at 0.52 μM in my original model while it was said to be 2.7 μM in an experimental study [105].

4.3.3.4 Baseline dopamine level

It was analyzed how striatal plasticity is affected by the baseline concentration of dopamine, which is known to be altered in Parkinson's disease and drug addiction (Fig. 4.13). At increased basal levels of dopamine ($[DA]_{\text{basal}} = 0.02$ μM;

dotted lines), the steady-state levels of active PKA and phosphorylated AMPA receptor were two times greater than control levels ($[DA]_{\text{basal}} = 0.01$ μM; solid lines). From this high-level initial state, even strong calcium input, as well as simultaneous calcium and dopamine inputs, resulted in LTD. Because initial levels of PP1 decreased (Fig. 4.13C) with increasing PKA inhibition (Fig. 4.13B) and responded in a larger amplitude to both calcium and dopamine inputs, causing dephosphorylation of AMPA receptors. Under dopamine depletion conditions ($[DA]_{\text{basal}} = 0$ μM; dashed lines), the steady-state level of the phosphorylated AMPA receptor was less than the control ($[DA]_{\text{basal}} = 0.01$ μM). Because of a decreased active PKA steady state, active PP1 level was initially higher with decreased responses to both calcium and dopamine inputs. This resulted in LTP with calcium input, as well as simultaneous calcium and dopamine inputs (Fig. 4.13D, dashed lines).

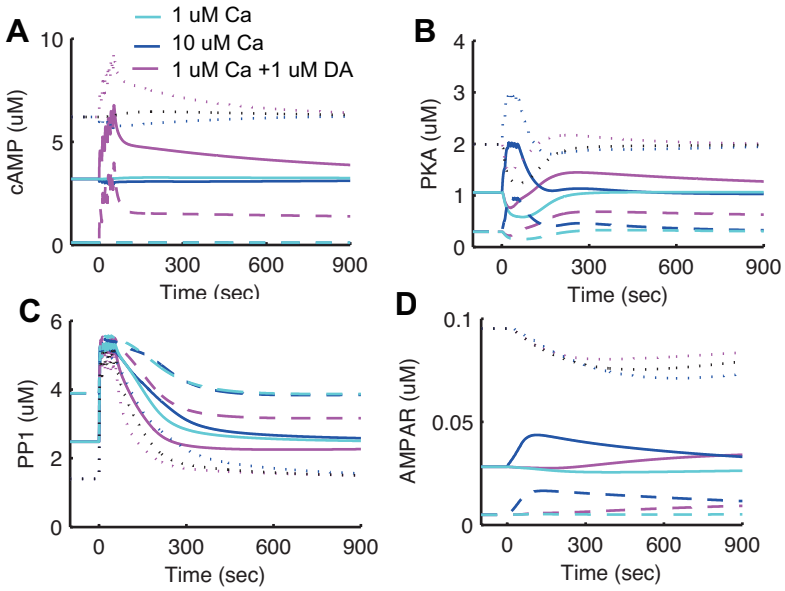

Figure 4.13. Transient responses at high basal dopamine levels. Time courses of (A) cAMP, (B) PKA, (C) PP1 and (D) AMPA receptor in the post-synaptic membrane, respectively, when basal dopamine level was altered. The cyan lines indicate 1 μM calcium influx, the blue lines indicate 10 μM calcium influx without dopamine input, and the magenta lines indicate 1 μM calcium influx together with 1 μM dopamine input. The solid lines indicate the 0.01 μM basal dopamine (control) condition, the dotted lines indicate the 0.02 μM condition, and the dashed lines indicate the 0 μM basal dopamine (dopamine depletion) condition.

4.3.3.5 Timing of calcium and dopamine inputs

The effect of calcium and dopamine input timing was tested under three conditions: 1) simultaneous initiation of calcium and dopamine inputs (control); 2) dopamine input preceding calcium input by 500 ms (DA preceding condition); and 3) dopamine input following calcium input with a 500-ms delay (DA following condition). Differences in input timing affected the AC5 response, with the DA following condition resulting in the greatest amplification(Fig. 4.14A). The amplified AC5 response was propagated through cAMP (Fig. 4.14C) to PKA (Fig. 4.14D). As a consequence, LTP was most effectively induced when dopamine input followed calcium input (Fig. 4.14E).

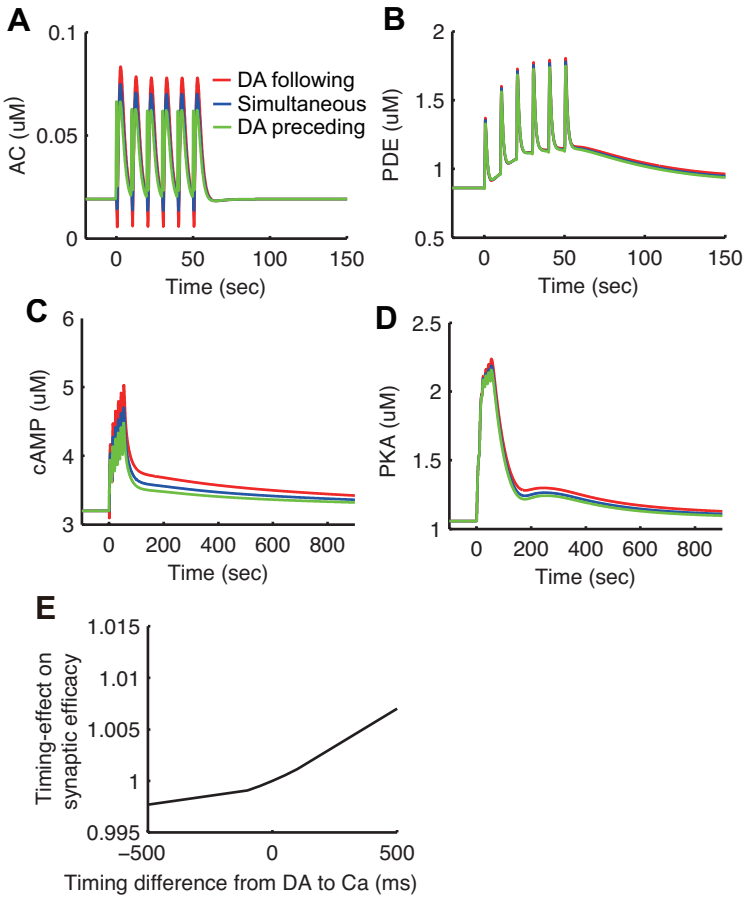

Figure 4.14. Transient responses to different temporal orders of calcium and dopamine inputs. (A-D) Time courses of AC, PDE cAMP, and PKA, respectively, in responses to 10 μM calcium and 1 μM dopamine input. Line colors denote four different temporal orders: dopamine followed by calcium with a 500 ms delay (red line); dopamine together with calcium (blue line); dopamine preceding calcium with a 500 ms delay (green line); (E) Timing-dependent plasticity when 1 μM dopamine input and 1 μM calcium input are given. The timing-effect on synaptic efficacy, denoted by the horizontal axis, was evaluated as the fraction of the synaptic efficacy in each timing condition over that in the condition where dopamine and calcium inputs were given simultaneously.

4.4 Discussion

To understand corticostriatal synaptic plasticity at the molecular level, a signaling cascade model for a single spine of a striatal medium spiny neuron was constructed. Strong calcium influx induced PKA activation through the PP2A-DARPP-32 pathway, which resulted in LTP. PKA was normally inhibited by DARPP-32 phosphorylation at Thr75. In addition, weak calcium input resulted in DARPP-32 phosphorylation at Thr75 through the PP2B-CK1-Cdk5 pathway, which ultimately resulted in PKA inhibition and LTD. In contrast, a strong calcium influx resulted in PP2A dephosphorylation at Thr75, ultimately disinhibiting (activating) PKA and leading to LTP. Previous studies have shown that CaMKII, not PKA activation, causes hippocampal LTP [151]. However, a marked feature of the striatal synaptic plasticity is that both CaMKII and PKA activation contribute to calcium-dependent LTP.

Dopamine activatd PKA through the AC5-cAMP pathway and then PKA activity was amplified by a PKA-PP2A-DARPP-32 positive feedback loop, leading to a threshold phenomenon. PKA phosphorylated AMPA receptors directly and indirectly reduced dephosphorylation of AMPA receptor by PP1 through DARPP-32 on Thr34 and I-1. These dual pathways provided for a robust regulation of AMPA receptor by PKA.

The major findings of this study are discussed below in relation to previous modeling and experimental studies.

4.4.1 Comparison with previous models

Several studies have modeled signal transduction in medium spiny neurons [9,65, 149]. The novelty of the present model is the incorporation of AMPA receptor phosphorylation and membrane trafficking to directly assess the effects of cascade dynamics on striatal synaptic plasticity. This allowed for the reproduction of both LTD and LTP in calcium- and dopamine-dependent plasticity and to predict interactions between calcium and dopamine inputs, as shown in Fig. 4.6, and effects of various manipulations on striatal synaptic plasticity. Embedding of the present model in a complete neuronal model, or even a neural network model, enables the assessment of the role of calcium- and dopamine-dependent plasticity in cellular and network functions. The model can also serve as the

basis for building simplified signaling cascade models for large-scale simulation and theoretical analysis.

The present signaling cascade model involving DARPP-32 differs from previous models in several points. The factors incorporated by this model but not by existing models [9,65,149] were inhibition of PDE by PKA, Ser137 effect on Thr34, and inhibition of PP1 by I-1. The CK1-Cdk5 pathway, which has been previously described [9], was critical for reproducing bidirectional phosphorylation of Thr75, which was dependent on calcium input intensity. In addition, the present study performed a rigorous analysis of bistability of positive feedback loop formed by PKA, PP2A, and DARPP-32 on Thr75, which was a source of a threshold-like response of PKA activity to both dopamine and calcium inputs.

The model prediction of Thr34 and Thr75 responses to dopamine and calcium input were consistent with the Fernandez model [65] if the calcium input levels from the Fernandez model were regarded as the strong calcium input for the present model. However, simultaneous calcium and dopamine inputs resulted in Thr34 dephosphorylation in the present model, but phosphorylation in the Lindskog model [149]. This discrepancy could be due to inactivation by the calcium-PP2B-Thr34 pathway was stronger than activation by the PKA-Thr34 pathway in present model.

4.4.2 CK1-Cdk5 pathway

DARPP-32 phosphorylation on Thr75 has been shown to because of glutamate, AMPA, or NMDA exposure, but returns to normal level within 10 min [170,174]. In addition, an mGluR agonist has been shown to potentiate Cdk5 activation and phosphorylation of DARPP-32 on Thr75 and Ser137, and returns to baseline levels after peaking at 2 min [152]. Assuming that an mGluR agonist induced weak calcium levels, and glutamate, AMPA, or NMDA produced strong calcium input, those experimental results were consistent with the present results, as shown in Fig. 4.4H.

In present model, phosphorylation of DARPP-32 on Thr75, as a result of weak calcium input, takes place through the CK1-Cdk5 pathway. Although CK1 activation is required for Cdk5 activation through signaling from mGluR [152], it is not known whether the pathway from CK1 to Cdk5 is direct. Similar to a

previous model, the present study assumed direct activation of Cdk5 by CK1 for simplicity [9]. Alternative mechanisms for inhibition of PP2A dephosphorylation on Thr75 exist - either through the calcium-AC5-cAMP-PKA pathway or the calcium-CaM-PDE-cAMP-PKA pathways. More quantitative data on the strengths of these pathways and additional *in silico* experiments are necessary to definitely determine the role of the CK1-Cdk5 pathway in calcium-dependent LTD.

4.4.3 AMPA receptors

AMPA receptor trafficking in the present model was derived from Hayer's model [103]. The primary modification comprised sequential phosphorylation of Ser845 by PKA followed by Ser831 phosphorylation by CaMKII, as proposed by Lee *et. al.* [143]. However, the LTP mechanism in the present striatal model differed from the hippocampal LTP by Lee *et. al.* [143]. Previous results demonstrated that the phosphorylation of Ser845 did not increase during LTP [143], and the present model showed that the phosphorylation of Ser845 increased during dopamine-dependent LTP, but did not increase during calcium-dependent LTP. In addition, PKA was required for striatal LTP [25] To address this feature in the present striatal model, most of the AMPA receptors were dephosphorylated at the baseline. This prediction was consistent with the lower phosphorylation level of Ser845 by reduced PKA levels due to inhibition by DARPP-32 in the striatum [210].
It should be noted, however, that the observation of sequential AMPA receptor phosphorylation by Lee *et al.* [143] in the hippocampus did not exclude a parallel phosphorylation model. It could be interpreted as a result of high PKA and low PPI concentration at the baseline in the hippocampus. It is a subject of future study whether a parallel phosphorylation model can also reproduce the striatal synaptic plasticity.

D1-type neurons express GluR1 and GluR2/3 in the spines [11, 53]. A previous hippocampal study [183] showed that GluR1 subunit trafficking was a result of stimulation, but that GluR2 subunit trafficking was constitutive. In addition, chronic treatment with the antidepressant maprotiline increases GluR1, but not GluR2 [223]. Moreover, GluR2-lacking AMPA receptors exhibit larger single-channel currents than GluR2-expressing AMPA receptors [222]. For these rea-

sons, trafficking of GluR1, but not GluR2, was modeled in the present study to ascertain whether synaptic plasticity responded to stimulus.
Some theoretical studies [36, 50] have predicted that NMDA receptor-mediated calcium influx results in bidirectional synaptic change. However, these studies modeled only AMPA receptor phosphorylation, but not trafficking, and also did not consider striatal synaptic plasticity.

Although the present model considered the number of AMPA receptors in the postsynaptic membrane as a measure of synaptic efficacy, previous studies have suggested that the conductance of AMPA receptor varies according to the phosphorylation state. For example, Ser831 phosphorylation increases conductance [54] and Ser845 phosphorylation increases open probability [8,194]. If these effects are taken into consideration, the amplitude of LTP could be larger, as observed in experiments [28, 30, 192, 235].

4.4.4 Bistability and long-term plasticity

Threshold dynamics due to the bistability of the positive feedback loop of PKA, PP2A, and Thr75 on DARPP-32 played an important role in reverting the LTD to LTP in dopamine-dependent plasticity. However, when embedded into the entire system, the loop did not exhibit complete bistability, as demonstrated by gradual conversion of synaptic conductance to baseline levels (Fig. 4.15). The possible mechanisms for longer-lasting synaptic plasticity are described below.
First, bistability of some proteins in the cascade has been reported, such as the bistability of CaMKII phosphorylation [103]. However, CaMKII activity did not last for an extended period of time in the present model. This was consistent with a previous study [144], which reported that CaMKII activity returns to baseline within 2-5 min. Hayer *et. al.* observed bistability of AMPA receptor phosphorylation and Catellani *et. al.* [35] mathematically determined bistability in the sequential AMPA receptor phosphorylation model. These bistable mechanisms were not incorporated in the present model, but may contribute to synaptic changes over longer periods of time.
Second, the present model did not consider increased levels of AMPA receptors and other proteins as a result of gene transcription. A possible link from the current model to longer-term synaptic plasticity is cAMP-response element binding

protein (CREB), which controls gene transcription for longer-term synaptic plasticity in the striatum [16]. CaMKII, PKA, and PP1 directly activate CREB, but also indirectly via extracellular signal-regulated kinase (ERK), which activates CREB [86, 119]. In addition, calcium activates mitogen-activated protein kinase kinase (MEK), which activates ERK [31].
PP1 activates striatal enriched phosphatase (STEP) [184], which inhibits ERK, and PKA inactivates STEP. As a result, CREB is inhibited by PP1 and activated by CaMKII and PKA. Therefore, activation of CaMKII and PKA, as well as inhibition of PP1, which results in AMPA receptor phosphorylation, can also trigger gene transcription through CREB activation.

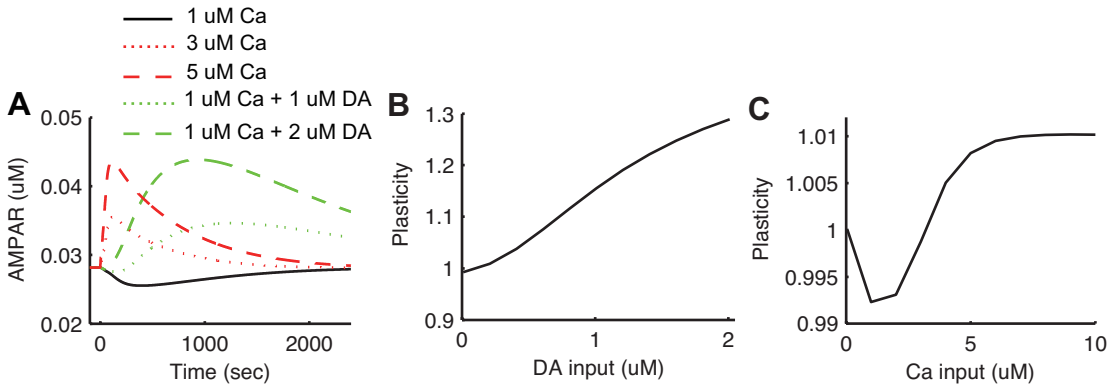

Figure 4.15. Synaptic plasticity at 40 min (A) Time course of AMPA receptors. The black line indicates 1 μM calcium input. The red dotted and dashed lines indicate 3 μM and 5 μM calcium input, respectively. The green dotted and dashed lines indicate 1 μM and 2 μM dopamine input combined with 1 μM calcium input, respectively. (B, C) Synaptic efficacy after 40 minutes of input ratio to pre-stimulus. Characteristics of dopamine- and calcium-dependent synaptic plasticity remain.

4.4.5 Model robustness

Approximately half of the model parameters were based on previous reports and databases [15, 56, 65, 139, 149, 208, 210], and the remaining half were designed to reproduce experimental findings [107, 152, 170–172, 174, 190, 211]. Model behavior robustness was determined by altering the kinetic parameters of the PKA-PP2A-Thr75 loop up to ten-fold (Fig. 4.12). Persistence of nonlinear threshold behavior,

despite shifts in thresholds, was also verified. Although the present model parameters reflected some uncertainty, the model served as a useful starting point for exploring the mechanisms influencing corticostriatal synaptic plasticity by testing alternative parameter values or incorporating additional pathways. The present model did not include a number of known pathways such as the effect of DARPP-32 Ser102 on phosphorylation of Thr75 [164].

4.4.6 Different types of corticostriatal synaptic plasticity

Membrane potential of striatal medium spiny neurons shifts between up- and down-states, depending on cortical inputs [237]. During the up-state, LTP is induced by cortical stimuli, even without dopamine input [2, 45, 46, 213]. LTP is also induced by cortical stimulation in a magnesium-free solution [24, 30, 42]. Both cases reflect calcium-dependent plasticity because of the large calcium influx through NMDA receptors.

Two types of medium spiny neurons exist: D1 receptor-expressing neurons that project to the direct pathway, and D2 receptor-expressing neurons that project to the indirect pathway [77,78]. In D1 neurons, dopamine increases cAMP via G-proteins and AC5, similar to the present model. However, in D2 neurons dopamine inhibits AC5 and decreases cAMP so the effect of dopamine input is opposite to that in D1 neurons.

4.4.7 Striatal synaptic plasticity and reinforcement learning

Schultz *et. al.* recorded the activities of dopamine neurons in the substantia nigra in monkeys and found that dopamine neurons encode error signals of reward prediction [202].

The reinforcement learning model of the basal ganglia posits that striatal neurons learn to compute expected reward based on the reward prediction error signal carried by dopamine neuron firing [202]. Dopamine-dependent synaptic plasticity plays a major role in learning. The medium spiny neurons are depolarized by glutamatergic inputs from the cortex that represent a sensory or a contextual state. When the acquired reward is more than expected, phasic dopamine neuron firing would induce LTP of the activated corticostriatal synapses. On the other hand, if the reward is less than expected, a pause in dopamine neuron

firing would cause LTD of those synapses. The glutamatergic input would not only cause depolarization and firing, but also induce changes in molecular states, such as the phosphorylation level of DARPP-32 and/or shift the threshold of the positive feedback loop, which would serve as the short-term memory of preceding states.

To support this scenario, the temporal order of calcium and dopamine input is a critical factor. Assuming that calcium flux by glutamatergic input is a fast process, the synaptic efficacy should be potentiated when calcium input (associated with a sensory or contextual state) precedes dopamine input (associated with a reward prediction error signal). My model is consistent with this point (Fig. S1). On the other hand, my model also predicts that the effect of the temporal order on synaptic plasticity is not strong enough. This suggests additional interactions between dopamine and calcium signaling. For example, dopamine modulates channels and , which affect the calcium influx through the interaction of glutamate receptor activation and back-propagating action potentials. To more precisely simulate calcium dynamics, I constructed a whole neuron model (see Section 3) and combined it with the signaling cascade model (see Section 5).

4.4.8 Dopamine-calcium interaction

There are several interaction pathways between calcium and dopamine signaling. In the upstream of PKA, calcium directly inhibits AC5 and indirectly cAMP through CaM and PDE. While calcium inhibition of AC5 depended on the timing between calcium and dopamine, PDE inhibition of cAMP did not depend on this timing very much. The stronger interaction of dopamine and calcium on PKA was through DARPP-32. Weak calcium input inhibited PKA through the phosphorylation of Thr75 by Cdk5, but strong calcium input activated PKA through the dephosphorylation of Thr75 by PP2A. While dopamine input reduced the increase of Thr75 by a weak calcium input, it did not affect the decrease of Thr75 by a strong calcium input.

Furthermore, the subsystem around the PKA-PP2A-DARPP-32 positive feedback loop showed bistability while PKA activity showed a threshold like response to cAMP activation by dopamine input. However, this loop became mono-stable with both activation of Cdk5 by a weak calcium input, leading to a low level of

PKA, and by activation of PP2A by a strong calcium input, leading to a high level of PKA.

4.4.9 Drugs and DARPP-32

Addictive drugs (e.g. cocaine and amphetamine) increase the basal level of dopamine by inhibiting the reuptake of dopamine and facilitating the release of presynaptic dopamine [165]. They ultimately decrease DARPP-32 phosphorylation on Thr75 and increase it on Thr34 [98]. In my model, increased basal dopamine levels caused LTD with the calcium and dopamine inputs which caused LTP under control conditions (Fig. 4.13). This result is consistent with the theory that the value of everything except for drugs decreases because of the impairment of appropriate learning in drug addiction [1].

4.4.10 More realistic modeling

My model is a deterministic model. However the number of molecules involved was in the region of several dozen to hundreds. This might be too small a number for deterministic simulation because few molecules are likely to behave randomly. For the positive feedback loop, stochastic factors may break or alter the characteristics of the bistability. Stochastic simulation would, therefore, be a logical next step.

In addition, my model assumed a spine as a single compartment. For more realistic simulation, it would better to consider diffusion. My model considered insertion into the postsynaptic membrane, but not diffusion. In hippocampal neurons, it was reported that the phosphorylated AMPAR was inserted into the membrane at the spine neck. The AMPAR then diffused and moved to the spine head [179].

Moreover, I considered only postsynaptic changes in this study. However, there are other factors to regulate the synaptic efficacy, for example, release probability from presynapse, the number of release sites, vesicle contents, diffusion of transmitters, spine size, spine shape dynamics and glutamate receptors conductance. Presynaptic elements, such as endocannabinoids, are also involved in synaptic plasticity [73, 154] Adding these elements to my model would make it more realistic.

5. Multi-Scale Model of Synaptic Plasticity in the Striatum

5.1 Introduction

So far, I have constructed an electric compartment model to predict calcium responses to the timing of inputs, including dopamine.I also constructed a molecular cascade model in the striatal medium spiny neuron and predicted the molecular dynamics underlying bidirectional plasticity of corticostriatal synapses depending on calcium and dopamine. However each stand-alone model could not predict synaptic changes due to physiological events; however, integration of these models make this possible.

In addition, according to the prediction of the electric compartment model, the timing dependence of peak and leaky integration of calcium were different. The leaky integration of calcium response was better fitted to experimental results from the cerebellum [224]. In the cerebellum, a positive feedback loop, consisting of PKC, Raf, MEK, MAPK, PLA2, and AA, leaky integrates calcium signals and induces cerebellar LTD [224]. Although the PKA-PP2A-DARPP-32 positive feedback loop possibly works as a leaky integrator of calcium, the results from the signaling cascade model did not show such a function.

Here, I integrated the signaling cascade model and the electric compartment model to predict synaptic change by physiological timed events and to understand the mechanisms of information processing as integration of these signals at the cellular and molecular levels. Furthermore, I investigated whether peak or leaky integration of calcium was more accurate to approximate changes in synaptic efficacy. I also investigated the underlying molecular mechanisms.

5.2 Integration of two models

The signaling cascade model and the electric compartment model operate at different levels, one is at the molecular level and the other is at the cellular level. In particular, the time scales and spatial scales were different. This made it difficult to combine the models. In a real brain, dopamine modulation of channels and receptors is mediated through signaling cascades. Here, for simplicity, I

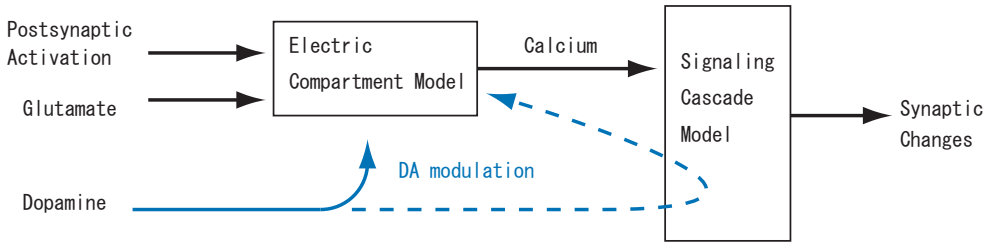

Figure 5.1. Multilevel modeling. The electric compartment model predicts calcium response to glutamate, dopamine, and activation of medium spiny neurons. The signaling cascade model predicts changes in synaptic efficacy induced by dopamine and calcium input. Combining them can predict synaptic efficacy by physiological triggers. A simple connection is that dopamine directly modulates the calcium prediction from the electric compartment model (solid arrow). In an actual neuron, dopamine modulation of calcium is through intracellular chemicals (dashed arrow).

just used output of the electric compartment model as a calcium input for the signaling cascade model (Fig. 5.2). To connect models, dumped files from the electric compartment model were manually loaded into the cascade model. The electric compartment model included dopamine modulation but not dopamine itself. That is, the time course of dopamine concentration was not considered. In the integration model, the time course of the dopamine concentration was approximated by the alpha function of Equation 4.6 from the signaling cascade model. Unless otherwise noted, the original parameter settings in Chapter 3 were used to calculate calcium change.

5.3 Simulations

5.3.1 High frequency stimulation

I first tested cortical high frequency stimulation (HFS) with postsynaptic spikes. 100 Hz cortical HFS was paired with supra-spike threshold depolarization of the postsynaptic cell for 0.1 s. The HFS was repeated 6 times with 10 s intervals (Fig. 5.3). Calcium change was generated by stimulation in the electric compartment model and applied to the signaling cascade model.

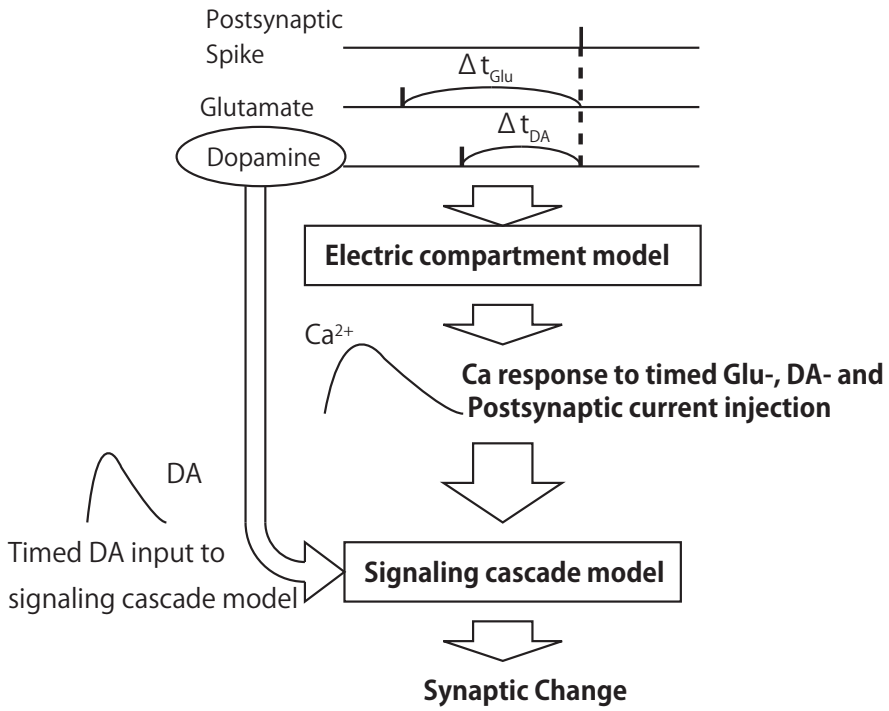

Figure 5.2. Procedure for the integration of models. The electric compartment model produced calcium responses to timed inputs of glutamate, dopamine and postsynaptic spike. The calcium transient was inputted to the signaling cascade model with timed dopamine input keeping the same timing as was used in the electric compartment model. Finally the signaling cascade model predicted synaptic change.

As a result, the calcium response in the down-state was bigger than that in the up-state. Synaptic efficacy showed short-term potentiation which did not last long. When synaptic efficacy was evaluated 10 min after the onset of input, it was potentiated in the up-state and depressed in the down-state. This corresponded with calcium (membrane potential) dependent synaptic plasticity.

Next, HFS was applied with timed dopamine input. Three timings were tested: $\Delta t_{DA} = -50$ ms, $\Delta t_{DA} = 0$ ms, and $\Delta t_{DA} = 50$ ms, in which dopamine timing Δt_{DA} was relative to the onset of HFS and had positive values when dopamine was preceded the HFS. As a result, calcium response and synaptic efficacy was potentiated when $\Delta t_{DA} > 0$ ms. Synaptic efficacy was potentiated more at $\Delta t_{DA} = 0$ ms than at $\Delta t_{DA} = 50$ ms. This was because dopamine effect lasted only 100 ms at most. In all cases, the larger the calcium level, the higher the induction of synaptic efficacy.

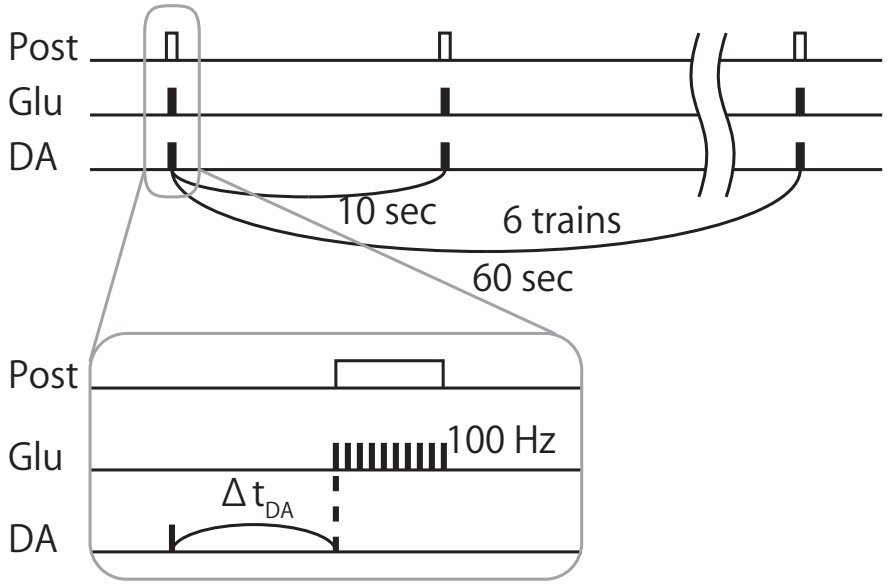

Figure 5.3. High frequency stimulation. Glutamate inputs were applied at 100 Hz with 0.1 s supra-threshold postsynaptic depolarization. This paired stimulation was repeated 6 times with 10 s intervals. Lower figure is an enlarged illustration of the upper figure. In some cases, stimulation contained dopamine input with timing, Δt_{DA}, relative to the onset of postsynaptic current injection.

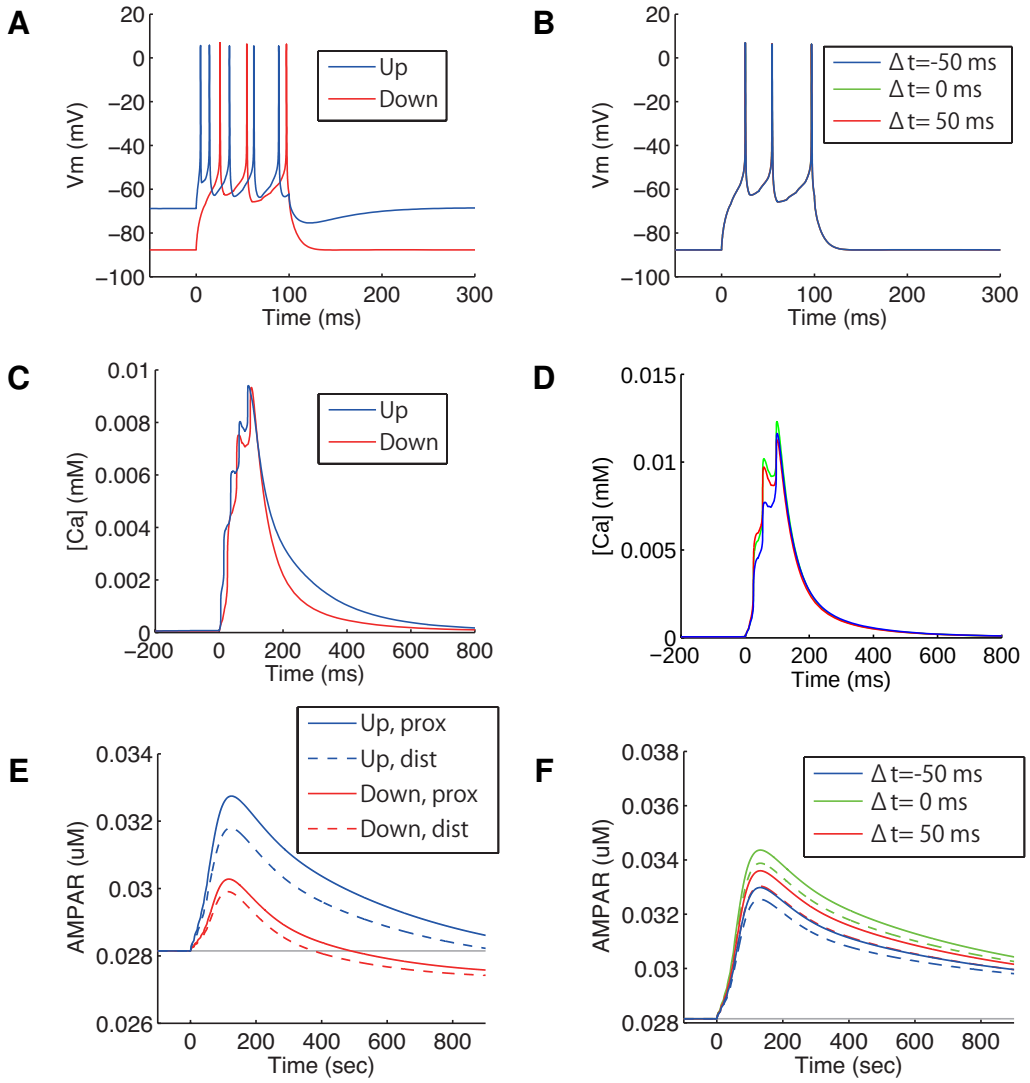

Figure 5.4. Synaptic plasticity by HFS. (A) Voltage and (C) calcium responses to HFS in the down-state (red) and up-state (blue). (B) Voltage and (D) calcium responses to HFS with dopamine input. Dopamine input was applied once at the timing of $\Delta t_{\mathrm{DA}} = -50$ ms (blue), $\Delta t_{\mathrm{DA}} = 0$ ms (green) and $\Delta t_{\mathrm{DA}} = 50$ ms (red). (E) Synaptic changes induced by calcium input of (C). The line colors are the same as in (C). The solid lines indicate a proximal spine and the dashed lines indicated a distal spine. (F) Synaptic changes induced by calcium input of (D) and timed dopamine inputs. The line colors are the same as in (D). The solid lines indicate a proximal spine and the dashed lines indicated a distal spine.

5.3.2 Spike-timing dependent plasticity

Spike-timing dependent plasticity was tested. In the simulation, glutamate input was paired with a postsynaptic spike with timing, Δt_{Glu}, which was the same as in Chapter 3. To evoke the postsynaptic spike, 2 ms current pulses were injected to the soma. Pawlak *et. al.* used glycine which is an NMDAR agonist [185], and NMDAR conductance was then multiplied 5 times in the simulation. In STDP studies, a pairing stimulation was normally repeated at low-frequency (LFS). For example, Fino *et. al.* used 100 pairing stimulations at 1 Hz, Pawlak *et. al.* used 60 pairing stimulations at 0.1 Hz, Shen *et. al.* used 10-15 trains of five bursts repeated at 0.1 Hz, with each burst composed of three bAPs and EPSPs at 50 Hz. In the simulation, the calcium change was repeated 100 times at 1 Hz (Fig.5.5) [66, 185, 204].

The calcium responses to timed glutamate input, which were obtained from the electric compartment model, are shown in Fig. 5.6 (A-C). The calcium responses were applied to the signaling cascade model as inputs. Then the calcium induced synaptic changes and the AMPAR concentration, 10 min after input, were evaluated (Fig. 5.6). This showed LTD in $\Delta t_{Glu} < 0$ ms and LTP in $\Delta t_{Glu} < 0$ ms in proximal spines. Although it still showed LTD for large negative Δt_{Glu}, it reproduced normal STDP. The shape of the STDP curve was similar to the curve of leaky integration of calcium rather than to that of peak calcium.

Next, four types of conditions were tested: a) a 2 ms current pulse was used to evoke a postsynaptic spike in the original parameter settings in the electric compartment model, which was the same as in Fig. 5.6, b) same as a) but a 30 ms current pulse was used, c) same as a) but in high AMPAR and low NMDAR conductance parameter settings, and d) same as c) but a 30 ms current pulse was used. As a result, normal STDP was reproduced in condition b) as well as in condition a). The model in high AMPAR and low NMDAR conductance parameter settings showed small differences among the glutamate timings and the shape was not consistent with any known STDP. The shapes of STDP curves in all four conditions were similar to the curve of leaky integration of calcium rather than to that of peak calcium.

For some simulated experiments, some protein activations were fixed at basal levels (Fig. 5.10). Although the fixation of PKA, PP2A and PP1 did not affect

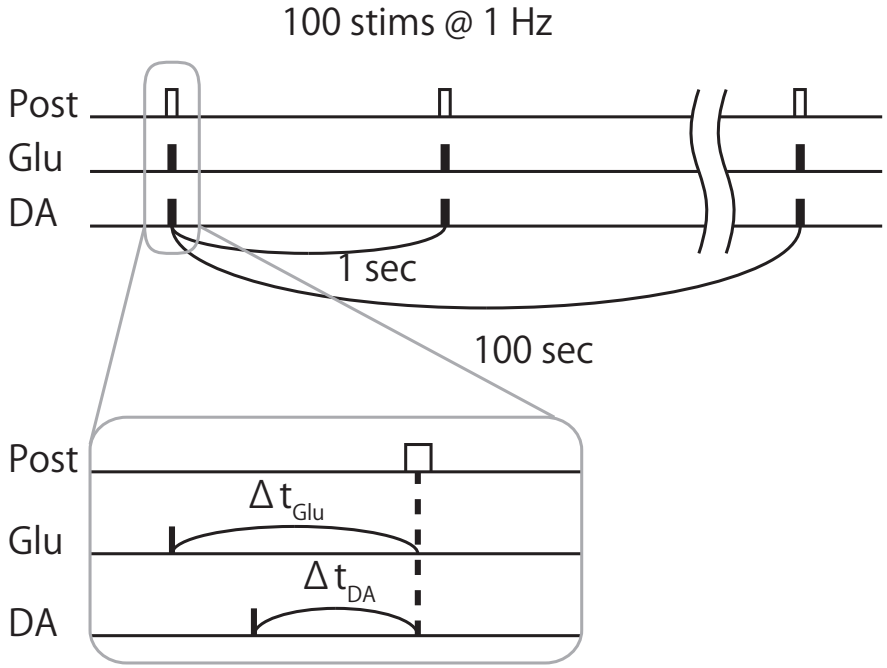

Figure 5.5. Low frequency stimulation. Timed stimulation of glutamate, dopamine and postsynaptic spike was repeated 100 times at 1 Hz. The lower figure is an enlarged illustration of the upper figure. Each stimulation contained timed glutamate input (and dopamine input) relative to postsynaptic spike with Δt.

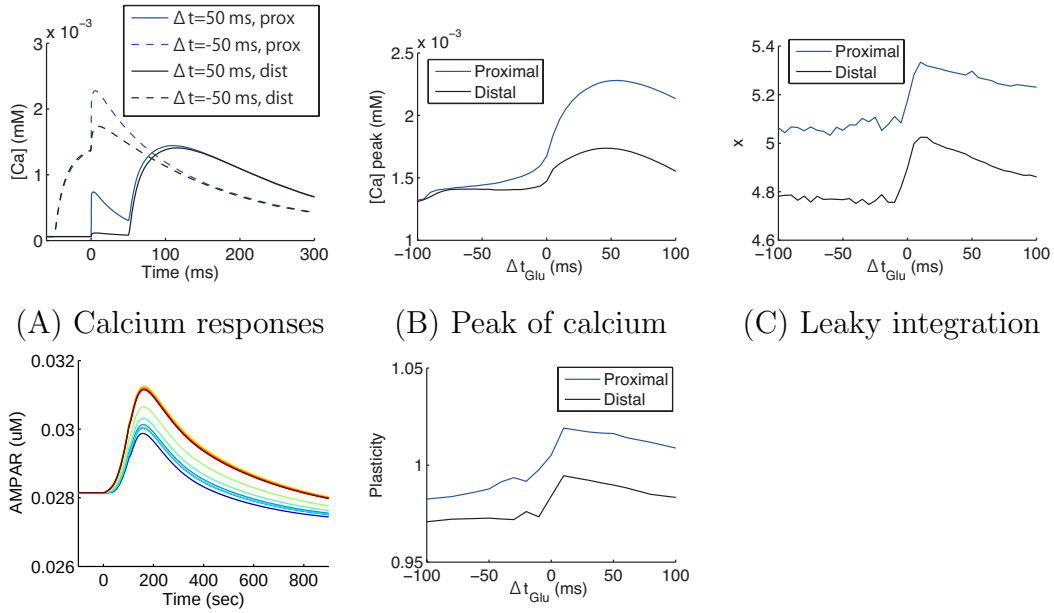

(A) Calcium responses (B) Peak of calcium (C) Leaky integration

(D) Synaptic changes (E) STDP

Figure 5.6. STDP. (A) Calcium response to $\Delta t_{\mathrm{DA}} = 50$ ms (dashed lines) and $\Delta t_{\mathrm{Glu}} = -50$ ms (solid lines) in proximal (blue) and distal (black) spines. (B) Peak and (C) leaky integration of calcium responses to glutamate timing at proximal (blue) and distal (black) spines. Leaky integration was calculated with Equation 3.38 with τ of 600 ms and a of 20. (D) Synaptic changes induced repeated calcium input mimicking LFS of timed input of glutamate and postsynaptic spike. Red-tinged color indicates $\Delta t_{\mathrm{Glu}} > 0$ ms and blue-tinged color indicates $\Delta t_{\mathrm{Glu}} < 0$ ms. (E) Synaptic plasticity evaluated at 10 min after onset of LFS in proximal (blue) and distal (black) spines.

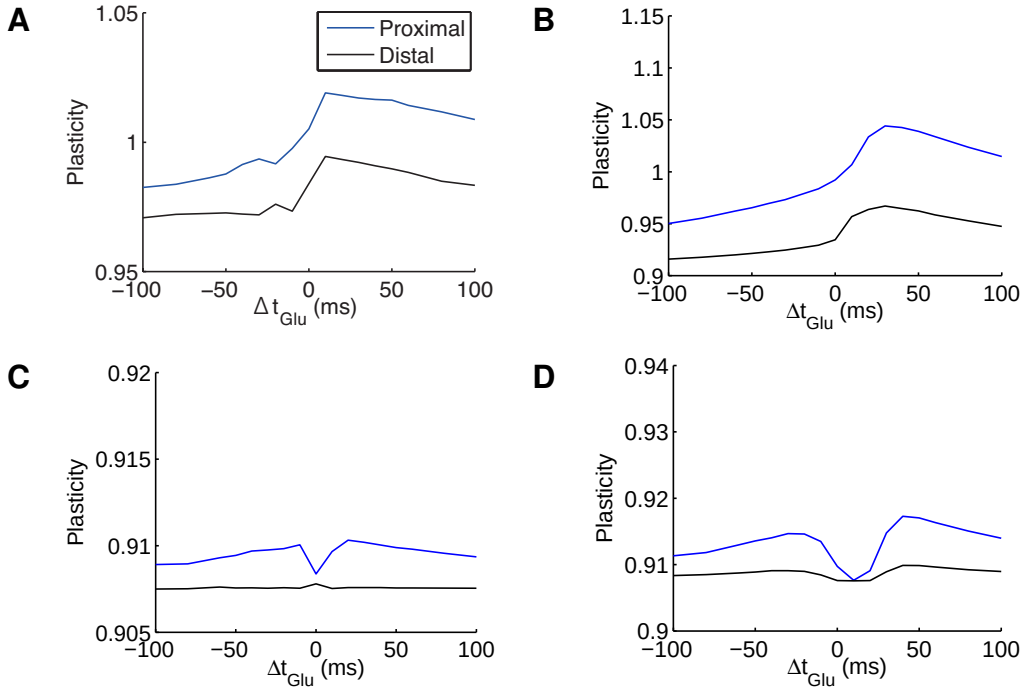

Figure 5.7. Comparison of STDPs. STDPs were evoked by LFS as in Fig. 5.6 but using different conditioning inputs. (A, B) Original parameter settings and (C, D) the other parameter settings which include a high AMPAR/NMDAR conductance ratio. (A, C) 2 ms (B, D) 30 ms postsynaptic current pulses were used to evoke postsynaptic spikes at proximal (blue) and distal (black) spine.

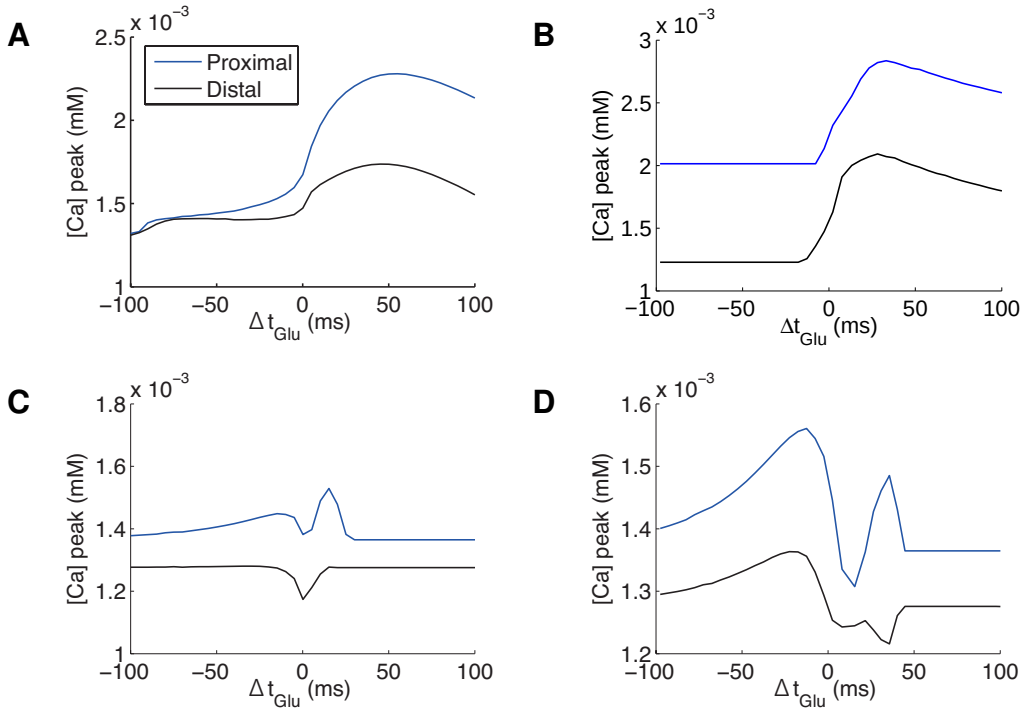

Figure 5.8. Comparison of calcium peaks. The calcium peaks used were those used in Fig. 5.7. (A, B) Original parameter settings and (C, D) the other parameter settings which include a high AMPAR/NMDAR conductance ratio. (A, C) 2 ms (B, D) 30 ms postsynaptic current pulses were used to evoke postsynaptic spikes at proximal (blue) and distal (black) spines.

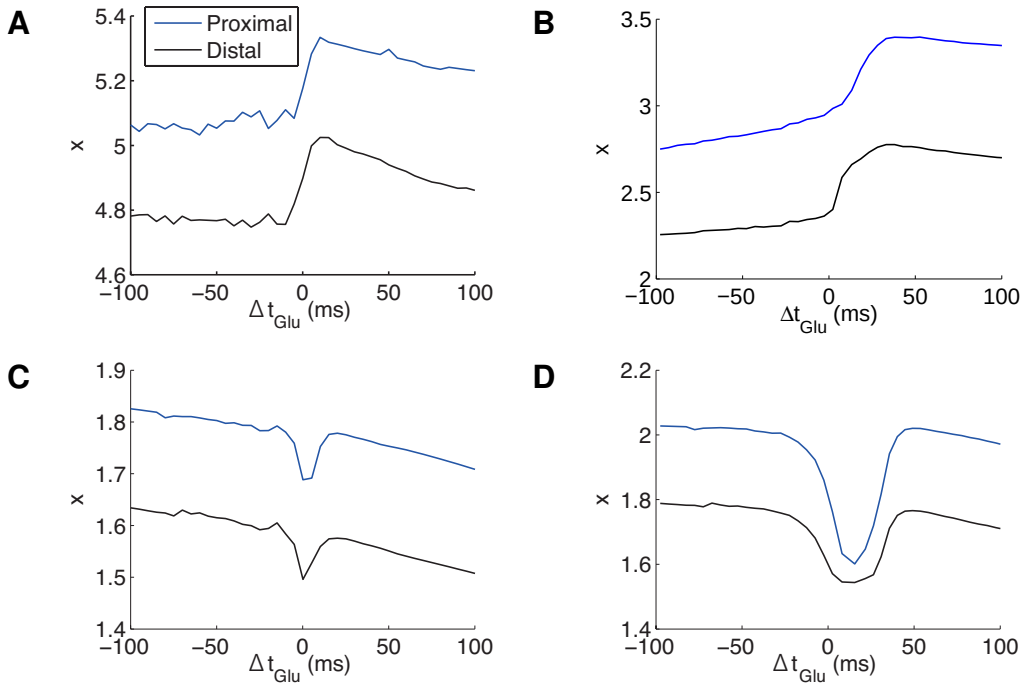

Figure 5.9. Comparison of leaky integration of calcium. The leaky integration of calcium values used were those used in Fig. 5.7. (A, B) Original parameter settings and (C, D) the other parameter settings which include a high AMPAR/NMDAR conductance ratio. (A, C) 2 ms (B, D) 30 ms postsynaptic current pulses were used to evoke postsynaptic spikes at proximal (blue) and distal (black) spines.

the STDP curve, the fixation of CaMKII activation did disturb the STDP curve.

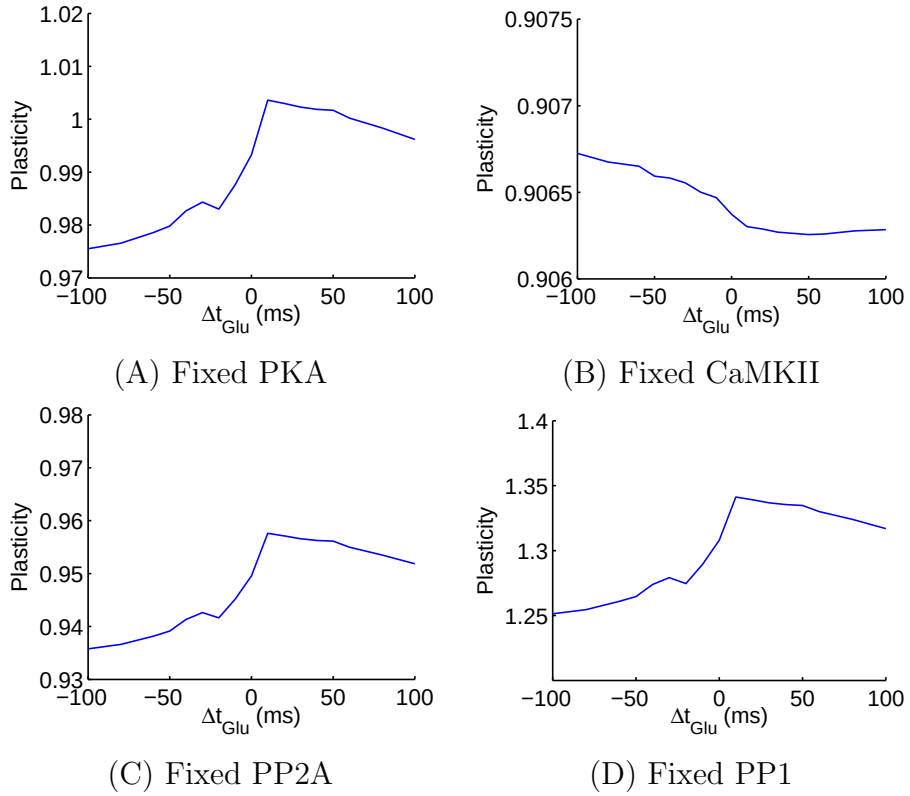

(A) Fixed PKA (B) Fixed CaMKII

(C) Fixed PP2A (D) Fixed PP1

Figure 5.10. Synaptic efficacy with fixation of enzymatic activity. The same experiment as shown in Fig. 5.7, but activation levels of (A) PKA, (B) CaMKII, (C) PP2A, and (D) PP1 were fixed at their basal levels.

5.3.3 STDP with dopamine

Dopamine input was applied to the STDP of glutamate and postsynaptic spike. Dopamine was applied to the electric compartment model and then the calcium response was calculated. Dopamine was also applied to the signaling cascade model using the same timings, and the stimulations were also repeated 100 times at 1 Hz. The shape of each dopamine input used was the same as in Section 4. Amplitude of dopamine input was 0.02 μM. The results showed that LTP was observed with dopamine for all timings of glutamate and dopamine.

To see the dopamine timing effect, I tested tricky dopamine input: although the value of the calcium input used in the signaling cascade model were obtained from the electric compartment model by inputs, including dopamine, dopamine input was not used in the signaling cascade model. In other words, dopamine input was used only for obtaining calcium input to the signaling cascade model. As a result, the STDP curves were similar to the dopamine presence conditions. The dopamine timing effect was not via the signaling cascade model, but via calcium. There was little effect of dopamine timing in the signaling cascade model; it functioned only for the elevation of synaptic efficacy in the signaling cascade model.

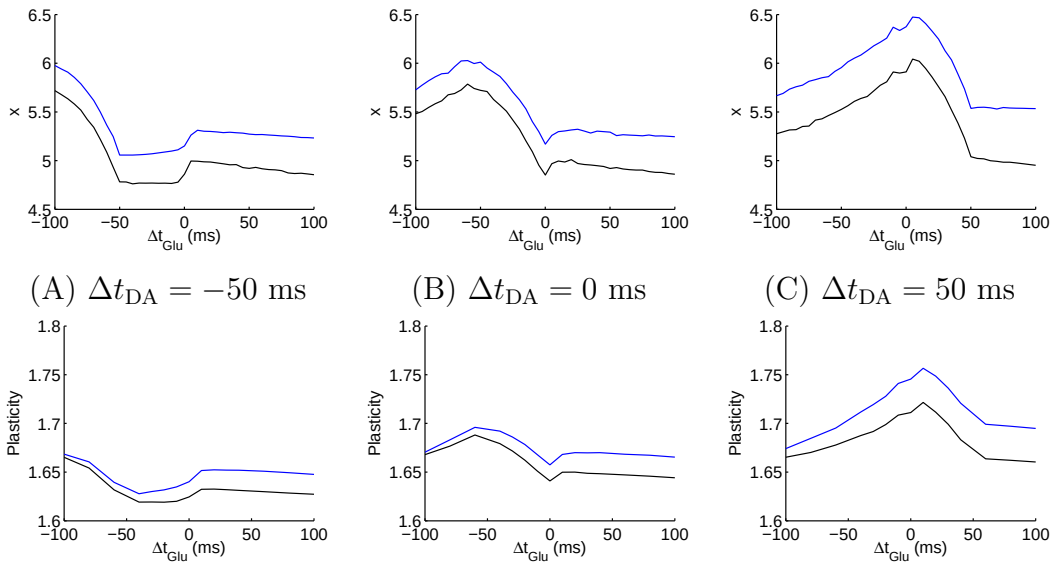

(A) $\Delta t_{\mathrm{DA}} = -50$ ms (B) $\Delta t_{\mathrm{DA}} = 0$ ms (C) $\Delta t_{\mathrm{DA}} = 50$ ms

(D) $\Delta t_{\mathrm{DA}} = -50$ ms (E) $\Delta t_{\mathrm{DA}} = 0$ ms (F) $\Delta t_{\mathrm{DA}} = 50$ ms

Figure 5.11. STDP with timed dopamine. Dopamine was applied to the signaling cascade model with calcium generated by the electric compartment model. Dopamine input was applied at the timing of (A, D) $\Delta t_{\mathrm{DA}} = 0$ ms, (B, E) $\Delta t_{\mathrm{DA}} = 100$ ms and (C, F) $\Delta t_{\mathrm{DA}} = -100$ ms relative to postsynaptic spike. (A-C) Leaky integration of calcium response for $\Delta t_{\mathrm{DA}} = -50$ ms, $\Delta t_{\mathrm{DA}} = 0$ ms, and $\Delta t_{\mathrm{DA}} = 50$ ms in proximal (blue) and distal (black) spines. (D-F) Synaptic plasticity in proximal (blue) and distal (black) spines.

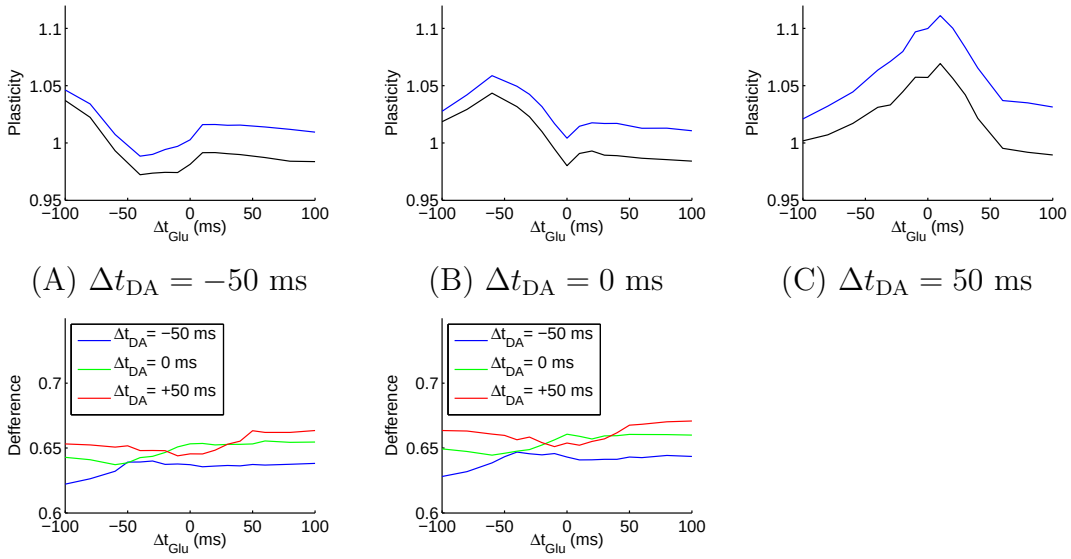

(A) $\Delta t_{\mathrm{DA}} = -50$ ms (B) $\Delta t_{\mathrm{DA}} = 0$ ms (C) $\Delta t_{\mathrm{DA}} = 50$ ms

(D) Differences @proximal (E) Differences @ distal

Figure 5.12. Dopamine effect on STDP. The same calcium input as in Fig. 5.11 was applied to the signaling cascade model, but dopamine was not applied to the signaling cascade model. That is dopamine was applied only to the electric compartment model. (A-C) Synaptic plasticity in proximal (blue) and distal (black) spines. Dopamine input was applied at the timing of (A) $\Delta t_{\mathrm{DA}} = 0$ ms, (B) $\Delta t_{\mathrm{DA}} = 100$ ms and (C) $\Delta t_{\mathrm{DA}} = -100$ ms relative to postsynaptic spike. (D, E) Difference of change in synaptic efficacy between the presence and absence of dopamine input to the signaling cascade model in (D) proximal and (E) distal spines. Timing of dopamine input to the electric compartment model was $\Delta t_{\mathrm{DA}} = -50$ ms (blue), $\Delta t_{\mathrm{DA}} = 0$ ms (green) and $\Delta t_{\mathrm{DA}} = 50$ ms (red).

5.3.4 Leaky integrators

To test whether leaky integration was a good approximation of synaptic efficacy and to determine which signaling cascade worked as a leaky integrator, various calcium inputs were applied to the signaling cascade model. These inputs had different amplitudes, $[Ca^{2+}]_{\text{stim}}$, and decay constants, τ, and are in Equation 5.1. Some of these inputs were the same leaky integration values each other which were calculated with Equation 3.38 ($\tau = 1$ ms and $a = 20$).

$$[Ca^{2+}](t) = [Ca^{2+}]_{\text{basal}} + [Ca^{2+}]_{\text{stim}} \times \frac{t}{\tau} \times \exp\left(1 - \frac{t}{\tau}\right), \tag{5.1}$$

The calcium inputs induced the activation of enzymes differentially, but CaMKII showed the same activation as in the leaky integrations for inputs of the same value (Fig. 5.13). Accordingly, synaptic efficacy was also the same as for the equivalent leaky integration of calcium. Hence, the leaky integration was a better approximation of the change in synaptic efficacy compared with peak calcium. It was concluded that the signaling cascade worked as a leaky integrator of calcium.

The leaky integration of dopamine was also tested in a similar way using DA input as calculated from Equation 5.2. Leaky integration of dopamine was calculated by Equation 5.3. As a result, the G-protein activation curve was overlapped that of the leaky integration of dopamine. Sequentially, PKA and synaptic efficacy showed the same activation as the leaky integration of dopamine.

$$[DA](t) = [DA]_{\text{basal}} + [DA]_{\text{stim}} \times \frac{t}{\tau} \times \exp\left(1 - \frac{t}{\tau}\right), \tag{5.2}$$

$$x(t) = \frac{a}{\tau} e^{-\frac{t}{\tau}} \int [DA](t) e^{\frac{t}{\tau}} dt \tag{5.3}$$

5.4 Conclusion and Discussion

I ran the simulation of the signaling cascae model using calcium prediction from the electric compartment model. The simulation reproduced experimentally reported corticostriatal synaptic plasticity to some extent only by simple connection

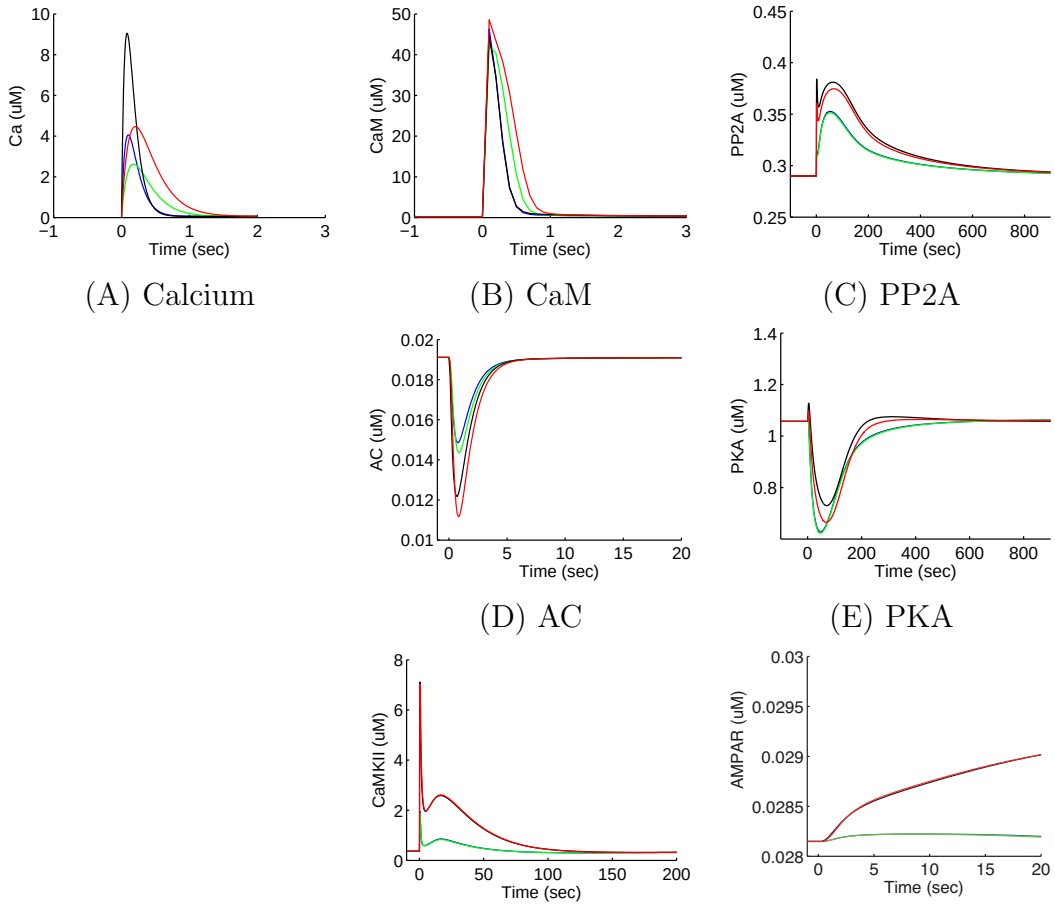

Figure 5.13. Leaky integration of calcium. To test the property of leaky integration of calcium, four types of calcium inputs were tested. (A) Four types of calcium inputs: 1) $\tau = 204$ ms, $[Ca^{2+}]_{\text{stim}} = 4.41$ μM, $x_{\tau=1 \text{ ms}} = 29.8$ (red), 2) $\tau = 82$ ms, $[Ca^{2+}]_{\text{stim}} = 9$ μM, $x_{\tau=1 \text{ ms}} = 30.7$ (black), 3) $\tau = 100$ ms, $[Ca^{2+}]_{\text{stim}} = 4$ μM, $x_{\tau 1= \text{ ms}} = 16.2$ (blue), and 4) $\tau = 178$ ms, $[Ca^{2+}]_{\text{stim}} = 2.56$ μM, $x_{\tau=1 \text{ ms}} = 16.0$ (green). τ and $[Ca^{2+}]_{\text{stim}}$ were the parameters used in Equation 5.1. x was the value of the leaky integration with a time constant of 1 ms and a of 20. The values of these inputs were mostly the same for 1) and 2), and, 3) and 4). (B-G) Responses of CaM, PP2A, AC (AC-Gsa-ATP Fig. C.2 in Appendix), PKA, CaMKII and Synaptic efficacy to the calcium inputs. Black and red lines, and blue and green lines are overlapped in (F) and (G).

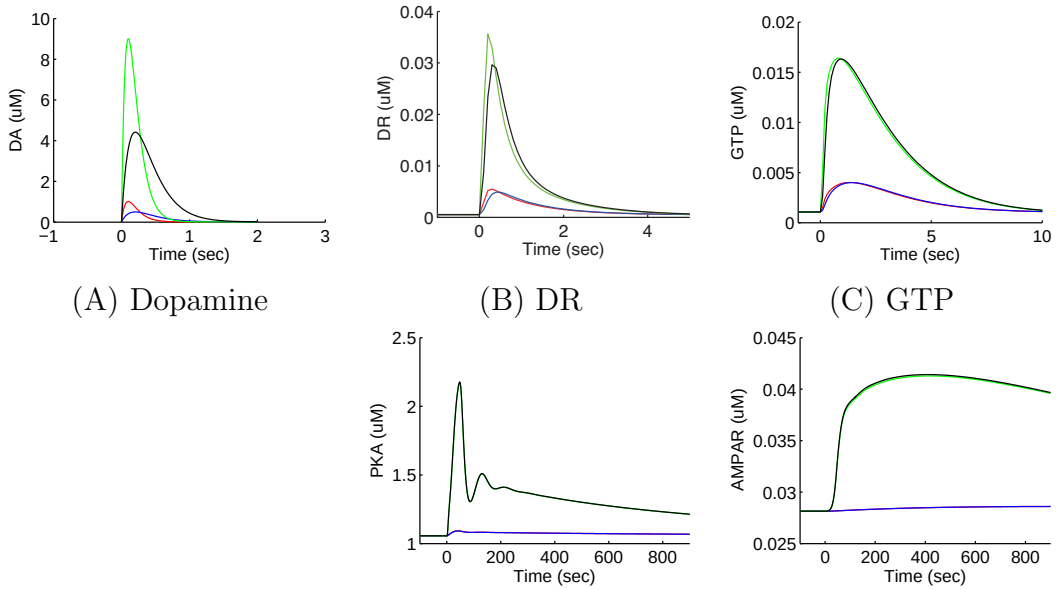

(A) Dopamine (B) DR (C) GTP

(D) PKA (E) AMPAR

Figure 5.14. Leaky integration of dopamine. To test the property of leaky integration of dopamine, four types of dopamine inputs were tested. (A) Four types of dopamine inputs: 1) $\tau = 204$ ms, $[DA]_{\text{stim}} = 0.49$ μM, $x_{\tau=600 \text{ ms}} = 5.8$ (blue), 2) $\tau = 100$ ms, $[DA]_{\text{stim}} = 1$ μM, $x_{\tau=600 \text{ ms}} = 5.8$ (red), 3) $\tau = 204$ ms, $[DA]_{\text{stim}} = 4.41$ μM, $x_{\tau=600 \text{ ms}} = 49.1$ (black), and 4) $\tau = 100$ ms, $[DA]_{\text{stim}} = 9$ μM, $x_{\tau=600 \text{ ms}} = 49.1$ (green). τ and $[DA]_{\text{stim}}$ were the parameters used in Equation 5.2. x was the value of the leaky integration with a time constant of 600 ms and a of 20. The values of these inputs were mostly the same for 1)- 2) and, 3)- 4). (B-G) Responses of dopamine receptor (D1R-DA-Gs in Fig. C.1 in Appendix),, G-protein (Gsa-GTP in Fig. C.1 in Appendix), PKA, and Synaptic efficacy to the dopamine inputs. Black and green lines, and blue and red lines are overlapped in (C-E).

of the two models. From the results using HFS, I reproduced calcium (voltage) dependent synaptic plasticity and dopamine dependent synaptic plasticity. When the timing of inputs was tested, timing dependence of LTP and LTD were reproduced.

I tested different parameter settings, such as high AMPAR/NMDAR conductance conditions, as used in the electric compartment model. Although the relationship between calcium peak and the temporal order of inputs depended on the duration of postsynaptic current pulse, the difference of synaptic efficacy due to the temporal order of inputs was small. High AMPAR/NMDAR conductance conditions would not be feasible in a real neural system.

I elucidated that the relationship between calcium and synaptic change was that leaky integration was a better approximation of the change in synaptic efficacy than the calcium peak. The Leaky integration of calcium was mediated by CaMKII, not by the PKA, PP2A and DARPP-32 positive feedback loop. On the other hand, the leaky integration of dopamine was mediated by G-protein coupled dopamine receptors. In this simulation, the dopamine timing effect on the synaptic efficacy was also tested. There was little dependence on dopamine timing in the signaling cascade model, which was also shown in Fig. 4.14 in Chapter 4. That is, dopamine timing effects on synaptic efficacy occur via calcium influx.

5.4.1 Connecting models

My integrated model can predict synaptic change by physiological events, which suggests that the two models were valid. However, I realized that the model parameters should be adjusted to reproduce both LTD and LTP. Actually NMDAR conductance was multiplied 5 times in the STDP simulation. This necessity of altering parameters would not be detectable without combining the models or experimentation.

Besides, in a real system, dopamine modulation occurs through intracellular chemical reactions. In this study, phenomenological dopamine modulation was used instead of the intracellular chemical reaction, even when the two models were connected. In additon, the production of IP_3 was modeled phenomenologicaly. This is because I used different simulators: NEURON Simulator was used for the electric compartment model and GENESIS/kinetikit was used for the sig-

naling cascade model, which made integration of the models difficult. Recently, there have been efforts to integrate such incompatible models. Multi Simulation Coordinator (MUSIC) is an Application Programming Interface (API) allowing large scale neuron simulators using Message Passing Interface (MPI), which can integrate major neuron simulators such as MOOSE (successor of GENESIS), NEURON, and NEST [19,33,59,80]. MUSIC would make realistic model integration possible. By integration using MUSIC it was possible to find more problems with my model and thus lead to better understanding of corticostriatal synaptic plasticity.

5.4.2 Multi- and large-scale modeling

My combined simulation was a multilevel simulation. Multi-scale simulation has generally some difficulties. If time- or spatial-scale, or computational accuracy is different at each level, simulation would not be efficient. Or, simply, integration may make the model complicated, which requires high performance computing. In this case, some model reduction or modification may be needed.

Why then, do we construct multi-scale modeling that has such difficulties? Actually, we can construct large-scale models using combinations of simple models, like the integrate-and-fire model. However such models cannot reproduce cell specific characteristics. A realistic model should be consistent with experimental data, which can be tested.

Recently, many simulation models have been developed and are available from databases, such as Model DB [113], BioModels Database [175], and DOQCS [208]. There are also mark-up languages to describe models, such as NeuroML [82] for the neuron model and Systems Biology Markup Language (SBML) [121] for the signaling cascade model. In addition, some coordination software, like MUSIC, exists. They make it easy to construct realistic large-scale models using ready-made models. I hope my models will also help such multi- and large-scale modeling.

5.4.3 Leaky integrators

The curve of the leaky integration of calcium for input timing fitted the STDP curve well. However, the two curves did not fit perfectly. This was because

of the effect of other proteins such as PKA and PP2A, which did not work as leaky integrators. Although the leaky integration curve fitted the STDP curve when leaky integration was calculated with time constant $\tau = 600$ ms, $\tau = 1$ ms was used in Fig. 5.13 and CaMKII activity did not overlap when $\tau = 600$ ms was used. This may be caused by whether the calcium response was bimodal or monomodal. This is that timed glutamate input to postsynaptic spike induced a bimodal calcium response but monomodal calcium change was used as inputs in Fig. 5.13.

Dopamine is integrated by G-protein coupled dopamine receptors. Dopamine can diffuse a significant distance from the synaptic cleft and dopamine receptors located at some distance from the synaptic cleft could receive low peak but prolonged dopamine stimulation. If it is not the peak, but the integration, of dopamine that is important, dopamine would give same the effect even on dopamine receptors located far from the synaptic cleft.

6. General Discussion

6.1 Summary

In this thesis, experimental and modeling studies of corticostriatal synaptic plasticity have been performed to elucidate electrophysiological and molecular mechanisms of corticostriatal synaptic plasticity in D1R expressing medium spiny neurons. I investigated synaptic plasticity in combination with the identification of the medium spiny neuron cell type. The two types of cell showed the same properties; HFS induced both LTP and LTD but only LTP was induced by HFS in magnesium-free solution. This suggested that differences between the cell types were not the basis of contrasting corticostriatal synaptic plasticity reports.

Then, to investigate the electrophysiological and molecular mechanisms of the synaptic plasticity in D1Ns, I constructed an electric compartment model and a signaling cascade model based on experimental data. The electric compartment model predicted calcium responses to the timing of glutamate and dopamine input and postsynaptic action potentials in various conditions. Both dopamine and glutamate input, preceding a postsynaptic spike, induced a high peak calcium response, but glutamate following a postsynaptic spike induced a higher leaky integration of calcium than glutamate preceding a postsynaptic spike when dopamine followed the postsynaptic spike. In the high AMPAR/NMDAR conductance condition, two types of calcium response were produced: Glu-Post induced a higher calcium response to a postsynaptic spike evoked by a 2 ms current injection, and Post-Glu induced a higher calcium response to a postsynaptic spike evoked by a 30 ms current injection. This could be a basis for the conflicting STDP observed in the striatum.

The signaling cascade model predicted changes in synaptic efficacy by dopamine and calcium input to investigate molecular mechanisms of dopamine- and calcium-dependent synaptic plasticity. According to my simulation results, the direction of change of the phosphorylation level of DARPP-32 depends on calcium input strength, which switches LTD and LTP. DARPP-32 with PKA and PP2A forms a positive feedback loop. The loop shows bistability, which induces dopamine dependent LTP.

Finally, by connecting the two models, I constructed a complete model predict-

ing synaptic efficacy induced by physiological triggers. The model reproduced calcium (membrane potential) dependent synaptic plasticity, dopamine dependent synaptic plasticity, and spike-timing dependent synaptic plasticity. However, the reversed shape of STDP was not reproduced, which was suggested from the electric compartment model using high AMPAR/NMDAR conductance conditions. The model showed that leaky integration of calcium was a better approximation of change in synaptic efficacy and it was mediated by CaMKII activity, and leaky integration of dopamine was mediated by G-protein coupled dopamine receptors.

To summarize the electrophysiological and molecular mechanisms of the synaptic plasticity in the striatum, dopamine potentiated synaptic efficacy by activating the PKA-PP2A-DARPP-32 positive feedback loop, but the dopamine timing effect was mediated mainly via calcium through NMDAR and calcium channels. Glutamate preceding a postsynaptic spike induced higher calcium influx via NMDAR and L-type calcium channels. This leaky calcium was integrated by CaMKII and induced potentiation of synaptic efficacy.

6.2 Experiments to test my model prediction

The models in this thesis used calcium as an input or output. However, nobody has experimentally investigated the direct relationship between calcium and synaptic plasticity in the striatum. Therefore, I attempted to investigate this using caged calcium, which makes it possible to use calcium as a direct input. Although I have not yet obtained any results, I discuss here a plan of the experiment.

Calcium can be uncaged using ultraviolet (UV) light, but the amount of UV a cell receivesis dependent on the depth of the cell from the surface of the slice. Therefore it is not possible to measure quantitatively how much calcium is generated by UV. Calcium imaging enables quantitative measurements. There are various calcium indicators, and usually fluorescence that is excited by green light is used with UV for uncaging. Therefore, two light sources, for imaging and uncaging, are required, which need complicated optics.

For photolysis uncaging, there are two approaches, using a laser or a lamp. A laser can stimulate a small region, whereas a broad area of slice can be irradiated by a lamp. Both approaches have merits and disadvantages. To observe

calcium signal in a dendrite, the cell is dyed using a fluorescent dye such as an Alexa dye. Then calcium signals can be measured. However, in our laboratory, calcium signals were measured only from the soma because dendrites were too dark. Although I cannot measure the response to cortical input in this case, it would be no problem to know how much calcium was generated by photolysis.

My model can be tested by measuring the change in synaptic efficacy by direct calcium stimulation. Control of duration and intensity of photolysis make it possible to give various shapes of calcium input. That is, I can test whether leaky integration or peak calcium is a good approximation of synaptic change. Calcium inputs and extracellular dopamine inputs with specific protein inhibitors can test the molecular dynamics underlying synaptic plasticity, which the model predicted. In addition, timed dopamine input using caged dopamine can be used to test my prediction that glutamate and postsynaptic spike evoked STDP was dependent on dopamine timing. Although this kind of experiment would be difficult to investigate many timing inputs, my model can lessen the experimental burden.

6.3 D2 neurons

In this study, I investigated medium spiny neurons expressing D1 type dopamine receptors. However, there is another type of medium spiny neuron in the striatum, which expresses D2 type dopamine receptors. Their electrophysiological properties are similar, but attenuation of the calcium transient with distance from the soma in D2 cells is smaller than that in D1 cells [52]. This attenuation is regulated by Kv4.2 channels. This result implies that the dopamine timing-dependent calcium transient could be observed even in distal dendrites in D2 cells.

Furthermore, dopamine has different effects on D1 and D2 cells [204, 216]. D1Rs activate AC via G protein $G_{s/olf}$, and D2Rs inhibit AC activity via G_i. The effects of D2Rs (Table 6.1) on channels are also different from D1Rs. For example, in contrast to D1 receptors, which increase NMDAR and L-type calcium currents, D2 receptors reduce AMPAR and L-type calcium currents.

	Dorsal		Ventral	
Channel	Effect	Ref.	Effect	Ref.
NaF	119%, hV1/2 3.2 mV	[217]	no change	[232, 244]
	no change, hV1/2 -16.9 mV		125%	[120]
CaL	(1.3) 76-81%	[109, 180, 197]	reduction	[186]
	(1.2) no change	[180]		
KAs	104-108%	[135, 218]	enhancement	[186]
Kir	unknown		85-98%	[186, 226, 227]
NMDAR	no change	[44, 67, 146, 148]	unknown	
AMPAR	72-85%	[108, 146]	unknown	
Glu	0-95%	[7, 118]	40-92%	[178, 241]

Table 6.1. Effects of dopamine modulation. This table was adopted from [162]. % means the change of the conductance. 100 % means no change.

6.4 Experimentation and modeling

In this thesis, realistic models were constructed. Although abstract models are helpful to discover principles of brain function, realistic models are necessary to fully understand brain function. Realistic models can be tested rigorously by experiment. The integration of experimentation and modeling would lead us to concrete knowledge of brain function, for example, what learning algorism is implemented by moleclues, neurons and neural curcuit, and what variables in reinforcement learning models are coded by which moleclues or neurons

Today, there are powerful experimental techniques to address this. One is the organotypic slice culture, which can maintain neuronal structure and the interactions between cells; cultures containing cortex, striatum, and even substantia nigra, with connections between the areas can be made [17]. Such a slice is difficult to achieve in an acute slice. Of course, culture conditions are simplified and cultured tissues may have different characteristics from *in vivo*. Model conditions are also simplifications of real biological systems and in this respect, the organotypic slice culture is similar to the model approach. Conversely, knowledge from culture studies is in good agreement with those from modeling. It would be

better to construct models based on culture studies to give predictions of brain function *in vivo*.

In the future, we will be able to construct a hybrid model of model and experimental culture. That is to say, it will be possible to embed a model into a culture or slice instead of individual neurons citePlenz:1996p1254. In addition, it is possible to manipulate neurons at the network level using channel rhodopsin, a light-gated ion channel, which enables the control of neuronal activity using light [20,163]. Combining them would be a new paradigm at the level of molecule and cell, which would enable us to understand cause-and-effect relationships, even at the system level.

Although this is speculation, it may be possible that the properties of corticostriatal synaptic plasticity depend on the magnitude of the values coded by striatal neurons. For example, a high-value coded neuron may hardly show LTP. If computational theory can predict what codes value in a cell, or how to distinguish the values coded by a cell, it would enable experiments to be performed to understand neural implementation of reinforcement learning.

6.5 Toward understanding neural mechanisms of reinforcement learning

The aim of computational neuroscience is to elucidate brain functions to the extent that we can build artificial machinery or computer programs, which solve the problems that the brain deals with using essentially the same principles as those used by the brain. As computer performance has increased, it has become possible to construct a detailed whole brain model *in silico* [158,176,203]. That is, it will also be possible to construct a model of the whole basal ganglia, which can learn autonomously through "trial-and-error", with detailed realistic properties that are capable of being tested by animal experiments.

Up to now, most reinforcement learning models were not biologically feasible at the level of cells and molecules. However, there is some biological reinforcement learning model [187]. In this model, STDP and dopamine modulated synaptic plasticity were used to produce the learning. The model was not biologically feasible in certain ways but it was a useful model as a first step to understand

the neural implementation of reinforcement learning. We will be able to understand the role of molecular and cellular dynamics in learning, by adding realistic features: the basal ganglia circuit, the topology of the corticostriatum, local striatal circuitry, cell characteristics including molecules, synapse location, synaptic forms, and detailed properties of synaptic plasticity. In this regard, the model proposed in this thesis is a stepping stone to further development and could contribute to a detailed understanding of synaptic plasticity induced by physiological triggers.

Furthermore, free-energy-based reinforcement learning could suggest principles of brain function [68]. Free-energy can be evaluated as a lower bound of expected surprise which is a kind of prediction error, That is, minimizing free-energy is adaptive change in the brain. In the framework of restricted Boltzmann machine, expected value of state and action was represented by negative free-energy. That is, minimizing free-energy is optimizing action to obtain a good state. Minimizing free-energy is the product of reward prediction error and the Hebb rule [181,198]. This is analogous to corticostriatal synaptic plasticity. There was an attempt to consider the Boltzmann machine with respect to a spiking neuron, even though it was not a reinforcement learning study [114]. Further development of such a theoretical study is hoped for in the future. Integration of theoretical, modeling, and experimental studies shall lead us to the truth.

References

[1] S. H. Ahmed. Neuroscience. Addiction as compulsive reward prediction. *Science*, 306(5703):1901–2, Dec 2004.

[2] G. Akopian, W. Musleh, R. Smith, and J. P. Walsh. Functional state of corticostriatal synapses determines their expression of short- and long-term plasticity. *Synapse*, 38(3):271–80, Dec 2000.

[3] G. E. Alexander, M. R. DeLong, and P. L. Strick. Parallel organization of functionally segregated circuits linking basal ganglia and cortex. *Annu Rev Neurosci*, 9:357–81, Jan 1986.

[4] G. W. Arbuthnott, C. A. Ingham, and J. R. Wickens. Dopamine and synaptic plasticity in the neostriatum. *J Anat*, 196 (Pt 4):587–96, May 2000.

[5] A. Artola and W. Singer. Long-term depression of excitatory synaptic transmission and its relationship to long-term potentiation. *Trends Neurosci*, 16(11):480–7, Nov 1993.

[6] B. W. Balleine, K. Doya, J. P. O'Doherty, and M. Sakagami. Current trends in decision making. *Ann N Y Acad Sci*, 1104:xi–xv, May 2007.

[7] N. S. Bamford, H. Zhang, Y. Schmitz, N.-P. Wu, C. Cepeda, M. S. Levine, C. Schmauss, S. S. Zakharenko, L. Zablow, and D. Sulzer. Heterosynaptic dopamine neurotransmission selects sets of corticostriatal terminals. *Neuron*, 42(4):653–63, May 2004.

[8] T. G. Banke, D. Bowie, H. Lee, R. L. Huganir, A. Schousboe, and S. F. Traynelis. Control of GluR1 AMPA receptor function by cAMP-dependent protein kinase. *J Neurosci*, 20(1):89–102, Jan 2000.

[9] P. E. Barbano, M. Spivak, M. Flajolet, A. C. Nairn, P. Greengard, and L. Greengard. A mathematical tool for exploring the dynamics of biological networks. *Proc Natl Acad Sci USA*, 104(49):19169–74, Dec 2007.

[10] V. A. Bender, K. J. Bender, D. J. Brasier, and D. E. Feldman. Two coincidence detectors for spike timing-dependent plasticity in somatosensory cortex. *J Neurosci*, 26(16):4166–77, Apr 2006.

[11] V. Bernard, P. Somogyi, and J. P. Bolam. Cellular, subcellular, and subsynaptic distribution of AMPA-type glutamate receptor subunits in the neostriatum of the rat. *J Neurosci*, 17(2):819–33, Jan 1997.

[12] I. Bezprozvanny, J. Watras, and B. E. Ehrlich. Bell-shaped calcium-response curves of Ins(1,4,5)P3- and calcium-gated channels from endoplasmic reticulum of cerebellum. *Nature*, 351(6329):751–4, Jun 1991.

[13] U. S. Bhalla and R. Iyengar. Emergent properties of networks of biological signaling pathways. *Science*, 283(5400):381–7, Jan 1999.

[14] J. A. Bibb. Role of Cdk5 in neuronal signaling, plasticity, and drug abuse. *Neurosignals*, 12(4-5):191–9, Jan 2003.

[15] J. A. Bibb, G. L. Snyder, A. Nishi, Z. Yan, L. Meijer, A. A. Fienberg, L. H. Tsai, Y. T. Kwon, J.-A. Girault, A. J. Czernik, R. L. Huganir, H. C. Hemmings, A. C. Nairn, and P. Greengard. Phosphorylation of DARPP-32 by Cdk5 modulates dopamine signalling in neurons. *Nature*, 402(6762):669–71, Dec 1999.

[16] H. Bito and S. Takemoto-Kimura. Ca(2+)/CREB/CBP-dependent gene regulation: a shared mechanism critical in long-term synaptic plasticity and neuronal survival. *Cell Calcium*, 34(4-5):425–30, Jan 2003.

[17] K. T. Blackwell, U. Czubayko, and D. Plenz. Quantitative estimate of synaptic inputs to striatal neurons during up and down states in vitro. *J Neurosci*, 23(27):9123–32, Oct 2003.

[18] P. Bonsi, A. Pisani, G. Bernardi, and P. Calabresi. Stimulus frequency, calcium levels and striatal synaptic plasticity. *Neuroreport*, 14(3):419–22, Mar 2003.

[19] J. Bower and D. Beeman. *The book of GENESIS: Exploring realistic neural models with the GEneral NEural SImulation System (2nd Ed.)*. New York: Springer, 1998.

[20] E. S. Boyden, F. Zhang, E. Bamberg, G. Nagel, and K. Deisseroth. Millisecond-timescale, genetically targeted optical control of neural activity. *Nat Neurosci*, 8(9):1263–8, Sep 2005.

[21] J. M. Bradshaw, Y. Kubota, T. Meyer, and H. Schulman. An ultrasensitive Ca2+/calmodulin-dependent protein kinase II-protein phosphatase 1 switch facilitates specificity in postsynaptic calcium signaling. *Proc Natl Acad Sci USA*, 100(18):10512–7, Sep 2003.

[22] P. Calabresi, D. Centonze, P. Gubellini, and G. Bernardi. Activation of M1-like muscarinic receptors is required for the induction of corticostriatal LTP. *Neuropharmacology*, 38(2):323–6, Feb 1999.

[23] P. Calabresi, D. Centonze, P. Gubellini, G. A. Marfia, and G. Bernardi. Glutamate-triggered events inducing corticostriatal long-term depression. *J Neurosci*, 19(14):6102–10, Jul 1999.

[24] P. Calabresi, P. Giacomini, D. Centonze, and G. Bernardi. Levodopa-induced dyskinesia: a pathological form of striatal synaptic plasticity? *Ann Neurol*, 47(4 Suppl 1):S60–8; discussion S68–9, Apr 2000.

[25] P. Calabresi, P. Gubellini, D. Centonze, B. Picconi, G. Bernardi, K. Chergui, P. Svenningsson, A. A. Fienberg, and P. Greengard. Dopamine and cAMP-regulated phosphoprotein 32 kDa controls both striatal long-term depression and long-term potentiation, opposing forms of synaptic plasticity. *J Neurosci*, 20(22):8443–51, Nov 2000.

[26] P. Calabresi, P. Gubellini, D. Centonze, G. Sancesario, M. Morello, M. Giorgi, A. Pisani, and G. Bernardi. A critical role of the nitric oxide/cGMP pathway in corticostriatal long-term depression. *J Neurosci*, 19(7):2489–99, Apr 1999.

[27] P. Calabresi, R. Maj, N. B. Mercuri, and G. Bernardi. Coactivation of D1 and D2 dopamine receptors is required for long-term synaptic depression in the striatum. *Neurosci Lett*, 142(1):95–9, Aug 1992.

[28] P. Calabresi, R. Maj, A. Pisani, N. B. Mercuri, and G. Bernardi. Long-term synaptic depression in the striatum: physiological and pharmacological characterization. *J Neurosci*, 12(11):4224–33, Nov 1992.

[29] P. Calabresi, N. Mercuri, P. Stanzione, A. Stefani, and G. Bernardi. Intracellular studies on the dopamine-induced firing inhibition of neostriatal neurons in vitro: evidence for D1 receptor involvement. *Neuroscience*, 20(3):757–71, Mar 1987.

[30] P. Calabresi, A. Pisani, N. Mercuri, and G. Bernardi. Long-term Potentiation in the Striatum is Unmasked by Removing the Voltage-dependent Magnesium Block of NMDA Receptor Channels. *Eur J Neurosci*, 4(10):929–935, Jan 1992.

[31] P. Calabresi, E. Saulle, G. A. Marfia, D. Centonze, R. Mulloy, B. Picconi, R. A. Hipskind, F. Conquet, and G. Bernardi. Activation of metabotropic glutamate receptor subtype 1/protein kinase C/mitogen-activated protein kinase pathway is required for postischemic long-term potentiation in the striatum. *Mol Pharmacol*, 60(4):808–15, Oct 2001.

[32] N. Caporale and Y. Dan. Spike Timing-Dependent Plasticity: A Hebbian Learning Rule. *Annu Rev Neurosci*, Feb 2008.

[33] N. T. Carnevale and M. L. Hines. *The NEURON Book*. Cambridge University Press, 2006.

[34] A. G. Carter and B. L. Sabatini. State-dependent calcium signaling in dendritic spines of striatal medium spiny neurons. *Neuron*, 44(3):483–93, Oct 2004.

[35] G. C. Castellani, A. Bazzani, and L. N. Cooper. Toward a microscopic model of bidirectional synaptic plasticity. *Proc Natl Acad Sci USA*, 106(33):14091–5, Aug 2009.

[36] G. C. Castellani, E. M. Quinlan, F. Bersani, L. N. Cooper, and H. Z. Shouval. A model of bidirectional synaptic plasticity: from signaling network to channel conductance. *Learn Mem*, 12(4):423–32, Jan 2005.

[37] N. G. Castro, M. C. de Mello, F. G. de Mello, and Y. Aracava. Direct inhibition of the N-methyl-D-aspartate receptor channel by dopamine and (+)-SKF38393. *Br J Pharmacol*, 126(8):1847–55, Apr 1999.

[38] W. A. Catterall. Structure and regulation of voltage-gated Ca2+ channels. *Annu Rev Cell Dev Biol*, 16:521–55, Jan 2000.

[39] D. Centonze, P. Gubellini, G. Bernardi, and P. Calabresi. Permissive role of interneurons in corticostriatal synaptic plasticity. *Brain Res Brain Res Rev*, 31(1):1–5, Dec 1999.

[40] D. Centonze, P. Gubellini, B. Picconi, P. Calabresi, P. Giacomini, and G. Bernardi. Unilateral dopamine denervation blocks corticostriatal LTP. *J Neurophysiol*, 82(6):3575–9, Dec 1999.

[41] D. Centonze, P. Gubellini, A. Pisani, G. Bernardi, and P. Calabresi. Dopamine, acetylcholine and nitric oxide systems interact to induce corticostriatal synaptic plasticity. *Reviews in the neurosciences*, 14(3):207–16, Jan 2003.

[42] D. Centonze, B. Picconi, P. Gubellini, G. Bernardi, and P. Calabresi. Dopaminergic control of synaptic plasticity in the dorsal striatum. *Eur J Neurosci*, 13(6):1071–7, Mar 2001.

[43] C. Cepeda, V. M. André, I. Yamazaki, N. Wu, M. Kleiman-Weiner, and M. S. Levine. Differential electrophysiological properties of dopamine D1 and D2 receptor-containing striatal medium-sized spiny neurons. *Eur J Neurosci*, 27(3):671–82, Feb 2008.

[44] C. Cepeda, C. S. Colwell, J. N. Itri, S. H. Chandler, and M. S. Levine. Dopaminergic modulation of NMDA-induced whole cell currents in neostriatal neurons in slices: contribution of calcium conductances. *J Neurophysiol*, 79(1):82–94, Jan 1998.

[45] S. Charpier and J.-M. Deniau. In vivo activity-dependent plasticity at cortico-striatal connections: evidence for physiological long-term potentiation. *Proc Natl Acad Sci USA*, 94(13):7036–40, Jun 1997.

[46] S. Charpier, S. Mahon, and J.-M. Deniau. In vivo induction of striatal long-term potentiation by low-frequency stimulation of the cerebral cortex. *Neuroscience*, 91(4):1209–22, Jan 1999.

[47] S. Choi and D. M. Lovinger. Decreased probability of neurotransmitter release underlies striatal long-term depression and postnatal development of corticostriatal synapses. *Proc Natl Acad Sci USA*, 94(6):2665–70, Mar 1997.

[48] D. M. F. Cooper. Molecular and cellular requirements for the regulation of adenylate cyclases by calcium. *Biochem Soc Trans*, 31(Pt 5):912–5, Oct 2003.

[49] I. Creese, D. R. Sibley, M. W. Hamblin, and S. E. Leff. The classification of dopamine receptors: relationship to radioligand binding. *Annu Rev Neurosci*, 6:43–71, Jan 1983.

[50] P. D'Alcantara, S. N. Schiffmann, and S. Swillens. Bidirectional synaptic plasticity as a consequence of interdependent Ca2+-controlled phosphorylation and dephosphorylation pathways. *Eur J Neurosci*, 17(12):2521–8, Jun 2003.

[51] Y. Dan and M.-M. Poo. Spike timing-dependent plasticity of neural circuits. *Neuron*, 44(1):23–30, Sep 2004.

[52] M. Day, D. Wokosin, J. L. Plotkin, X. Tian, and D. J. Surmeier. Differential excitability and modulation of striatal medium spiny neuron dendrites. *J Neurosci*, 28(45):11603–14, Nov 2008.

[53] Y. P. Deng, J. P. Xie, H. B. Wang, W. L. Lei, Q. Chen, and A. Reiner. Differential localization of the GluR1 and GluR2 subunits of the AMPA-type glutamate receptor among striatal neuron types in rats. *J Chem Neuroanat*, 33(4):167–92, Jul 2007.

[54] V. Derkach, A. Barria, and T. R. Soderling. Ca2+/calmodulin-kinase II enhances channel conductance of alpha-amino-3-hydroxy-5-methyl-4-isoxazolepropionate type glutamate receptors. *Proc Natl Acad Sci USA*, 96(6):3269–74, Mar 1999.

[55] F. Desdouits, D. Cohen, A. C. Nairn, P. Greengard, and J.-A. Girault. Phosphorylation of DARPP-32, a dopamine- and cAMP-regulated phosphoprotein, by casein kinase I in vitro and in vivo. *J Biol Chem*, 270(15):8772–8, Apr 1995.

[56] F. Desdouits, J. C. Siciliano, P. Greengard, and J.-A. Girault. Dopamine- and cAMP-regulated phosphoprotein DARPP-32: phosphorylation of Ser-137 by casein kinase I inhibits dephosphorylation of Thr-34 by calcineurin. *Proc Natl Acad Sci USA*, 92(7):2682–5, Mar 1995.

[57] F. Desdouits, J. C. Siciliano, A. C. Nairn, P. Greengard, and J.-A. Girault. Dephosphorylation of Ser-137 in DARPP-32 by protein phosphatases 2A and 2C: different roles in vitro and in striatonigral neurons. *Biochem J*, 330 (Pt 1):211–6, Feb 1998.

[58] J. Ding, J. D. Peterson, and D. J. Surmeier. Corticostriatal and thalamostriatal synapses have distinctive properties. *J Neurosci*, 28(25):6483–92, Jun 2008.

[59] M. Djurfeldt, J. Hjorth, J. M. Eppler, N. Dudani, M. Helias, T. C. Potjans, U. S. Bhalla, M. Diesmann, J. H. Kotaleski, and O. Ekeberg. Run-Time Interoperability Between Neuronal Network Simulators Based on the MUSIC Framework. *Neuroinformatics*, Mar 2010.

[60] T. Doi, S. Kuroda, T. Michikawa, and M. Kawato. Inositol 1,4,5-trisphosphate-dependent Ca2+ threshold dynamics detect spike timing in cerebellar Purkinje cells. *J Neurosci*, 25(4):950–61, Jan 2005.

[61] K. Doya. Metalearning and neuromodulation. *Neural Networks*, 15(4-6):495–506, Jan 2002.

[62] K. Doya. Reinforcement learning: Computational theory and biological mechanisms. *HFSP J.*, 1(1):30, Jan 2007.

[63] M. D. Ehlers. Reinsertion or degradation of AMPA receptors determined by activity-dependent endocytic sorting. *Neuron*, 28(2):511–25, Nov 2000.

[64] J. A. Esteban, S.-H. Shi, C. Wilson, M. Nuriya, R. L. Huganir, and R. Malinow. PKA phosphorylation of AMPA receptor subunits controls synaptic trafficking underlying plasticity. *Nat Neurosci*, 6(2):136–43, Feb 2003.

[65] E. Fernandez, R. Schiappa, J.-A. Girault, and N. L. Novère. DARPP-32 is a robust integrator of dopamine and glutamate signals. *PLoS Comput Biol*, 2(12):e176, Dec 2006.

[66] E. Fino, J. Glowinski, and L. Venance. Bidirectional activity-dependent plasticity at corticostriatal synapses. *J Neurosci*, 25(49):11279–87, Dec 2005.

[67] J. Flores-Hernández, C. Cepeda, E. Hernández-Echeagaray, C. R. Calvert, E. S. Jokel, A. A. Fienberg, P. Greengard, and M. S. Levine. Dopamine enhancement of NMDA currents in dissociated medium-sized striatal neurons: role of D1 receptors and DARPP-32. *J Neurophysiol*, 88(6):3010–20, Dec 2002.

[68] K. Friston. The free-energy principle: a rough guide to the brain? *Trends Cogn Sci (Regul Ed)*, 13(7):293–301, Jul 2009.

[69] R. C. Froemke and Y. Dan. Spike-timing-dependent synaptic modification induced by natural spike trains. *Nature*, 416(6879):433–8, Mar 2002.

[70] R. C. Froemke, M.-M. Poo, and Y. Dan. Spike-timing-dependent synaptic plasticity depends on dendritic location. *Nature*, 434(7030):221–5, Mar 2005.

[71] F. Fujiyama, E. Kuramoto, K. Okamoto, H. Hioki, T. Furuta, L. Zhou, S. Nomura, and T. Kaneko. Presynaptic localization of an AMPA-type glutamate receptor in corticostriatal and thalamostriatal axon terminals. *Eur J Neurosci*, 20(12):3322–30, Dec 2004.

[72] F. Fujiyama, T. Unzai, K. Nakamura, S. Nomura, and T. Kaneko. Difference in organization of corticostriatal and thalamostriatal synapses between patch and matrix compartments of rat neostriatum. *Eur J Neurosci*, 24(10):2813–24, Nov 2006.

[73] M. Garcia-Munoz, P. Patino, E. Masliah, S. J. Young, and P. M. Groves. Glutamate-dependent long-term presynaptic changes in corticostriatal excitability. *Neuroscience*, 73(1):109–19, Jul 1996.

[74] W. V. Geit, P. Achard, and E. D. Schutter. Neurofitter: A parameter tuning package for a wide range of electrophysiological neuron models. *Frontiers in Neuroinformatics*, Jan 2007.

[75] C. R. Gerfen. The neostriatal mosaic. I. Compartmental organization of projections from the striatum to the substantia nigra in the rat. *J Comp Neurol*, 236(4):454–76, Jun 1985.

[76] C. R. Gerfen. Synaptic organization of the striatum. *Journal of electron microscopy technique*, 10(3):265–81, Nov 1988.

[77] C. R. Gerfen. Molecular effects of dopamine on striatal-projection pathways. *Trends Neurosci*, 23(10 Suppl):S64–70, Oct 2000.

[78] C. R. Gerfen, T. M. Engber, L. C. Mahan, Z. Susel, T. N. Chase, F. J. Monsma, and D. R. Sibley. D1 and D2 dopamine receptor-regulated gene expression of striatonigral and striatopallidal neurons. *Science*, 250(4986):1429–32, Dec 1990.

[79] T. S. Gertler, C. S. Chan, and D. J. Surmeier. Dichotomous anatomical properties of adult striatal medium spiny neurons. *J Neurosci*, 28(43):10814–24, Oct 2008.

[80] M. Gewaltig and M. Diesmann. *NEST (Neural Simulation Tool)*. Scholarpedia, 2007.

[81] J.-A. Girault, H. C. Hemmings, K. R. Williams, A. C. Nairn, and P. Greengard. Phosphorylation of DARPP-32, a dopamine- and cAMP-regulated

phosphoprotein, by casein kinase II. *J Biol Chem*, 264(36):21748–59, Dec 1989.

[82] N. H. Goddard, M. Hucka, F. Howell, H. Cornelis, K. Shankar, and D. Beeman. Towards NeuroML: model description methods for collaborative modelling in neuroscience. *Philos Trans R Soc Lond, B, Biol Sci*, 356(1412):1209–28, Aug 2001.

[83] S. Gong and X. W. Yang. Modification of bacterial artificial chromosomes (BACs) and preparation of intact BAC DNA for generation of transgenic mice. *Current protocols in neuroscience*, Chapter 5:Unit 5.21, May 2005.

[84] S. Gong, C. Zheng, M. L. Doughty, K. Losos, N. Didkovsky, U. B. Schambra, N. J. Nowak, A. Joyner, G. Leblanc, M. E. Hatten, and N. Heintz. A gene expression atlas of the central nervous system based on bacterial artificial chromosomes. *Nature*, 425(6961):917–25, Oct 2003.

[85] F. Gonon, J. B. Burie, M. Jaber, M. Benoit-Marand, B. Dumartin, and B. Bloch. Geometry and kinetics of dopaminergic transmission in the rat striatum and in mice lacking the dopamine transporter. *Prog Brain Res*, 125:291–302, Jan 2000.

[86] T. D. Gould and H. K. Manji. DARPP-32: A molecular switch at the nexus of reward pathway plasticity. *Proc Natl Acad Sci USA*, 102(2):253–4, Jan 2005.

[87] A. A. Grace. Gating of information flow within the limbic system and the pathophysiology of schizophrenia. *Brain Res Brain Res Rev*, 31(2-3):330–41, Mar 2000.

[88] P. Greengard. The neurobiology of dopamine signaling. *Biosci Rep*, 21(3):247–69, Jun 2001.

[89] P. Greengard, P. B. Allen, and A. C. Nairn. Beyond the dopamine receptor: the DARPP-32/protein phosphatase-1 cascade. *Neuron*, 23(3):435–47, Jul 1999.

[90] P. Greengard, A. C. Nairn, J.-A. Girault, C. C. Ouimet, G. L. Snyder, G. Fisone, P. B. Allen, A. A. Fienberg, and A. Nishi. The DARPP-32/protein phosphatase-1 cascade: a model for signal integration. *Brain Res Brain Res Rev*, 26(2-3):274–84, May 1998.

[91] A. J. Gruber, S. A. Solla, D. J. Surmeier, and J. C. Houk. Modulation of striatal single units by expected reward: a spiny neuron model displaying dopamine-induced bistability. *J Neurophysiol*, 90(2):1095–114, Aug 2003.

[92] P. Gubellini, A. Pisani, D. Centonze, G. Bernardi, and P. Calabresi. Metabotropic glutamate receptors and striatal synaptic plasticity: implications for neurological diseases. *Prog Neurobiol*, 74(5):271–300, Dec 2004.

[93] P. Gubellini, E. Saulle, D. Centonze, C. Costa, D. Tropepi, G. Bernardi, F. Conquet, and P. Calabresi. Corticostriatal LTP requires combined mGluR1 and mGluR5 activation. *Neuropharmacology*, 44(1):8–16, Jan 2003.

[94] J. L. Guillou, H. Nakata, and D. M. Cooper. Inhibition by calcium of mammalian adenylyl cyclases. *J Biol Chem*, 274(50):35539–45, Dec 1999.

[95] K. Håkansson, M. Lindskog, L. Pozzi, A. Usiello, and G. Fisone. DARPP-32 and modulation of cAMP signaling: involvement in motor control and levodopa-induced dyskinesia. *Parkinsonism Relat Disord*, 10(5):281–6, Jul 2004.

[96] P. J. Hallett, R. Spoelgen, B. T. Hyman, D. G. Standaert, and A. W. Dunah. Dopamine D1 activation potentiates striatal NMDA receptors by tyrosine phosphorylation-dependent subunit trafficking. *J Neurosci*, 26(17):4690–700, Apr 2006.

[97] S. Halpain, J.-A. Girault, and P. Greengard. Activation of NMDA receptors induces dephosphorylation of DARPP-32 in rat striatal slices. *Nature*, 343(6256):369–72, Jan 1990.

[98] M. Hamada, J. P. Hendrick, G. R. Ryan, M. Kuroiwa, H. Higashi, M. Tanaka, A. C. Nairn, P. Greengard, and A. Nishi. Nicotine regulates

DARPP-32 (dopamine- and cAMP-regulated phosphoprotein of 32 kDa) phosphorylation at multiple sites in neostriatal neurons. *J Pharmacol Exp Ther*, 315(2):872–8, Nov 2005.

[99] C. Hansel, A. Artola, and W. Singer. Relation between dendritic Ca2+ levels and the polarity of synaptic long-term modifications in rat visual cortex neurons. *Eur J Neurosci*, 9(11):2309–22, Nov 1997.

[100] J. Harvey and M. G. Lacey. Endogenous and exogenous dopamine depress EPSCs in rat nucleus accumbens in vitro via D1 receptors activation. *J Physiol (Lond)*, 492 (Pt 1):143–54, Apr 1996.

[101] J. Harvey and M. G. Lacey. A postsynaptic interaction between dopamine D1 and NMDA receptors promotes presynaptic inhibition in the rat nucleus accumbens via adenosine release. *J Neurosci*, 17(14):5271–80, Jul 1997.

[102] Y. Hashimotodani, T. Ohno-Shosaku, H. Tsubokawa, H. Ogata, K. Emoto, T. Maejima, K. Araishi, H.-S. Shin, and M. Kano. Phospholipase Cbeta serves as a coincidence detector through its Ca2+ dependency for triggering retrograde endocannabinoid signal. *Neuron*, 45(2):257–68, Jan 2005.

[103] A. Hayer and U. S. Bhalla. Molecular switches at the synapse emerge from receptor and kinase traffic. *PLoS Comput Biol*, 1(2):137–54, Jul 2005.

[104] H. C. Hemmings, P. Greengard, H. Y. Tung, and P. Cohen. DARPP-32, a dopamine-regulated neuronal phosphoprotein, is a potent inhibitor of protein phosphatase-1. *Nature*, 310(5977):503–5, Jan 1984.

[105] H. C. Hemmings, A. C. Nairn, and P. Greengard. DARPP-32, a dopamine- and adenosine 3':5'-monophosphate-regulated neuronal phosphoprotein. II. Comparison of the kinetics of phosphorylation of DARPP-32 and phosphatase inhibitor 1. *J Biol Chem*, 259(23):14491–7, Dec 1984.

[106] H. C. Hemmings, K. R. Williams, W. H. Konigsberg, and P. Greengard. DARPP-32, a dopamine- and adenosine 3':5'-monophosphate-regulated neuronal phosphoprotein. I. Amino acid sequence around the phosphorylated threonine. *J Biol Chem*, 259(23):14486–90, Dec 1984.

[107] C. M. Hempel, P. Vincent, S. R. Adams, R. Y. Tsien, and A. I. Selverston. Spatio-temporal dynamics of cyclic AMP signals in an intact neural circuitm. *Nature*, 384(6605):166–9, Nov 1996.

[108] E. Hernández-Echeagaray, A. J. Starling, C. Cepeda, and M. S. Levine. Modulation of AMPA currents by D2 dopamine receptors in striatal medium-sized spiny neurons: are dendrites necessary? *Eur J Neurosci*, 19(9):2455–63, May 2004.

[109] S. Hernandez-Lopez, T. Tkatch, E. Perez-Garci, E. Galarraga, J. Bargas, H. Hamm, and D. J. Surmeier. D2 dopamine receptors in striatal medium spiny neurons reduce L-type Ca2+ currents and excitability via a novel PLC[beta]1-IP3-calcineurin-signaling cascade. *J Neurosci*, 20(24):8987–95, Dec 2000.

[110] S. M. Hersch, B. J. Ciliax, C. A. Gutekunst, H. D. Rees, C. J. Heilman, K. K. Yung, J. P. Bolam, E. Ince, H. Yi, and A. I. Levey. Electron microscopic analysis of D1 and D2 dopamine receptor proteins in the dorsal striatum and their synaptic relationships with motor corticostriatal afferents. *J Neurosci*, 15(7 Pt 2):5222–37, Jul 1995.

[111] O. Hikosaka, K. Nakamura, and H. Nakahara. Basal ganglia orient eyes to reward. *J Neurophysiol*, 95(2):567–84, Feb 2006.

[112] M. L. Hines and N. T. Carnevale. NEURON: a tool for neuroscientists. *The Neuroscientist : a review journal bringing neurobiology, neurology and psychiatry*, 7(2):123–35, Apr 2001.

[113] M. L. Hines, T. Morse, M. Migliore, N. T. Carnevale, and G. M. Shepherd. ModelDB: A Database to Support Computational Neuroscience. *J Comput Neurosci*, 17(1):7–11, Jan 2004.

[114] G. Hinton and A. Brown. Spiking boltzmann machines. *ADVANCES IN NEURAL INFORMATION PROCESSING SYSTEMS*, 12, 2000.

[115] W. R. Holmes. The role of dendritic diameters in maximizing the effectiveness of synaptic inputs. *Brain Res*, 478(1):127–37, Jan 1989.

[116] S. Hoops, S. Sahle, R. Gauges, C. Lee, J. Pahle, N. Simus, M. Singhal, L. Xu, P. Mendes, and U. Kummer. COPASI–a COmplex PAthway SImulator. *Bioinformatics*, 22(24):3067–74, Dec 2006.

[117] F. W. Hopf, M. G. Cascini, A. S. Gordon, I. Diamond, and A. Bonci. Cooperative activation of dopamine D1 and D2 receptors increases spike firing of nucleus accumbens neurons via G-protein betagamma subunits. *J Neurosci*, 23(12):5079–87, Jun 2003.

[118] K. S. Hsu, C. C. Huang, C. H. Yang, and P. W. Gean. Presynaptic D2 dopaminergic receptors mediate inhibition of excitatory synaptic transmission in rat neostriatum. *Brain Res*, 690(2):264–8, Sep 1995.

[119] S. C. Hu, J. Chrivia, and A. Ghosh. Regulation of CBP-mediated transcription by neuronal calcium signaling. *Neuron*, 22(4):799–808, Apr 1999.

[120] X.-T. Hu, Y. Dong, X.-F. Zhang, and F. J. White. Dopamine D2 receptor-activated Ca2+ signaling modulates voltage-sensitive sodium currents in rat nucleus accumbens neurons. *J Neurophysiol*, 93(3):1406–17, Mar 2005.

[121] M. Hucka, A. Finney, H. M. Sauro, H. Bolouri, J. C. Doyle, H. Kitano, A. P. Arkin, B. J. Bornstein, D. Bray, A. Cornish-Bowden, A. A. Cuellar, S. Dronov, E. D. Gilles, M. Ginkel, V. Gor, I. I. Goryanin, W. J. Hedley, T. C. Hodgman, J.-H. Hofmeyr, P. J. Hunter, N. S. Juty, J. L. Kasberger, A. Kremling, U. Kummer, N. L. Novère, L. M. Loew, D. Lucio, P. Mendes, E. Minch, E. D. Mjolsness, Y. Nakayama, M. R. Nelson, P. F. Nielsen, T. Sakurada, J. C. Schaff, B. E. Shapiro, T. S. Shimizu, H. D. Spence, J. Stelling, K. Takahashi, M. Tomita, J. Wagner, J. Wang, and S. Forum. The systems biology markup language (SBML): a medium for representation and exchange of biochemical network models. *Bioinformatics*, 19(4):524–31, Mar 2003.

[122] A. Hudmon and H. Schulman. Neuronal CA2+/calmodulin-dependent protein kinase II: the role of structure and autoregulation in cellular function. *Annu Rev Biochem*, 71:473–510, Jan 2002.

[123] A. Hudmon and H. Schulman. Structure-function of the multifunctional Ca2+/calmodulin-dependent protein kinase II. *Biochem J*, 364(Pt 3):593–611, Jun 2002.

[124] V. Janssens, J. Jordens, I. Stevens, C. V. Hoof, E. Martens, H. D. Smedt, Y. Engelborghs, E. Waelkens, and J. Goris. Identification and functional analysis of two Ca2+-binding EF-hand motifs in the B"/PR72 subunit of protein phosphatase 2A. *J Biol Chem*, 278(12):10697–706, Mar 2003.

[125] J. G. Johnston, C. R. Gerfen, S. N. Haber, and D. van der Kooy. Mechanisms of striatal pattern formation: conservation of mammalian compartmentalization. *Brain Res Dev Brain Res*, 57(1):93–102, Dec 1990.

[126] B. M. Kampa, J. Clements, P. Jonas, and G. J. Stuart. Kinetics of Mg2+ unblock of NMDA receptors: implications for spike-timing dependent synaptic plasticity. *J Physiol (Lond)*, 556(Pt 2):337–45, Apr 2004.

[127] B. M. Kampa, J. J. Letzkus, and G. J. Stuart. Dendritic mechanisms controlling spike-timing-dependent synaptic plasticity. *Trends Neurosci*, 30(9):456–63, Sep 2007.

[128] Y. Kawaguchi. Neostriatal cell subtypes and their functional roles. *Neurosci Res*, 27(1):1–8, Jan 1997.

[129] Y. Kawaguchi, C. J. Wilson, S. J. Augood, and P. C. Emson. Striatal interneurones: chemical, physiological and morphological characterization. *Trends Neurosci*, 18(12):527–35, Dec 1995.

[130] A. E. Kelley. Memory and addiction: shared neural circuitry and molecular mechanisms. *Neuron*, 44(1):161–79, Sep 2004.

[131] J. N. Kerr and J. R. Wickens. Dopamine D-1/D-5 receptor activation is required for long-term potentiation in the rat neostriatum in vitro. *J Neurophysiol*, 85(1):117–24, Jan 2001.

[132] J. N. D. Kerr and D. Plenz. Dendritic calcium encodes striatal neuron output during up-states. *J Neurosci*, 22(5):1499–512, Mar 2002.

[133] J. N. D. Kerr and D. Plenz. Action potential timing determines dendritic calcium during striatal up-states. *J Neurosci*, 24(4):877–85, Jan 2004.

[134] M. M. King, C. Y. Huang, P. B. Chock, A. C. Nairn, H. C. Hemmings, K. F. Chan, and P. Greengard. Mammalian brain phosphoproteins as substrates for calcineurin. *J Biol Chem*, 259(13):8080–3, Jul 1984.

[135] S. T. Kitai and D. J. Surmeier. Cholinergic and dopaminergic modulation of potassium conductances in neostriatal neurons. *Advances in neurology*, 60:40–52, Jan 1993.

[136] C. B. Klee, G. F. Draetta, and M. J. Hubbard. Calcineurin. *Adv Enzymol Relat Areas Mol Biol*, 61:149–200, Jan 1988.

[137] C. Koch. *Biophysics of Computation*. Oxford University Press, Jan 2004.

[138] C. Koch and I. Segev. *Methods in Neuronal Modeling: From Ions to Networks*. MIT Press, Jan 1998.

[139] R. Kötter. Postsynaptic integration of glutamatergic and dopaminergic signals in the striatum. *Prog Neurobiol*, 44(2):163–96, Oct 1994.

[140] R. Kötter and J. R. Wickens. Interactions of glutamate and dopamine in a computational model of the striatum. *J Comput Neurosci*, 2(3):195–214, Sep 1995.

[141] A. C. Kreitzer. Physiology and pharmacology of striatal neurons. *Annu Rev Neurosci*, 32:127–47, Jan 2009.

[142] S. Kuroda, N. Schweighofer, and M. Kawato. Exploration of signal transduction pathways in cerebellar long-term depression by kinetic simulation. *J Neurosci*, 21(15):5693–702, Aug 2001.

[143] H. K. Lee, M. Barbarosie, K. Kameyama, M. F. Bear, and R. L. Huganir. Regulation of distinct AMPA receptor phosphorylation sites during bidirectional synaptic plasticity. *Nature*, 405(6789):955–9, Jun 2000.

[144] I. Lengyel, K. Voss, M. Cammarota, K. Bradshaw, V. Brent, K. P. S. J. Murphy, K. P. Giese, J. A. P. Rostas, and T. V. P. Bliss. Autonomous activity of CaMKII is only transiently increased following the induction of long-term potentiation in the rat hippocampus. *Eur J Neurosci*, 20(11):3063–72, Dec 2004.

[145] J. J. Letzkus, B. M. Kampa, and G. J. Stuart. Learning rules for spike timing-dependent plasticity depend on dendritic synapse location. *J Neurosci*, 26(41):10420–9, Oct 2006.

[146] M. S. Levine, Z. Li, C. Cepeda, H. C. Cromwell, and K. L. Altemus. Neuromodulatory actions of dopamine on synaptically-evoked neostriatal responses in slices. *Synapse*, 24(1):65–78, Sep 1996.

[147] T. Li, L. E. Chalifour, and H. K. Paudel. Phosphorylation of protein phosphatase 1 by cyclin-dependent protein kinase 5 during nerve growth factor-induced PC12 cell differentiation. *J Biol Chem*, 282(9):6619–28, Mar 2007.

[148] J. Y. Lin, R. Dubey, G. D. Funk, and J. Lipski. Receptor subtype-specific modulation by dopamine of glutamatergic responses in striatal medium spiny neurons. *Brain Res*, 959(2):251–62, Jan 2003.

[149] M. Lindskog, M. Kim, M. A. Wikström, K. T. Blackwell, and J. H. Kotaleski. Transient calcium and dopamine increase PKA activity and DARPP-32 phosphorylation. *PLoS Comput Biol*, 2(9):e119, Sep 2006.

[150] J. Lisman. A mechanism for the Hebb and the anti-Hebb processes underlying learning and memory. *Proc Natl Acad Sci USA*, 86(23):9574–8, Dec 1989.

[151] J. Lisman, H. Schulman, and H. Cline. The molecular basis of CaMKII function in synaptic and behavioural memory. *Nat Rev Neurosci*, 3(3):175–90, Mar 2002.

[152] F. Liu, X. H. Ma, J. Ule, J. A. Bibb, A. Nishi, A. J. DeMaggio, Z. Yan, A. C. Nairn, and P. Greengard. Regulation of cyclin-dependent kinase 5 and casein kinase 1 by metabotropic glutamate receptors. *Proc Natl Acad Sci USA*, 98(20):11062–8, Sep 2001.

[153] F. Liu, D. M. Virshup, A. C. Nairn, and P. Greengard. Mechanism of regulation of casein kinase I activity by group I metabotropic glutamate receptors. *J Biol Chem*, 277(47):45393–9, Nov 2002.

[154] D. M. Lovinger, E. C. Tyler, and A. Merritt. Short- and long-term synaptic depression in rat neostriatum. *J Neurophysiol*, 70(5):1937–49, Nov 1993.

[155] R. C. Malenka and M. F. Bear. LTP and LTD: an embarrassment of riches. *Neuron*, 44(1):5–21, Sep 2004.

[156] R. Malinow and R. C. Malenka. AMPA receptor trafficking and synaptic plasticity. *Annu Rev Neurosci*, 25:103–26, Jan 2002.

[157] N. I. Markevich, J. B. Hoek, and B. N. Kholodenko. Signaling switches and bistability arising from multisite phosphorylation in protein kinase cascades. *J Cell Biol*, 164(3):353–9, Feb 2004.

[158] H. Markram. The blue brain project. *Nat Rev Neurosci*, 7(2):153–60, Feb 2006.

[159] F. A. Middleton and P. L. Strick. Basal ganglia and cerebellar loops: motor and cognitive circuits. *Brain Res Brain Res Rev*, 31(2-3):236–50, Mar 2000.

[160] C. Missale, S. R. Nash, S. W. Robinson, M. Jaber, and M. G. Caron. Dopamine receptors: from structure to function. *Physiol Rev*, 78(1):189–225, Jan 1998.

[161] N. Mons and D. M. Cooper. Selective expression of one Ca(2+)-inhibitable adenylyl cyclase in dopaminergically innervated rat brain regions. *Brain Res Mol Brain Res*, 22(1-4):236–44, Mar 1994.

[162] J. T. Moyer, J. A. Wolf, and L. H. Finkel. Effects of dopaminergic modulation on the integrative properties of the ventral striatal medium spiny neuron. *J Neurophysiol*, 98(6):3731–48, Dec 2007.

[163] G. Nagel, T. Szellas, W. Huhn, S. Kateriya, N. Adeishvili, P. Berthold, D. Ollig, P. Hegemann, and E. Bamberg. Channelrhodopsin-2, a directly light-gated cation-selective membrane channel. *Proc Natl Acad Sci USA*, 100(24):13940–5, Nov 2003.

[164] A. C. Nairn, P. Svenningsson, A. Nishi, G. Fisone, J.-A. Girault, and P. Greengard. The role of DARPP-32 in the actions of drugs of abuse. *Neuropharmacology*, 47 Suppl 1:14–23, Jan 2004.

[165] E. J. Nestler. Molecular basis of long-term plasticity underlying addiction. *Nat Rev Neurosci*, 2(2):119–28, Feb 2001.

[166] K. A. Neve, J. K. Seamans, and H. Trantham-Davidson. Dopamine receptor signaling. *J Recept Signal Transduct Res*, 24(3):165–205, Aug 2004.

[167] T. Nevian and B. Sakmann. Spine Ca2+ signaling in spike-timing-dependent plasticity. *J Neurosci*, 26(43):11001–13, Oct 2006.

[168] S. M. Nicola, D. J. Surmeier, and R. C. Malenka. Dopaminergic modulation of neuronal excitability in the striatum and nucleus accumbens. *Annu Rev Neurosci*, 23:185–215, Jan 2000.

[169] E. S. Nisenbaum, P. G. Mermelstein, C. J. Wilson, and D. J. Surmeier. Selective blockade of a slowly inactivating potassium current in striatal neurons by (+/-) 6-chloro-APB hydrobromide (SKF82958). *Synapse*, 29(3):213–24, Jul 1998.

[170] A. Nishi, J. A. Bibb, S. Matsuyama, M. Hamada, H. Higashi, A. C. Nairn, and P. Greengard. Regulation of DARPP-32 dephosphorylation at PKA- and Cdk5-sites by NMDA and AMPA receptors: distinct roles of calcineurin and protein phosphatase-2A. *J Neurochem*, 81(4):832–41, May 2002.

[171] A. Nishi, J. A. Bibb, G. L. Snyder, H. Higashi, A. C. Nairn, and P. Greengard. Amplification of dopaminergic signaling by a positive feedback loop. *Proc Natl Acad Sci USA*, 97(23):12840–5, Nov 2000.

[172] A. Nishi, G. L. Snyder, and P. Greengard. Bidirectional regulation of DARPP-32 phosphorylation by dopamine. *J Neurosci*, 17(21):8147–55, Nov 1997.

[173] A. Nishi, G. L. Snyder, A. C. Nairn, and P. Greengard. Role of calcineurin and protein phosphatase-2A in the regulation of DARPP-32 dephosphorylation in neostriatal neurons. *J Neurochem*, 72(5):2015–21, May 1999.

[174] A. Nishi, Y. Watanabe, H. Higashi, M. Tanaka, A. C. Nairn, and P. Greengard. Glutamate regulation of DARPP-32 phosphorylation in neostriatal neurons involves activation of multiple signaling cascades. *Proc Natl Acad Sci USA*, 102(4):1199–204, Jan 2005.

[175] N. L. Novère, B. Bornstein, A. Broicher, M. Courtot, M. Donizelli, H. Dharuri, L. Li, H. Sauro, M. Schilstra, B. Shapiro, J. L. Snoep, and M. Hucka. BioModels Database: a free, centralized database of curated, published, quantitative kinetic models of biochemical and cellular systems. *Nucleic Acids Res*, 34(Database issue):D689–91, Jan 2006.

[176] M. Oberlaender, V. J. Dercksen, R. Egger, M. Gensel, B. Sakmann, and H.-C. Hege. Automated three-dimensional detection and counting of neuron somata. *J Neurosci Methods*, 180(1):147–60, May 2009.

[177] P. O'Donnell and A. A. Grace. Physiological and morphological properties of accumbens core and shell neurons recorded in vitro. *Synapse*, 13(2):135–60, Feb 1993.

[178] P. O'Donnell and A. A. Grace. Tonic D2-mediated attenuation of cortical excitation in nucleus accumbens neurons recorded in vitro. *Brain Res*, 634(1):105–12, Jan 1994.

[179] M. C. Oh, V. A. Derkach, E. S. Guire, and T. R. Soderling. Extrasynaptic membrane trafficking regulated by GluR1 serine 845 phosphorylation primes AMPA receptors for long-term potentiation. *J Biol Chem*, 281(2):752–8, Jan 2006.

[180] P. A. Olson, T. Tkatch, S. Hernandez-Lopez, S. Ulrich, E. Ilijic, E. Mugnaini, H. Zhang, I. Bezprozvanny, and D. J. Surmeier. G-protein-coupled receptor modulation of striatal CaV1.3 L-type Ca2+ channels is dependent on a Shank-binding domain. *J Neurosci*, 25(5):1050–62, Feb 2005.

[181] M. Otsuka, J. Yoshimoto, and K. Doya. Robust Population Coding in Free-Energy-Based Reinforcement Learning. In *Proceedings of the 18th international conference on Artificial Neural Networks, Part I*, page 386. Springer, 2008.

[182] M. T. Pacheco-Cano, J. Bargas, S. Hernández-López, D. Tapia, and E. Galarraga. Inhibitory action of dopamine involves a subthreshold Cs(+)-sensitive conductance in neostriatal neurons. *Experimental brain research Experimentelle Hirnforschung Expérimentation cérébrale*, 110(2):205–11, Jul 1996.

[183] M. Passafaro, V. Piëch, and M. Sheng. Subunit-specific temporal and spatial patterns of AMPA receptor exocytosis in hippocampal neurons. *Nat Neurosci*, 4(9):917–26, Sep 2001.

[184] S. Paul, G. L. Snyder, H. Yokakura, M. R. Picciotto, A. C. Nairn, and P. J. Lombroso. The Dopamine/D1 receptor mediates the phosphorylation and inactivation of the protein tyrosine phosphatase STEP via a PKA-dependent pathway. *J Neurosci*, 20(15):5630–8, Aug 2000.

[185] V. Pawlak and J. N. D. Kerr. Dopamine receptor activation is required for corticostriatal spike-timing-dependent plasticity. *J Neurosci*, 28(10):2435–46, Mar 2008.

[186] M. F. Perez, F. J. White, and X.-T. Hu. Dopamine D(2) receptor modulation of K(+) channel activity regulates excitability of nucleus accumbens neurons at different membrane potentials. *J Neurophysiol*, 96(5):2217–28, Nov 2006.

[187] W. Potjans, A. Morrison, and M. Diesmann. A spiking neural network model of an actor-critic learning agent. *Neural computation*, 21(2):301–39, Feb 2009.

[188] C. J. Price, P. Kim, and L. A. Raymond. D1 dopamine receptor-induced cyclic AMP-dependent protein kinase phosphorylation and potentiation of striatal glutamate receptors. *J Neurochem*, 73(6):2441–6, Dec 1999.

[189] D. V. Raju, T. H. Ahern, D. J. Shah, T. M. Wright, D. G. Standaert, R. A. Hall, and Y. Smith. Differential synaptic plasticity of the corticostriatal and thalamostriatal systems in an MPTP-treated monkey model of parkinsonism. *Eur J Neurosci*, 27(7):1647–58, Apr 2008.

[190] S. V. Rakhilin, P. A. Olson, A. Nishi, N. N. Starkova, A. A. Fienberg, A. C. Nairn, D. J. Surmeier, and P. Greengard. A network of control mediated by regulator of calcium/calmodulin-dependent signaling. *Science*, 306(5696):698–701, Oct 2004.

[191] J. N. Reynolds, B. I. Hyland, and J. R. Wickens. A cellular mechanism of reward-related learning. *Nature*, 413(6851):67–70, Sep 2001.

[192] J. N. Reynolds and J. R. Wickens. Substantia nigra dopamine regulates synaptic plasticity and membrane potential fluctuations in the rat neostriatum, in vivo. *Neuroscience*, 99(2):199–203, Jan 2000.

[193] J. N. J. Reynolds and J. R. Wickens. Dopamine-dependent plasticity of corticostriatal synapses. *Neural Networks*, 15(4-6):507–21, Jan 2002.

[194] K. W. Roche, R. J. O'Brien, A. L. Mammen, J. Bernhardt, and R. L. Huganir. Characterization of multiple phosphorylation sites on the AMPA receptor GluR1 subunit. *Neuron*, 16(6):1179–88, Jun 1996.

[195] J. E. Rubin, R. C. Gerkin, G.-Q. Bi, and C. C. Chow. Calcium time course as a signal for spike-timing-dependent plasticity. *J Neurophysiol*, 93(5):2600–13, May 2005.

[196] E. Saka, M. Iadarola, D. J. Fitzgerald, and A. M. Graybiel. Local circuit neurons in the striatum regulate neural and behavioral responses to dopaminergic stimulation. *Proc Natl Acad Sci USA*, 99(13):9004–9, Jun 2002.

[197] H. Salgado, F. Tecuapetla, T. Perez-Rosello, A. Perez-Burgos, E. Perez-Garci, E. Galarraga, and J. Bargas. A reconfiguration of CaV2 Ca2+ channel current and its dopaminergic D2 modulation in developing neostriatal neurons. *J Neurophysiol*, 94(6):3771–87, Dec 2005.

[198] B. Sallans and G. Hinton. Reinforcement Learning with Factored States and Actions. *The Journal of Machine Learning Research*, Jan 2004.

[199] K. Samejima, Y. Ueda, K. Doya, and M. Kimura. Representation of action-specific reward values in the striatum. *Science*, 310(5752):1337–40, Nov 2005.

[200] S. N. Schiffmann, F. Desdouits, R. Menu, P. Greengard, J. D. Vincent, J. J. Vanderhaeghen, and J.-A. Girault. Modulation of the voltage-gated sodium current in rat striatal neurons by DARPP-32, an inhibitor of protein phosphatase. *Eur J Neurosci*, 10(4):1312–20, Apr 1998.

[201] S. N. Schiffmann, P. M. Lledo, and J. D. Vincent. Dopamine D1 receptor modulates the voltage-gated sodium current in rat striatal neurones through a protein kinase A. *J Physiol (Lond)*, 483 (Pt 1):95–107, Feb 1995.

[202] W. Schultz, P. Dayan, and P. R. Montague. A neural substrate of prediction and reward. *Science*, 275(5306):1593–9, Mar 1997.

[203] H. S. Seung. Reading the book of memory: sparse sampling versus dense mapping of connectomes. *Neuron*, 62(1):17–29, Apr 2009.

[204] W. Shen, M. Flajolet, P. Greengard, and D. J. Surmeier. Dichotomous dopaminergic control of striatal synaptic plasticity. *Science*, 321(5890):848–51, Aug 2008.

[205] H. Z. Shouval, M. F. Bear, and L. N. Cooper. A unified model of NMDA receptor-dependent bidirectional synaptic plasticity. *Proc Natl Acad Sci USA*, 99(16):10831–6, Aug 2002.

[206] H. Z. Shouval and G. Kalantzis. Stochastic properties of synaptic transmission affect the shape of spike time-dependent plasticity curves. *J Neurophysiol*, 93(2):1069–73, Feb 2005.

[207] J. A. Shuen, M. Chen, B. Gloss, and N. Calakos. Drd1a-tdTomato BAC transgenic mice for simultaneous visualization of medium spiny neurons in the direct and indirect pathways of the basal ganglia. *J Neurosci*, 28(11):2681–5, Mar 2008.

[208] S. Sivakumaran, S. Hariharaputran, J. Mishra, and U. S. Bhalla. The Database of Quantitative Cellular Signaling: management and analysis of

chemical kinetic models of signaling networks. *Bioinformatics*, 19(3):408–15, Feb 2003.

[209] P. J. Sjöström and S. B. Nelson. Spike timing, calcium signals and synaptic plasticity. *Curr Opin Neurobiol*, 12(3):305–14, Jun 2002.

[210] G. L. Snyder, P. B. Allen, A. A. Fienberg, C. G. Valle, R. L. Huganir, A. C. Nairn, and P. Greengard. Regulation of phosphorylation of the GluR1 AMPA receptor in the neostriatum by dopamine and psychostimulants in vivo. *J Neurosci*, 20(12):4480–8, Jun 2000.

[211] G. L. Snyder, S. Galdi, A. A. Fienberg, P. B. Allen, A. C. Nairn, and P. Greengard. Regulation of AMPA receptor dephosphorylation by glutamate receptor agonists. *Neuropharmacology*, 45(6):703–13, Nov 2003.

[212] W. J. Song and D. J. Surmeier. Voltage-dependent facilitation of calcium channels in rat neostriatal neurons. *J Neurophysiol*, 76(4):2290–306, Oct 1996.

[213] J. P. Spencer and K. P. Murphy. Bi-directional changes in synaptic plasticity induced at corticostriatal synapses in vitro. *Experimental brain research Experimentelle Hirnforschung Expérimentation cérébrale*, 135(4):497–503, Dec 2000.

[214] K. W. Sung, S. Choi, and D. M. Lovinger. Activation of group I mGluRs is necessary for induction of long-term depression at striatal synapses. *J Neurophysiol*, 86(5):2405–12, Nov 2001.

[215] D. J. Surmeier, J. Bargas, H. C. Hemmings, A. C. Nairn, and P. Greengard. Modulation of calcium currents by a D1 dopaminergic protein kinase/phosphatase cascade in rat neostriatal neurons. *Neuron*, 14(2):385–97, Feb 1995.

[216] D. J. Surmeier, J. Ding, M. Day, Z. Wang, and W. Shen. D1 and D2 dopamine-receptor modulation of striatal glutamatergic signaling in striatal medium spiny neurons. *Trends Neurosci*, 30(5):228–35, May 2007.

[217] D. J. Surmeier, J. Eberwine, C. J. Wilson, Y. Cao, A. Stefani, and S. T. Kitai. Dopamine receptor subtypes colocalize in rat striatonigral neurons. *Proc Natl Acad Sci USA*, 89(21):10178–82, Nov 1992.

[218] D. J. Surmeier and S. T. Kitai. D1 and D2 dopamine receptor modulation of sodium and potassium currents in rat neostriatal neurons. *Prog Brain Res*, 99:309–24, Jan 1993.

[219] T. Suzuki, M. Miura, K. Nishimura, and T. Aosaki. Dopamine-dependent synaptic plasticity in the striatal cholinergic interneurons. *J Neurosci*, 21(17):6492–501, Sep 2001.

[220] P. Svenningsson, A. C. Nairn, and P. Greengard. DARPP-32 mediates the actions of multiple drugs of abuse. *The AAPS journal*, 7(2):E353–60, Jan 2005.

[221] P. Svenningsson, A. Nishi, G. Fisone, J.-A. Girault, A. C. Nairn, and P. Greengard. DARPP-32: an integrator of neurotransmission. *Annu Rev Pharmacol Toxicol*, 44:269–96, Jan 2004.

[222] G. T. Swanson, S. K. Kamboj, and S. G. Cull-Candy. Single-channel properties of recombinant AMPA receptors depend on RNA editing, splice variation, and subunit composition. *J Neurosci*, 17(1):58–69, Jan 1997.

[223] C.-H. Tan, X. He, J. Yang, and W.-Y. Ong. Changes in AMPA subunit expression in the mouse brain after chronic treatment with the antidepressant maprotiline: a link between noradrenergic and glutamatergic function? *Experimental brain research Experimentelle Hirnforschung Expérimentation cérébrale*, 170(4):448–56, Apr 2006.

[224] K. Tanaka, L. Khiroug, F. Santamaria, T. Doi, H. Ogasawara, G. C. R. Ellis-Davies, M. Kawato, and G. J. Augustine. Ca2+ requirements for cerebellar long-term synaptic depression: role for a postsynaptic leaky integrator. *Neuron*, 54(5):787–800, Jun 2007.

[225] K. Tang, M. J. Low, D. K. Grandy, and D. M. Lovinger. Dopamine-dependent synaptic plasticity in striatum during in vivo development. *Proc Natl Acad Sci USA*, 98(3):1255–60, Jan 2001.

[226] N. Uchimura, H. Higashi, and S. Nishi. Hyperpolarizing and depolarizing actions of dopamine via D-1 and D-2 receptors on nucleus accumbens neurons. *Brain Res*, 375(2):368–72, Jun 1986.

[227] N. Uchimura and R. A. North. Actions of cocaine on rat nucleus accumbens neurones in vitro. *Br J Pharmacol*, 99(4):736–40, Apr 1990.

[228] M. Umemiya and L. A. Raymond. Dopaminergic modulation of excitatory postsynaptic currents in rat neostriatal neurons. *J Neurophysiol*, 78(3):1248–55, Sep 1997.

[229] H. Urakubo, M. Honda, R. C. Froemke, and S. Kuroda. Requirement of an allosteric kinetics of NMDA receptors for spike timing-dependent plasticity. *J Neurosci*, 28(13):3310–23, Mar 2008.

[230] H. Usui, R. Inoue, O. Tanabe, Y. Nishito, M. Shimizu, H. Hayashi, H. Kagamiyama, and M. Takeda. Activation of protein phosphatase 2A by cAMP-dependent protein kinase-catalyzed phosphorylation of the 74-kDa B" (delta) regulatory subunit in vitro and identification of the phosphorylation sites. *FEBS Lett*, 430(3):312–6, Jul 1998.

[231] Z. Wang, L. Kai, M. Day, J. Ronesi, H. H. Yin, J. Ding, T. Tkatch, D. M. Lovinger, and D. J. Surmeier. Dopaminergic control of corticostriatal long-term synaptic depression in medium spiny neurons is mediated by cholinergic interneurons. *Neuron*, 50(3):443–52, May 2006.

[232] F. J. White, X. T. Hu, and X.-F. Zhang. DA D2 receptors in the ventral striatum: multiple effects or receptor subtypes? *Nihon shinkei seishin yakurigaku zasshi = Japanese journal of psychopharmacology*, 17(2):91–5, Apr 1997.

[233] J. R. Wickens and G. W. Arbuthnott. *Structural and functional interactions in the striatum at the receptor level*, volume 21. chapter IV, Elsevier, Jan 2005.

[234] J. R. Wickens and G. W. Arbuthnott. *Gating of Cortical Input to the Striatum*. chapter 19, Elsevier, 2010.

[235] J. R. Wickens, A. J. Begg, and G. W. Arbuthnott. Dopamine reverses the depression of rat corticostriatal synapses which normally follows high-frequency stimulation of cortex in vitro. *Neuroscience*, 70(1):1–5, Jan 1996.

[236] C. J. Wilson. Striatal D2 receptors and LTD: yes, but not where you thought they were. *Neuron*, 50(3):347–8, May 2006.

[237] C. J. Wilson and Y. Kawaguchi. The origins of two-state spontaneous membrane potential fluctuations of neostriatal spiny neurons. *J Neurosci*, 16(7):2397–410, Apr 1996.

[238] J. A. Wolf, J. T. Moyer, M. T. Lazarewicz, D. Contreras, M. Benoit-Marand, P. O'Donnell, and L. H. Finkel. NMDA/AMPA ratio impacts state transitions and entrainment to oscillations in a computational model of the nucleus accumbens medium spiny projection neuron. *J Neurosci*, 25(40):9080–95, Oct 2005.

[239] S. N. Yang, Y. G. Tang, and R. S. Zucker. Selective induction of LTP and LTD by postsynaptic [Ca2+]i elevation. *J Neurophysiol*, 81(2):781–7, Feb 1999.

[240] L. C. Yeung, G. C. Castellani, and H. Z. Shouval. Analysis of the intraspinal calcium dynamics and its implications for the plasticity of spiking neurons. *Phys. Rev. E*, 69(1 Pt 1):011907, Jan 2004.

[241] C. Y. Yim and G. J. Mogenson. Neuromodulatory action of dopamine in the nucleus accumbens: an in vivo intracellular study. *Neuroscience*, 26(2):403–15, Aug 1988.

[242] G. W. D. Young and J. Keizer. A single-pool inositol 1,4,5-trisphosphate-receptor-based model for agonist-stimulated oscillations in Ca2+ concentration. *Proc Natl Acad Sci USA*, 89(20):9895–9, Oct 1992.

[243] X.-F. Zhang, D. C. Cooper, and F. J. White. Repeated cocaine treatment decreases whole-cell calcium current in rat nucleus accumbens neurons. *J Pharmacol Exp Ther*, 301(3):1119–25, Jun 2002.

[244] X.-F. Zhang, X. T. Hu, and F. J. White. Whole-cell plasticity in cocaine withdrawal: reduced sodium currents in nucleus accumbens neurons. *J Neurosci*, 18(1):488–98, Jan 1998.

[245] R. S. Zucker. Calcium- and activity-dependent synaptic plasticity. *Curr Opin Neurobiol*, 9(3):305–13, Jun 1999.

Appendix

A. Publications

- Journal Paper
  - Nakano T, Doi T, Yoshimoto J, Doya K. A kinetic model of dopamine- and calcium-dependent striatal synaptic plasticity. *PLoS Computational Biology*, 6(2): e1000670, Feb 2010.

- Conferences
  - Nakano T, Yoshimoto J, Wickens J, Doya K. Calcium responses model in striatum dependent on timed input sources. *19th International Conference on Artificial Neural Networks (ICANN)*, Part I: 249-58, Limassol, Cyprus, Sep 2009. (Oral presentation, refereed full paper)
  - 中野高志, 吉本潤一郎, Wickens J, 銅谷賢治. 線条体における入力タイミングに依存するカルシウム応答モデル. 情報処理学会 第 *17*回バイオ情報学研究会, 沖縄県恩納村, 2009 年 5 月. (Oral presentation, in Japanese)
  - 中野高志, 吉本潤一郎, Wickens J, 銅谷賢治. 線条体における入力タイミング依存のカルシウム応答モデル. 脳と心のメカニズム 第 *9*回 冬のワークショップ, 留寿都, 2009 年 1 月. (Poster presentation, in Japanese)
  - Vickers C, Nakano T, Wickens J. Dopamine dependent plasticity in the corticostriatal system. *6th Forum of European Neuroscience*, Geneva, Switzerland, Jul 2008.(Poster presentation)
  - 吉本潤一郎, 中野高志. 機械学習と学習システムとしての脳—学習理論とシステム生物学の接点—. 特定領域「バイオ操作」若手研究者第 3 回ワークショップ, 沖縄, 2008 年 7 月. (招待講演) (Oral presentation, in Japanese)
  - 中野高志, 土居智和, 吉本潤一郎, 銅谷賢治. 線条体シナプス可塑性とそのシグナル伝達経路モデル. シナプス研究会, 岡崎, 2007 年 12 月. (Poster presentation, in Japanese)
  - Nakano T, Doi T, Yoshimoto J, Doya K. A kinetic model of the molecular cascade for corticostriatal synaptic potentiation and depression. *NEURO-*

SCIENCE 2007: Society for Neuroscience, 676.5, BN06, San Diego, CA, Nov 2007. (Poster presentation)

- Nakano T, Doi T, Yoshimoto J, Doya K. A kinetic model for molecular mechanisms of corticostriatal synaptic plasticity. *Neuro2007: The 17th Annual Meeting of the Japanese Neural Network Society*, Yokohama, Japan, O2P-B16, Sep 2007. (Oral presentation)
- 中野高志, 土居智和, 吉本潤一郎, 銅谷賢治. 線条体シナプス可塑性の分子機構のシミュレーション研究. 情報処理学会 第 *9* 回バイオ情報学研究会, 沖縄, 2007 年 6 月. (Oral presentation, in Japanese)
- Nakano T, Doi T, Yoshimoto J, Doya K. A kinetic model of molecular cascade for striatal synaptic potentiation and depression. *Brain reward systems: Fondation des Treilles*, Provence, May 2007. (Oral presentation)
- Nakano T, Doi T, Yoshimoto J, Doya K. A Kinetic Model of Corticostriatal Synaptic Plasticity, *7th International Conference of Systems Biology (ICSB 2006)*, Yokohama, Oct 2006. (Poster presentation)
- 中野高志, 土居智和, 吉本潤一郎, 銅谷賢治. 皮質線条体可塑性の細胞内シグナル伝達のシミュレーション. 日本神経回路学会第 *16* 回全国大会, 44-45, 名古屋, 2006 年 9 月. (Poster presentation, in Japanese)

- Workshops
  - システム神経生物学スプリングスクール (SNSS2010). 京都, 2010 年 3 月 14 日-3 月 16 日.
  - Australian Course in Advanced Neuroscience (ACAN). Australia, April 20 - May 10, 2008.
  - システム神経生物学スプリングスクール (SNSS2008). 京都, 2008 年 2 月 29 日-3 月 2 日.
  - システム神経生物学スプリングスクール (SNSS2007). 大阪, 2007 年 3 月 9 日-3 月 11 日.
  - Okinawa Computational Neuroscience Course (OCNC 2006), Okinawa, June 28th - July 7th, 2006

- Award
  - 2009 年 情報処理学会バイオ情報学研究会学生奨励賞
    (2009 SIGBIO Best Student Presentation Award)

- Model
  - The signaling cascade model is available at ModelDB (accession numbers 126098).
    https://senselab.med.yale.edu/modeldb/ShowModel.asp?model=126098

B. Model Parameters in Signaling Cascade Model

Table B.1. Initial concentrations I

Group	Name	InitialConc (uM)	Note	Reference
PKA	R2C2	3.59		Estimated
	R2C2-cAMP2	0.10		
	R2C2-cAMP4	4.88e-3		
	R2-cAMP4	0.69		
	PKA-active	0.06		
	PKA-D75	1.23		
	PKA-D75-137	0.05		
PP1	PP1-active	2.30		[139]
	PP1-D34	0.24		
	PP1-D34-137	0.03		
	PP1-D34-75	5.30e-5		
	PP1-D34-75-137	7.84e-6		
	PP1-D	0.24		
	PP1-D75	5.32e-5		
	PP1-D137	0.01		
	PP1-D75-137	2.31e-6		
I1	I1	0.68		[139]
	PP1-I1	0.01		
	PP1-I1-p	2.20		
	I1-p	6.73e-4		
PP2B	CaNAB	0.27		[139]
	CaNAB-Ca2	9.69		
	CaNAB-Ca4	0.13		
	CaMCa4-CaNAB	9.55e-4		
	CaMCa3-CaNAB	0.01		
	CaMCA2-CaNAB	0.01		

Table B.2. Initial concentrations II

Group	Name	InitialConc (uM)	Note	Reference
CaMKII	CaMKII	18.89		[139]
	CaMKII-CaM	2.90e-3		
	CaMKII-Thr286	0.33		
	CaMKII-Thr306	0.01		
	tot-CaM-CaMKII	0.02	*	
	tot-autonomous-CaMKII	0.34	*	
	CaMKII-act	0.36	*	
	CaMKII-Thr286p-CaM	0.02		
	CaMKII-Thr286-305	0.01		
	basal-CaMKII	2.00		
CaM	CaM-TR2-Ca2	0.21		Estimated
	CaM-Ca3	4.54e-3		
	CaM	58.40		
	CaM-Ca4	1.27e-5		
		58.61		
DARPP-32	D	34.97		[15]
	D34	0.01		
	D137	1.37		
	D75	9.92		
	D34-75	2.36e-6		
	D34-137	4.55e-4		
	D34-75-137	1.07e-7		
	D75-137	0.39		
PP2A	B1	2.37		[139]
	B2	2.10		
	PP2A-PKA	0.01		
	PP2A-Ca	1.21e-3		
	B1-2Ca	3.49e-4		
	PP2A	0.42		
	B2p	0.02		

tot-CaM-CaMKII = CaMKII-CaM + CaMKII-Thr286p-CaM

tot-autonomous-CaMKII = CaMKII-Thr286-305 + CaMKII-Thr286

CaMKII-act = tot-CaM-CaMKII + tot-autonomous-CaMKII

Table B.3. Initial concentrations III

Group	Name	InitialConc (uM)	Note	Reference
GluR	GluR	0.02		Estimated
	GluR-845p	0.01		
	GluR-831p-845p	1.46e-3		
	GluR-I-831p-845p	0.01		
	GluR-I-845p	0.07		
	GluR-I	0.16		
	Bulk-AMPAR	9.00	buffered	
	Anchor	11.56		
DR	D1R	0.06		Estimated
	D1R-Gs	0.44		
	D1R-DA	9.89e-4		
	D1R-DA-Gs	5.36e-4		
	Gs-GDP	2.54		
	bc	0.03		
	Gsa-GTP	1.07e-3		
	Gsa-GDP	4.18e-3		
AC	AC	2.34		[149]
	AC-Gsa	1.93e-3		
	cAMP	0.22		
	ATP	2000.00	buffered	
	AC-Ca	0.16		
	ACGsa-Ca	1.28e-4		
	ACGsa-Ca-ATP	1.07e-3		
	AC-Gsa-ATP	0.02		
PDE	PDE2	1.11		[149]
	PDE2-p	0.86		
	PDE1	3.98		
	PDE1-CaM	5.04e-6		
PP2C	PP2C	1.26		Estimated
CK1	CK1p	0.48		Estimated
	CK1	0.02		
Cdk5	CDK5p	0.07		Estimated
	CDK5	0.50		

Table B.4. Enzymatic reactions I

Group	Enzyme	Substrate	Product	Km (uM)	kcat (sec-1)	Initial conc of complex	Reference
PKA	PKA-act	I1	I1p	5	1.4	8.83e-3	Estimated
	PKA-act	PP2A	PP2Ap	1	1.2	1.36e-1	Estimated
	PKA-act	D	D34	2.4	2.7	9.41e-1	[105, 139]
	PKA-act	D137	D34-137	2.4	2.7	3.68e-2	[105, 139]
	PKA-act	GluR	GluR-845p	2	1	5.67e-4	Estimated
	PKA-act	GluR-I	GluR-I-845p	2	1	5.23e-3	Estimated
	PKA-act	PDE	PDE2-p	7.5	9	9.56e-3	[13]
PDE	PDE1	cAMP	AMP	39.7	9	2.22e-2	[13]
	PDE1-CaM	cAMP	AMP	4.60	18	2.43e-7	[13]
	PDE2	cAMP	AMP	39.7	18	6.20e-3	[13]
	PDE2-p	cAMP	AMP	19.841	20	9.62e-3	[13]
PP1	PP1-act	CaMKII-Thr286p-CaM	CaMKII-CaM	5.1	0.35	7.31e-3	[13]
	PP1-act	CaMKII-Thr286	CaMKII	5.1	0.35	1.49e-1	[13]
	PP1-act	CaMKII-Thr286-305	CaMKII-Thr286	5.1	0.35	6.00e-3	[13]
	PP1-act	CaMKII-Thr286-305	CaMKII-Thr306	5.1	0.35	6.00e-3	[13]
	PP1-act	CaMKII-Thr306	CaMKII	5.1	0.35	6.00e-3	[13]
	PP1-act	GluR-845p-831p	GluR-845p	100	1	3.36e-5	[210]
	PP1-act	GluR-845p	GluR	100	3	1.91e-4	[210]
	PP1-act	GluR-I-845p-831p	GluR-845p	100	1	1.63e-4	[210]
	PP1-act	GluR-I-845p	GluR-I	100	3	1.71e-3	[210]

Enzymatic Reactions and Parameters Used in the Model. In our simulation, we used the ration of kb to kcat is fixed to 4, which is default setting of GENESIS/kinetikit. Km is calculated by Km = (kb+kcat)/(kf*NA*V), where V is volume and NA is Avogadro's number.

Table B.5. Enzymatic reactions II

Group	Enzyme	Substrate	Product	Km (uM)	kcat (sec-1)	Initial conc of complex	Reference
PP2A	PP2A-PKA	D75	D	0.37	6.7	2.37e-1	Estimated
	PP2A-PKA	D34-75	D34	0.37	6.7	5.63e-8	Estimated
	PP2A-PKA	D75-137	D137	0.37	6.7	9.28e-3	Estimated
	PP2A-PKA	D34-75-137	D34-137	0.37	6.7	2.56e-9	Estimated
	PP2A-PKA	GluR-831p-845p	GluR-845p	30	1	4.33e-7	[210]
	PP2A-PKA	GluR-845p	GluR	30	3	2.46e-6	[210]
	PP2A-PKA	GluR-I-831p-845p	GluR-I-845p	30	1	2.10e-6	[210]
	PP2A-PKA	GluR-I-845p	GluR-I	30	3	2.21e-5	[210]
	PP2A-Ca	D75	D	0.372	6.7	3.23e-2	Estimated
	PP2A-Ca	D34-75	D34	0.372	6.7	7.67e-9	Estimated
	PP2A-Ca	D75-137	D137	0.372	6.7	1.26e-3	Estimated
	PP2A-Ca	D34-75-137	D34-137	0.372	6.7	3.49e-10	Estimated
	PP2A-Ca	GluR-831p-845p	GluR-845p	30	1	5.90e-8	[210]
	PP2A-Ca	GluR-845p	GluR	30	3	3.35e-7	[210]
	PP2A-Ca	GluR-I-831p-845p	GluR-I-845p	30	1	2.86e-7	[210]
	PP2A-Ca	GluR-I-845p	GluR-I	30	3	3.01e-6	[210]

Enzymatic Reactions and Parameters Used in the Model. In our simulation, we used the ration of kb to kcat is fixed to 4, which is default setting of GENESIS/kinetikit. Km is calculated by Km = (kb+kcat)/(kf*NA*V), where V is volume and NA is Avogadro's number.

Table B.6. Enzymatic reactions III

Group	Enzyme	Substrate	Product	Km (uM)	kcat (sec-1)	Initial conc of complex	Reference
PP2B	CaMCa2-CaNAB-Ca4	D34	D	0.0136	6.8	5.02e-3	[56]
	CaMCa2-CaNAB-Ca4	D34-75	D75	0.0136	6.8	1.10e-6	[56]
	CaMCa2-CaNAB-Ca4	D34-137	D137	0.0136	2	2.12e-4	[56]
	CaMCa2-CaNAB-Ca4	D34-75-137	D75-137	0.0136	2	5.00e-8	[56]
	CaMCa2-CaNAB-Ca4	PP1-D34	PP1-D	0.0136	6.8	1.13e-1	[56]
	CaMCa2-CaNAB-Ca4	PP1-D34-75	PP1-D75	0.0136	6.8	2.47e-5	[56]
	CaMCa2-CaNAB-Ca4	PP1-D34-137	PP1-D137	0.0136	2	1.55e-2	[56]
	CaMCa2-CaNAB-Ca4	PP1-D34-75-137	PP1-D75-137	0.0136	2	3.65e-6	[56]
	CaMCa2-CaNAB-Ca4	I1p	I1	4	3	2.79e-3	Estimated
	CaMCa2-CaNAB-Ca4	PP1-I1p	PP1-I1	5	1.4	1.07e-6	Estimated
	CaMCa2-CaNAB-Ca4	CK1p	CK1	2	6	1.51e-3	Estimated
	CaMCa3-CaNAB-Ca4	D34	D	0.0136	6.8	1.01e-2	[56]
	CaMCa3-CaNAB-Ca4	D34-75	D75	0.0136	6.8	2.21e-6	[56]
	CaMCa3-CaNAB-Ca4	D34-137	D137	0.0136	2	4.27e-4	[56]
	CaMCa3-CaNAB-Ca4	D34-75-137	D75-137	0.0136	2	1.01e-7	[56]
	CaMCa3-CaNAB-Ca4	PP1-D34	PP1-D	0.0136	6.8	2.28e-1	[56]
	CaMCa3-CaNAB-Ca4	PP1-D34-75	PP1-D75	0.0136	6.8	4.98e-5	[56]
	CaMCa3-CaNAB-Ca4	PP1-D34-137	PP1-D137	0.0136	2	3.12e-2	[56]
	CaMCa3-CaNAB-Ca4	PP1-D34-75-137	PP1-D75-137	0.0136	2	7.36e-6	[56]
	CaMCa3-CaNAB-Ca4	I1p	I1	4	3	2.15e-6	Estimated
	CaMCa3-CaNAB-Ca4	PP1-I1p	PP1-I1	5	1.4	5.61e-3	Estimated
	CaMCa3-CaNAB-Ca4	CK1p	CK1	2	6	3.04e-3	Estimated
	CaMCa4-CaNAB-Ca4	D34	D	0.0136	6.8	1.70e-2	[56]
	CaMCa4-CaNAB-Ca4	D34-75	D75	0.0136	6.8	3.72e-6	[56]
	CaMCa4-CaNAB-Ca4	D34-137	D137	0.0136	2	2.33e-3	[56]
	CaMCa4-CaNAB-Ca4	D34-75-137	D75-137	0.0136	2	5.50e-7	[56]
	CaMCa4-CaNAB-Ca4	PP1-D34	PP1-D	0.0136	6.8	7.56e-4	[56]
	CaMCa4-CaNAB-Ca4	PP1-D34-75	PP1-D75	0.0136	6.8	1.65e-7	[56]
	CaMCa4-CaNAB-Ca4	PP1-D34-137	PP1-D137	0.0136	2	3.19e-5	[56]
	CaMCa4-CaNAB-Ca4	PP1-D34-75-137	PP1-D75-137	0.0136	2	7.53e-9	[56]
	CaMCa4-CaNAB-Ca4	I1p	I1	4	3	1.61e-7	Estimated
	CaMCa4-CaNAB-Ca4	PP1-I1p	PP1-I1	5	1.4	4.20e-4	Estimated
	CaMCa4-CaNAB-Ca4	CK1p	CK1	2	6	2.27e-4	Estimated

Enzymatic Reactions and Parameters Used in the Model. In our simulation, we used the ration of kb to kcat is fixed to 4, which is default setting of GENESIS/kinetikit. Km is calculated by Km = (kb+kcat)/(kf*NA*V), where V is volume and NA is Avogadro's number.

Table B.7. Enzymatic reactions IV

Group	Enzyme	Substrate	Product	Km (uM)	kcat (sec-1)	Initial conc of complex	Reference
CaMKII	tot-CaM-CAMKII	CaMKII-CaM	CaMKII-Thr286p-CaM	113.6	0.5	4.88e-7	[13]
	tot-CaM-CAMKII	CaMKII-Thr286	CaMKII-Thr286-305	113.6	6	5.54e-5	[13]
	tot-autonomous-CaMKII	CaMKII-CaM	CaMKII-Thr286p-CaM	175	0.5	5.69e-6	[13]
	tot-autonomous-CaMKII	CaMKII-Thr286	CaMKII-Thr286-305	175	6	6.45e-4	[13]
	CaMKII-act	GluR-845p	GluR-845p-831p	150	1	2.00e-5	Estimated
	CaMKII-act	GluR-I-845p	GluR-I-845p-831p	150	1	1.80e-4	Estimated
CK1	CK1p	D	D137	3.4	3	1.91e-1	[56]
	CK1p	D34	D34-137	3.4	3	5.90e-5	[56]
	CK1p	D75	D75-137	3.4	3	5.43e-2	[56]
	CK1p	D34-75	D34-75-137	3.4	3	1.29e-8	[56]
	CK1p	CDK5	CDK5p	0.6	4	1.55e-2	Estimated
Cdk5	CDK5p	D	D75	4	3	6.01e-1	Estimated
	CDK5p	D34	D34-75	4	3	1.85e-4	Estimated
	CDK5p	D137	D75-137	4	3	2.35e-2	Estimated
	CDK5p	D34-137	D34-75-137	4	3	7.82e-6	Estimated
PP2C	PP2C	D137	D	3	1	5.74e-1	Estimated
	PP2C	D34-137	D-34	3	1	1.91e-4	Estimated
	PP2C	D75-137	D75	3	1	1.63e-1	Estimated
	PP2C	D34-75-137	D34-75	3	1	4.50e-8	Estimated

Enzymatic Reactions and Parameters Used in the Model. In our simulation, we used the ration of kb to kcat is fixed to 4, which is default setting of GENESIS/kinetikit. Km is calculated by Km = (kb+kcat)/(kf*NA*V), where V is volume and NA is Avogadro's number.

Table B.8. Binding Reactions I

Group	Reaction			kf (uM-1sec-1)	kb (sec-1)	Reference
DA	D1R + DA	↔	D1R-DA	1.11	10	[149]
	D1R-Gs + DA	↔	D1R-Gs-DA	3.33	10	[149]
	D1R + Gs-GDP	↔	D1R-Gs	0.06	0.0003	[149]
	D1R-DA + Gs-GDP	↔	D1R-Gs-DA	0.6	0.001	[149]
	D1R-Gs-DA	→	D1R-DA+Gsa-GTP+bc	20 s-1	0 uM-2s-1	[149]
	Gs-GTP	→	Gs-GDP	10 s-1	0	[149]
	Gsa-GDP+bc	→	Gs-GDP	100	0	[149]
AC	AC+Ca	↔	AC-Ca	1	0.9	[149]
	AC + Gsa-GTP	↔	AC-Gsa	38.5	50	[149]
	AC-Ca+Gsa-GTP	↔	ACGsa-Ca	19.2	25	[149]
	AC-Gsa+ATP	↔	AC-Gsa-ATP	0.128	0.261	[149]
	ACGsa-Ca+ATP	↔	ACGsa-Ca-ATP	0.06	0.131	[149]
	AC-Gsa-ATP	↔	cAMP+AC-Gsa	28.46 s-1	0.259 uM-1s-1	[149]
	ACGsa-Ca-ATP	↔	cAMP+ACGsa-Ca	14.23 s-1	0.13 uM-1s-1	[149]
PDE	PDE1 + CaM	↔	PDE-CaM	0.1	1	[149]
	PDE-p	→	PDE	0.1 s-1	0	[13]
PKA	R2C2 +2cAMP	↔	R2C2-cAMP2	0.035 uM-2s-1	0.06	Estimated
	R2C2-cAMP2 +2cAMP	↔	R2C2-cAMP4	0.27 uM-2s-1	0.28	Estimated
	R2C2-cAMP4	↔	2PKA-act+R2-cAMP4	0.05 s-1	0.085 uM-2s-1	Estimated
	PKA-act+D75	↔	Inhibited-PKA1	4.6	2.4	Estimated
	PKA-act+D75-137	↔	Inhibited-PKA2	4.6	2.4	Estimated
PP1	PP1-I1	→	PP1-act+I1	1 s-1	0 uM-1s-1	[13]
	PP1-act+I1-p	↔	PP1-I1-p	150	0.1	[13]
	PP1-act+D34	↔	PP1-D34	100	0.2	[139]
	PP1-act+D34-75	↔	PP1-D34-75	100	0.2	[139]
	PP1-act+D34-137	↔	PP1-D34-137	100	0.2	[139]
	PP1-act+D34-75-137	↔	PP1-D34-75-137	100	0.2	[139]
	PP1-D	→	PP1-act+D	10 s-1	0 uM-1s-1	Estimated
	PP1-D75	→	PP1-act+D75	10 se-1	0 uM-1s-1	Estimated
	PP1-D137	→	PP1-act+D137	10 se-1	0 uM-1s-1	Estimated
	PP1-D75-137	→	PP1-act+D75-137	10 se-1	0 uM-1s-1	Estimated

Binding reactions and parameters used in the model

Table B.9. Binding Reactions II

Group	Reaction			kf (uM-1sec-1)	kb (sec-1)	Reference
PP2A	PP2A-B1+2Ca	↔	PP2A-B1-2Ca	0.082 uM-2s-1	2	Estimated
	PP2A-B2p	→	PP2A-B2	8.3 s-1	0	Estimated
	PP2A+PP2A-B2p	↔	PP2A-PKA	7.4	6.8	Estimated
	PP2A+PP2A-B1-2Ca	↔	PP2A-Ca	1	0.12	Estimated
PP2B	Ca+CaNAB	↔	CaNAB-Ca2	10008 uM-2s-1	1	[13]
	Ca+CaNAB-Ca2	↔	CaNAB-Ca4	3.6 uM-2s-1	1	[13]
	CaMCa2+CaNAB-Ca4	↔	CaMCa2-CaNAB-Ca4	0.24	1	[13]
	CaMCa3+CaNAB-Ca4	↔	CaMCa3-CaNAB-Ca4	22.38	1	[13]
	CaMCa4+CaNAB-Ca4	↔	CaMCa4-CaNAB-Ca4	600	1	[13]
CaMKII	CaMKII	→	CaMKII-Thr286	0.003 s-1	0	[13]
	CaMKII+CaM	↔	CaMKII-CaM	50	5	[13]
	CaMKII-thr286+CaM	↔	CaMKII-thr286-CaM	1000	0.1	[13]
CaM	CaM + Ca	↔	CaM-Ca2	72 uM-2s-1	72	[13]
	CaM-Ca2+ Ca	↔	CaM-Ca3	3.6	10	[13]
	CaM-Ca3+ Ca	↔	CaM-Ca4	0.465	10	[13]
AMPAR	GluR	→	IR+Anchor	0.0008 s-1	0 uM-1s-1	[103]
	IR+Anchor	↔	GluR-845p-831p	0.018	1	[103]
	GluR-I	↔	Bult-AMPAR	1 s-1	0.018	[103]
	GluR-I-845p	→	Bult-AMPAR	2e-05 s-1	0	[103]
	GluR-I-845p-831p	→	Bult-AMPAR	2e-05 s-1	0	[103]
CK1	CK1	→	CK1p	1.54 s-1	0	Estimated
CDK5	CDK5p	→	CDK5	0.9 s-1	0	Estimated

Binding reactions and parameters used in the model

C. Detailed Illustrations of Reactions

Illustrations of reactions used in Chapter 4.

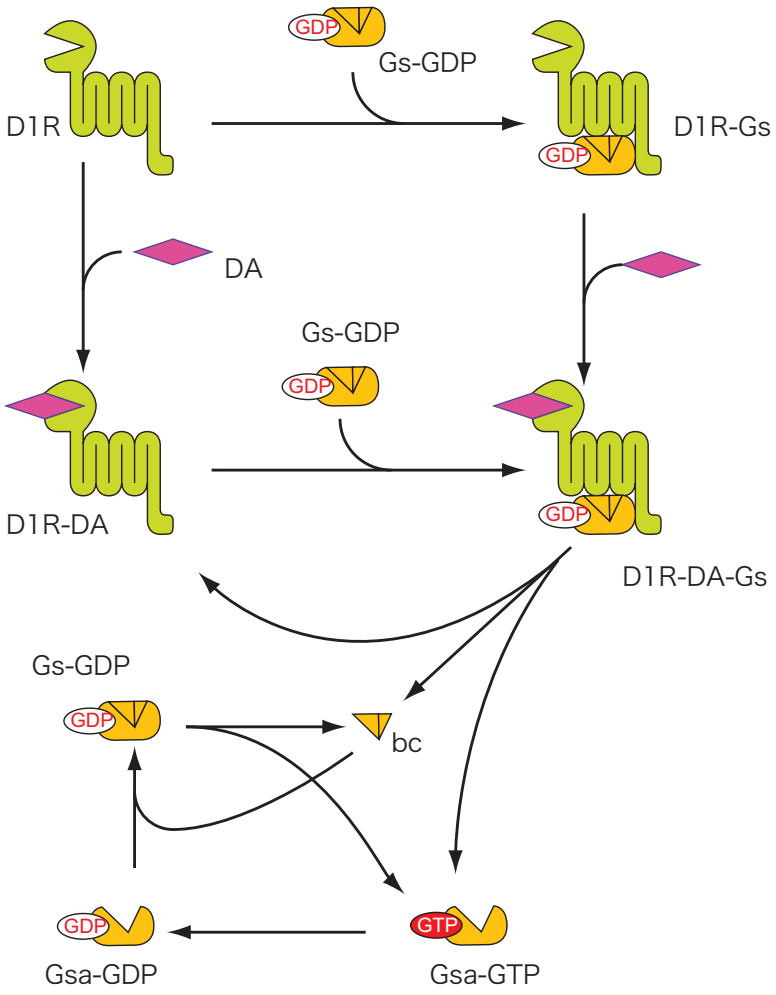

Figure C.1. Dopamine receptor

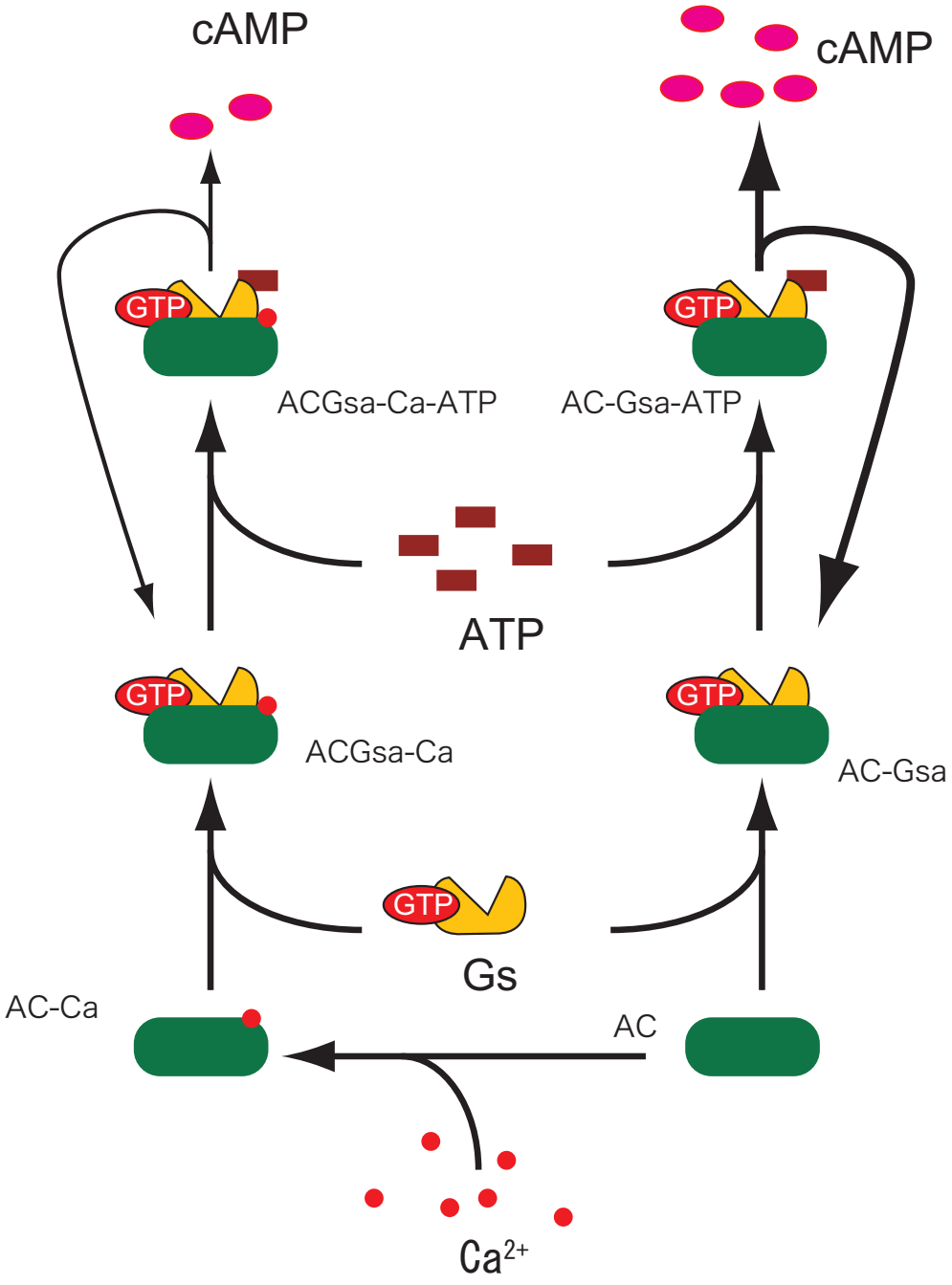
cAMP
cAMP
GTP
GTP
ACGsa-Ca-ATP
AC-Gsa-ATP
ATP
GTP
GTP
ACGsa-Ca
AC-Gsa
GTP
Gs
AC-Ca
AC
Ca2+

Figure C.2. AC

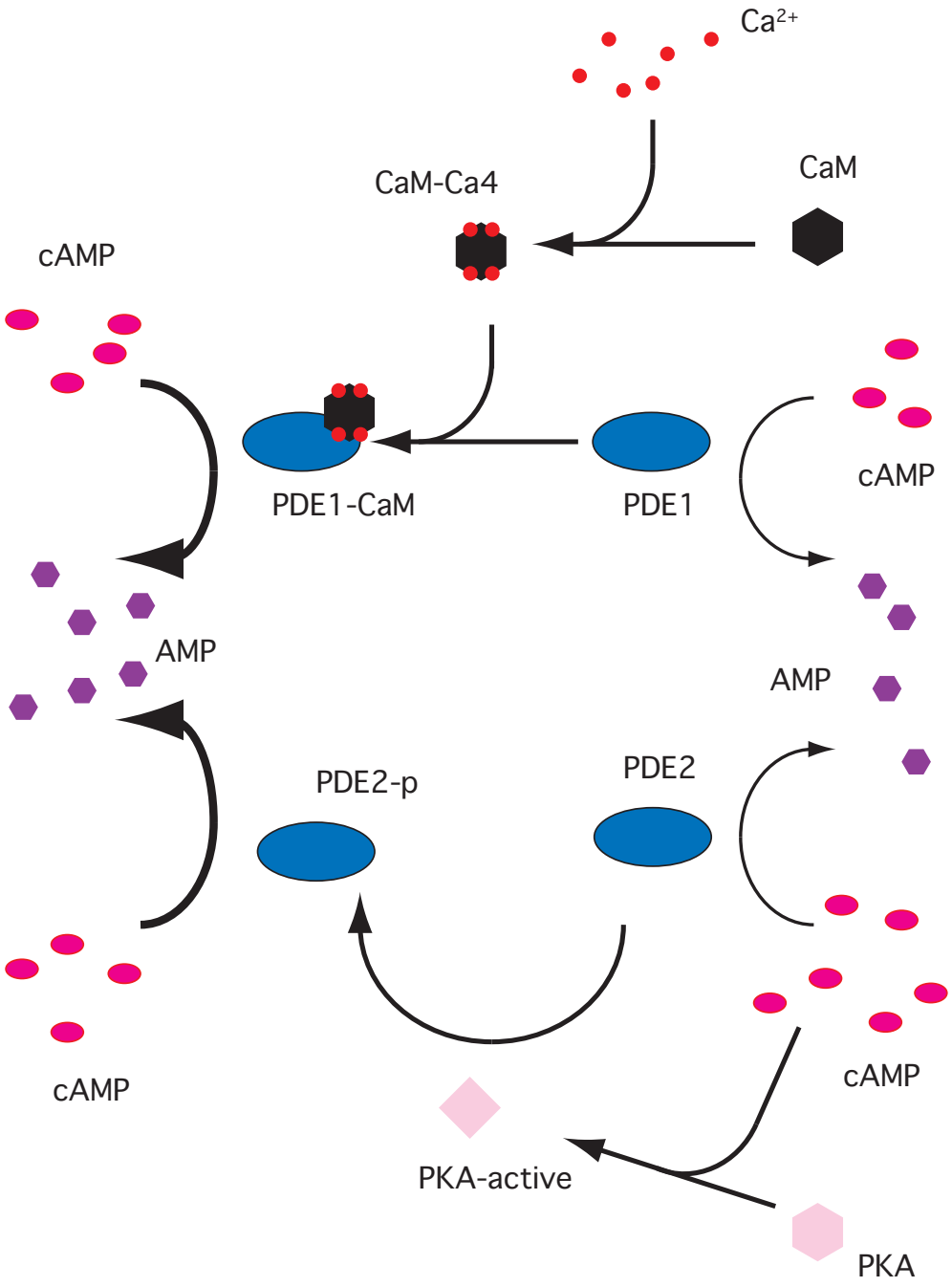

Figure C.3. PDE

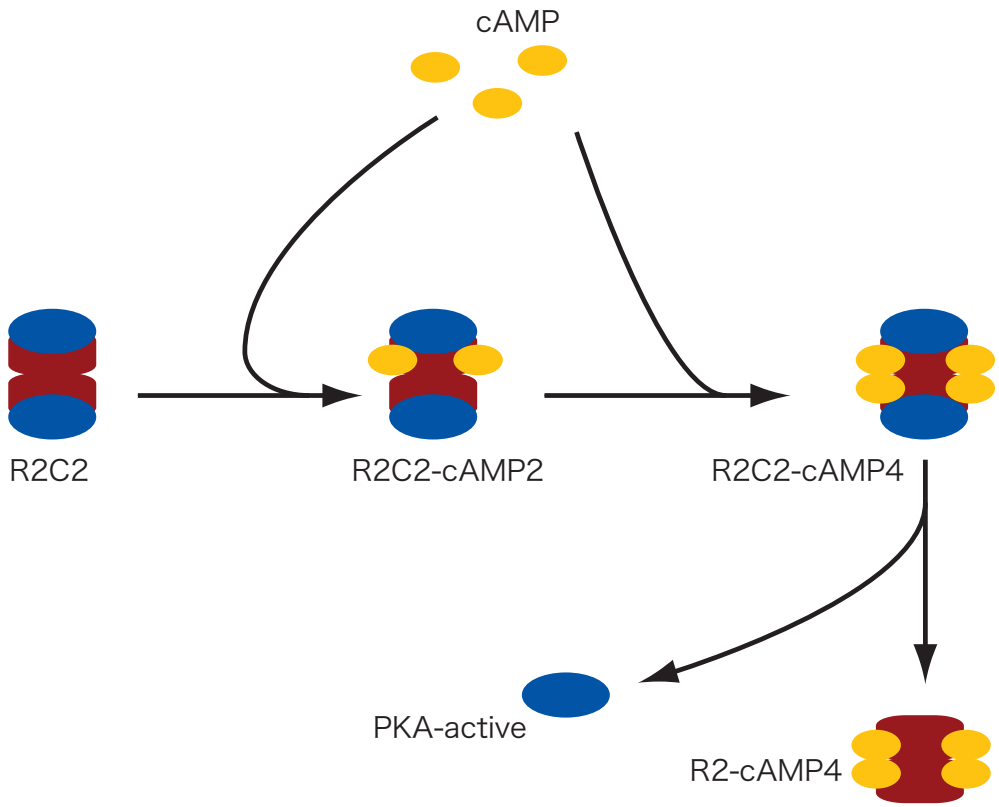

Figure C.4. PKA

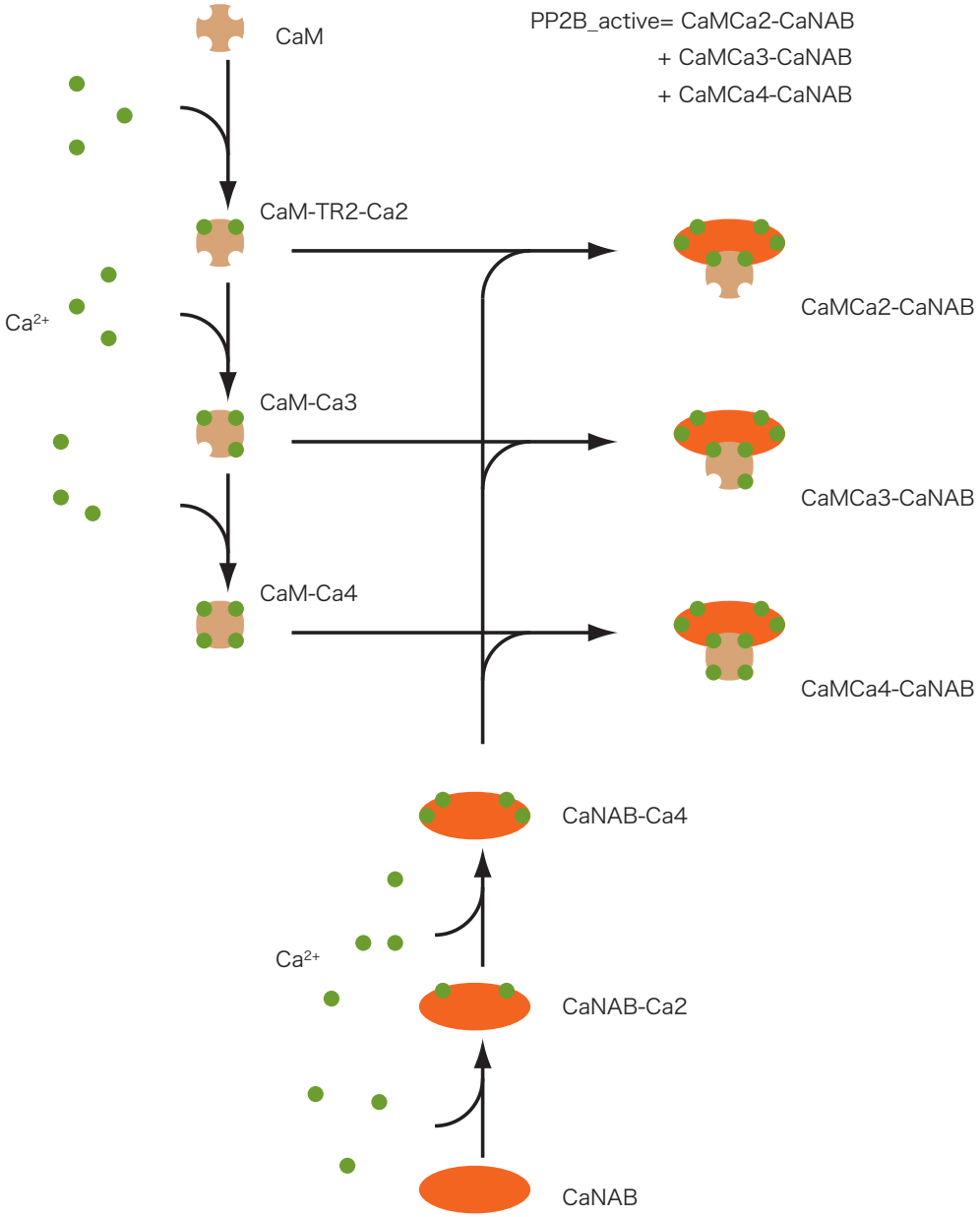

Figure C.5. CaM and PP2B

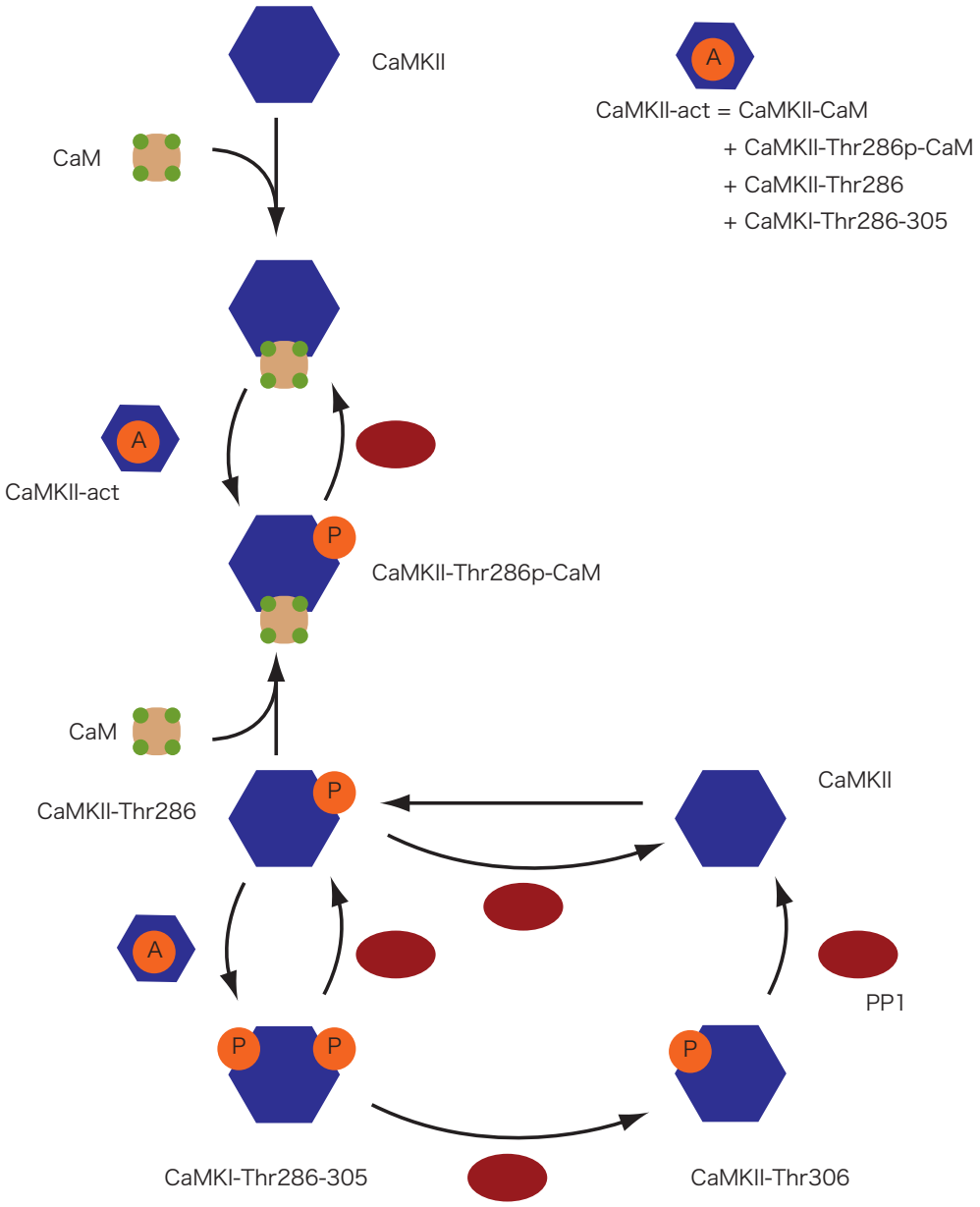

Figure C.6. CaMKII

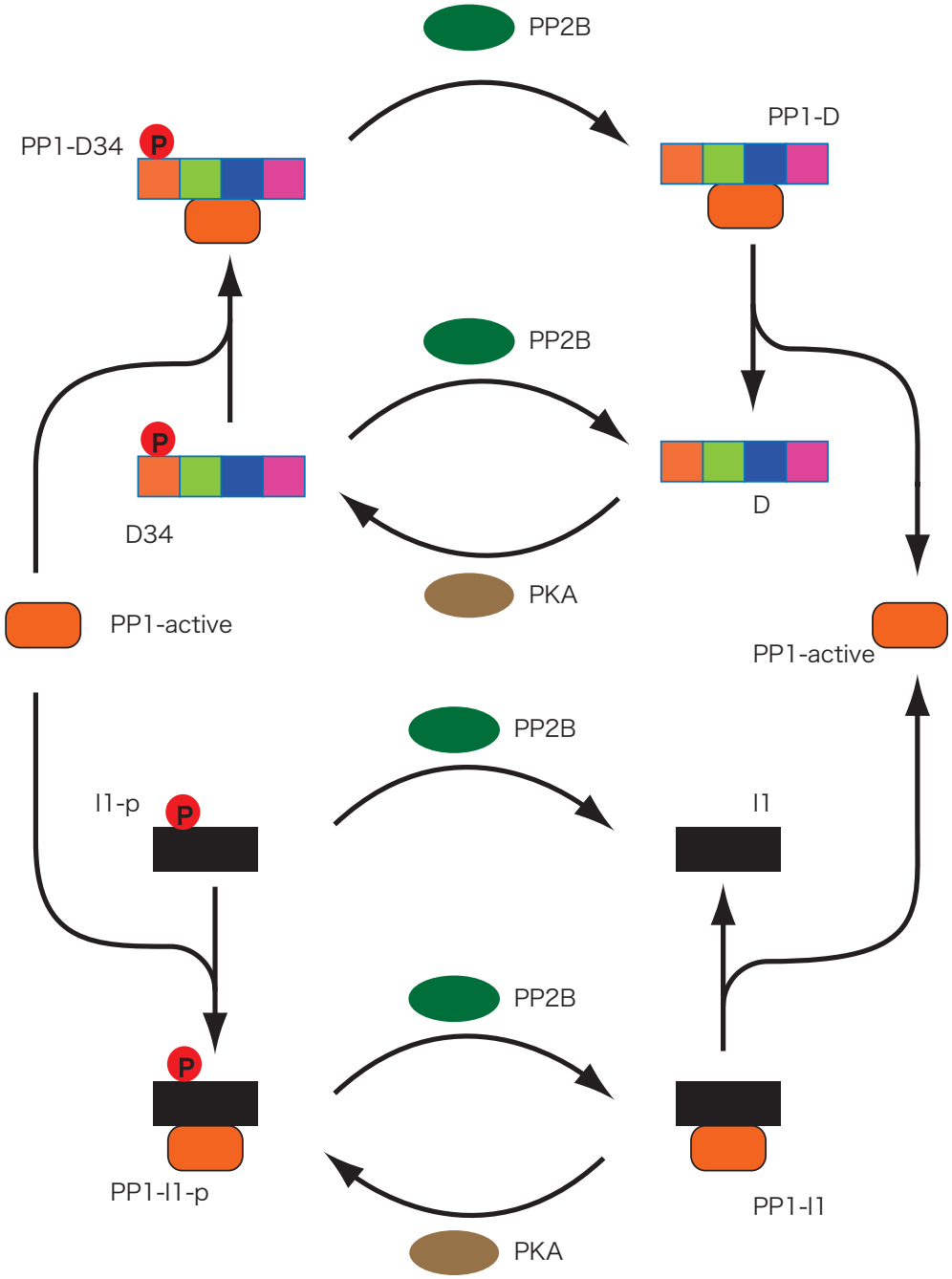

Figure C.7. PP1

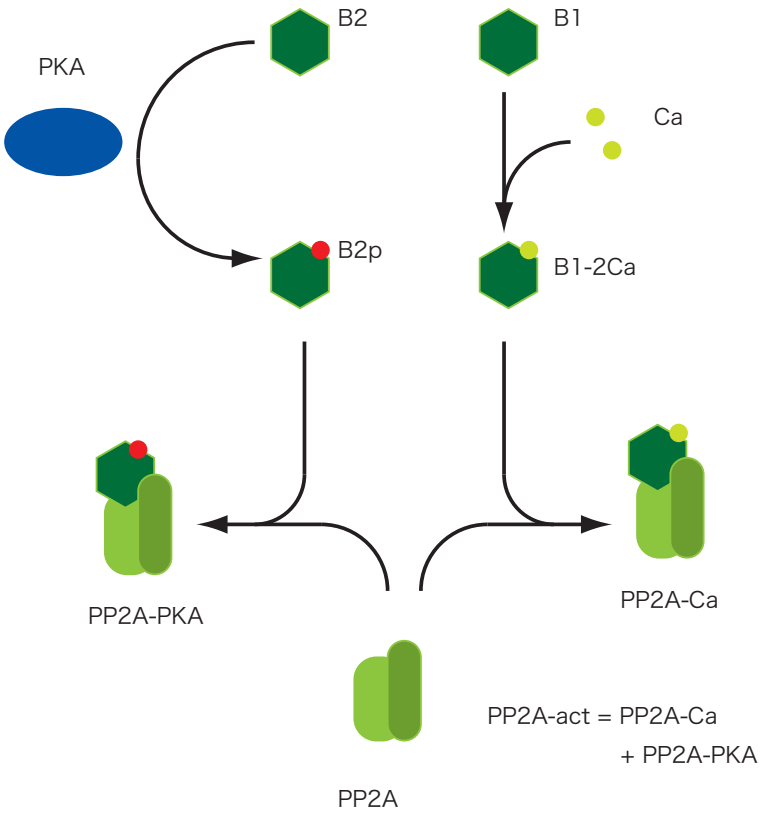

Figure C.8. PP2A

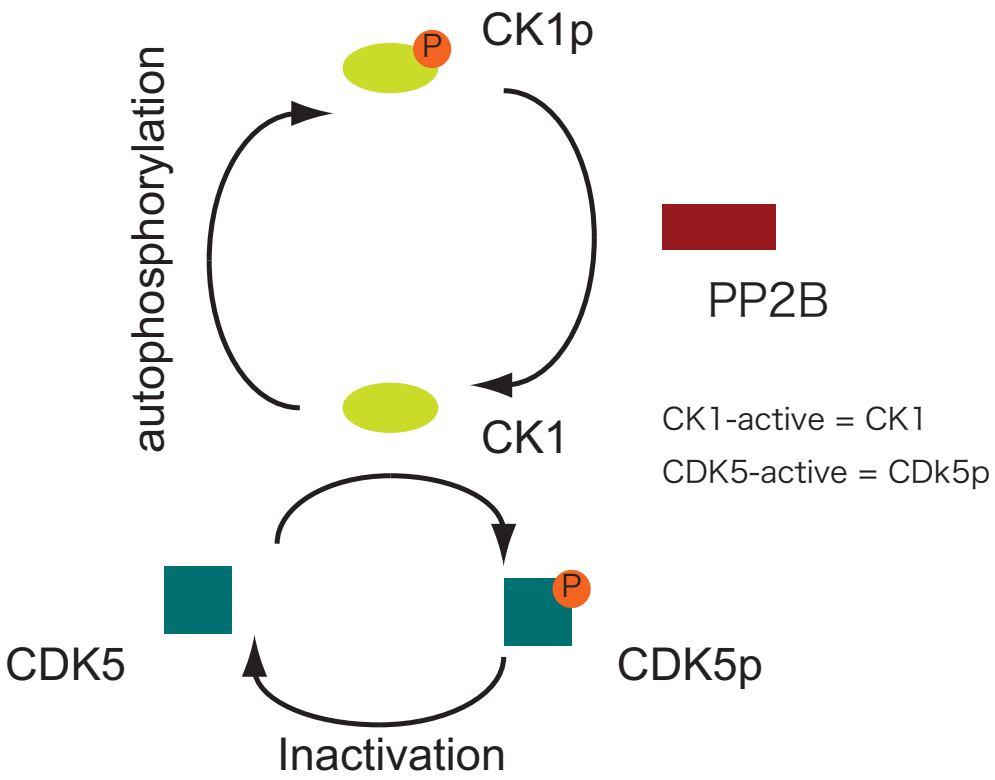

Figure C.9. CK1 and Cdk5

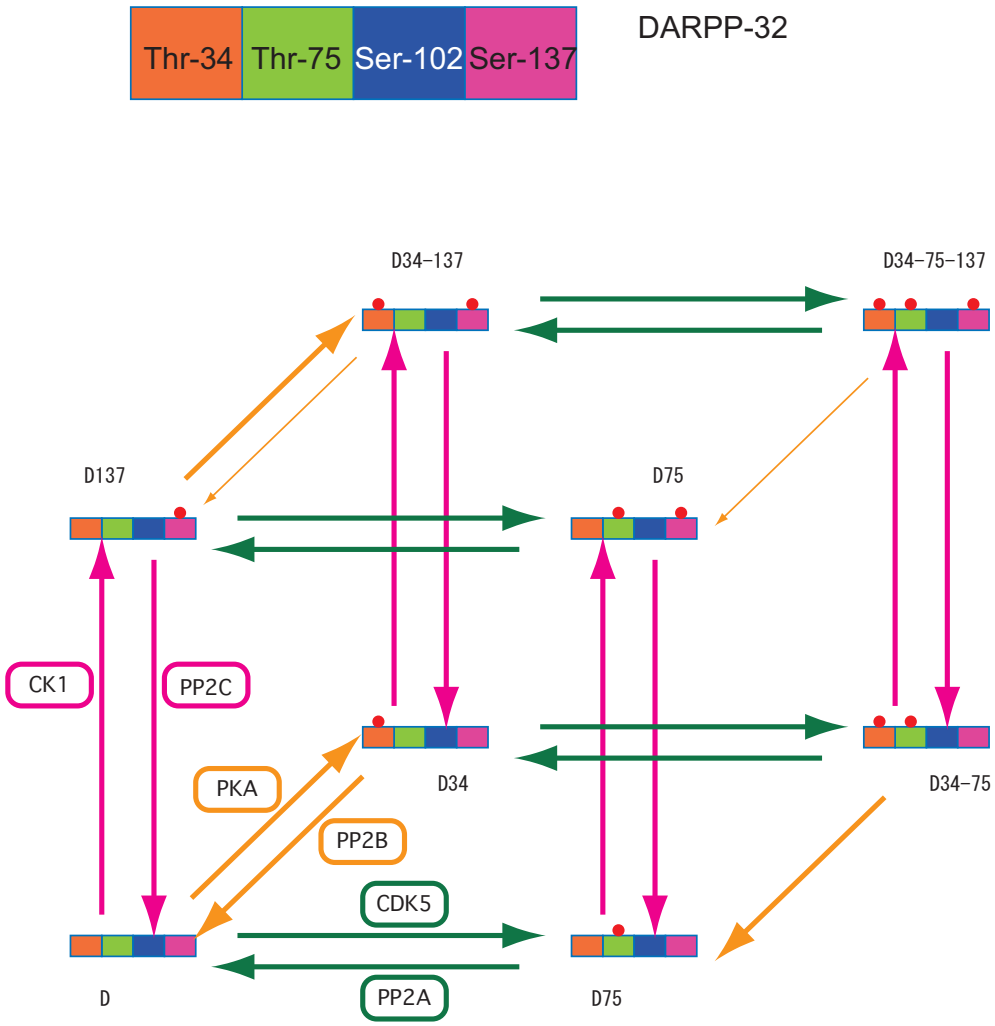

Figure C.10. DARPP-32